Inter-Satellite Communication Links for Sensor Networks in Low Earth Orbits

Saad Ali Malik

Department of Engineering

University of Leicester

This dissertation is submitted for the degree of

Doctor of Philosophy

Embedded Systems Group May 2019

This thesis is dedicated to my father (Nazakat Ali Khan), mother (Ismat Malik), wife (Ammara) and children (Ahdia, Taha, Ayesha, Ibrahim & Tayyab) ...

Declaration

I hereby declare that except where specific reference is made to the work of others, the contents of this dissertation are original and have not been submitted in whole or in part for consideration for any other degree or qualification in this, or any other university. This dissertation is my own work and contains nothing which is the outcome of work done in collaboration with others, except as specified in the text and Acknowledgements.

Saad Ali Malik
May 2019

ACKNOWLEDGEMENTS

First and foremost, all praises and thanks to the Creator of the Universe for granting me an opportunity to conduct research as a PhD scholar.

I am sincerely grateful to my principle supervisor, Prof. Vladimirova, for accepting me as her student. I acknowledge her future vision and insight of the evolving space engineering applications, which has resulted in considerable research in the emerging field of space based wireless sensor networks. Her extra efforts, vigilance, and focused approach guided me through the turbulent voyage called PhD. She kept my moral high, always believing in me, ushering me onwards, at times when all hope seemingly lost. It would not be wrong to state, that this thesis is the fruit of her unwavering trust, patience, extra support and clear guidance.

The technical advice by my additional supervisors Prof. Warrington at Leicester and Prof. Sweeting at Surrey, pushed me through the deadlocks during research. The critical review by the examiners (Dr. Stocker and Dr. Hobbs) is highly appreciated, who took time to read every line of the thesis, while acknowleding the contributions, also indicated room for improvement.

During the course of PhD, the administrative staff, librarian and technicians at Surrey Space Centre, U.K., Engineering Department of Leicester, UK, and Institute of Space Technology, Pakistan, have been kind enough to assist me generously in technical and administrative matters.

The wonderful caring and helpful colleagues at Surrey and Leicester left a lifelong mark in my memories. At times of dire financial needs Prof. Adel would exempt house rent payment schedules; the smiles, laughs and assurances of Karen, lending ears of Thibault, solemn assurances by Jean Paul, wise advice by Adbul-Haleem, daily chats with Rizuan, Hassaan, Naveed, Fayyaz, listening to my thoughts by Shujahat, Mohammad and Omar, to name a few.

Last but not the least, the exemplary support extended by my wife, kids and parents, backing me up at times of extreme despair; when every path taken seemed to lead to a dead end, every oath taken apparently broke — thank you for not letting go of the trust in me.

I have been blessed to work under the supervision of experts in their field, to meet the kindest, generous colleagues — *may Allah blesseth thee all.*

Inter-Satellite Communication Links for Sensor Networks in Low Earth Orbits

Saad Ali Malik

Abstract

Unlike the inter-Satellite communications link (ISL) being used in current space missions, emerging scenarios require point to multi-point links with additional support for autonomous networking amongst multiple satellites. Be it for formation flying or space based wireless sensor networks, these distributed satellite systems require revised communications system design to provide for the various physical topologies, dynamic channel characteristics and user requirements. All three factors being mission specific, that is why, little literature is published, in which physical aspects of the link or the communications system design or the channel is discussed. This thesis determines channel characteristics and performance of OFDM modem for three physical topologies for a proposed mission scenario, bridging the gap in literature. The mission is used as the basis for investigating the impact of relative motion and in-orbit environment on propagating EM waves.

The proposed multipoint sensing mission namely the ionosphere monitoring mission (IMM) comprises pico/nano class of satellites in a mother daughter configuration, to take finer measurement of the plasma bulk properties in LEO.

Three physical topologies for ISL are identified. Relative motion is studied for (a) free flying CubeSats acting as sensor, (b) a sensor satellite with respect to a relay satellite and (c) several relay satellites in a string-of-pearl configuration. The Doppler shift is nominal tens of Hz for the first and third case, however, the Doppler shift is in kHz for case b. Thus a third order PLL is required in receiver stage.

Contrary to what is assumed in literature, the communications channel is identified to exhibit fading. The dynamic fading (fast and slow) can reach up to 20 dB. To cope with the dynamic channel behaviour a reconfigurable OFDM modem is described. This channel is modelled in MATLAB as a Time Delay Line (TDL) structure, and used to evaluate the performance of OFDM modem for data rates up to 1 Mbps. The hardware-in-the-loop simulation methods, assisted in laying a much needed foundation for a testbed for evaluating ISL.

Table of Contents

List of Figures

List of Tables

Nomenclature

Roman Symbols

A	Amplitude of signal
a	Orbital Elements: Semi-major Axis of elliptical orbit
A_{aper}	Surface Area of Antenna
$\mathbf{B}$	Magnetic field.
I	Current
$\dot{(\cdot)}$	Time derivative of the enclosed function
e	Eccentricity of elliptical orbit in orbital parameters
e_{elec}	Charge on electron in magneto-ionic theory.
f_c	Operational frequency or carrier wave frequency.
F_s	Force exerted by spring.
i	Orbital Elements: Inclination (angle of Ellipse wrt Equatorial plane)
k	Springs constant as defined in Hooke's law.
$L_{\oplus}$	Geomagnetic Latitude
L	Longitudinal component of vector field w.r.t. propagating wave normal
m_e	Mass of electron
n_e	Number of electrons per unit volume, Electron concentration (electrons/m^3)
N_T	Total electron content along a path.
P_r	Power received by the Antenna in Watts (W)
P_t	Power fed to the Antenna in Watts (W)
$R_{\oplus}$	Radius of Earth as defined in JGM-3
s	Length of propagation path in ionized gas.
T	Transverse component of vector field w.r.t. propagating wave normal
T_{rev}	Orbit period

$\vec{\mathrm{h}}$	Angular momentum of orbit
$\vec{\mathrm{r}}$	Position Vector of satellite in ECI frame
$\vec{r}_a$	Apogee radius
$\vec{r}_p$	Perigee radius
$\vec{\mathrm{v}}$	Velocity Vector of satellite in ECI frame
V	Voltage
x,y,z	Rectangular coordinate axis

Greek Symbols

χ	Absorption index i.e. negative imaginary part of η
ε	Dielectric constant
ε_0	Electric permittivity of free space
η	Complex refractive index of magneto-ionic medium
j	Current density
κ	Absorption coefficient
μ	Real part of η
μ_0	Magnetic permittivity of free space
ν	Collision frequency of electrons
Ω	Orbital Elements: Right Ascension of the ascending node (angle from vernal equinox to line of nodes
ω	Orbital Elements: Argument of Perigee (angle from the line of ascending node to point of perigee)
ω_{wave}	Angular wave-frequency
ω_N^2	$= 4\pi N e_{elec}^2/\varepsilon_0 m$
τ	Time duration; Pulse width (as per context)
Θ	Faraday Rotation angle.
ζ	Charge density

Acronyms / Abbreviations

1U	CubeSat of 10cm x 10cm x 10cm, mass 1kg
2U	CubeSat of 10cm x 10cm x 20cm, mass 2kg
3U	CubeSat of 10cm x 10cm x 30cm, mass 3kg
BER	Bit error rate
BoL	Beginning of Life

CME	Coronal Mass Ejection
DSN	Distributed Sensor Networks
ECI	Earth Centric Inertial Frame of reference
EM	Electro-Magnetic Waves or fields
EoL	End of Life
ESA	European Space Agency
ES	Earth Station or Ground Station
FER	Frame error rate
FFTB	Formation Flying Test Bed for space missions
FIR	Finite Impulse Response Filter
GEO	Geosynchronous Earth Orbit
GL	Ground Link for tracking,telemetry and telecommand.
GM	Geiger-Muller energetic particle counter
GPS	Global Positioning (Satellite) Systems
HEO	Highly Elliptic Earth Orbit
HF	High Frequency
IIR	Infinite Impulse Response Filter
IMM	Ionosphere Monitoring Mission
ISL	Inter-Satellite Communications Link
JAXA	Japan Aerospace Exploration Agency
LEO	Lower Earth Orbit
LP	Langmuir Probe
LVLH	Local Vertical Local Horzontal Body fixed frame
LV	Launch Vehicle
MaNET	Mobile Adhoc Networks
MEO	Medium Earth Orbit
NASA	National Aeronautics and Space Administration
NOAA	National Oceanic and Atmospheric Administration
OBC	On-Board Controller
OBDH	On-Board Data Handler
p/n	Part Number of a Manufacturers catalogue.

PMEL	Pacific Marine Environmental Laboratory
P-POD	Polytechnic Pico Orbital Deployer
RF	Radio Frequency
SBWSN	Space Based Wireless Sensor Networks
SDR	Software Defined Radios
SER	Symbol error rate
SMAD	Space Mission Analysis and Design
SOSUS	Sound Surveillance System
TEC	Total Electron Content
TT&C	Telemetry, Tracking and Tele-Command
UHF	Ultra High Frequency
VHF	Very High Frequency
VLSI	Very-Large Scale Integration
w.r.t	with respect to
WSN	Wireless Sensor Networks

CHAPTER 1

INTRODUCTION

> "It is difficult to say what is impossible, for the dream of yesterday is a hope of today and the reality of tomorrow."
>
> — ROBERT H. GODDARD

Currently, space industry is passing through a phase of rapid changes. Cost effective solutions serve as a new leitmotif for scientists, engineers, researchers, entrepreneurs and technologists, to capitalise on. Adapting commercial-off-the-shelf (COTS) components [1], incorporating miniaturised electro-mechanical systems [2, 3] and legislating commercial access to space [4, 5], are the factors contributing to the introduction of smart, efficient technologies in space systems engineering. Very small satellites once considered "academic toys", not only lead a rejuvenated small satellite industry, but are acknowledged as a prime contributor to novel distributed satellite systems (DSS) not realisable earlier due to high costs and technical issues.

An application of DSS is multipoint sensing, for which multiple satellites are deployed. This thesis investigates physical aspects of the communications system used for inter-satellite links in such a mission scenario. An end to end communications system performance evaluation demonstrates severity of link disruption, while highlighting the need of a reconfigurable system, for a highly dynamic channel identified in low Earth orbits.

1.1 Thesis Background and Related Work

This thesis is the result of a research work initiated in the VLSI Design and Embedded Systems (VDES) research group at Surrey Space Centre (SSC), UK, which culminated at the Embedded systems research group at the University of Leicester, UK, following the move by the principal supervisor. Mission scenario and CubeSat development issues were covered at SSC, whereas, radio propagation issues were investigated at Leicester; both works are being presented in this thesis.

At the Surrey Space Centre, the research group was investigating enabling technologies [6] for two novel applications of wireless sensor networks in space:

1. Sun sensors, star sensors, Albedo, temperature, voltage, pressure and a plethora of other sensors particularly in a space science mission, all linked to a central processing unit, is an example of a sensor network in space. The harnesses connecting these sensors makes up 10% of the dry mass [7], so replacing the harnesses with wireless links can reduce overall financial cost and development times. So the first application targets intra-spacecraft wireless sensor networks. To this regard commercially available Motes developed for terrestrial WSN application were evaluated for their operations in harsh space environments [8].
2. The second application of WSN is to deploy several sensor satellites in large numbers, so as to improve the spatial and temporal resolution of the measurement, thus overcoming the inherent ambiguity arising in single point sensing. With regards to the second application, three sub-problems were being investigated:
   a) A mass producible low cost spacecraft platform having a very small size, which could be used as a sensor satellite.
   b) Adopting commercially available terrestrial wireless technologies for establishing autonomous ad hoc networks in space.
   c) Investigate low powered high processing capabilities.

The focus of research in this thesis is the second application i.e. SBWSN, for which inter-satellite links need to be evaluated.

SBWSN is a relatively new concept in space missions, therefore little literature is published. Clare [9] suggested the use of multi-hop networks for inter-planetary environments. Vladimirova [6] embarked on adopting wireless local area network technologies for space application with a focus on using small low cost mass producible satellites to act as sensors. Dubois [10] suggested the use of ad hoc networking technology for Solar system exploration. Clare and Dubois both presented a general overview of possible technologies which could be used, backing their claims with simulation based results of higher layers avoiding the physical layer issues. Whereas, Vladimirova [11, 12] took a system specific approach, investigating terrestrial wireless networking technologies such as IEEE 802.11 [13], IEEE 802.16 [14] and Zigbee [15] for space applications. ESPACENET [16] programme, which is a consortium of several universities and space agencies, marked the seriousness shown towards the concept of wireless sensor networks in space. DSS, ESPACENET and SBWSN can be envisioned as the next logical extra terrestrial application of the Distributed Sensor Network (DSN) programme initiated by the Department of Advanced Research Projects Agency (DARPA) in 70s [17]. Enabling technologies which have already been addressed are described to clarify the context of the research presented in this thesis.

The development of low cost spacecraft platform started back in the mid 90s. Academia took interest in smaller student led satellite projects to educate its graduates in project management and gaining hands-on-experience. OPAL [18] being one of the pioneering student satellites, followed by CanSat [19], SNAP-1 [20], CubeSat [21, 22], to name a few. PCBSat [23, 24] and ChipSat [25] are contributions by the VDES group. These small satellite platforms compared to typical micro satellites in terms of financial costs, mass and size and shape, are illustrated in Figure 1.1.

Amongst the small satellites, CubeSat platform got wide acceptance in academia and picked up by venture capitalists. Pumpkin Inc. [26] started selling CubeSat structures fitted with a flight ready on-board computer (OBC), and private ventures, such as ISIS, eased CubeSat's integration with the Launch Vehicle (LV). The ease with which CubeSat structure could be bought and interfaced to a LV, is a major factor which made CubeSat the de facto pico/nano satellite standard, widely accepted in academia and industry alike [27].

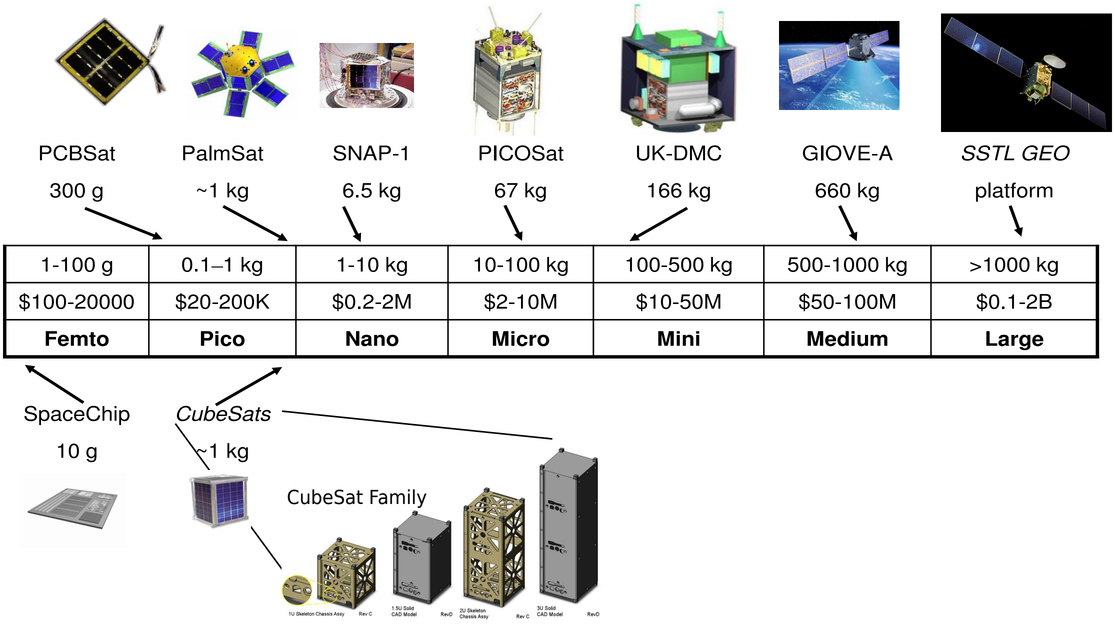

Fig. 1.1 Small satellite schematics with projected development costs adopted from [23].

An example of a DSS mission using inter-satellite links to form a network was proposed in the VDES group at Surrey [24, 28], laying the foundations for future SBWSN applications [29]. Equipped with a COTS radio, it was assumed, that a mesh network would be formed and the inter-satellite links would assist in distributed operations such as exchange of data for relay, or on-board processing. The radio operating at 900 MHz, it was assumed, that the channel would not have any deteriorating impact other than the free space path loss, when deployed in Low Earth Orbits (LEO).

ESPACENET research programme [16] systematically addressed various aspects of SBWSN. A multi-band antenna for small satellites was developed at a partner university [30], which could be used with a beam forming algorithm suggested by VDES researcher Sidibeh [31]; both works assumed the use of 3 axis stabilised satellites, and no deterioration due to communications channel on the inter-satellite link.

IEEE 802.11 and IEEE 802.15 which is extensively used in WSN analysis were evaluated for SBWSN by Sidibeh [32, 33], in the VDES group. He identified, by a modification in the IEEE 802.11 Medium Access Controller (MAC) algorithm can be adopted for space application. The MAC uses carrier sense multiple access (CSMA) [34] with collision avoidance (CA) technique, requiring single frequency of operations, without the need for a priori knowledge of the location of network nodes (members of the network). Paul [35] within the VDES group, implemented an orthogonal frequency division multiplexing (OFDM) modem on a field programmable gate array (FPGA), interfaced to "SpaceWire", aiming at intra-spacecraft WSN applications. Wu [36, 12] contributed by developing a hardware-in-the-loop (HIL) testbed to investigate networking protocols for space applications, and evaluated a routing algorithm [37]. The network simulator used in the process called NS-2 [38].

In addition to the above emerging application, ISL, has been an active research topic for formation flying missions, LEO communication satellite networks, and GEO based tracking and data relay missions. Surprisingly, all investigations regarding inter-satellite links tackled for the above stated applications, focused on either of the following aspects:

1. the geometrical aspect of the link [39, 40, 41], i.e. placement of satellites in a constellation to optimise orbital parameters for line of sight [42, 43, 44, 45],
2. the technical issues of pointing accuracies arising from the use of fine beam width LASER or millimetre waves [46, 47, 48, 49]; addressing the particular issue of correctly pointing quickly and reducing mechanical jitter in the rotary mechanisms.
3. the generation of LASER [50, 51] and the necessary circuitry.

1.2 Motivation

In all the works described above, the inter-satellite environment was assumed simply to act as free space, thus free space path loss model was used in performance evaluations i.e. signal strength decreases with the inverse square of the distance and is directly dependant on the wavelength of radiation (Friis formula [52]).

On the contrary, it is well known that the satellite to ground links suffer from signal degradation which has been attributed to turbulent behaviour of not only the neutral atmosphere below 90 km altitude, but also the ionised gas in the 90 to 1500 km altitude [53]. The signal degradation is called scintillation, i.e. rapid changes in amplitude and phase of the received signal. Scintillation has been extensively studied and its effects modelled by several authors, some of the notable works are Loo's statistical model [54] for a land mobile satellite channel, Bello's general theory of stochastic processes to identify channel characteristics [55]. Works by Fremouw, Bogusch and Rino on satellite to ground scintillation modelling [56, 57, 58, 59, 60, 61], are enough evidence to evaluate the in-orbit space environment for time varying fading properties for satellite to satellite links as well. This is the primary factor instigating the research presented in this thesis.

The second factor motivating the work presented in this thesis is the application of inter-satellite links for the emerging very small satellites (Figure 1.1). The successful deployment of the pico/nano class of satellites since 2000 is remarkable. In the first decade of the 21st century, these small satellites were only mocked as "educational toys", whereas, today they are driving a multi-million dollar industry. The potential use of these very small satellites is being investigated by major space agencies, for example initiatives by NASA [62] and ESA [63]. It is foreseen that in the near future, distributed satellite systems based on these very small satellites would play a pivotal role in Earth observation missions in general and space science missions in particular, as identified in the reports: the NASA Sun-Earth Enterprise [64] and ESA Cosmic Vision (2015–2025) [65]. Furthermore, it is intriguing that even though ISL has been demonstrated as early as 70s, only a few space missions incorporate ISL as discussed in Section 2.2. To use small satellites to form a sensor network in space as part of a SBWSN, the satellites need to be equipped with inter-satellite communications systems; which is a challenge in its own aspect.

A communications system comprises several sub-systems, which work in cohesion to pass the generated message from one the transmitter to the receiver. To understand the impact of the operational environment and the design of these sub-systems, a brief overview of communications systems is given in the following section.

1.3 Inter-Satellite Communications System Design

A communications system be it for ground links or inter-satellite links (Figure 1.2) is formed of three fundamental elements.

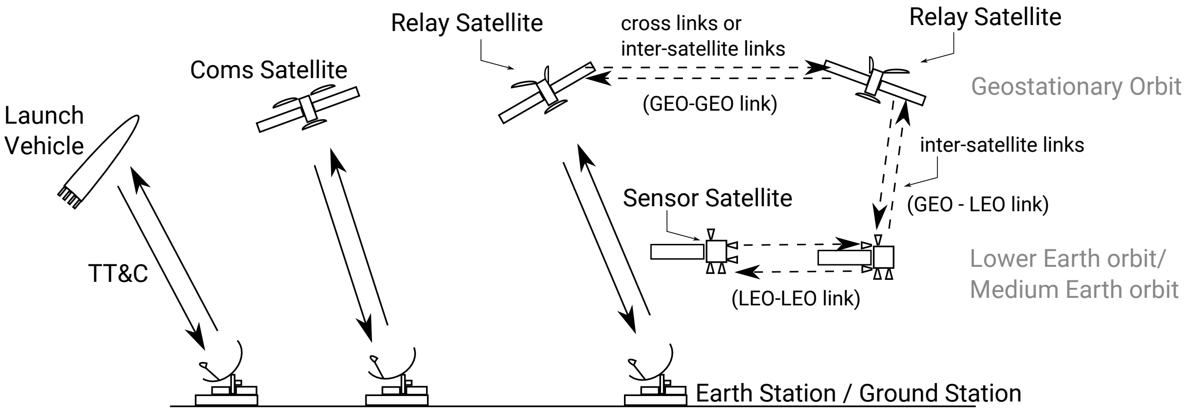

Fig. 1.2 Types of satellite communications links, distinguished as satellite to ground links (GL), and satellite to satellite links (ISL).

The elements are: a **baseband modem**, an **analogue front end (AFE)** and an **antenna system**. The **modem** is acronym for **mod**ulation and **dem**odulation. A message is passed to the modem, which generates appropriate waveforms, which are then converted to analogue form, and radiated after passband modulation. Over the wireless link, the interaction of the environment with propagating EM waves, distort the transmitted waveforms. The distorted waveform is captured at the receiver end, and the receiver demodulates the carrier to baseband signal after tuning into the carrier frequency. The baseband modem at the receiver again synchronise the internal timer to the incoming waveform start and end time, so that the message is extracted from the waveform. The three elements are illustrated as functional blocks in the Figure 1.3. A detailed description of modem and the working of the synchroniser is given in Appendix B for the interested reader.

The **wireless link** in Figure 1.3 represents the path or paths followed by the wave radiated from transmitting antenna, while reaching the receiver. In this path the interaction with the medium (metal, air, water, or ionised gas) causes the propagating electromagnetic wave to change its characteristics. The observable parameters of interest are:

- the loss of power,
- change in frequency,
- change in path direction,

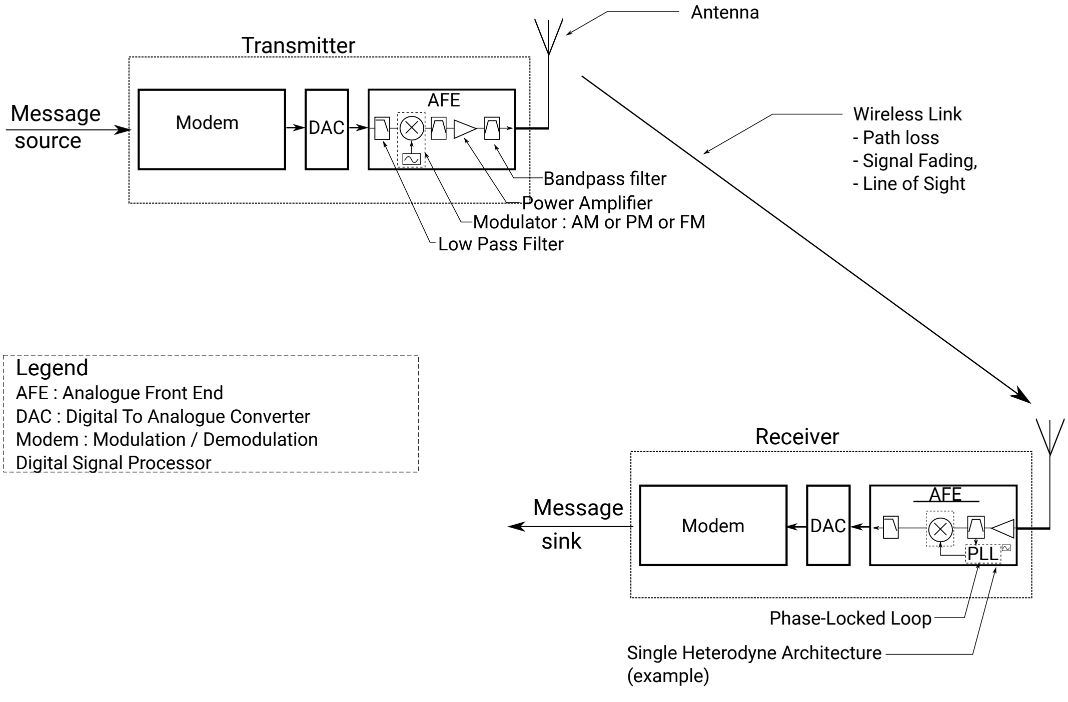

Fig. 1.3 A simplified block diagram representing the transmitter, the wireless link and the receiver. Message fed to the transmitter, is radiated in the form of electromagnetic waves, captured by receiving antenna and extracted by the modem from the distorted waveform received.

- changes in amplitude and phase of the wave, and
- the changes in field polarisation.

Different media affect the propagation depending on the fundamental carrier frequency in use, e.g. ultra sonic waves are used for underwater communications, whereas, microwaves are extensively used for terrestrial as well as space communications. Microwaves get attenuated so much so that they cannot be used for underwater communications. Similarly the effects are different for low density ionised gas and turbulent considerably denser ionised gas in different regions in space.

Capturing effects of the medium in the form of a mathematical expression or a computer algorithm, helps in evaluating the performance of baseband modulation schemes. The models thus formed, are called **communications channel models**. Several channel models have been developed that are in use today, but choosing the correct model, which truly depicts the operational environment is of utmost importance. Otherwise, excellent designs which have been simulated using computers could fail in the field tests.

Furthermore, in addition to the interaction with the medium, other objects in the vicinity of transmitter and receiver are also important. They either reflect, scatter or absorb the electromagnetic fields of the propagating waves. In the case of scattering, reflection or refraction, multiple replicas of the same transmitted waveform can be received but delayed by a small amount of time and diminished in power. The interference of the signals at the receiver is generally referred to as a multipath effect, which results in fading, i.e. changes in amplitude as well as phase.

In addition to the environment, the motion of the transmitter and receiver, affects not only the rate of fading observed at the receiver but the relative motion also introduces a shift in frequency, i.e. the well known Doppler frequency shift phenomenon. The receiver must be able to handle the shift of frequency, otherwise, the communications link cannot be established, because, receiver would not be able to lock on the predefined carrier frequency.

Testing is an important phase during the design process, for which testbeds are necessary. Tests are conducted physically as well as using computer based simulations. The design, testing and validation of each element of the communications system is carried out independently, since the background theories governing the design as well as implementation are different.

The elements of a communications system in general and the channel impact is simulated as illustrated in Figure 1.4. When the channel exhibits simple properties, the receiver design becomes simple; whereas, as soon as the channel exhibits complex properties, receiver design becomes more complex. The fading type of channel is the most deteriorating, for which appropriate mitigating techniques must be employed. Therefore, characterising the communications channel to assess the receiver performance for a given modulation scheme is a critical factor in assessing inter-satellite links in particular.

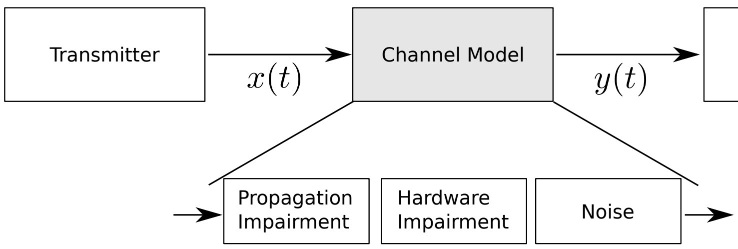

Fig. 1.4 Functional elements of a communications system.

The metric to evaluate the performance of the modem under the influence of the channel, is the bit error rate (BER). BER is defined as the number of bits found in error when compared to the transmitted bits. The BER is calculated for different signal (bit) to noise power ratio or in baseband bit energy to noise energy ratio E_b/N_0, typically the ratio varies from 0 to 20 dB. At least 100 bits are required to be transmitted* averaged over a repetition of 5 to 10 experiments for each E_b/N_0, to achieve a valid statistics. The result is plotted in the form shown in Figure 1.5. Figure 1.5 highlights the marked difference in performance of a BPSK modem under three different channel models of different characteristics namely; (i) additive white Gaussian noise (AWGN), (ii) multipath fading channel with a direct line of sight component using Rician statistics, (iii) multipath fading depicting non line of sight communications using Rayleigh statistics. Therefore, it is of utmost importance to characterise the channel adequately and appropriately, for inter-satellite links for the environment in which SBWSN is to operate.

BER is a metric to determine the performance of end-to-end communications system performance when compared for different transmission schemes under the influence of the same channel. BER can be determined at the design stage by simulating all the elements of communications system, which becomes complex. Alternatively, baseband modem can be modelled, and evaluated for the impact of impairments caused by hardware and channel, which then require their own respective models in the same simulation environment in which modem is modelled. Hardware in the loop simulation allows us to remove models for hardware based impairments, since actual hardware is used in conjunction with soft form baseband modem. Only channel is required to be modelled, and complete end to end system performance can be evaluated. Therefore selection of a computer based simulation environment is critical to such performance evaluation studies. Simulation of communications systems design and its issues are described in detail in [66, 67].

The Matrix Laboratory (MATLAB) [68] is a versatile simulation environment suitable for functional level studies, whereas the Advanced Design Systems (ADS) [69] is better equipped for circuit level design studies. The proof-of-concept at the functional level suffices for this thesis, therefore, MATLAB is the

*Actually at least 100,000 bits are used, since computer memory is cheap today, even for personal desktops.

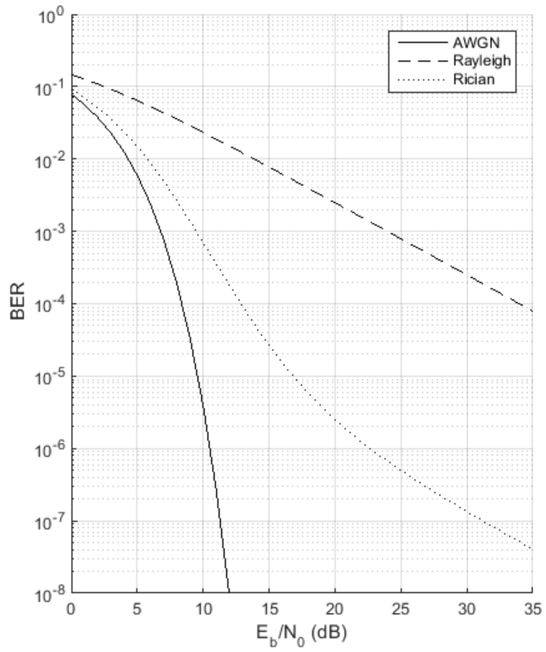

Fig. 1.5 Theoretical BER performance curves for AWGN, Rician and Rayleigh fading channels (using MATLAB BERTool for BPSK, diversity factor 1, assuming perfect synchronisation).

appropriate simulation tool. Matlab has built in functions for general channel models, digital modulation schemes and handy functions needed in testing algorithm integrity, modem performance, as well as translating the algorithm to a hardware specific code providing hardware-in-the-loop simulation for a selected DSP hardware. The functional blocks of a software defined radio (SDR) [70] to be implemented on a digital signal processor can be easily modelled for testing and development in MATLAB.

Assuming, the models for the modem and ISL channel, are already available (in some form) for testing / simulation studies, then the investigation can be carried out using the test setup configuration shown in Figure 1.6.

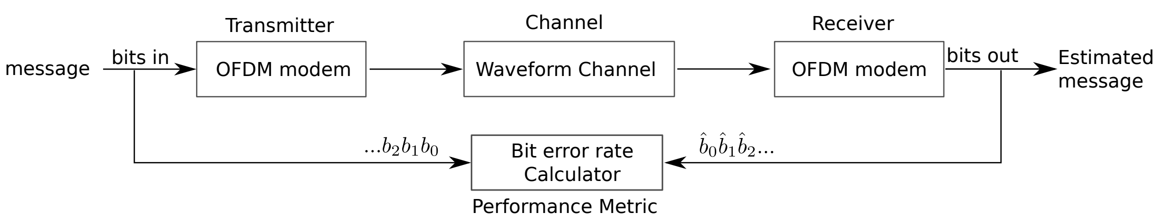

Fig. 1.6 Test setup for evaluating digital modem performance under the influence of channel.

However, it turns out, that performance evaluation of inter-satellite links is not easy. In any order, neither a channel model for ISL is available apart from the free space path loss model, nor the transmission scheme has been identified in literature for use with SBWSN.

The space environment not only has an impact on the design of electronics, mechanical structures and thermal, it has a significant impact on the propagating electromagnetic waves. The space environment varies significantly from near planetary regions, to inter-planetary space. It is not possible to study all regions, for their prospective impact on communications channel, therefore, scope of work has to be confined to one region only.

The placement of the satellite thus, plays a significant role in inter-satellite link evaluation studies. Where they are placed, determines the in-orbit environment, which can then be studied for communications channel characteristics. The placement also identifies the physical topology of the link. The physical topology governs the power requirements, the pointing of antenna, and the distance being covered to support the requisite data rates.

The selection of spacecraft platform, placement in space, and the overall communications system requirements is mission specific, therefore, a mission scenario is critical for conducting useful investigations. The interdependent nature of the factors is illustrated in the Figure 1.7.

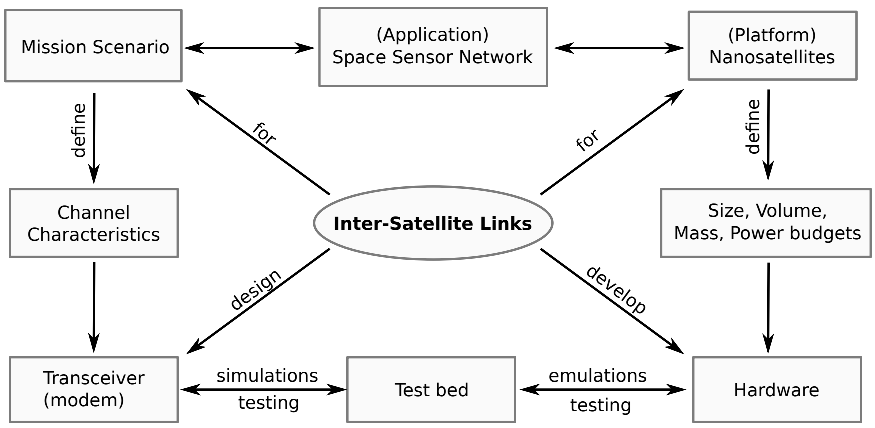

Fig. 1.7 The ISL dependency block diagram.

1.4 Research Objectives & Scope of Work

The research objective of this thesis is to evaluate the communications channel characteristics and use its model to determine the performance of digital modulation schemes, so that the performance of the inter-satellite link under a certain modulation scheme / transmission scheme be evaluated.

In order to limit the scope of work within the confines of this study, several assumptions are made whose impact on ISL investigations is listed as follows:

(i) SBWSN is assumed to be deployed in Earth bound circular polar orbits at altitudes less than 1000 km. The operational environment is therefore the environment found in LEO, which is investigated for inter-satellite communications channel characteristics.

(ii) SBWSN comprises small satellites of the pico or nano class, which are generally deployed in free flight mode. Therefore their relative motion is governed by their deployment mechanism.

(iii) The networking protocol in use is the modified IEEE 802.11. Therefore, the antenna radiation patterns need to be isotropic which is the requirement of the medium access controller used in IEEE 802.11. Since modified IEEE 802.11 is a strong candidate for the SBWSN, therefore, one of its modulation scheme should be evaluated for performance evaluation and design features.

(iv) The scope of research does not include design and development of antenna, analogue front end, and the implementation of modem on FPGA or DSP.

Based on the above assumptions, the main objective along with the sub-problems, addressed in this thesis can be listed as follows:

1. Determine the values of Doppler frequency shifts caused by the relative motion of the satellites. Limit the scope of work by identifying useful orbits, for which a SBWSN mission scenario be defined. The following cases be investigated for the relative motion of:
   a) a sensor satellite with respect to a sensor satellite (a case of motion of satellites in the same or different orbits, presumably in close proximity).
   b) a sensor satellite with respect to a relay satellite (a case when satellites are in different orbits).
   c) a relay satellite with respect to a relay satellite (a case of satellites in same orbits but at large distances).
2. Determine the source of fading i.e. multipath or otherwise, by studying the in-orbit environment where the SBWSN operates. The impact of the following factors on propagating EM waves should be investigated;
   a) ionised gas,
   b) space debris,
   c) meteors and their trails,
   d) other spacecrafts in close proximity.
3. Based on the outcome of the above two factors, determine a suitable mathematical model or algorithm to be used in computer based simulation studies, for the identified channel characteristics. Determine a channel model for the channel.
4. Evaluate the performance of OFDM modem (one of the transmission schemes used in IEEE 802.11) under the identified channel model, in a suitable computer simulation environment at the functional level rather than the circuit level. If required, model the modem in the computer simulation environment.

As it turned out, the OFDM modem and the communications channel both needed to be modelled in MATLAB.

1.5 Thesis Structure

The rest of the thesis is structured in the following chapters.

Chapter 2 is a survey of existing missions which employ inter-satellite links as their main mission objective, highlighting the fact that existing communications systems need to be improved to undertake networking requirements posed in the future applications. PROX-1 being the only space protocol in its preliminary stages, focused on addressing the issues arising in spacecraft proximity operations such as perceived in local area networks. Networking is not part of the protocol suite, it only defines a physical layer specifications of orbiting spacecraft and a planetary rover, tested for on Mars.

Chapter 3 is a case study the outcome of which is the development of an application mission scenario highlighting operational requirements for inter-satellite links as perceived in the context of space based wireless sensor network concept.

Chapter 4 investigates the relative motion of the member satellites of a SBWSN, to determine the Doppler frequency shift experienced between two communicating satellites. SBWSN comprises of smaller sensor nodes called sensor satellites, whereas, slightly larger satellites are used as data relay satellites. The motion of sensors with each other, and with respect to the relay satellite is marked important. Three cases are examined, namely (a) relative motion of free flying CubeSats in LEO, (b) a sensor satellite with respect to a relay satellite and (c) a relay satellite with respect to a relay satellite in the same orbit (string of pearl orbit configuration).

Chapter 5 investigates the propagation effects due to interaction of EM waves with in-orbit environment. The effects are separately studied for interaction with ionised gas, space debris, meteors, and the presence of member satellites in close proximity. A tapped delay line (TDL) structure is used to model the fading characteristics.

Chapter 6 evaluates the impact of the channel modelled in the previous chapter on the baseband design of orthogonal frequency division multiplex (OFDM) design. OFDM is one of the physical layer specified for data transmission over wireless links in IEEE 802.11 b protocol, being considered for use in SBWSN. The modem and channel both are modelled, in MATLAB, and the performance of modem evaluated.

Chapter 7 summarises the work presented in this thesis and concludes the findings. This work is in no means complete, rather a starting point for further investigations in the light of the current findings, which are suggested as future work.

1.6 Publications

Some of the results found in this thesis have been reported in the following publications:

1. T. Vladimirova, C. P. Bridges, J. R. Paul, S. A. Malik and M.N.Sweeting. "Space-Based Wireless Sensor Networks: Design Issues", Proceedings of 2010 IEEE Aerospace Conference, 6–13 March 2010, pp. 1–14, March 2010, Big Sky, MT, Digital Object Identifier: 10.1109/AERO.2010.5447031
2. S. A. Malik, T. Vladimirova and E.M. Warrington, "Upper Ionosphere Plasma FDTD Formulation for Inter-Satellite Link Analysis", Proceedings of 12th International Conference on Ionospheric Radio Systems and Techniques (IRST), paper 7.3, 15–17 May 2012, Royal York Hotel, York, UK, IET.
3. S. A. Malik and T. Vladimirova, "Space-based wireless sensor networks: Ionosphere Monitoring Mission", Poster Presentation, 2013, University of Leicester, UK.

CHAPTER 2

A LITERATURE SURVEY OF INTER-SATELLITE LINKS

Renewed interest in Inter-Satellite Links (ISL) is instigated by the need identified in current and emerging space missions requiring multiple spacecraft. In the broad sense such missions can be divided into different categories based on the application namely; Formation Flying, Tracking and Data relay, Rendezvous & Docking and Networks of Sensors. Although, in essence, ISL is a communications system, but, the underlying design of hardware and the use of a transmission scheme (modulation/demodulation) is unique to the application.

After a brief overview of the telecommunications systems employed in space missions in section 2.1, the class of existing missions which employ inter-satellite links are discussed in section 2.2. The emerging multi-spacecraft based missions classified as Distributed Satellite Systems (DSS) are discussed in section 2.3, which require ISL as one of the enabling technologies, for establishing autonomous networks in space. In section 2.4, work published in literature and carried out in research groups which directly contribute to the enabling technologies are described.

The chapter concludes after assessing the current contributions in section 2.4, and pointing out the requirement of systematic evaluation of physical inter-satellite links in section 2.6 for the emerging application of a network of several small satellites i.e. space based wireless sensor networks.

2.1 Introduction to Telecommunications in Space Systems

Telecommunications is an essential and integral part of space mission. Telecommunications systems in space communications has two operational entities, one in space called the space segment and the other on ground called ground segment. The space segment work in close conjunction with the command and data subsystem [71] of the spacecraft. The space segment of the telecommunications subsystem is of particular interest in this thesis, therefore, it is described in subsection 2.1.1, as it works closely with the on-board computer also called the command and data handling system.

The telecommunications system on ground plays a critical part in establishing the link between the spacecraft and ground stations. Therefore, the two segments work in conjunction, designed specifically to establish the links for the appropriate distances, data transfer rates, and the quality of the links, which is dictated by the mission. The telecommunications system link budget is a critical preliminary design factor, which acts as the requirements for the hardware design engineer. An extreme link budget example is given in subsection 2.1.2 to illustrate the requirement assessment for the distances involved in space communications.

In addition to the telecommunications system used by the communications satellites payload, is called the "transponder", which is also a telecommunications system, however, its purpose and design is different. It is discussed in subsection 2.1.3.

Owing to the digital communications design techniques, baseband modulation schemes being employed in current space telecommunications system, as well as being envisioned for future missions, is briefly described in subsection 2.1.4.

2.1.1 Command and Data System

It is referred to as "command and data system" (CDS), command and data handling system, or on-board computer and data handler (OBC&DH). On board is the term generally used to differentiate space segment technology from the technology implemented in ground segment.

The system handles three digital data streams, namely:

Science or payload data is the information the spacecraft was designed to acquire. Typically it requires high data rates.

Engineering or Health data is the information required to assess the operational status or health of spacecraft systems. This data is called telemetry, which is sent down to (downlink) ground at moderate rates.

Commands are the instructions from ground to spacecraft critical to the operations, which are generally executed at a specific time instance, asking attitude controller to fire thrusters or requesting particular status of a subsystem. Commands are critical, any error in the uploaded commands, can jeopardise the mission. Therefore they are transmitted with extreme care, at the lowest data rate. The command stream is thoroughly tested on ground before being uploaded to spacecraft.

The command and the communications systems are closely related, as illustrated in Figure 2.1. The CDS has extensive interfaces, one with the communications subsystem, and the other is with other subsystems and onboard sensors. The function of the computer is to provide computational needs of spacecraft, execute commands and process the data for downlink. That is why it is often called OBC&DH.

The International Consultative Committee for Space Data Systems (CCSDS), has played a significant role in standardising the CDS system for spacecraft. They publish their recommendations online [72] in the form of colour coded books i.e. Blue (Recommended standards) , Magenta (recommended practices), Green (Informational Reports), Orange (Experimental) and Yellow (Record). Silver colour is reserved for historical archives. With the aid of these recommendations, it is easier to assess the types of commands, telemetry and high volume data, their framing and control bit usage.

Since CDS is mainly concerned with handling commands and data, the data rates become important in the scenario. An uplink command for an interplanetary mission such as Mars Global Surveyor was 7.8 / 500 bps, and an engineering downlink rate of 250 / 2000 bps. However, for Earth orbiting satellites, the Earth Observer EO-1 can establish an uplink at 4000 bps, and the science data downlink at 105 Mbps.

It is recommended to use a error correction algorithm to be able to detect and correct errors in command words. CCSDS[72, 73] recommends the use of Reed-Solomon (255,233) for the downlink data as the outer code, with a convolutional code as the inner code. For the uplinks CCSDS recommends commands to be encoded using BCH (63,56) block codes. Error correction codes are a standard processing block in wireless communications, therefore are explained very well see for instance [74, 75, 60]. They serve to reduce the error rate, thus reducing the necessity of re-transmission of data, indirectly saving bandwidth and time. For instance, consider transmitting the same data three times to determine the location of error, that too with little certainty. For small command words it is feasible, but with engineering or science payload data is inefficient.

The operational status of spacecraft systems is sent as engineering data (health), based on which ground station sends commands to spacecraft. The telemetry data is the information sent from spacecraft to

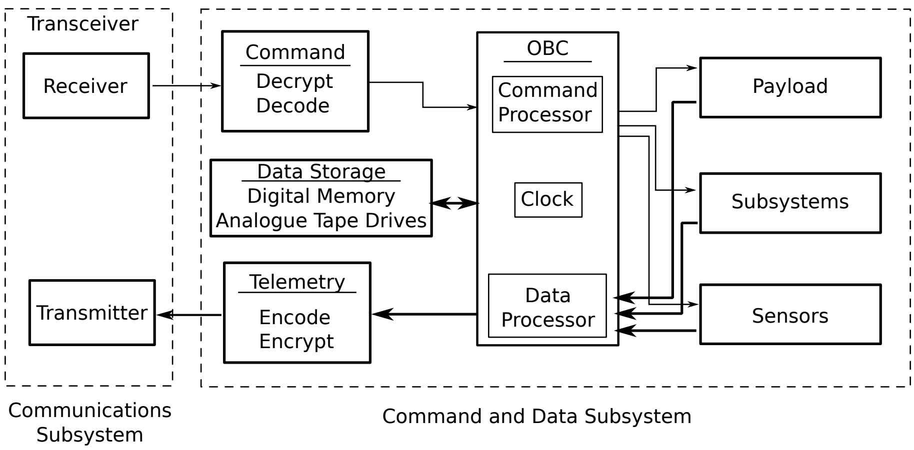

Fig. 2.1 Spacecraft command and data system closely integrated with communications subsystem [71].

earth, comprising of science data, engineering data and imaging data. The science data are moderate in volume, with stringent quality and transmission accuracy. Engineering data report the status of spacecraft instruments and systems (health of spacecraft). These data are low in volume and need to be of only moderate quality. Imaging data are of high volume. Due to redundancy in image data, they need to be of only moderate quality [71].

2.1.2 Telemetry link Example

The link budget is an important preliminary design factor for telecommunications system evaluation. With the aid of an example of deep space communications with the deep space probe Voyager, active parameters are described.

The interplanetary space is essentially filled with ionised gas called plasma [76]. It is essentially same as free space as far as propagation of microwave signals is concerned. In the absence of weather effects the Earth's atmosphere is almost completely transparent at 2.3 GHz (S-band) and 8.4 GHz (X-band), which are the frequencies used in deep space telecommunications [77]. Therefore the calculation of received signal strength is a geometrical problem.

Let the transmitted power by P_t at distance r from the receiver on Earth. If the power were radiated isotropically, the power flux density at the receiver ρ, would be the transmitted power divided by the area of a sphere of radius r. The actual flux density is increased by a factor equal to the gain of the transmitting antenna G_t. Thus

$$\rho = \frac{P_t G_t}{4\pi r^2} \tag{2.1}$$

where $4\pi r^2$ is the area of a sphere of radius r. The received signal level P_r is obtained by multiplying the flux density at the receiver by the area of receiving antenna A_r times the antenna efficiency μ i.e.

$$P_r = \rho \mu A_r \tag{2.2}$$

This shows that the received power can be increased by three actions namely;

- First by increasing the transmit power. This has system repercussions. A spacecraft transmit power of 20 watts means with 40 % efficiency, it requires 50 watts of power generated.
- Secondly, the transmitting gain of antenna can be increased, to focus the radiation more intensely on the receiver. Better focusing requires a larger spacecraft antenna constrained by size and weight, and the ability to aim (pointing) the resulting narrow beam.
- Thirdly, the receiving antenna area can be increased to collect as much of the incoming signal power as possible.

The link budget is illustrated with the example of Voyager a deep space probe, illustrating the functional requirements of satellite to ground links, particularly the minute details covered to establish communications link.

The Voyager spacecraft transmitting $P_t = 21.3$ W at 8.4 GHz, with the $G_t = 6.5 \times 10^4$ (unit less), and the distance from Jupiter to Earth being 6.8×10^{11} m. Thus the power flux density at the receiver is

$$\rho = 2.383 \times 10^{-19} \quad \mathrm{W/m^2} \tag{2.3}$$

With an antenna that has a 64-m diameter dish with $A_r = 3.2 \times 10^3 \quad \mathrm{m}^2$ which has an efficiency of 42%, the received signal power is

$$P_r = 3.05 \times 10^{-16} \quad \mathrm{W} \tag{2.4}$$

The reception process introduces most of the noise that corrupts the receiving signal. Every object radiate energy at radio frequencies. The deep space network (DSN) of NASA employs cryogenically cooled maser amplifiers so that the total system noise power corrupting the received signal is very low [77]. In typical operation condition at 8.4 GHz, the DSN station receiving system equivalent noise temperature is 28.5 K. The noise spectral density is

$$N_0 = kT \tag{2.5}$$

where k is Boltzmann's constant = 1.38×10^{-20} mW/K Hz, and T is the system equivalent noise temperature = 28.5 K. Thus,

$$N_0 = 3.933 \times 10^{-22} \quad \mathrm{W/Hz} \tag{2.6}$$

There are other losses in the entire link other than that due to distance such as circuit losses and antenna pointing losses etc. For the Voyager telemetry link, the total loss is $L = 0.7$ (unitless). When the loss is 0.7 then the factor representing the retained, useful power is 0.3 (i.e. 1-0.7).

Therefore the received signal-to-noise-power-spectral-density ratio is;

$$\frac{P_r L}{N_0} = 5.428 \times 10^5 \mathrm{Hz} \tag{2.7}$$

How efficiently this signal-to-noise-power-spectral-density ratio is being used determines the ultimate telemetry capability. **And it is the choice of modulation and coding that determines the efficiency**

with which the signal to noise ratio is used. For Voyager, imaging data, the acceptable telemetry data quality has a bit error probability of 5×10^{-3}. Voyager uses PCM/PSK/PM modulation and convolutional code with Viterbi decoding, which requires a received signal-to-noise-power-spectral-density ratio of 2.05×10^5 Hz, for a data rate of 115.2 kbps. The above calculation illustrates the small margin to cover uncertainties.

2.1.3 Transponders

A term commonly used in satellite communications engineering literature is “Transponders”, which is a special type of communications system [78]. It should not be confused by the telecommunications systems for CDS. According to Gardner [79, p.161], a transponder receives a signal, processes it in some manner and re-transmits the signal at increased power.

A transponder is said to be coherent if its transmitted frequency f_t is a rational multiple of its received frequency f_r; i.e. $f_t = (m/n)f_r$ where m and n must be integers. With this definition of coherence, there are exactly m cycles out for every n cycles that enter the transponder. The frequency received at the ground can be multiplied by m/n and the result can be compared against the frequency originally transmitted from ground; their difference is the two way Doppler shift.

Early coherent transponders often used $n = 1$ thus the output frequency was a harmonic (usually the second) of the input. A transponder of this type need not be phase-locked to be coherent. Our interest here is in an offset transponder in which neither m nor n is unity. Coherence in offset transponders is almost always obtained by means of phase-lock techniques. A block diagram of a typical phase-locked transponder is shown in Figure 2.2.

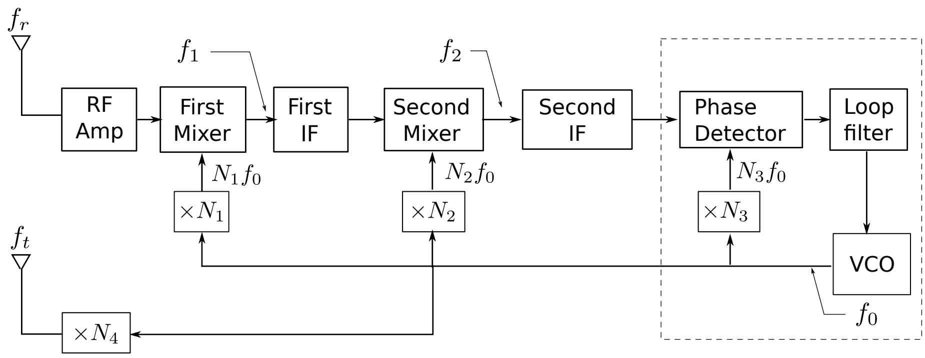

Fig. 2.2 Phase-lock transponder [79, p.162].

Double superheterodyne conversion is illustrated in the receiver portion, but single or triple conversion operate on the same principle. All mixer and phase-detector injection voltages are obtained as harmonics of a single local oscillator. Operation of the first mixer can be described as

$$f_r = N_1 f_0 \pm f_1 \tag{2.8}$$

whereas the operation of the second mixer is given as,

$$f_1 = N_2 f_0 \pm f_2 \tag{2.9}$$

and the phase-lock requirement is

$$f_2 = N_3 f_0 \tag{2.10}$$

where nomenclature is defined in Figure 2.2, and the choice of plus or minus signs depends on whether low-side or high-side injection, respectively is used. A combination of these three equations and elimination of the two intermediate frequencies results in

$$f_r = f_0(N_1 \pm N_2 \pm N_3) \tag{2.11}$$

Because the transmitted frequency is $f_t = N_4 f_0$, the ratio of output frequency to input frequency is

$$\frac{f_t}{f_r} = \frac{N_4}{N_1 \pm N_2 \pm N_3} \tag{2.12}$$

which is a rational number, therefore the transponder is coherent if it is locked.

In modern transponders, after the first IF, demodulation and modulation is also carried out, thus getting the name of re-generators. The advantage is obvious in the link budget design, because the noise does not carry forward.

2.1.4 Bandwidth Efficient Digital Modulation

The digital modulation schemes used for bandwidth efficient satellite to ground links are also applicable to the inter-satellite links. Therefore, they are included in the related works.

Traditionally space agencies employ sub-carriers as a simple means to separate different data types, ensuring separation of radio frequency (RF) carrier and the baseband spectra. Using sub-carriers means large bandwidth, because generally overlap is not allowed. One effort carried out was to replace more traditional square-wave sub-carriers with sine-waves, but was not acceptable [80]. Current digital modulation schemes allow the possible use of many types of waveforms.

In space communications transmit power is a critical resource, which is utilised efficiently by utilising the power amplifier in saturation mode. This practice requires that the signal (waveform) should have a constant envelope, otherwise clipping is introduced due to over amplification. This constraint means the modulation schemes that can be employed are those which have a constant envelope of the modulated carrier. Relaxing the condition of constant envelope potentially eases the restrictions on power and bandwidth efficiency to the extreme limit of Nyquist-type signalling, which in theory is band-limited and capable of achieving maximum power efficiency.

A three phase study conducted by the CCSDS in response to an action item from the SFCG identified ten modulation schemes commonly used or planned by space agencies for bandwidth-efficient applications. The 10 modulations so identified were: PCM/PM/NRZ, PCM/PM/Biphase, QPSK, MSK, 8-PSK, BPSK/NRZ, BPSK/Biphase, OQPSK, GMSK, and FQPSK-B. The objective of the study was to compare these modulation methods, using a combination of simulation and analysis in terms of E_b/N_0 required to maintain the data bit error probability at a given constant level.

The study based on simulations included the non-linear system parameters including European Space Agency's (ESA) Solid State Power Amplifier (SSPA) model in full saturation mode. The conclusions drawn from the study are; FQPSK-B delivers the narrowest bandwidth (highest throughput) with reasonable end-to-end loss compared with BPSK/NRZ while GMSK comes in a close second in terms of bandwidth efficiency. At the other extreme turbo-coded rate 1/3 BPSK/NRZ is the clear choice for achieving power efficiency at the expense of bandwidth that meets the requirements for deep-space applications. Trellis-coded 8-PSK with or without filtering is also an excellent choice for bandwidth efficient operations. Finally combining the CCSDS-recommended error-correction coding with PCM/PM/NRZ and with BPSK/NRZ are reasonable choices when both power and bandwidth are considerations. The results are summarised in Figure 2.3a and Figure 2.3b.

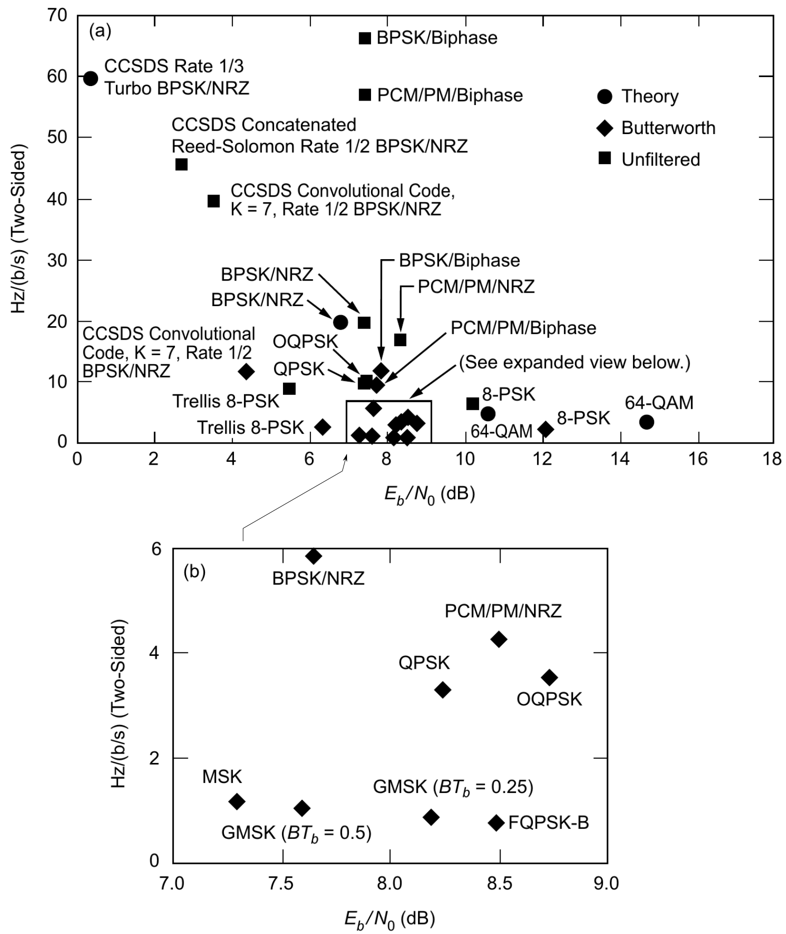

(a) Bit error probability of 10^{-3} .

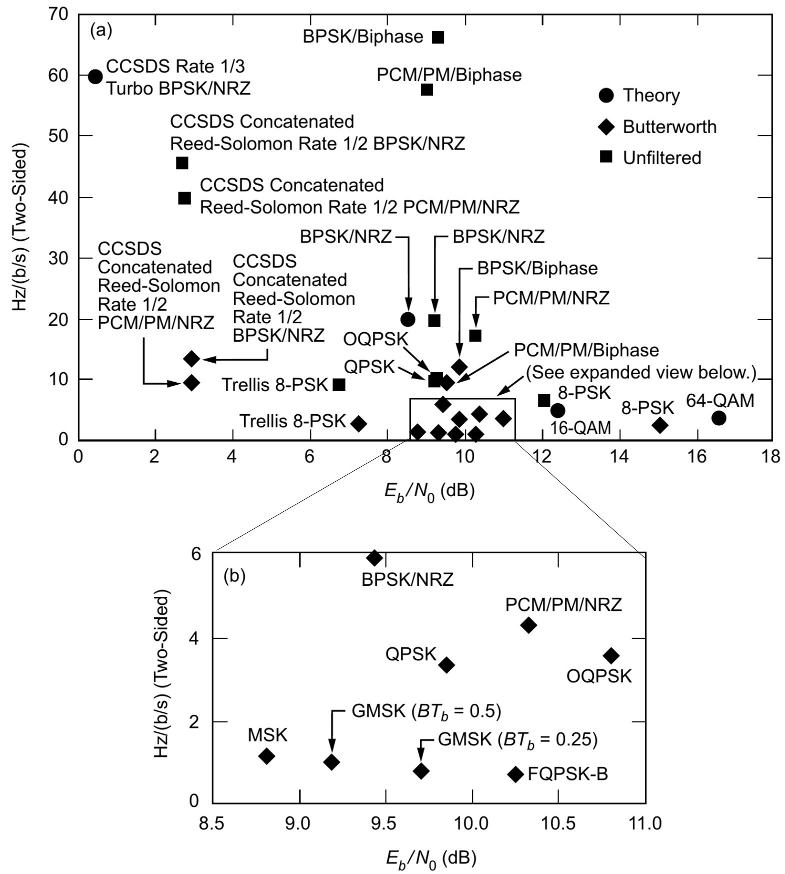

(b) Bit error probability of 10^{-4}.

Fig. 2.3 The power-bandwidth trade-off for respective bit error probabilities [80].

2.2 Existing Missions Employing Inter-Satellite Links

Although hundreds of space missions have successfully flown since 1957, only a handful of missions employ inter-satellite links*. It can be observed from Table 2.1, that ISL experiments were conducted as early as 1970's. The communications link established between two amateur satellites as an experiment when they were in range, and the link lost when out of range. The first dedicated mission to experiment ISL is the LES 8 and LES 9 in the Lincoln laboratories experimental satellite series. Early links were demonstrated for microwave links. With the anticipated increase in data flow between communications satellite deployed in GEO, later development work shifted from microwave based to optical based ISL.

It can be observed from Table 2.1 that a wide range of frequencies are in use. Prior to mid 90's, all links were between geostationary satellite to lower orbits i.e. low Earth orbits or medium Earth orbits. The links were intermittent, established only on visible line of sight.

In late 90s, deployment of IRIDIUM constellation, each satellite was equipped with 4 ISL, designed for continuous links. After the turn of the century, it is observed, that ISL is used by science missions requiring tight relative motion control. ISL not only measures inter-satellite distances in such missions, it also provides relative position data to each member of the mission to employ relative motion control mechanism. Such missions are called formation flying missions.

Although Global positioning system (GPS) employs several spacecraft to provide precise navigation and guidance signals from MEO, however, inter-satellite links in their constellation is only planned for the next generation GLONASS and Galileo, replacing the old system.

The type of links, and the spacecraft using ISL, both are important parameters. A survey of inter-satellite link technology for selected mission types, from large GEO based satellites to recent nano-class satellites, is given in Annex A.

The salient features of existing mission with inter-satellite links is summarised in Table 2.2.

The analogue front end of communications systems design depends on the operational frequency used by the radiating carrier waves. The wavelength in optical range dictate a different set of underlying technologies from that used in microwaves or millimeter waves. Most of the literature after 1970s had its focus on optical based long distance inter-satellite links [51, 82, 50]. That is one of the reason why most of the literature considers ISL as free space path loss only, since plasma is transparent to optical wavelengths. A hybrid system using RF and Laser together has been suggested [48]. The reason to opt for laser over microwave links is their high bandwidth support, which means high data rate, almost no interference, high security and timely transfer of large amounts of data. It was perceived correctly, that large amounts of data between GEO satellites would be carried out by ISL, however, few examples are seen practically, that too are microwave links.

*Inter-Satellite links (ISL) also known as Cross-Links (X-Links) in American literature and inter-orbital links by ESA.

Table 2.1 Space missions using inter-satellite links (ISL) (modified from [81]).

Year	Mission	ISL Frequency	Link Configuration (From-To)
1972-78	OSCAR 6,7,8	146 MHz	LEO–LEO
1976	LES-8&9	36,38 GHz	GEO–GEO
1983-	TDRSS	C, Ku, Ka	GEO–GEO/LEO/MEO
1985-	Luch (Altair)	UHF, Ka	GEO–LEO (MIR Space Station)
1994	ETS-6	2, 23, 32 GHz, Optical	GEO–LEO/MEO
1997-	Navstar Block IIR	UHF	
1997-	IRIDIUM	23 GHz	LEO–LEO
1998	Comets (ETS-7)	2 GHz	LEO–GEO (TDRSS)
1994-2003	Milstar I/II	60 GHz	GEO–GEO/LEO/MEO
1998	Spot-4	Optical	LEO–GEO
2001	Artemis	S, Ka, Optical	GEO–LEO/MEO/Aircraft
2002	Adeos-II	2, 26 GHz	LEO–GEO (Artemis)
2005	OICETS	Optical	LEO–GEO
2010	AEHF (MilStar Followup)	60 GHz	GEO–GEO, GEO–LEO
Planned	IRIDIUM Next	23 GHz	LEO–LEO
Planned	Galileo & GLONASS		MEO–MEO

Laser is not widely adopted as the main communications link [50] for satellite to satellite links, owing to the complexity and technology readiness level. The lack of interest is due to observed malfunction either as a result of leakages in gas, or mechanical failure [46, 47, 83, 48] The heavy mechanical pointing mechanism needed for precise pointing of laser, is another discouraging factor [84]. The disadvantages are being overcome by current technology, therefore in the near future optical links would be a norm, as is evident from its selection in the Micro-Satellite Swarms mission [85].

2.2.1 Inter-Satellite links in Formation Flying Missions

Another group of satellites not covered in Table 2.1 is known as Formation Flying (FF) space missions, where inter-satellite communications links are being investigated for both communications as well as relative motion assessment.

The Formation Flying (FF) missions and Rendezvous missions, rely on inter-satellite links to provide precise range (inter-satellite distance) and range rate measurement between the two spacecraft. The range measurements enable the on-board processors to compute the necessary thrust vectors required to adjust spacecraft velocities [86], so that the two spacecraft formation is maintained within acceptable margins. The precision of range estimation, and the accuracy of formation control are the key attributes of such missions, which are anticipated features of some SBWSN as well.

Table 2.2 Salient features of communications systems used in inter-satellite experiments on-board LES-8&-9, ATS-6, ETS-VI.

	LES-8 , LES-9			ATS-6	ETS-VI			
	Downlink	**G/L**	**ISL Exp.**	**TDRS Exp.**	**ISL**	**ISL**	**ISL/GL**	**ISL/GL**
Transmitter:								
Freq.	200–400 MHz (UHF Band)	36/38 GHz	36/38 GHz	2063 MHz (S-band)	2108.4 MHz (S Band)	23.3875 GHz (K band)	38 GHz	GaAlAs Laser diodes
Power Out	32 W / 8 W	0.5	0.5	20 W	0.9 W SSPA	3W SSPA		14 mW
EIRP	25/18 dBW	21 dBW	39 dBW	48.0 dBW	34.2 dBW	36.2 dBW		
Antenna:								
Type	3 Crossed Dipoles on ground plane	Horn	Parabola Dish	30 ft Parabola, Switched Feeds	5.8ft Hexagon Phased Array 19 Elements	80 cm Parabola Dish	40 cm Parabola Dish	7.5 cm Telescope
Beam Width	35 deg	10	1.15	13.2 deg		0.2 deg		1.7 or 3.4 (mdeg)
Gain	8 dB	24 dB	42.6 dB	36.4 dB		34.7/36.3 (Tx/Rx)	37/41 (Tx/Rx)	
Polarization						Circ	Circ	
Antenna Steering Platform:		Fixed	Mech.		Elec.	Mech.	Mech.	Mech.
Azimuth			$\pm$ 104 deg		$\pm$ 10 dg			
Elevation			$\pm$ 10 deg					
Pointing					$\geqslant$ 1.1 deg	$\pm$ 9.8 deg	$\pm$ 9.8 deg	Coarse 32, Fine 2 (mrad)
Receiver:								
Freq.	240–400 MHz	36/38 GHz	36/38 GHz	2253 MHz	2287.5 MHz	25.85 GHz	43.0 GHz	0.51 micron Avalanche PhotoDiode
Sys. Noise	1000 K	1400 K			1.5 dB NF	5dB NF	5.2 dB NF	
G/T	-20 dB/K	$\geq$ -8 dB/K	$\geqslant$ 10dB/K	7.0 dB/K	-4 dB/K	6.4 dB/K		
Bit Rate		10 or 100 kbps			1.5 Mbps, 300 kbps	10 Mbps	10 Mbps	1 Mbps
Modulation		DPSK, 8 Tone FSK			PSK/CDMA			

2.2.1.1 Current FF Mission Capabilities

The capabilities of selected missions is stated in Table 2.3. It can be noted that currently formation flying mission comprise of two members, whereas, future missions anticipate more members, more autonomous on-board computing capabilities.

Since FF based missions are being pursued actively, therefore literature abounds in their problems-solution discussions; testing of such links, placement in optimal orbits of such satellites to reduce the fuel consumption, minimizing navigation and guidance estimate errors, and real time algorithms to run on spacecraft computers, are some of the general topics under discussion [86, 87, 90, 91, 92, 93, 94, 95]. Our interest is in the inter-satellite links for multiple spacecraft, whereas, for formation flying missions, currently only point to point links are being evaluated. Since precise measurements are required to maintain the relative distances using inter-satellite links, therefore carefully designed equipment is used see the ISL module used in GRACE [96] and PRISMA [87].

2.2.1.2 Testbeds

The performance of the link under scintillation effects, which also affects the precision of the range measurements via ISL, is also a concern for precise measurements. In the space industry, a hybrid method of testing systems is utilised, which is described since testing is a critical aspect of communications systems designed for space. A typical procedure followed is that the hardware is physically developed and then tested under a simulated channel environment. testbeds developed exclusively for inter-satellite

Table 2.3 Formation Flying mission capabilities in terms of proximity maneuver allowable windows (taken from [87]).

Mission	Date	Altitude [km]	Along Track Separation [km]	Comments
GRACE	2002	450	220 ±50	Ground based relative orbit control, precise K band ISL.
E0-1/LandSat	2001	700	450 ±85	Ground based control, ISL.
CloudSat/Calipso	2006			"A-Train" of satellites.
DART/Mublcom	2005			Autonomous rendezvous attempt failed, collision occurred due to false estimation of ISL range [88].
XSS-11	2005			Demonstrated Rendezvous operations with a Launch Vehicle upper stage [89].
PRISMA	2010	700	0.1 to 2.0 ± 0.025	Autonomous precise FF, maintained over week long time intervals. ISL using UHF @ 19.2 kbps [87]
CANX-4&5	2015	LEO	< 5 km	In-orbit demonstration of autonomous FF. ISL using S-band @ 10 kbps

link testing, which were published in literature are mentioned, here, which also serve as a reference for future development in this area of research.

Jet Propulsion Laboratory (JPL) uses a Formation Flying Test Bench (FFTB) [97], whose functional block diagram is shown in Figure 2.4. The testbed allows performance evaluation of autonomous formation flying algorithms [86, 98, 93] developed for guidance, navigation and control. The information gathered by differential GPS technique to measure inter-satellite locations [99, 100], is compared with the measurements using ISL, under the effects of relative motion and charged particles (see section 5.3 for details). The measurement is carried out by the on board ISL hardware, and compared with the known ISL distance measured by GPS.

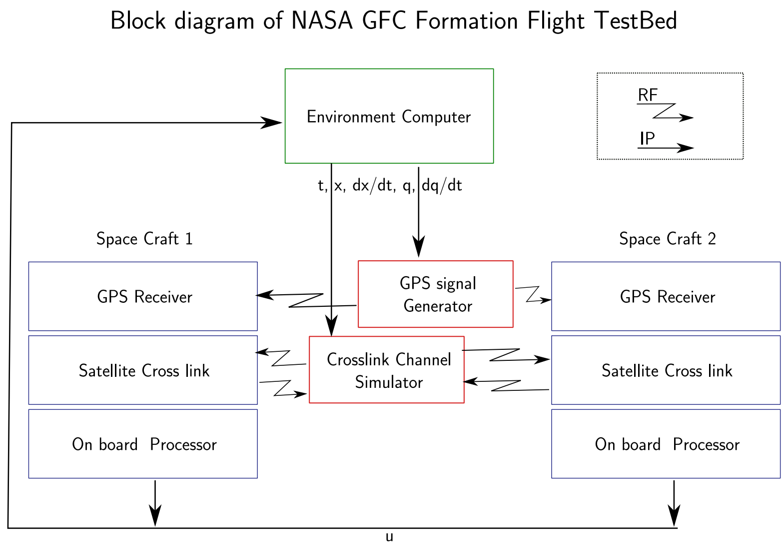

Fig. 2.4 Formation Flying Testbed block diagram used by Jet Propulsion Laboratories (JPL) (courtesy of [91]).

The electrical hardware is based on Field Programmable Gate Array (FPGA) technology. The block diagram of the JPL formation flying testbed is redrawn in Figure 2.5. This hardware was originally built for STARLIGHT project back in 2001. A similar testing mechanism is used by newer missions such as PRISMA [87]. The relative distance measurements are evaluated based on availability, acquisition of signal, and accuracy, emulating the GPS receiver on-board a fast moving satellite.

The key features of JPL FFTB are as follows:

1. testbed can support testing of simultaneous four links.
2. testbed can allow testing of 2 FF satellites using GPS receivers, since there are only two GPS receivers and one GPS signal generator.
3. Cables are used with high attenuation to interface the RF communications links. This provides better control on emulating link attenuation.

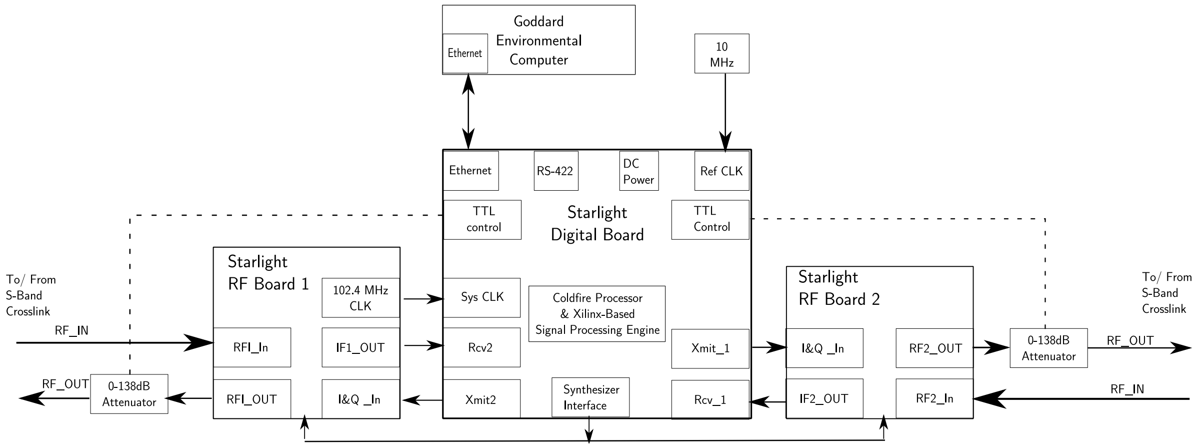

Fig. 2.5 Starlight mission ISL hardware testbed (courtesy of [101]).

4. Communications hardware is based on Field Programmable Gate Array (FPGA), with configurable band pass filters, that can support frequency up to 2GHz. For higher frequencies, external up converters are required.
5. The platform supports digital communications waveforms, since digital baseband modem is implemented.

The future trend in inter-satellite communications link for formation flying is summarised in Figure 2.6. The current state of the art is point to point for two satellites, whereas, future formation flying missions require autonomous operations; where ad hoc networks are formed without ground intervention, exchanging messages to achieve goals for which tasks would be determined by powerful on-board processors. These goals are in line with the distributed satellite systems as well as envisioned in space based wireless sensor networks, which place a significant demand on the design of inter-satellite communications systems, to support not only reliable data transfers, but allow autonomous networks to be formed, and assist in data routing particularly for the ad hoc networks, where a node can join or leave without a central controller keeping track of its presence within the range of network.

From the literature survey, it is evident that currently, point to point links are being employed, where microwave is the preferred technology over optical links.

2.3 Emerging Demands of Inter-Satellite Links

As opposed to the existing utility of ISL, emerging mission scenarios require more than two spacecraft to collaborate, such missions are categorized as distributed space systems (DSS). At the turn of the century, the two major space agencies, NASA in their Earth-Sun-Enterprise and ESA in their Cosmic Vision, identified the need for pro-active environment prediction, for their 2010-2025 time frame [102]. In the identified requirements, collaborative DSS based missions have been identified to play a significant role,

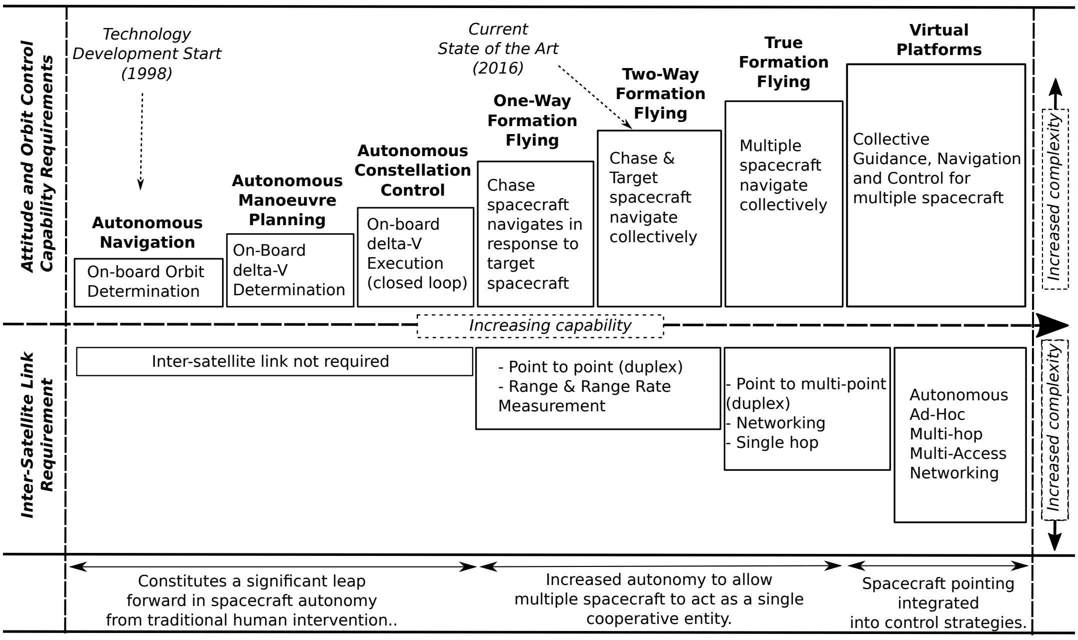

Fig. 2.6 Space Formation Flying technology staircase, indicating requirement on inter-satellite links.

for which inter-satellite link is a key enabling technology to support networking. ISL in such missions must be characterized. In this section, published literature which has already identified system level requirements are described, so as to identify the current state of the art in ISL.

Kwadrat [103] defines the Distributed Space Systems (DSS) as those “missions which consist of multiple space platforms that act in consort gathering data to achieve a single science objective. ” The members of DSS gather science data from various spatial and temporal perspectives for reduction into a single format that is more informative than that provided by any of the individual platforms within the distribution. Examples of this are spacecraft with radiation sensors that form the synthetic apertures that are the basis of optical and radio-based interferometers, and the multi-perspective images that provide time-sequenced images of certain natural phenomena. Two distinct categories of DSS missions are described. (a) Ground based data reduction requires that all of the science data be transferred to the ground via an independent space-ground link capability that is associated with each member of the distribution. (b) Space based data reduction requires that one or more spacecraft collect and process the data from the other members of the distribution. This alternative requires inter-satellite links to transfer science data amongst the members. In such circumstances, the data might be processed entirely, partially, or just repackaged prior to being transferred to the mission ground segment. He emphasizes that the the choice of data transfer alternatives i.e. the use of inter-satellite links depends on the mission design / objectives.

Current space mission architectures are based on monolithic spacecraft, with little or no provision for sharing information or rapid allocation of resources in response to events, rather, data is fused and processed after receiving it on Earth. Science missions fall in two categories, **long term monitoring**, or

exploratory missions. Long term monitoring missions are characterized by large, multiple instrument platforms and complex labor intensive ground operations. Exploratory missions provide for one time scientific discovery campaigns, which are generally more focused and bear lower costs, which may lead to a follow on longer term monitoring mission. Extensive planning activity is associated with getting a mission response to a specific event or positioning at a location.

Distributed Spacecraft Technology Requirement Analysis (DSTRA) [102] identifies five broad themes for investigating enabling technologies;

1. Systems and architecture development tools
2. Miniaturization production manufacture test and calibration
3. Data networks and information management
4. orbit control planning and operations
5. Launch and deployment

The key five research areas or possible investment are described in Table 2.4.

2.3.1 Notional Architectures

One can divide the emerging DSS missions on the basis of orbit configurations, as notional architectures [103]:

- Global constellations
- Virtual platforms
- Sensorwebs
- Precise formation flying

Global Constellations : The NEW Millennium Program Space Technology 5 (ST-5) is planning to validate technologies including satellite cross links, relative navigation and ground systems constellation operations. Future constellations of 100s of spacecraft are envisioned for which small spacecraft production techniques are also being investigated. Example constellation missions include:

- **Global Precipitation (E0S-9)** — The proposed measurement approach considers nine satellites , a large active radar satellite, flying in a constellation with eight passive radar receivers.
- **Atmospheric chemistry/ozone** (WX-2, OP-3, and follow-on missions) — Constellations provide the ability to conduct multi-point occultation and GPS soundings.
- Under the **Sun-Earth Connection science theme**, in*situ* magnetosphere and radiation measurement missions such as Magnetospheric Constellation employs as many as 100 spacecraft to conduct simultaneous multi-point observations.

Table 2.4 Key areas for Distributed Spacecraft Technology investment [102].

Technology Area	Drivers	Recommended Technology Investment
1. Systems and Architecture development tools	• Formulation and development of systems of systems • Legacy systems integration • Interoperability • Design for mass production	• Concurrent engineering tools to asses interoperability of heterogeneous systems of systems. • Engineering for manufacture, production and integration and test.
2. Miniaturisation, Production, Test and Calibration	• Mass production of spacecraft and instruments • Mass and volume reduction • Instrument calibration. • Cross-platform calibration.	• Instrument miniaturisation and mass production. • Cross-platform calibration procedures and benchmarks • Integration and testing using production-line procedures and the Internet
3. Data networks and information management	• High volume of data with constrained processing growth • Data fusion • Interoperability standards	• Model-based data compression • Symmetric uplinks (receivers, C&DH) • space to space communications protocols and standards • Interoperability standards
4. Orbit Control, Planning and Operations	• Standards for interoperability of heterogeneous systems • Scalable and miniature precision impulse bit propulsion • Cross platform control	• Closed-loop cross-platform control • Autonomous on board planning • Precision impulse bit miniature micro-newton thrusters • Interoperability standards, cross platform goal driven commanding.
5. Launch and Deployment	• Reduce launch costs • increase launch frequency • Maintain and refresh orbiting assets	• Advances in this area to be driven by the commercial sector • Continued development of RLV and new propulsion technologies.

1. **Notional Architecture** for global constellations similar to that of IRIDIUM:
   a) All spacecraft are identical replicas, carrying a single moderate resolution instrument.
   b) Instrument is nadir pointing, 10% coverage overlap at the equator,
   c) 705 km polar orbit typical of Earth Observation missions
   d) Walker delta pattern , 16 planes of 24 satellites each are required, total 384 satellites.

Virtual platforms are defined as a system employing two or more spacecraft flying in formation and registered as if the observations were made and coordinated as a single spacecraft. All elements must be within direct line of sight of each other at all times. These missions exploit coordinated position to enable or add value to the measurement concept. This architecture enables the creation of large synthetic apertures and permits simultaneous stereo or multi-angular views of the same ground track.

Example Virtual Platforms used for missions include:

1. A simple case discussed would be that of **EO-1** which consists of two spacecraft viewing the same ground track.
2. US Air forces proposed **TechSat 21 mission**. This mission would fly several small spacecraft in a formation, and demonstrate a distributed array radar application — a technology demonstration mission.

Notional architectures for a virtual platform in the US Air force TechSat 21 orbital configuration is a good starting point. One larger master platform and four co-orbiting smaller platforms. The spacecraft are in three orbital planes, with the larger spacecraft occupying the central plane, and two of the smaller platforms are phased at each of the other two planes so that it appears as if they are orbiting the larger platform as the entire spacecraft mission orbits the Earth.

Precision Formation Flying exploits coordinated precise, relative position knowledge and control to add value to a measurement concept. This category require multiple platforms to fly in a very accurate formation where relative range knowledge and control becomes the major driver. Position knowledge and control requirements often exceeds the accuracy of GPS navigation by several orders of magnitude. Examples include time varying gravity field measurements and interferometric, very high-resolution imagery.

Sensorwebs have been proposed as the key architectural ingredient enabling the Earth Science Vision. For this study, they are defined as an architecture that utilises multiple vantage points and a mixture of sensor types to achieve synergistic observations of the Earth. Such an architecture exploits information technology (processing power, modelling, and algorithms) to add value to a measurement concept. Data fusion and real-time measurement coordination and communication across platform and systems create a leveraged system of systems.

The sensorwebs envisions coordinating and obtaining measurements from various vantage points including LEO, GEO, and L1. New orbit types such as "pole sitters" are also envisioned. Enabled by new propulsion technologies like solar sail or plasma thrusters, these non-Keplerian orbits would provide continuous view of Earths polar region. Data will also be provided from instruments carried on other platforms such as International Space Station.

Another set of notional architectures on the basis of multi-point sensing is defined by Clare. Clare [9] points out that multi-point sensing missions can fall into one of the following categories;

1. **Pixellation / Voxellation**; "in which each sensor data can be perceived as a local 'pixel', and collectively the complete 'picture' can be visualised. The advantage is significant, over a single platform based sensor". Example missions are, Magneto-spheric Constellation (MC) [104], Cluster [105], ACE+ [106] and SWARM [107]. Plasma Bubble study using PCBSat [29], the synthetic

aperture radar (SAR) based on satellites such as TerraSAR [108] and PRISMA [87], falls in the same category..

2. **Beam formation**; "where emitting EM waves from a remote object are observed by several sensors, placed at strategic positions, each having the capability to direct the received waves towards a central point where all signals are combined to achieve higher signal to noise (SNR) ratio;" Example missions are Terrestrial Planet Finder (TPF) [109], Laser interferometer space antenna (LISA) [110] and multiple input multiple output synthetic aperture radar (MIMO-SAR) techniques being sought for TANDEM-L [111].
3. **Tomography / Rendering**; "where a remote object is viewed from several perspectives corresponding to projections, and these are combined to form a higher dimensional representation" as proposed in the STEREO mission [112]. Satellites can also pick reflected GPS signals from Earth to study ocean tide waves [113].

2.3.2 Functional Considerations

Functional requirements of ISL can be grouped as follows, based on the assumption that networks of several spacecraft are formed;

1. antenna control,
2. physical layer,
3. data link layer and
4. network layer functions.

Antenna control fulfils the requirements associated with selection, control, and scheduling of the on-board antennas. Those functions associated with the modulation of data, the transmission of RF signals, the receipt of RF signals, and the demodulation of data represent requirements that are traditionally associated with transceivers and the physical layer of a data network communications system*. The data link function requirements manage the flow and ensure reliable data block exchanges over the links. The network function requirements cover the routing of datagrams to and from the payload equipment via ISL to members of the network.

The physical topology of the network can be assessed from the orbital deployment as a constellation, a formation flying or a free flying mission. In the case of constellation and formation flying the relative distances are well known and positions are well coordinated, whereas, it is not the case in free flying missions. The topology is envisioned to consist of larger spacecraft to interact with smaller members of the constellation or formation or cluster, similar to a "mother-daughter" relationship. The mother spacecraft supporting daughter spacecraft. Similarly, the "motherships" could in turn become the "daughters" of one "great grandmother" to form a hierarchical multilevel structure of nested "Centralised

*Refer to the OSI 7 layer model differentiating the functions of each layer.

Distributions". On the other hand, hybrid topologies can lend themselves to mixtures of networking architectures that consist of Local Area Networks (LANs) for the Centralised or Distributed Topologies and Wide Area Networks (WANs) for the higher level Distributed or Centralised Topologies [103]. ESPACENET also anticipates similar network topology, but focusing on ad hoc networking for very small satellites acting as daughters.

The anticipated ISL are expected to carry the following four types of data between distributed spacecraft:

1. science (medium to high volumes of data),
2. navigation (low volume),
3. command, and
4. spacecraft health data (low volume).

The volume and kinds of data depend on the objectives of the mission. For example, formation flying missions requiring tight coupling between the spacecraft will experience frequent transfers of navigation and command data via ISL within the distribution. Centralised formation flying missions collecting science imaging data may need to frequently transfer high volumes of science data from collector spacecraft across the crosslinks for pre-processing on a mothership prior to relaying the reduced data to the ground segment on a space-ground link. Spacecraft on-board storage will help determine the frequency and volume of science data transfers thereby specifying the crosslink channel capacity requirements for the mission.

Since constellation operations do not require precision autonomous navigation operations, navigation will be a low frequency data transfer operation for this type of DSS. The anticipated maximum cross-link data rates for navigation, command, and health data are on the order of 1 kbps each. Science data rates may vary from a few bps up to 100 Mbps or more (e.g. remote sensing optical or multi-spectral

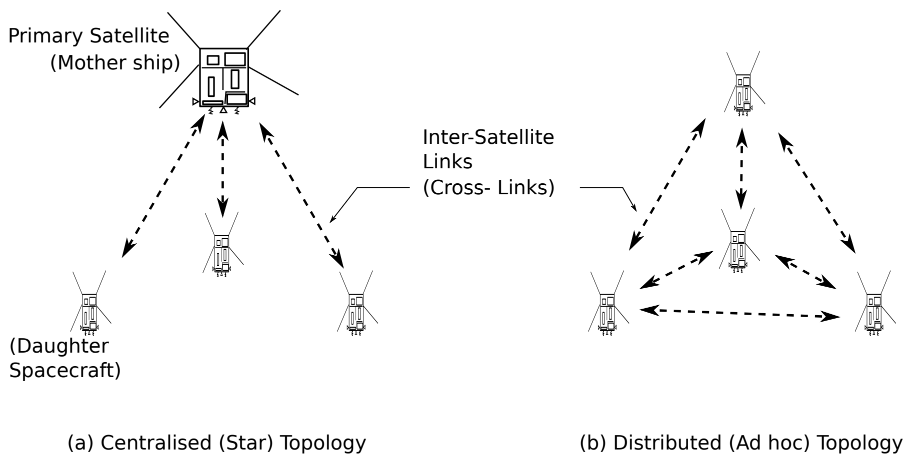

Fig. 2.7 Basic topologies in the formation flying cross-links [103]

imagers such as used by DMC[114]). Estimating the total bandwidth required for space and earth science distributed spacecraft missions using crosslinks requires a simple calculation using the probable number of simultaneously operational crosslinks, the probabilities that mission crosslinks need narrow, medium, or wide bandwidth communication capabilities, and the associated maximum data rate with the narrow, medium, or wide bandwidth capability [103] .

Since multiple access is deemed necessary for the networks, the multiple access techniques available today would be a necessary feature of the ISL. The multiple access techniques and their advantages are summarised in Table 2.5.

The main issues arising in the design of inter-satellite links of emerging missions depends on the relative distance, the change in relative distances, the placement in space, and the underlying application which generates the message that is to be exchanged with the members of DSS or SBWSN. The selection of antenna, data rates, the bandwidth, the power, are interdependent specifications / requirements, which are mission specific. Little literature is published which addresses the physical layer issues, even though general SBWSN concepts have been floated. However, considerable work has been carried out under the project of ESPACENET, which is summarised in the following section, to act as the current state of the art in SBWSN.

2.3.3 Frequency Bands for Inter-Satellite Links

ISL is generally considered for GEO to GEO links and formation flying missions. Recently, LEO to LEO links have also been employed (section 2.2). ISL do not require uplink or downlink, or propagation through the atmosphere, in general. All links use directional antennas for point to point links. In the emerging applications such as ESPACENET and SBWSN concept, point to multi-point links are required. To the author's best knowledge no requirements have been published in the open literature with regards to ISL at the time of writing this thesis. The purpose of this section is to review the licensed and unlicensed frequency bands currently in use and discuss considerations applicable to ISL.

International Telecommunications Union (ITU) regulates the most important resource in telecommunications i.e. the operational (carrier) frequency and the bandwidth occupied by the transmitted signal for a particular service. It regulates the frequency by providing license to the operator, be it a terrestrial or space application. However, certain unlicensed bands are also provided, which could be used for SBWSN, in particular for COTS based hardware used in ISL.

2.3.3.1 Licensed Frequency Bands

The licensed frequency bands by international regulatory authorities (ITU-R, and ITU-T) are listed in Table 2.6. However, we have observed that lower frequencies have been used in earlier experiments

Table 2.5 Basic Multiple Access Methods for Inter-Satellite Links [103].

Method	Basic Characteristics	Advantages	Disadvantages
Time Division Multiple Access (TDMA)	• Unique time slots must be assigned to each S/C ISL • Each ISL transaction in the distribution limited to the assigned time slot	• Single frequency needed • Low cost due to replicate ISL design	• Transmissions restricted to one ISL at a time • Time synchronisation needed between each S/C • Propagation delay corrections must be applied when ISL signal path lengths vary in order to avoid signal collision • The greater the number of S/C the longer is the duty cycle for the transmission, resulting in a lower overall data throughput for distribution • Changing S/C separation distances requires dynamic assessment of time slots allocations to compensate for variable signal delays
Frequency Division Multiple Access (FDMA)	• Unique frequency needed for each ISL	• Multiple ISL transmissions can occur simultaneously	• One centre frequency needed for each ISL implementation • The larger the number of S/C, larger bandwidth required • Increased cost due to frequency variation in the ISL design
Code Division Multiple Access (CDMA)	• The ISL signal must be randomly spread across a portion of the frequency bandwidth via a PN code	• Multiple ISL transmissions can occur simultaneously • Relative range measurements can be simultaneously made with the communications	• Total number of ISL are restricted by the code noise floor • Complex signal processing • Complexity adds to overall cost
Random Access (RA) e.g. ALOHA	• Transmission attempted when no other operations detected • If an ongoing transmission detected, the attempt is deferred by a random amount of time till next attempt	• Single frequency needed for operations • Low cost system due to replicated design	• One transmission possible at a time, therefore data through put is time limited (access time) • Collision probability increases with longer distances due to propagation delays masking ongoing transmission • With increase in number of S/C, increased time of access limiting the DSS throughput
Spatial Access (SA)	• High gain antennas isolate beams and prevent ISL interference between different links	• Continuous ISL services can take place with minimal probability of interference	• Cost of ISL system increases significantly due to cost of high gain antenna, as well as its beam steering capability

see Table 2.1. Keeping ISL at high frequency serves several purposes such as little interference with terrestrial wireless services, since these frequencies are naturally filtered through the neutral atmosphere of Earth. Secondly, larger bandwidth is available which can support higher data transfer rates, and the physical size of antenna reduces. However, pointing requirements increase with the use of directional antenna i.e. satellites attitude and antenna structures must support precise pointing.

Table 2.6 Frequency bands allocated for Inter-Satellite links [115].

Inter-satellite Service(s)	
Radio Frequency	**Optical Frequency**
22.55 - 23.55 GHz	0.8 - 0.9 μm (AlGaAs Laser Diode)
24.45 - 24.75 GHz	1.06 μm (Nd:YAG Laser Diode)
32.00 - 33.00 GHz	0.532 μm (Nd:YAG Laser Diode)
54.25 - 58.20 GHz	10.6 μm (CO_2 Laser Diode)

2.3.3.2 Unlicensed Frequency Bands

The ITU allows the amateur radio users to operate satellites in unlicensed frequency bands shown in Table 2.7. The world amateur radio societies put a lot of effort to allow ITU to provide additional bandwidth in GHz range. Currently, most of the amateur satellites use UHF (430.00, 2400 MHz) band of frequencies for uplink and downlink.

Although currently, the number of users in the unlicensed band are few, but as the users would grow, issues arising from intentional or unintentional interference of carriers would need regulations. Just as ISM bands are regulated strictly in terrestrial applications, similar regulations are perceived for operations in space.

The available ISL frequency bands would suffice for operational requirements in the context of SBWSN, therefore no need of applying for additional frequency is envisaged.

2.4 Related Works

Enabling technologies for a SBWSN [11, 117] span over many fields from technology development to fleet management. However, immediate need of the hardware are:-

1. low cost, mass producible spacecraft platforms,
2. inter-satellite communications links,
3. high performance, low powered processing / data management*,
4. miniature thrusters to provide for spacecraft orbit and attitude control,

*to support distributed computing and networking algorithms or navigational algorithms

Table 2.7 International Telecommunication Union Amateur Satellite Service Frequency Allocations [116], comparison between 1971 and 1979 allocations.

1971 WARC			1979 WARC		
Frequency	Units	Comments	Frequency	Units	Comments
7.00 – 7.100	MHz		7.00–7.100	MHz	
14.000 – 14.250	MHz		14.000–14.250	MHz	
21.000 – 21.450	MHz		21.000–21.450	MHz	
			24.890–24.990	MHz	
28.000-29.700	MHz		28.000-29.700	MHz	
144.000-146.000	MHz		144.000-146.000	MHz	
435.000-438.000	MHz		435.000-438.000	MHz	
			1.26-1.27	GHz	Uplink Only
			2.40-2.45	GHz	
			3.40-3.41	GHz	In Regions 2 & 3 only
			5.65-5.67	GHz	Uplink only
			5.83-5.85	GHz	Downlink only
			10.45-10.50	GHz	
24.00-24.05	GHz		24.00-24.05	GHz	
			47.0-47.2	GHz	Amateur Exclusive
			75.5-76.0	GHz	Amateur Exclusive
			76-81	GHz	
			142-144	GHz	Amateur Exclusive
			144-149	GHz	
			241-248	GHz	
			248-250	GHz	Amateur Exclusive

5. interoperability between several communications systems.

From the operational perspective, fleet management becomes challenging. Inter-satellite links ease the management by providing access to members via a single point of contact from the ground.

2.4.1 Emergence of Pico/Nano/Femto Class of Satellites

The birth of small satellite engineering is attributed to the pioneering Orbiting Satellite Carrying Amateur Radio (OSCAR) and Radio-Sputnik (RS) series of satellites [116], produced by the international amateur radio satellite (AMSAT) community and their Russian counterparts. From OSCAR-1 (1961) the amateur satellites grew in sophistication till OSCAR-8 (end of 1970). Since none of the satellites carried on-board computers, therefore, they acted as pure “relays in orbit”.

OSCAR-9 (UoSAT-1) and OSCAR-11 (UoSAT-2) [1] are considered the pioneers of the modern concept of *smaller, faster, cheaper* breed of amateur satellites. The two satellites carried a built in microprocessor and other commercial-off-the-shelf (COTS) micro-electronics, thus establishing the basis of adapting COTS for space environment. The remarkable time to develop UoSat-1&2 by dedicated university led teams [118] demonstrate effective cost of effort. Whereas, student led satellite projects namely the OPAL [18, 119] and EMERALD [120] missions, took about 8 years from concept to in-orbit operations, which far exceeded nominal project time of 2 years available to a graduating engineer. The experience gained from OPAL and EMERALD indicated the need to simplify payload and sub-system [121], by reducing the size, limiting the mass and standardising the shape of satellite. The effect is that with simpler mission concepts, same teams work similar to dedicated engineers on a project would. The result is smaller spacecraft concept designs namely;

- CubeSat [121], a free flying satellite in a 10 cm cube.
- CanSat [19], a free flying satellite in a soda can.
- SNAP-1 [20], a small nano satellite platform with active propulsion.
- PalmSat [122], a satellite the size of the palm of a hand.
- ChipSat [123], a basic free flying satellite in the form of an integrated chip.
- PCBSat [23] a free flying satellite on a printed circuit board half the height of 10 cm cube.

Apart from PCBSat, ChipSat, rest of the satellites have in-orbit experience. Amongst them, only CubeSat has demonstrated more than a decade of in-orbit operations see for instance the Xi-IV CubeSat [124].

The new group of very small satellites is classified into pico/nano/femto classes of satellites, illustrated in Figure 1.1. Although pico/nano class of satellites are sought to be simpler than conventional satellites, nevertheless they are complex [125], heralding challenges for the mission designer, and systems engineer. For instance design of real time operating system to operate on simple low resourced microprocessors, low powered data storage capabilities, low powered data communications, smaller sensor designs, and so on.

These platforms hold great potential, however, the size does limit the application. "Such small satellites cannot cater for all mission types, especially where large transmitter powers, antenna arrays or optical apertures are required for applications such as direct broad cast TV, mobile voice / data communications from geostationary orbits or for high resolution Earth or astronomical imaging," [125, ch.18]. However, when deployed at altitudes less than 1000 km, they have demonstrated in-orbit readiness. A broad set of applications are listed as follows;

- These miniature satellites are particularly suitable for hands-on-training for young scientists, engineers, experiencing technical and managerial aspects of mission design.
- These are suitable for fulfilling amateur communications, remote sensing and space science applications.
- The satellites can make affordable constellations possible.
- The satellites are feasible to demonstrate new technologies in orbit.

The small satellites have gained wide acceptance in the academia and national space agencies [63, 62] for which inter-satellite links are one of the current research activity [126].

2.4.2 Data Link Layer

OSI (open system interconnection) [127] suggests 7 functional layers for a data network communicating via physical link, of which the first is the physical layer whose responsibility is to transmit bits in the form of electrical signals over a shared medium, example specifications are Ethernet (IEEE 802.3) for wired local area network, Wifi (IEEE 802.11 [128]) for wireless local area network and WiMax (IEEE 802.16 [14]) for wireless wide area network. Since the medium is being shared, a medium access control (MAC) mechanism is also required which is addressed in the data link layer e.g. collision* avoidance (CA) [129], collision detection (CD) [130] within the family of carrier sense multiple access (CSMA) algorithms [34]. CSMA/CA is used in IEEE 802.11 data link layer, referred to as the medium access control (MAC) algorithm.

When several nodes are connected, then the sender of data must know the destination, for which, the network entities should know the route to be taken by the data packets to reach the destination, just like postal service, logical addresses are maintained to mark possible routes to each entity or node. Route determination and management is the goal of the network layer see for details [131, 132, 133]. Rest of the functionality is not necessarily required to establish a network, but they are required for addressing compatibility of formats of data e.g. distinguishing multimedia related data from email related data from facsimile data from control data.

The Table 2.8 highlights physical layer specifications adopted by variants of the IEEE 802.11 protocol for wireless local area networks. DSSS and OFDM are the two main physical transmission schemes proposed and implemented by original equipment manufacturers (OEM) devices.

Table 2.8 IEEE 802.11 standard physical layer evolution.

Release Date	Standard	Frequency (GHz)	Bandwidth (MHz)	Modulation	Antenna	Max Data Rate
1997	802.11	2.4	20	DSSS[a],FHSS[b]	-	2 Mbps
1999	802.11 b	2.4	20	DSSS	-	11 Mbps
1999	802.11 a	5	20	OFDM[c]	-	54 Mbps
2003	802.11 g	2.4	20	DSSS,OFDM	-	542 Mbps
2009	802.11 n	2.4, 5	20, 40	OFDM	MIMO[d]	600 Mbps
2013	802.11 ac	5	40, 80,160	OFDM	MIMO[e]	6.93 Gbps

[a]Direct Sequence Spread Spectrum
[b]Frequency Hopping Spread Spectrum
[c]Orthogonal Frequency Division Multiplex
[d] Multiple Input Multiple Output, 4 spatial streams
[e]Multiple Input Multiple Output, 8 spatial streams

*When two or more nodes transmit simultaneously on the same medium, then the signals interfere, destroying the waveforms in a manner, that the represented data is corrupted, considered as lost. This phenomenon is called collision of packets / data in computer networks.

The typical data rates and modulation schemes of IEEE 802.11 standards are listed in Table 2.8. The carrier frequency operating in industrial, scientific and medical (ISM) license free frequency bands i.e 2.4 and 5 GHz, one of the reason of low cost but widely used standard. Sidibeh [32] evaluated the MAC layer and proposed changes in its internal timers which keep track of the control messages required in network establishment.

2.5 Analysis of ISL Research for SBWSN

Like many advanced technologies, the origin of WSNs is seen in military and heavy industrial applications. The first wireless network that bore any real resemblance to a modern WSN is the Sound Surveillance System (SOSUS), developed by the United States Military in the 1950s to detect and track Soviet submarines. This network used submerged acoustic sensors – hydro phones – distributed in the Atlantic and Pacific oceans. This sensing technology is still in service today, albeit serving more peaceful functions of monitoring undersea wildlife and volcanic activity [134].

The Defence Advanced Research Projects Agency (DARPA) started the Distributed Sensor Network (DSN) program in 1980 to formally explore the implementation challenges. With the birth of DSN and its progression into academia through partnering universities such as Carnegie Mellon University and the Massachusetts Institute of Technology Lincoln Labs, WSN technology soon found a home in academia and civilian scientific research. Governments and universities eventually began using WSNs in applications such as air quality monitoring, forest fire detection, natural disaster prevention, weather stations and structural monitoring [135]. The concept has perpetuated from its terrestrial application to space [33].

Examples of influential academic/industrial initiatives on WSN are the following:

- UCLA Wireless Integrated Network Sensors (1993)
- University of California at Berkeley PicoRadio program (1999)
- Adaptive Multi-domain Power Aware Sensors program at MIT (2000)
- NASA Sensor Webs (2001)
- ZigBee Alliance (2002)
- Centre for Embedded Network Sensing (2002)
- Space based wireless sensor network (2002)
- ESPACENET (2008)

It is but natural that the WSN finds its application in space. The following typical DSS applications also benefit from the enabling technologies being developed for SBWSN:

- Rendezvous missions; requiring navigation and guidance based on ISL.
- Formation Flying (FF) missions; requiring navigation and guidance based on ISL.

- Global Communication Systems; requiring data hand-over from one satellite to the other i.e telephone calls handed over to satellites similar to a cellular network.
- Tracking and Data Relay; when LEO satellites are not visible to ground stations, GEO based satellites provide a reliable link.
- Interplanetary Environmental Sensing; be it for planetary surfaces or in the outer atmosphere.

A number of concurrent developments have been undertaken since the turn of the century, particularly in the first decade, which are directly required in SBWSN, particularly the work on ISL used in FF missions. The existing research in the SBWSN can be summarised as follows:

1. Pico/nano satellite research has resulted in SNAP-1 [20], PalmSat [122], ChipSat [136, 123, 23], PCBSat [29] at SSC, UK, whereas CubeSat [21] from PolyTech collaboration with CalTech, USA.
2. Deployment mechanism: P-POD and likes are space qualified.
   - PCBSat and CubeSat have a standard deployer called **P-POD** [22] which can be interfaced to major space launch vehicles,
   - It has been tested on DNEPR (Russian) and PSLV (Indian) for cluster deployment, thus gaining extensive space heritage-+.
3. SNAP-1 which was launched in 2000, carried ISL capability. However, ISL was demonstrated by the nano-satellites CAN-X 4&5 [137] in 2014 for their autonomous formation flying mission. Some notable ISL works are listed below:
   - Single carrier based **UHF transceivers** using BPSK, or QPSK.
     - Custom transceivers were used in SNAP-1, Can-X 4&5, operating in UHF band.
     - The only proposed cross link channel simulator is [101], where ISL is considered free space, thus only path loss is modelled.
     - Folding antennas [138] for CubeSat are being investigated, phased array antenna with electrically steerable beam suggested to support IEEE 802.11 based network [139, 32].
   - IEEE 802.11 has been investigated for its data link protocol found to be feasible with minor modifications in internal timers [31].
   - The Routing problem is the next critical factor that needs addressing after adopting physical and data link layers for SBWSN. Although routing algorithms have been investigated for terrestrial WSN [133] but not from the perspective of SBWSN. Routing in Mobile Ad hoc networks (MANET) is a similar problem [132]. Issues in LEO satellite network routing has been considered in [140].
   - Delay tolerant network issues have been investigated by Muri [131] for nano satellite networks.
4. Design of testbeds in the context of SBWSN lacks investigation, but it bears similarity to testbeds developed for formation flying missions.
   - A SBWSN network testbed has was proposed by Wu [36], which also assumed a simple free space path loss model, whereby relative motion and Doppler Shift were not taken into account.
   - Formation Flying cross link testbeds [101, 97] incorporate scintillation effects to study range estimation accuracy using cross links.

5. Saratoga [141] , a UDP file transfer protocol has been tested for LEO to ground link, which can be used in SBWSN.

From the above summary, it can be seen, that various enabling technologies required for a functional SBWSN have been addressed, such as design of small mass producible spacecraft to act as sensors, development of enabling technologies e.g. ISL for such small spacecraft, adopting networking protocols, and launch vehicles capable of deploying clusters of small spacecraft. However, it is found, that despite the advances in a broad range of enabling technologies, the physical layer issues and the pertaining testing mechanism have not been tackled, which constitute a gap in the present state of the art.

2.6 ISL Evaluation Methodology for SBWSN

Testing is an important aspect in research and development, and in the context of ISL, physical testing is of utmost value. Since, it is difficult to conduct field tests for ISL in space as and when required, therefore, most of the development is perceived to be carried out using simulation tools, in which the channel models would play a critical role. Although, most of the literature assumes free space path loss for point to point links for their extremely high carrier frequencies, however, SBWSN is perceived to operate in bands allocated AMSATs or ISM, to avail existing COTS for ISL designs. Therefore, a testing mechanism to evaluate the performance of ISL is also one of the critical enabling technologies required in developing future SBWSN.

The current inter-satellite link development is focused on Formation Flying missions, where two satellites require point-to-point links. The ISL is employed to measure inter-satellite distance, in addition to communications links for passing navigation and guidance data. The testbeds for such missions have been developed by ESA and JPL (as discussed earlier in section 2.2.1.2), which is currently restricted to testing point to point links between two satellites. Whereas, in the case of SBWSN, point to multipoint links are required, where, multiple satellites want to establish communication links.

Unlike FF testbeds, SBWSN has to test the network protocol suite incorporating the impact of link outages the cause of which is when the satellites move out of range of the link, or loss of signal due to deep fades observed when satellites traverse parts of turbulent ionosphere. Furthermore, any change in the physical layer data throughput rate, in turn affect the higher layer performance. Therefore, for end to end network performance measure, additional features are to be incorporated in the testbed for SBWSN. One of the features is to provide physical interfaces to four or more radios, so that completely developed sensor satellites and relay satellite, be tested for networking under normal as well as adverse conditions. It is pointed out here, that the interdisciplinary nature of ISL for SBWSN, demands a systematic approach to the development and testing of multiple aspects of the network. Since the physical layer performance governs the overall end to end performance of the network, therefore, special care must be done in incorporating the physical link quality in other network layer performance evaluation. The testbed is

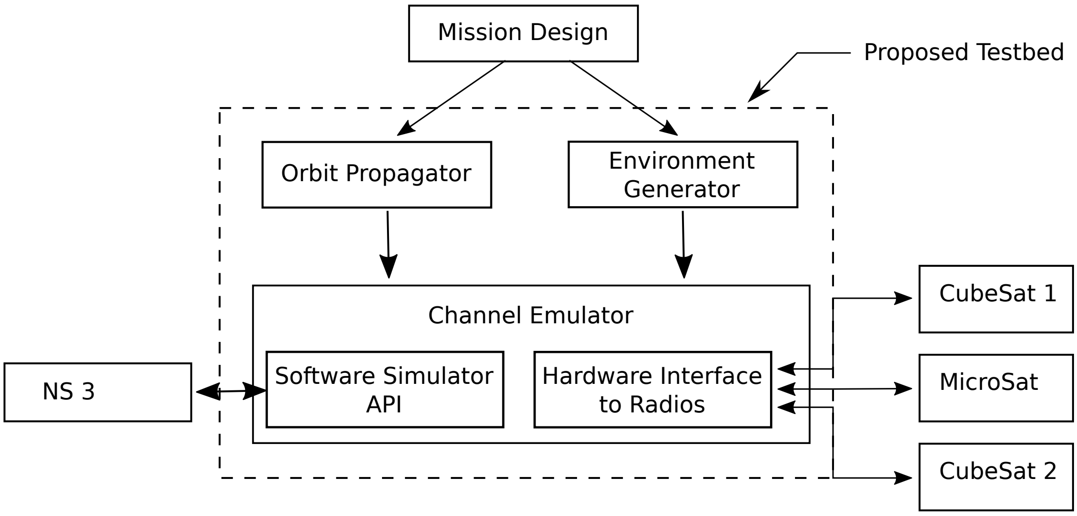

Fig. 2.8 Proposed testing mechanism for evaluating inter-satellite links for a SBWSN. NS-3 is a third party network simulator. The satellites represent the fully developed ISL hardware for members of SBWSN.

a pure simulation environment, with a separate module to allow physical hardware interface to fully developed ISL modules of satellites.

In the light of the above discussion, a testing mechanism is proposed. The functional modules are illustrated in the Figure 2.8. These functional blocks are complex, and must be developed in stages; initially only for simulation based studies in baseband, then allowing hardware interface, and finally a complete hardware emulator and simulator with defined APIs to interact with other network simulators.

For the purposes of this research, the functional blocks to be part of the proposed testbed are worked out first. Although a hardware based testbed is useful, hardware based test equipment tend to be costly, therefore, simulation based tools would be developed and used in this research work.

The major modules perceived in SBWSN testbed are:

- an environment generator,
- an orbit propagator, and
- a channel emulator, whose purpose is to generate impairments for the ISL.

Although not being considered part of the testbed, that a mission scenario evaluator/developer would be required eventually, since the testbed depends on the input from mission scenario. Automating this process would be useful.

It is envisioned that the testbed would operate in the following sequence:

1. A mission scenario is worked out first, in which the placement of satellites in line with the mission objectives is carried out, resulting in orbital configurations of the SBWSN i.e. the initial state of the

physical topology of the members of the SBWSN is identified. The in-orbit environment is identified based on the region of deployment. The orbital parameters are then passed to the orbit propagator.

2. The testbed takes input in the form of orbital parameters, and a specified region of interest. The trajectory of each SBWSN member is computed to identify inter-satellite link geometries useful in determining line of sight.
3. The environment generator, determines the state of plasma, space debris or other elements in the identified orbits, so that any impairments caused by such elements could be computed.
4. The channel impairment generator, would compute expected degradation on selected links during the, based on the inputs from orbit propagator and environment generator.
5. Finally, once the computations are completed, the impaired ISL is ready for use. In this thesis, it is being perceived for evaluating the performance of physical layer i.e. the performance of analogue front end, the baseband modem.

The mission scenario is studied for possible mission deployments. Based on the information of the environment and the orbital propagator, a link tester would generate impairments i.e. channel deteriorating effects on the communications links. For each new point the link range, and link quality would vary, therefore, numerical orbit propagator is perceived.

In this manner, the networking protocols running on-board satellites, could be tested, for disruptions caused in physical links. It is important to understand, that, physical links may or may not be guaranteed in the case of SBWSN, therefore, testing in such an environment is critical to the overall performance of SBWSN protocol suite.

2.7 Conclusion

Although the concept of wireless sensor networks is appealing and several concurrent developments have enhanced the current state of the art of enabling technologies for SBWSN, but the physical aspects of the communications links between the satellites are deliberately left, since they are considered mission specific. It is true, that a general treatise of physical link issues is not fruitful, because the possible topological configurations are mission specific e.g. the location and manner of deployment of satellites dictate the inter-satellite link geometries, line of sight, and relative dynamics of the satellites. Furthermore, the communications channel characteristics for such ISL, depend on the in-orbit environment, the type of antenna used for ISL, and the operational frequency of the carrier wave. Performance evaluation of a modem is therefore mission specific as explained in the dependency chart illustrated in Figure 1.7 and described in section 1.3. Incorporating all of the above stated factor in the performance evaluation tests is the identified need for space based wireless sensor networks. A testing mechanism, that would capture the deteriorating effects of in-orbit environment and the motion of satellites, on the inter-satellite links. So that, the impact of deteriorated physical layer performance could reflect upon the working of the higher layers of the complete networking protocol suite being used. For example, in the case of IEEE 802.11, data link layer performance depends on the performance of physical layer. And the performance of the appropriate network layer protocol depends on the combined performance of data link and physical link layers.

Since, the SBWSN concept itself is novel, and a handful of mission scenarios have been worked out in detail, therefore, for ISL investigations, a mission scenario depicting the SBWSN concept is required. Using the concept mission as the basis of specifying the physical topological configurations, relative motion would be assessed. The specified region of deployment would help in studying the in-orbit environment from its impact on propagating electromagnetic waves. Hence building blocks of the proposed testbed would thus be laid out, which can be further developed in future, since developing such a multi-disciplinary testbed as a complete module is out of the scope of this research.

As discussed in section 2.6, a testbed or a testing mechanism is essential to the current study, which is not available at the time of writing of this thesis. Therefore, as per the functional requirements outlined earlier, the rest of the thesis is structured along the lines of the proposed ISL evaluation methodology for SBWSN, i.e. first a SBWSN mission scenario is identified, based on which the relative motion would be evaluated, then, the environment in the identified orbit would be assessed, and communications channel characteristics would then be determined. If the channel characteristics can be simulated using existing channel models, then existing models would be used, and the requisite changes in the set of parameters would be done.

It is important to ascertain the true nature of the channel in which the link is to operate, to ensure acceptable operations of the ISL device, be it to support standard specifications defined by IEEE 802.11 or PROX-1 standards or be it to support custom specifications defined by the design engineer.

CHAPTER 3

DEFINITION OF A MULTI-POINT SENSING MISSION FOR IONOSPHERE MONITORING

According to the Space based Wireless Sensor Network (SBWSN) concept, several small satellites act as sensors, communicating with each other, exchanging engineering data i.e. operational status of sub-systems as well as passing measurements. The data is passed either to a central processing facility in-orbit or on ground. The information is thus extracted from the data, and distributed to concerned users/applications. The sensor network may be placed in Earth bound orbits, even about a larger spacecraft (geostationary communications satellite), on other planets, asteroid, moons, or sent farther away from Earth in deep space. The transmission/modulation scheme would perform differently for different environments. A generic communications system design becomes too complex to cater to deteriorating effects of all possible environments. In addition to the environment, each spacecraft design poses its own constraints e.g. smaller satellites have less resources thus are able to support simpler antenna systems, generate less electrical power, thus are less capable, whereas, larger satellites can carry large furled parabolic mesh surfaces acting as high gain directional antenna, generate more power, and thus can handle complex operations in orbit. The mission payload / instrument determines volume of data to be transferred between the sensor. The nature of data itself may be critical or time constrained. The above stated factors i.e. the environment, spacecraft platform, the data volumes and the user requirements, together, determine communications system design specifications.

This Chapter defines an application mission scenario to highlight operational requirements for inter-satellite links as perceived from the point of view of the SBWSN concept. It defines the mission objectives from which the region of spacecraft deployment determining the type of anticipated orbits. Since the ionosphere is to be monitored by measuring the electron density at multiple points, the region of interest lies in Low Earth Orbit (LEO) at altitudes below 1,100 km.

3.1 Introduction

The main purpose of a communications system is to transmit the message as far as possible, as correctly as possible. Therefore, it is of utmost importance to identify the properties of the environment that affect the wireless link, which are referred to as **communications channel characteristics**, or commonly known as **channel models** in the telecommunications industry. Some of the effects of a communications channel on the transmission are discussed to highlight the significance of confining the scope of research to a particular environment in space.

When the message is transmitted in the form of digital data, then the data transfer rates is one of the design specifications i.e. the number of bits transmitted in one second. Therefore, a bit when represented by a waveform is confined in time. A system designed to transfer at low data rates operating at a distance within a certain environment, may not be able to operate at all for a higher data transfer rate, for the same distance and environment. The environment effects on the wireless link is more distorting in the case of high data transfer rate, than lower rates. Identifying the minimum and maximum data transfer rate requirements is one of the fundamental design specification.

Satellites are placed in orbits, in which they are constantly in motion. Relative motion of satellites cause receiver side carrier wave shifted from the originally set value. There are many ways to place satellites in orbits, depending on the underlying application scenario. When multiple satellites are deployed, then they can be deployed as part of a constellation, cluster, or swarms. The constellation design sparked interest during the 80s and 90s , where, communications satellites were being evaluated for placement in LEO or MEO, e.g. the IRIDIUM, TELEDESIC, BigLEO mission concepts, of which only IRIDIUM is the only constellation with inter-satellite links. The consideration for constellation design was to determine the minimum number of satellites to be placed in such a manner, that all parts of the globe are covered by the radiation patterns of the antennas on board such satellites. Notable constellation design theories are Walker [142, 143], Ballard [44] and more recently a different form of visualisation applied to the same orbits known as Flower Constellations [42, 144, 43] (see Annex D for example Walker constellations).

Therefore, the knowledge of the environment and its distorting effects on the wireless link along with the data transfer rates and the relative motion of satellite, is not only essential but critical to the design of the communications system to support inter-satellite communications. Being a new concept, there is a handful of published literature [145, 39, 35, 40, 146, 41, 147, 37, 139, 103], addressing the inter-satellite communications system (COMS-ISL) design issues for specific space based wireless sensor network based mission scenarios.

The aim of this chapter is to define an example **SBWSN mission scenario** to highlight the underlying issues which directly affect the **communications system for inter-satellite links (COMS-ISL)**. COMS-

ISL refers to the transmission schemes implemented on the hardware transceiver including the baseband modem, analogue front ends, and the antenna sub-system.

The factors which are derived from mission objectives, and affect COMS-ISL design are as follows:

- The payload defines the data transfer rate requirements; based on the volume of data generated by science payload, data transfer rate requirements are ascertained.
- The payload is selected on the basis of phenomenon to be studied. The occurrence of phenomenon in space determines the region of interest, therefore orbits are selected which cover the region of interest. The selection of orbits directly influence the design of communications system in two ways
  (a) The in-orbit environment can be specified, which can be investigated for communications channel characterisation. Which inturn determine suitable modulation schemes to be used to support the specified data rates.
  (b) The placement in orbits, also determine the inter-satellite relative motion, which can be used to determine the Doppler Frequency shifts and shift rates, observed at the receiver side — one of the critical design specification for phase-locked loop (PLL) based tuning circuits in the analogue front end of the receiver.
- The payload also defines the supporting bus-systems, which must be confined to the smallest possible spacecraft platform so that overall mission cost be reduced as perceived in SBWSN [11, 33]. The hardware design of communications system is then restrained by the available resources in terms of mass, volume, electrical power, and placement within the selected class of satellite — an important hardware design consideration.
- The payload defines the attitude control method of spacecraft, whether it is to be spin stabilised or 3-axis stabilised. The selected attitude control mechanism directly influences the type of antenna sub-system to be used as the radiating element for the communications system.

The above stated factors lead to the following aims and objectives of this chapter:

1. Define the science payload, by identifying a pressing issue in the space science community requiring multi-point sensing space mission:
   a) Prefer commercially available systems also called commercial off the shelf systems (COTS) for the payload instrumentation and associated electronics.
   b) Determine the electrical power requirements, mass, shape, sizes, for which smallest pico/nano class of satellite be suitable.
   c) Determine the volume of data generated by each payload, so that data rate requirements for COMS-ISL be considered.
   d) Define the attitude control requirement of science payload
2. Identify associated bus-system needed to support the science payload.
3. For the region of interest, determine suitable types of orbits.
4. Determine the feasibility of the concept mission scenario (a feasibility metric needs to be defined).

The feasibility of the mission scenario defined above depends on the following three factors:

(i) **Low cost:** The mission would only cost less when unit cost of satellite itself is considerably low, i.e. pico/nano class of satellites be preferred, since they are inherently low cost platforms compared with conventional mini/micro satellites (Figure 1.1). The per unit cost can be lowered by utilising COTS in the development of satellites, therefore one of the feasibility metric factor is the use of COTS, along with the preference of pico/nano satellites.

(ii) **Science return:** An enhanced science return is possible by improving the spatial and temporal resolutions of the measurements, which translates in to the use of multiple satellites with the same measurement instrument deployed in the region of interest. The use of multiple sensors also overcomes the inherent ambiguity arising from single point measurement. Therefore, a feasibility factor would be the use of small science instruments which could fit in the confines of pico/nano class of satellites.

(iii) **Technical feasibility:** A low cost mission can be scientifically feasible, but engineering issues may prohibit its practical realisation on technical grounds. To evaluate technical feasibility the following are to determined: (a) ease of integration and availability of bus-systems for the satellite development (preference given to COTS), (b) ease of deployment of such satellites in orbit, (c) ease of operational and management issues and (d) graceful death of satellites so that in-orbit space is available for reuse as well as to reduce man made space debris a major cause of damage to satellites.

3.2 Significance of the Ionosphere

The Earth's ionosphere has a direct impact on technology used in our daily life, particularly radio based services. The disturbances occurring in the ionosphere [148] affect the radio applications [149] as illustrated in a summarised form in Figure 3.1. Its significance is highlighted by the following services and activities:

- Long distance communications using high frequency (HF) bands i.e. 3-30 MHz. The transmitted waves directed towards the sky, bend as the rays refract while passing through the various electron densities in ionosphere. The turbulence in the nominal electron density change the refractive index of ionosphere, causing change in direction of propagation, resulting in a loss of reception at the destined location. Scintillation i.e. the rapid changes in phase and amplitude of the received signal, is frequently observed at the receiver, is also known to be the effect of turbulent nature of ionosphere. In addition to the HF long distance communications, the TV broadcasting via satellites, the communications line between railways and electrical power house grid stations get damaged due to severe solar storms (severe turbulence in ionosphere and above).

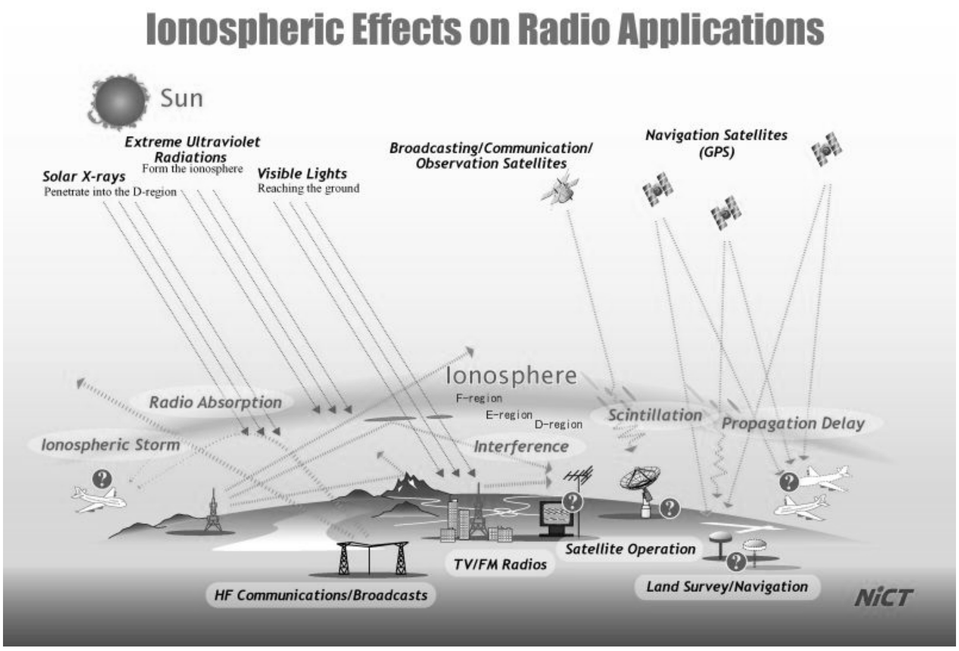

Fig. 3.1 An illustration of effects of ionosphere turbulence on electronic assets in use today (courtesy of NiCT [149]).

- Global Positioning Satellite Service (GPS) [150], deployed in medium Earth orbits (MEO), continuously transmit radio signals, which are used to determine the location for navigational purposes e.g. GPS receivers in car. While passing through the ionosphere, the actual wave parameters change, resulting in erroneous position, at the receiver. The turbulence in electron density, increases the positional errors, even loss of signal in severe conditions.
- The surge in electron density essentially increases with the onset of highly energetic particles, which can penetrate not only space assets in orbit, but can be a source of danger to humans travelling in aeroplanes while flying near the poles [151].
- The international ionosphere reference (IRI) model constantly relies on measured parameters to correct its prediction accuracy which depends on in*situ* measurements to accommodate anomalies [152].
- The science community is interested in the morphology of the disturbing structures found in ionosphere [153], correlating with events triggered in space or from Earth [154, 155].
- The study of Ionosphere has been emphasised by major space agencies in their long term goals. NASA has set ionosphere related missions in its "Sun-Earth Connection" programme [64]. ESA acknowledge the space weather significance and monitoring of ionosphere in its "Cosmic Vision" programme [65].

Although the Ionosphere is studied from ground based instruments, however, real insight is achieved from the in*situ* measurements by space missions.

3.2.1 Space Science Missions to Explore the Ionosphere

In this section a brief history of the ionosphere exploratory missions is discussed. Since the early space age, several missions have been sent to study the Earth's ionosphere for its constituents, the dynamics, and interaction with solar and cosmic radiations. The ability to diagnose ionised gas for its constituent particles, statistical estimates of its density, temperatures, and velocity vectors improved with each successful mission flown, thus a flight heritage developed, which resulted in a better understanding of plasma behaviour in ionosphere. Since the same ionospheric plasma forms the atmosphere causing atmospheric drag to lower earth orbiting satellites, the modelling of this part of atmosphere becomes an integral part of space mission designs. The knowledge accumulated helped in developing more accurate and complex set of instruments [156], spacecraft and ionosphere models [157]. Satellites carrying payloads to measure the chemical composition, temperature and drift velocity of various particle species were sent in ionosphere.

The early Explorer comprising a set of five satellites named Atmosphere Explorer were launched in sequence between 1963 till 1976 [158]. These satellites were placed in orbits which mutually completed the coverage of all latitude ranges, from equatorial to polar, flying at heights from 150 km to several thousand kilometres. The sampling rate was about 0.1 to 1 Hz (considered low). These missions were able to take long uninterrupted measurements, providing valuable insight to the ionosphere.

In 1991, a satellite couple named Dynamics Explorer (DE) was launched which studied the wave activity in ionosphere. Both satellites had a perigee of about 300 km and 460 km, carrying a payload to measure electromagnetic emissions, plasma parameters and super thermal charged particle fluxes. A series of space missions to study electromagnetic emissions, turbulence and instabilities in ionospheric plasma were Viking, AKTIVNY, APEX, and FREJA [159]. These satellites had a perigee between 440 and 650 km and apogee of several thousand kilometres. The scientific payload included electro-meters and magneto-meters.

New possibilities of on-board data processing system was realised in FREJA which allowed transmitting not only the spectra but also the wave form of plasma emissions including high frequency Langmuir oscillations. This helped in observing the generation and decay relationship of wave processes in different frequency bands.

Monitoring was not the specific goal of any of the above mentioned missions. The scientific payload was switched on only in the region of interest for example, the two Auroras, the equatorial region or higher latitude. Probably the first time monitoring was realised, was by the French mission Demeter [155], a micro satellite placed in circular sun synchronous orbit at an altitude of 700 km in June 2004. The distinguishing feature was the objective to register electromagnetic emissions in the ionosphere triggered from "below" i.e. the Earth quakes, tsunami, volcanic activity; these signatures are of interest to different researchers which is the basis of a proposed cluster mission to monitor ionosphere see [154].

Both spectra and wave forms of the measured data could be transmitted with the aide of modern on board data processing units, therefore high speed communications links are required. The payload was switched off at latitudes higher than 70°, therefore only selected region could be investigated.

Missions sent earlier in Earth's Ionosphere were to study and enhance the capabilities of the spacecraft engineering and measurement instruments. Spacecraft designs have shown a trend towards lighter and more capable spacecraft, where resources are designed around the payload, such as shown in Figure 3.2. In this design approach either more instruments could be added to the payload, or the instrument could optimally utilise the available resources. In either case the science return of the mission increases [160]. Distributing the payload to several small satellites would allow distributed satellite systems to operate, with a much higher spatial and temporal resolution, as well as a reduced payload to mass ratio, allowing capable spacecraft, with lesser complexity in design and much higher science returns.

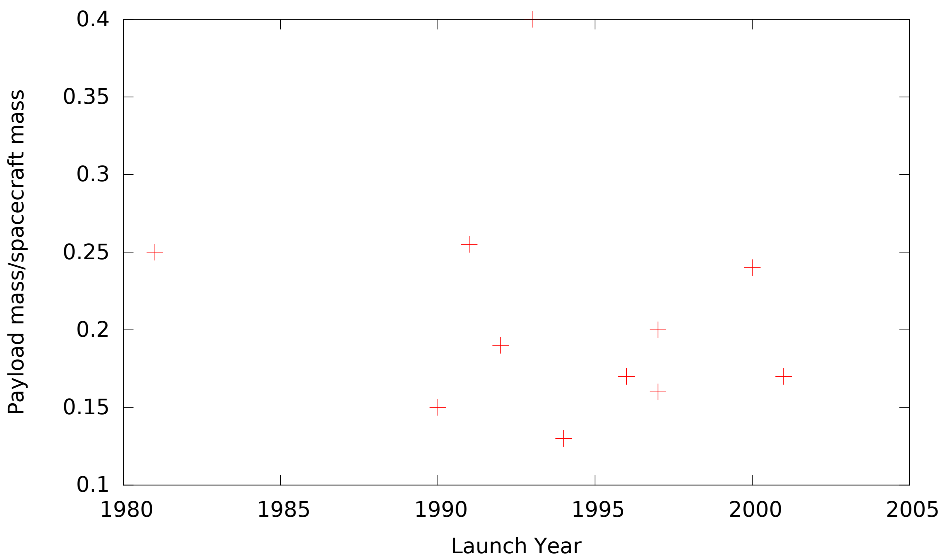

Fig. 3.2 Payload to mass ratio of a few spacecraft missions (adapted from [160])

3.2.2 Space Plasma Instruments

The purpose of this section is to review instruments used in ionosphere exploration, which could be deployed on very small spacecraft. By identifying the instruments the data transfer rates can be assessed, which is essential in determining the ISL data throughput requirements.

Today a single spacecraft carries a plethora of scientific instruments.

Since any measurement instrument has a limited measurement range, therefore, other instruments extend the measurement range as well as sensitivity. On STEREO mission, the set of instruments taking measurement are listed in Table 3.1. The particle and wave nature of plasma is investigated by separate measurement instruments, having their own range and frequency. The data rates would assist in determining the base requirement of communications systems.

Each of the mentioned science payloads can form a separate sensor satellite, thus various size and shapes of emerging sensor satellites are envisioned. For the sake of system level evaluation only the smallest simplest instrument which can fit in CubeSat would suffice to prove the concept being propagated in this chapter.

Table 3.1 The scientific instruments in the particle and fields package (IMPACT) on STEREO mission [161], illustrating the typical mass and data rates of space plasma physics on a single spacecraft.

Experiment	Instrument	Measurement	Range	Mass (kg)	Power (W)	Data (bps)	Time Resolution
SW	STE	Electron Flux and Anisotropy	2-100 keV	0.35	0.20	34	1 min
	SWEA	3D electron distribution core and halo density, temp, anisotropy	0.3 keV	1.41	1.10	41	1 min
MAG	MAG	Vector field	$\pm 500nT$ $\pm 65536nT$	0.55	0.38	76	0.25 s
SEP	SIT	He to Fe ions	0.03-2 MeV/nuc	0.84	0.64	60	30 s
		^{3}He	0.15-0.25 MeV/nuc				
	SEPT	Diff. electron flux.	20-400 keV	0.79	0.60	30	1 min
		Diff. proton	20 -7000keV				1 min
		Anisotropies	As above				15 min
	LET	Ion Mass 2-28 and anisotropy	1.5-40 MeV/nuc	0.51	0.18	80	1-15min
		^{3}HeIons flux and anisotropy	1.5-1.6 MeV/nuc				1-15min
		H ions flux and anisotropy	1.5-3.5 MeV				1-15min
	HET	Electrons flux and anisotropy	1-8 MeV	0.33	0.07	30	1-15 min
		H	13-100 MeV				1-15 min
		He	13-100 MeV				1-15 min
		^{3}He	15-60 MeV/nuc				15 min
	SEP	—	—	1.69	1.44	—	—
Common	IDPU	—	—	1.78	3.22	33 or 126	—

3.3 Mission Objectives

In this section a scientifically feasible mission scenario, based on the overview of the SBWSN concept above, is determined. The proposed ionosphere monitoring mission has a two-fold agenda: (i) to address a long outstanding science community demand for a multi-point sensing mission for space plasma [161] and (ii) to demonstrate the feasibility of the space based wireless sensor network concept [117, 33, 162].

3.3.1 Scientific Goals

- To address the much needed multi-point sensing requirements by space plasma physicist. The region selected for study is Earth's ionosphere, which lie in the lower Earth orbits i.e. altitude less than 1000 km.
- To determine a minimal set of science instruments needed to take meaningful measurements of plasma bulk properties. The charged particle (electron) density is to be determined at different vantage points.

3.3.2 Technical Demonstration Goals

- To define the mission on the lines anticipated in the concept of space based wireless sensor networks.
- To confine the size of spacecraft to pico or nano class of satellites.
- To determine the physical topology of the network formed by satellites either in free flight mode, or regular mode with orbit control.
- To demonstrate the use of modified IEEE 802.11 b protocol, in establishing ad hoc networks in space.

Unlike monolithic single spacecraft based missions, the proposed mission is based on distributed satellite system (DSS) comprising several satellites of various sizes, whose aim is to provide for "the necessary requirement of continuous uninterrupted data with **substantial temporal and spatial resolution**" [161] to assist the space plasma physicist in getting a better picture of the complex interaction of terrestrial and extra terrestrial phenomenon with ionosphere[157, 153] specifically for its effects on space assets [163].

3.4 Sensor Network Hierarchy

When plasma density in Earths ionosphere is to be measured, the region of interest spans over three dimensions covered by the latitude, longitude and the altitude. Plasma variations are not only limited spatially, but also temporally varying from a few seconds to several months of turbulence. Several sensors taking simultaneous measurements are thus desired.

Since the sensors are continuously in orbit, their orbital speed and the minimum time to setup a measurement dictates the lower limits of spatial and temporal resolution. Consider at an altitude of 600 km, the average speed in orbit is about 7 km/s, so 7000 m has been traversed in one second. When the time to take one measurement is say 1 msec, then 70 m has been traversed already. Where the requirement is to take measurements at less than 70 m separation, faster response instruments are required.

Using smaller low cost satellite platforms not only reduces the cost of the mission, the smaller size of satellite reduces the contamination caused by wake generated around the moving satellite in plasma, and reduces the risk of destruction due to collision of satellites in close proximity.

The smaller size of satellites has a down side; smaller size, lesser volume for science instrument, lesser power generation capability, consequently compact systems design which tends to be complex particularly from the Electromagnetic Interference (EMI) and Electromagnetic Compatibility (EMC) conformance testing. Smaller size of spacecraft also means that the communications system particularly the high gain antennas, high power amplifiers operating in the carrier frequency range become not only power hungry, but fitting the system in small confines of the spacecraft becomes a challenge.

Therefore in view of anticipated smaller communications system on the sensor satellites, rather than a direct communications link with ground, a slightly larger satellite than the smaller sensors, equipped with higher gain antenna, sensitive receiver and high power transmitter is envisioned to act as a relay. The relay satellite is considered an integral part of the sensor network, whose purpose is to gather data from sensors passing it on to the ground station (GS), similar to WiFi range extender used in home today. The relay satellite can be a larger nano or microsatellite such as the Surrey Satellite Technologies Ltd. (SSTL) series of satellites (UoSat) [164] (depicted as the microsatellite in Figure 3.3).

It is important to highlight here, that the same transmission scheme must be used in both the sensors and relay satellites, different modulation schemes are not compatible. The network of sensors is depicted as a block diagram indicating inter-satellite distances. A complete route of data transfer from sensor to ground station is clearly indicated in Figure 3.3. However, the same route of data transfer in Figure 3.4, depicts a more factual picture by considering in orbit placement.

Important factors pertaining to the inter-satellite communications design are the distances between the sensors, the distance between the sensor and the relay satellite, and between relay to relay satellite. It is anticipated that the relay satellite would be a constellation of several satellites in a string of pearl configuration. Whereas, the pico satellite having no orbit control mechanism, would be in free flight mode, their orbits would be governed by natural forces acting on them, as well as the initial conditions at the time of deployment in orbits. The nano satellites with orbit control mechanism may be able to maintain a close proximity operation for a limited period of time. Since they would operate in close proximity as compared to conventional satellites, they are to form clusters to distinguish them from constellations. It is pertinent to mention here, there is no clear definition of the terms constellations,

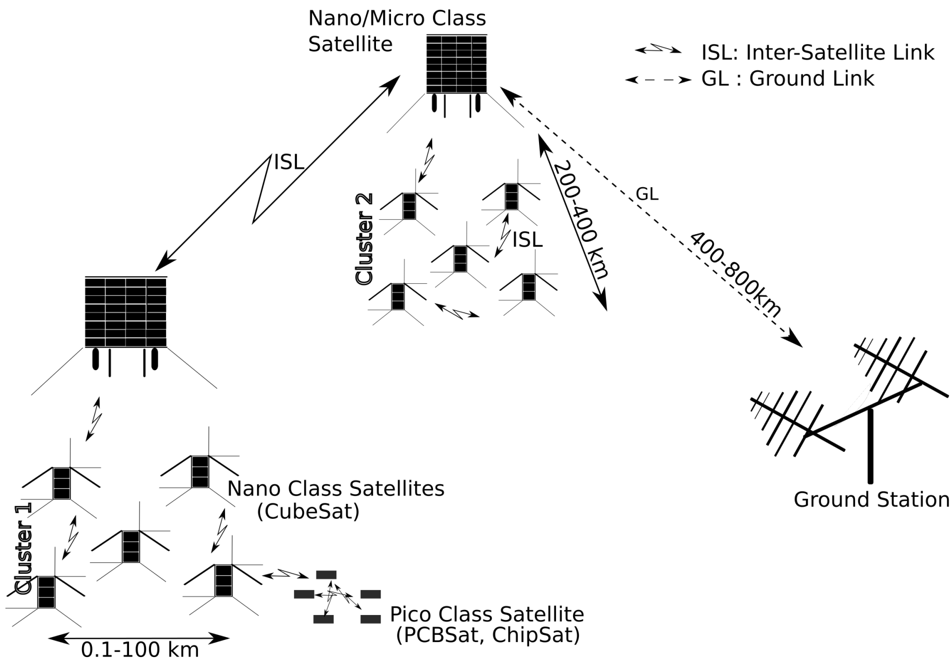

Fig. 3.3 Ionosphere monitoring mission (IMM) network hierarchy of larger mother satellites acting as relay to smaller sensors.

clusters or swarms used in distributed satellite system literature, therefore the definition stated above is meant in this thesis.

Furthermore, it is envisioned that to improve spatial resolution, a nano satellite be harbouring a pico satellite, which could be released to take measurements the length of the tether less than a few tens of meters. The purpose is to take measurements of the fine scale phenomenon, which is missed by the high speed satellites in orbit. The mother - daughter concept is illustrated in Figure 3.10 described in detail in sec 3.6.

The satellites responsible for sensing shall be referred to as **SenSat**, which would be pico or nano class of satellites preferably less than 10 kg mass. The satellites responsible for relaying data from sensors to ground station shall be referred to as **ReSat**, which are either nano or micro satellites preferably of the mass less than 30 kg.

SenSat takes measurements, ReSat relays the data from each sensor back to Earth. The data can take possible routes of which only the first two routes are considered for evaluating technical issues.

1. The link from sensor to sensor to relay satellite to Earth (depicted as route 1 by solid line in Figure 3.4).
2. The link from sensor to sensor to relay to Geo satellite to earth (depicted as route 1 then route 2 by dashed line in Figure 3.4).
3. the link from sensor to Geo satellite to earth (this option is not evaluated in this dissertation).

4. the link from sensor to earth directly (this option is always possible, however, not all sensors can be accessed at one time).

3.5 Science Payload : Instrument Selection & Description

The purpose of this section is two fold (a) to determine whether the science instrument can fit on the smallest satellite platform, preferably pico or nano class of satellites, and (b) to determine the data being generated in terms of volume so as to assess data transfer rates from inter-satellite communications system.

3.5.1 Magnetometer

The required ranges and accuracies of magnetic field measurements appropriate to different plasma environments in Earth environment are shown in Table 3.2. Since these DC measurements would be taken from a moving platform, there will inevitably be a temporal variation, which will be characterised as part of the future work stated in section 7.3.

The commercially available 3-axis flux gate magnetometer by Honeywell Inc. (Figure 3.5) has been selected, which meets the range and accuracy requirements posed in Table 3.2. The magnetic field vector sensor requires additional electrical circuitry, to make it compatible for interface with the on board processor (computer requiring digital data). Honeywell also sell sensor with the additional electrical

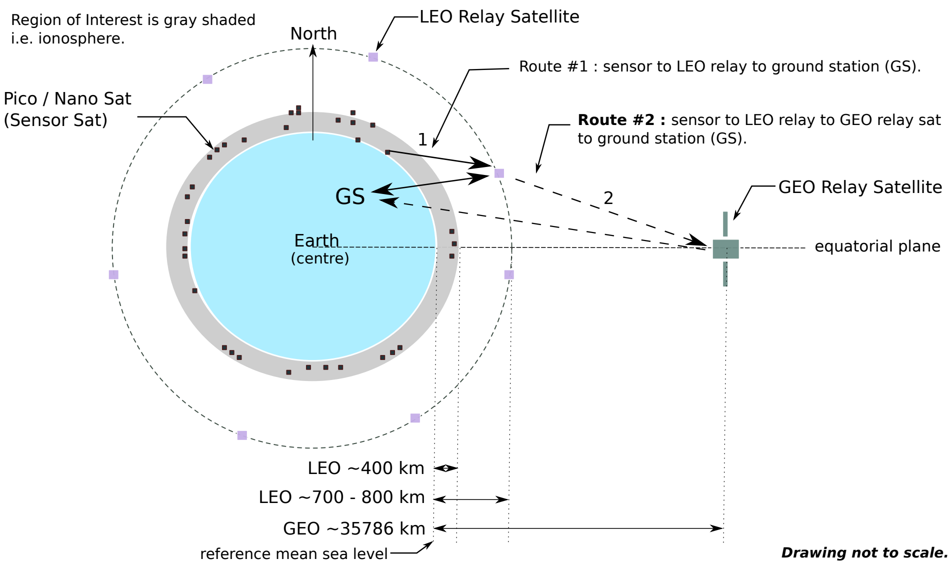

Fig. 3.4 Communications link routes from sensor to ground station (GS) as perceived in the proposed mission (IMM).

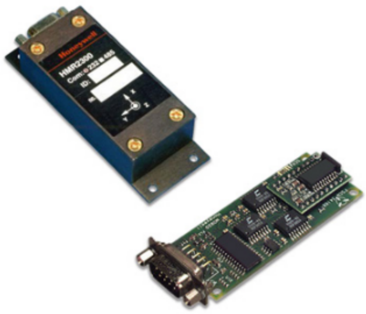

Fig. 3.5 The space qualified 3-axis magnetometer from Honeywell Inc. with and without cover, proposed for use inIMM [165].

Table 3.2 DC magnetic field measurement requirements in space science missions [161].

Environment	Range (nT)	Required Accuracy
Earth's field and low-Earth Orbit	$0-45,000$	$\sim 0.1-1$
Magnetosphere	$0-10,000$	$\sim 0.05-0.2$
Inner Heliosphere	$0-100$	$\sim 0.05-0.1$
Outer Heliosphere	$0-30$	~ 0.01

Table 3.3 The science payload magnetometer salient features and specifications from its data sheet [165].

Feature	Specifications	Comments
Digital Interface	RS-232 & RS-485	
Magnetic Field Range	± 2 Gauss	Sample rate varies from 10 to 154 samples per second
Power Consumption	0.525 Watts	
Sensor Type	Tri-axial flux gate	3-axis vector measurement
Size	$10.57 \times 3.81 \times 2.23$ cm	

digitisation circuit as part number HMR 2300 [165], which is taken as the basis for determining the data volume and data transfer rates*. Salient features of the product HMR2300 are shown in Table 3.3.

The instrument can measure all three axis that makes it "tri-axial" magnetometer. The sensor can generate a minimum of 480 bps using 10 samples per second, to a maximum of 7392 bps when 150 samples per second are selected. The analogue to digital conversion (digitisation) is 16 bit for each sample per axis. The small size makes it suitable for use in small confines such as in pico or nano satellite. In 1U CubeSat, the illustrated magneto meter may not fit easily, however, for 2U and above, the size is appropriate.

*Market survey and selection of the most appropriate equipment is not the intention here, rather determining the data transfer rates from an actual instrument which had been purchased and is available in house at the time of writing this thesis.

3.5.2 Langmuir Probe

The expected range of measurement in Earth's ionosphere [155] for the bulk properties of plasma such as the electron density are stated in Table 3.4. A preliminary search for commercial availability did not prove to be useful, therefore, a paper design of the Langmuir probe is carried out, which is described in this section. The aim is to estimate the power, mass and data transfer rate requirements of the instrument.

Table 3.4 Electron density, temperature ranges expected in Earth's ionosphere [155].

Parameter	Range	Units
Electron density N_e	10^8 - 5×10^{11}	m^{-3}.
Electron temperature T_e	600 - 10000	Kelvin
Spacecraft potential v_s	$\pm$ 3	Volts

Starting from the geometry to determine the size, shape and volume requirements of the instrument which leads to the spacecraft platform selection. The Langmuir Probe has two basic geometries (a) simple wire, and (b) a spherical ball. The two types of probe, and the magnetometer used on board DEMETER space mission are illustrated in Figure 3.6.

3.5.2.1 Probe Structure

The construction and working of the wire type probe is simpler than spherical. Moreover, the line can be twirled to fit within the small confines of the pico or nano satellite. It is recommended in [166], that the probe should consider the following points summarised as follows, detailed in Appendix E.2;

- The length of the probe be at least 30 cm, so that it could be immersed away from the wake of satellite, and probe the unaffected plasma. A smaller probe can also be used but its theory is complex, example of probe used in DEMETER, of diameter 3mm and length 7.5 cm [155].
- Two probes are suggested [155]; one aligned with the spin axis, and the other perpendicular to the spin axis as illustrated in Figure 3.7c. Thus as the spinning satellite moves, the two probes take simultaneous measurements thus incorporating directional plasma density with respect to the velocity vector .
- The LP be biased in a symmetric sweep mode with in the bias voltages ± 5 or ± 7 Volts (see Figure 3.7a).
- An in built cleansing mechanism be incorporated, with in the electronics of the probe.

3.5.2.2 Functional Description of Langmuir Probe

A brief functional description follows, where as detailed functional considerations are described in The voltage sweep from negative to positive region attract ions and electrons which cause a current to flow in

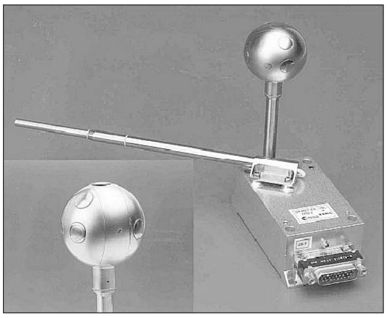

(a) Cylindrical and spherical shaped Langmuir Probe.

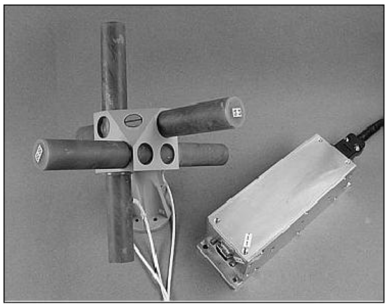

(b) Tri-Axial magnetometer.

Fig. 3.6 Custom built (science grade flight model) Langmuir probe and magnetometer used on-board DEMETER mission for illustration only (courtesy of [155]).

Langmuir Probe. The measured current when plotted against the applied voltage, makes a characteristic curve of current against applied voltage. The distinct regions of the curve provide parameters which are used in expressions which provide estimates of electron, and ion density as well as their temperature. The detailed description of LP working in described in Appendix E.2. The functional block diagram, the current voltage characteristic curve, and the placement of probe on the spacecraft is illustrated in Figure 3.7.

From the functional block diagram, the probe requires a voltage sweep generator of dual polarity and a sensitive electric current measuring electro-meter. A quick survey of market for available components that make up the electrical part acquiring the current and digitising the current and voltage. A preliminary assessment of power consumption and generated data can be carried out, which is briefly discussed as follows.

A paper design of the Langmuir Probe is described in section E.2.4, from which the electrical power consumption is estimated. The data volume generated is estimated based on the assumptions described in section E.2.5. Based on the working described in relevant sections, the electrical power and data budgets are described in the following section.

3.5.3 Budget Estimates of Payload Power & Data

The power budget estimate for our instruments using preliminary paper design is tabulated in Table 3.5. The values are worked out using basic components for the electronics for the probe, which is the electro-meter, voltage sweep generator and ADC/DAC. The magnetometer values are taken from its data sheet. These estimates allow the selection or design of electrical power, on-board computing and data handling and communications systems design.

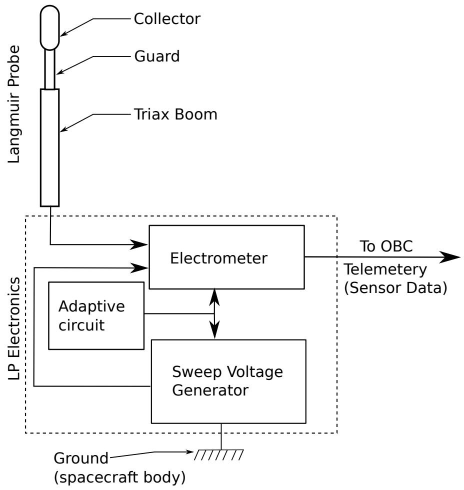

(a) Electronic Function

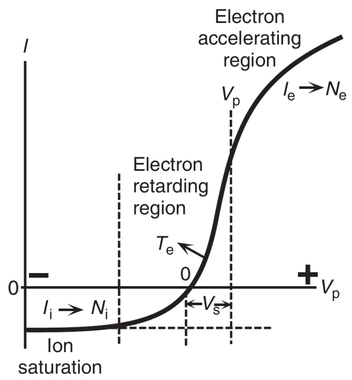

(b) $I-V$ Curve

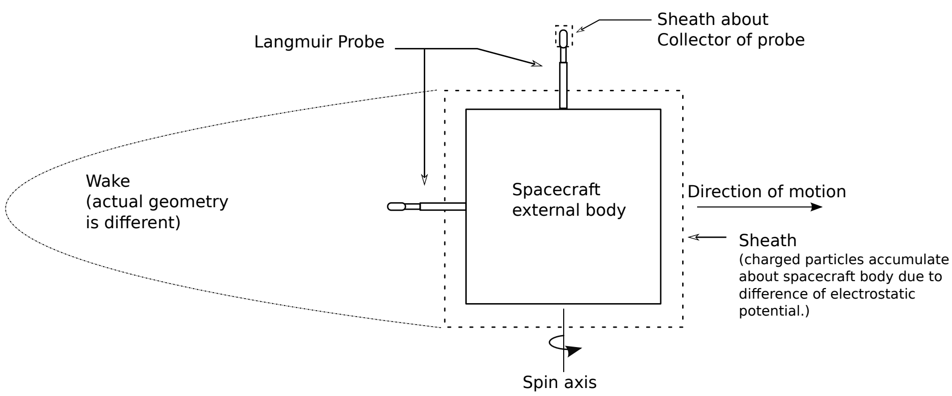

(c) Satellite Placement

Fig. 3.7 LP functional requirement, reference curve to determine electron density and placement on spacecraft attracting charged particles around collector, and the wake formed behind the spacecraft [166].

Table 3.5 Estimated Budgets for power, mass and data rates for science payload.

Payload	**Mass** (g)	**Size** (cm)	**Power** (W)	**Data** (bps)	**Comments**
LP	≤ 500	≤ 10	-	-	Diameter 0.3mm
LP Electronics	≤ 98	9.8 x 9.8 x 3	≤ 2	≤ 30000	Worst case scenario.
Mag. meter	≤ 98	10.57x3.81x2.23	≤ 0.525	≤ 7392	max sample rate

3.6 Proposed Satellite Bus-Systems

For normal operations, the science payload is to be mounted on a platform called the bus systems – an analogy of payload being the passengers and bus taking them safely to a destination while protecting them from the outside heat, dust & smoke. In case of spacecraft, the payload is supported by the sub-systems of the spacecraft, while protecting the payload from hazardous space environment.

The spacecraft platform could spin about its axis and be small in size so as to reduce contamination of ionised gas forming a plasma wake about the satellite [76, 167], but be large enough to hold the payload, and associated electronics, electrical and mechanical systems.

The basic functional bus systems for a satellite are listed briefly as follows.

1. **The electrical power system** (EPS) which generates electrical power for the rest of the systems. The main source of energy is the solar panels, which convert solar energy into electrical. A secondary source is rechargeable battery, which is generally used in times when solar light is not available, or when additional power by any of the sub-system is required.
2. **On-board computer and data handling system**: (OBC & DH) is the brains, where the microprocessor is programmed to carry out tasks at specified times. It also handles the data being stored in the memory, determining errors and correcting errors due to interaction of charged particles in-orbit. OBC interfaced to all other systems, gathers operational / working status (health) of systems, detecting system level faults, and passing the satellite health to ground operators.
3. **Attitude determination and control**: (ADC) determines whether the specified side of satellite is facing Earth, stars, or the Sun. The orientation of each side of satellite is generally referred to its “attitude”, which is first determined with the aide of several sensors, and then corrected using generated momentum by several means (momentum wheels, gravity gradients, or propellant based thrusters).
4. **Orbit control**: is a set of systems comprising compressed propellant and thrusters whose thrust is controlled by electronic valves. The thrusters assist in controlling / maintaining the attitude and orbit. This system is part of ADC therefore, together, it is called attitude and orbit control system (AOCS). In very small satellites these propellants and thrusters are left out to ease the complexity of design, thus the satellite operate in free flight mode i.e. its movement is controlled after ejection by natural forces.
5. **Thermal control**: keeps the temperature of within the housing maintained at each subsystem requirements.
6. **Communications and antenna system**: (COMS) is the next critical system of satellites, comprises electrical circuits for communications, and antenna. The type of antenna depends on the link budget calculations. The purpose of communications link is to allow monitoring of spacecraft operational parameters by the ground based operators / engineers. It also allows ground staff to upload tasks, commands to the OBC, which then schedules each task as per prescribed criterion. The purpose of beacon signal generator is to generate low data rate signals which are picked up by ground stations worldwide indicating that the satellite is alive.
7. **Inter-satellite communications system** (ISL) is in addition to the above stated typical set of sub-systems. For the space based wireless sensor network or any distributed satellite system, ISL is a primary communications system of the same critical level as ground communications system.

3.6.1 Sensor Satellite Bus System and Structure

The proposed bus system functional block diagram of the IMM sensor satellite is illustrated in Figure 3.8. The core intelligence lies with the central processor, and associated memory banks. The processor is linked to other bus-systems via electrical and mechanical interfaces. Each system provides a basic form of its status which is directly linked to the beacon signal generator. Keeping a separate beacon signal generator is to add redundancy and avoiding single point of failure. If the main ground link becomes inoperational at the time of launch or afterwards, then beacon signal generator can still send a simple form of telemetry (engineering data) indicating the operational status of satellite. Beacon signal is one way only, therefore no ground to satellite command upload is possible.

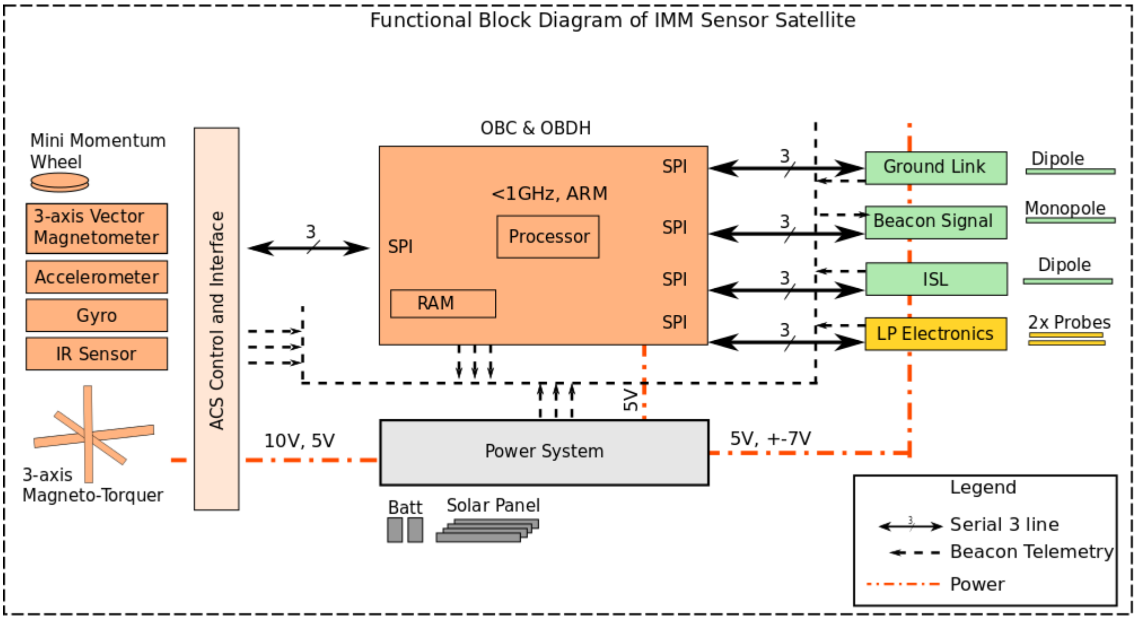

Fig. 3.8 The proposed bus-system architecture for pico/nano class satellites, used in IMM.

The inter-satellite link module and the ground link module can be made same, or different. Having the same modules, implies, hardware redundancy, so if one fails the other takes over. However, the concept of SBWSN is to allow each sensor satellite via a relay satellite.

The antenna for telemetry and telecommand is kept simple i.e. a dipole (see [26] for commonly used antenna on CubeSat). Antenna for beacon signal generator is kept mono-pole. Both can be kept folded before deployment and unfolded afterwards.

3.6.1.1 Sensor Satellite Physical Structure

ReSat and SenSat are assumed to be housing similar bus-systems. The only difference is that ReSat being larger than SenSat, can generate more electrical power from solar panels, can have better attitude and orbit control and house powerful transmitters interfaced to high gain directional or omni-directional antennas. Whereas, SenSat is much smaller in size, cost and mass, therefore, has less on-board resources to spare for bus-systems.

As is with any engineering problem, either an available solution or a custom design built is the first deciding factor. At the time when this dissertation started, at SSC, the available in house platforms were SNAP, CubeSat, PCBSat, and ChipSat. The simplest and effective platform for ease of development is the CubeSat and PCBSat, since unlike SNAP, they do not house any on-board propellant therefore, associated issues with attitude control are eliminated — simpler system design. With ChipSat, each system has to be designed using nano-technology, which again is complex and an active research field. Whereas, for CubeSat many sub systems including its flight ready structure are available as COTS, therefore, a satellite bus which can support a custom science instrument can be developed in a short time (section F).

Although CubeSat initially specified 3 basic structural platforms referred to as 1U, 2U and 3U [168], however, it has evolved into several possible configurations i.e. 0.5U, 6U, 12U as illustrated in Figure 3.9. PCBSat is similar to 0.5U, so two PCBSats can be combined to form a 1U CubeSat.

With the preliminary analysis, it is evident that magnetometer along with its electronics cannot be housed within 1U CubeSat, however, if magnetometer is separated into its sensor and electronics part, it can be

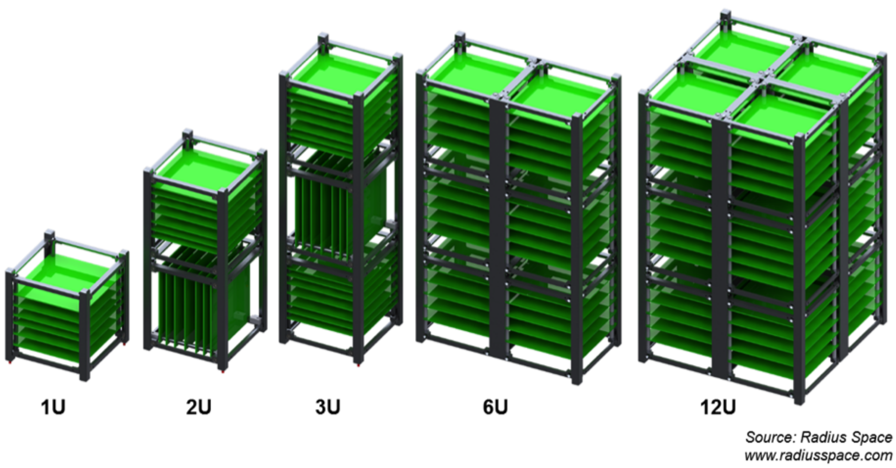

Fig. 3.9 Various configurations of CubeSat from a single unit to several units combined (courtesy of Radius Space).

fitted within 1U or less. Same is true with the Langmuir Probe. Furthermore, power requirements of LP are not readily met by 1U or less, owing to smaller solar panels fitted to its sides. A custom design of solar panels which could unfurl after deployment, can be a solution to the above stated power deficit. Increasing number of solar panels would affect other sub-systems as well, by taking up available volume which has to be shared with other bus-systems i.e. OBC, ADCS, COMS, ISL.

With the above considerations, it is safe to assume that 3U is a suitable structure for the sensor satellite. Furthermore, it is being proposed that PCBSat can be fitted in the extra space vacant. The PCBSat would act as daughters to the 3U CubeSat, providing extra resolution in measurement where and when needed. The daughters are attached to the main CubeSat with tethers, with the objective to retrieve them back when required. Since PCBSat houses similar electronics, including ISL, it can communicate with CubeSat, in close proximity. (Actual implementation and its issues are not discussed here, since the aim is to determine the impact on communications system for satellite to satellite links.)

The physical structure supporting the bus-systems and the sensors, along with the mother and daughter configuration is illustrated in Figure 3.10. The larger 3U CubeSat houses two PCBSats. The placement of antennas, LP, and the solar panels is illustrated. The bus-systems are single or double PCB cards interfaced with 20-pin headers shown yellow and dark blue blocks.

The probe and the dipole antenna configuration is also shown. The placement of the electrical sub-system and approximate sizes are also depicted, which gives a good idea of the space management and wiring considerations.

The main issue arising in the CubeSat platform is generating enough electrical power for the requisite payload and the communications systems. Primarily electrical power is generated from the solar panels. Increasing the solar panels in a manner that they are collapsed, during the launch phase is anticipated. Unfurling the solar panels would increase the surface area which captures the solar energy and converts it into electrical energy. Increasing the size of solar panels allows the increased area capturing solar energy. Therefore solar panels are to unfold when in orbit. The double surface area would roughly double the solar power generation. The use of on-board rechargeable batteries is essential. The batteries provide unaccounted for power surge required in burst transmissions or cleansing the probes, or discharging the spacecraft body.

To keep the centre of gravity in the middle, all electronics including the heaviest of batteries are placed roughly in the centre. The solar panels are of equal size, weight and are collapsible, extendable back to compensate for the change in centre of gravity when PCBSat are ejected.

A gravity gradient boom can be installed, or a furled antenna can be placed in the other vacant space above the electronics part.

Initially the antenna and probes are in a collapsed configuration, so the sensor satellite is just a rectangle. As soon as satellite is deployed, the antenna unfurl, the solar panels open up and unfurl, and with

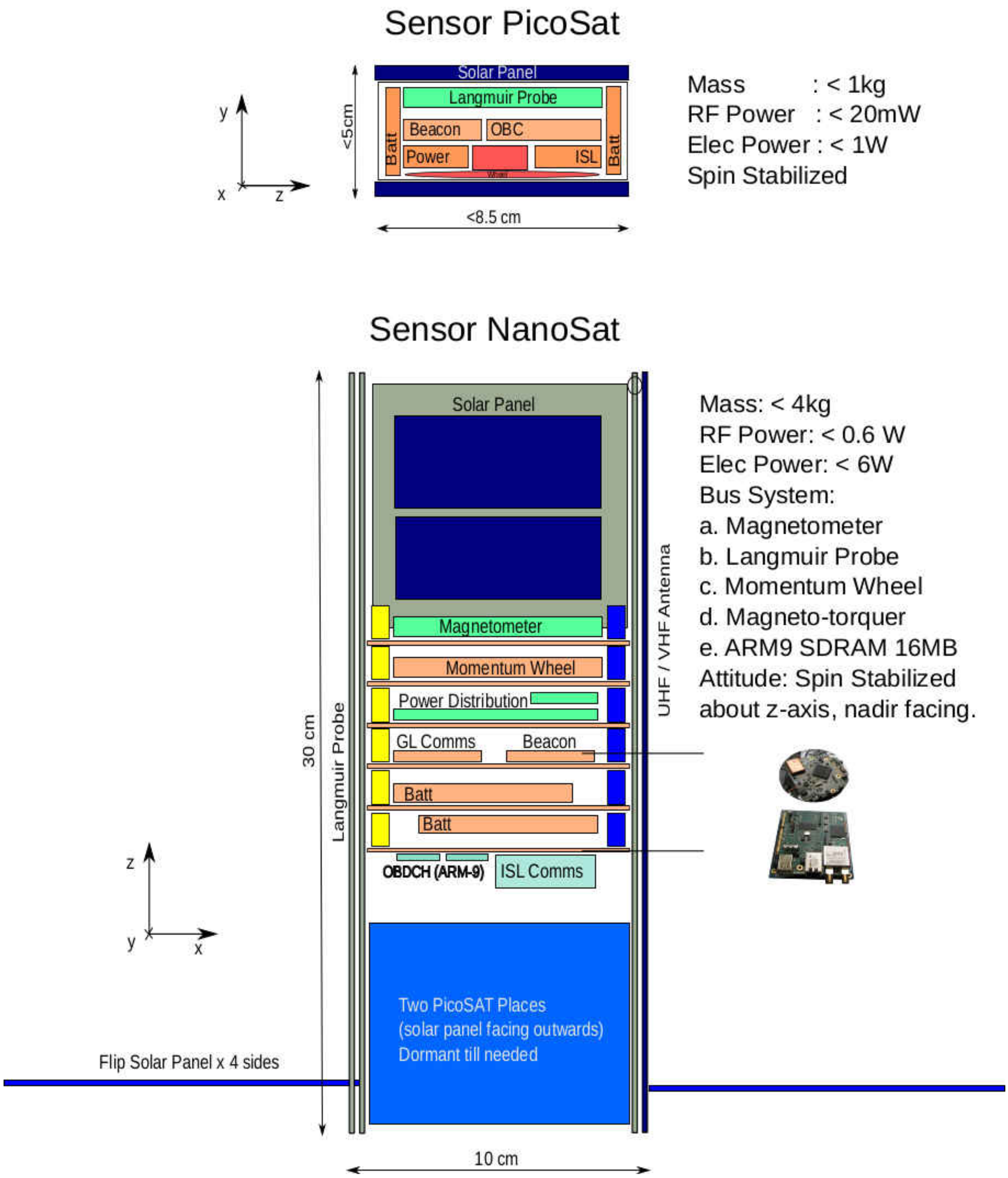

Fig. 3.10 The proposed mother daughter sensor satellite configuration for IMM.

the availability of electrical power, beacon signal starts generating its signal. Then initial checks are conducted by OBC, determining links with sub-systems. When all sub-systems reply, passively the satellite shifts its attitude to the desired

Since, inter-satellite communications is not a general requirements, therefore, its architecture, and possible hardware configuration is discussed, to complete the preliminary design definition of mission.

3.7 Inter-Satellite Link Hardware Sub-System

The purpose of this system is to enable the satellites (or any spacecraft) with capabilities to establish a communication link , transfer data and release the link after successful data transfer. The functional requirements assist the designer to select the most appropriate hardware and system architecture, based on several technology options available today, which are not known at this stage.

3.7.1 Implementation Choices

ISL is essentially a communications device, such as used for the ground link, whose basic functional block diagram is shown in Figure 3.11. As soon as the underlying architecture is defined, the components selection is simple. From implementation point of view, there are two options and third is a hybrid as briefly described as follows;

1. **Hardwired** is implemented be fixing the functionality of baseband modem, its oscillators and amplifier circuit. It is the most easy implementation, and is usually easier to optimise to consume less power. Since there is no room for other mode of operations unlike the other two implementations described as follows, only a hardware failure is possible. Therefore two redundant hardware implementation complimenting each other are desirable especially in space communications.
2. **Hybrid** is based on the digital processing technology, where the baseband is a software code. The digital signal is transmitted after conversion to analogue, and upgraded to the desired frequency. The designer has the choice of keeping some parts hardwired (fixed) and other configurable. For instance, the frequency conversion can be fixed, since it is governed by licensing authorities, and is not changed. The baseband signal processing also called MODEM can be soft coded. In this implementation, the most power hungry is the digital to analogue converters and the processors, depending on the processing power. Support for wider band of operations is power hungry.
3. **Software Defined** in which the analogue front end converts the signal directly to a digital signal without the steps of up conversion or down conversion, and all signal processing such as noise cancellation, automatic gain control, frequency tuning, synchronisation and baseband symbol detection is carried out in software. This is the most configurable solution but is also fragile. Any change in the code would render the complete system inoperative.

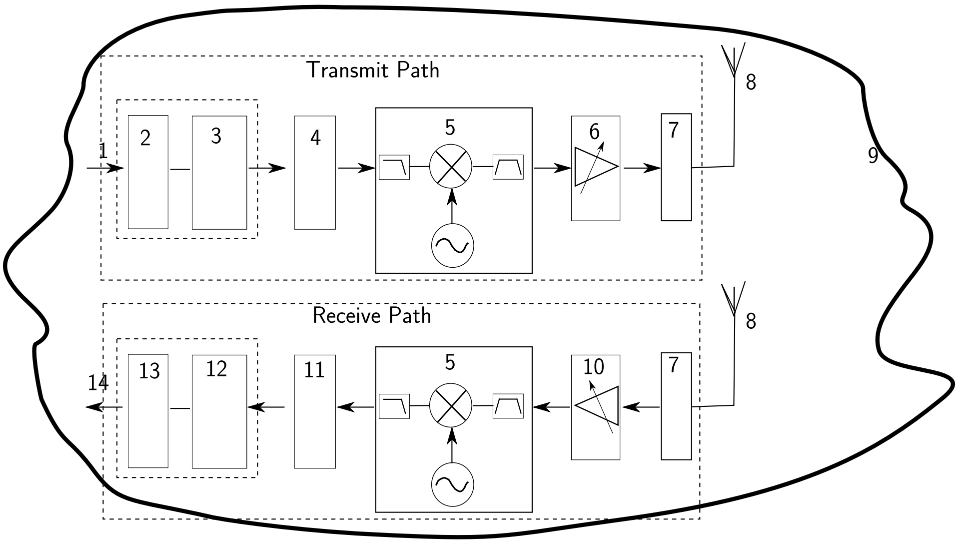

1. Digital Source
2.-3. Digital Signal Processing unit; Digital Mapper and Waveform Generator
4. Digital To Analog Converter
5. Frequency Converter. Up converter for Transmit, and Downconverter for Receive.
6. Power Amplifier
7. Antenna Matching Circuit
8. Antenna with its accessories
9. Operational Environment, also includes Channel.
10. Low Noise Amplifier
11 Analog to Digital Converter
12 -13 DSPU, with waveform estimator and demapper
14. Digital Sink.

Fig. 3.11 A digital communications functional block diagram illustrating the functionality of fundamental components and the flow path of signal. Each block can be implemented independently has a separate hardware or as soft code on digital signal processor. The operational environment governs the selection of implementation method e.g. underwater operations vs nuclear reactor operations or space operations.

For our consideration, the channel behaviour is unpredictable, and hostile. Therefore a configurable system is desirable. It would allow the link to be optimised to the actual channel characteristics observed at the receiver. Therefore the receiver should be intelligent enough to assess the channel.

The fundamental requirement is to support networking. IEEE 802 family of protocols based networking protocol for wireless access mature and well defined, the basis for the space compatible CCSDS "Proximity-1" protocol suggested by the European space consortium, are the two strong candidates. It is believed that any of the two would be required to work, therefore additional processing power for their medium access controller, and routing is to be kept in the hardware.

With the above two governing factors, we opt for a hybrid software defined radio implementation, so that maximum configuration options are available to the system designers as software codes, even after launch. Reconfiguration is an essential feature for systems deployed in unknown territories, therefore a software defined radio approach enables easy updates of the baseband modulation schemes as well as receiver design.

3.7.2 Frequency Selection

Today we have devices which can operate at various regions of the electromagnetic spectrum. The radio frequencies (RF) or microwave links is a generic term which refers to any communications system that does not use optical band.

There are two options when selecting the operational frequency which lies in the spectrum in the (a) Optical range and (b) Radio Frequency. Optical communications is carried out using laser, and tend to be less power hungry than their counter parts, but at the expense of additional support for maintaining high pointing accuracy [85, 84].*.

*Optical terminals have been suggested for range finding for soft landing on asteroids [169], mechanical systems tend to be heavy.

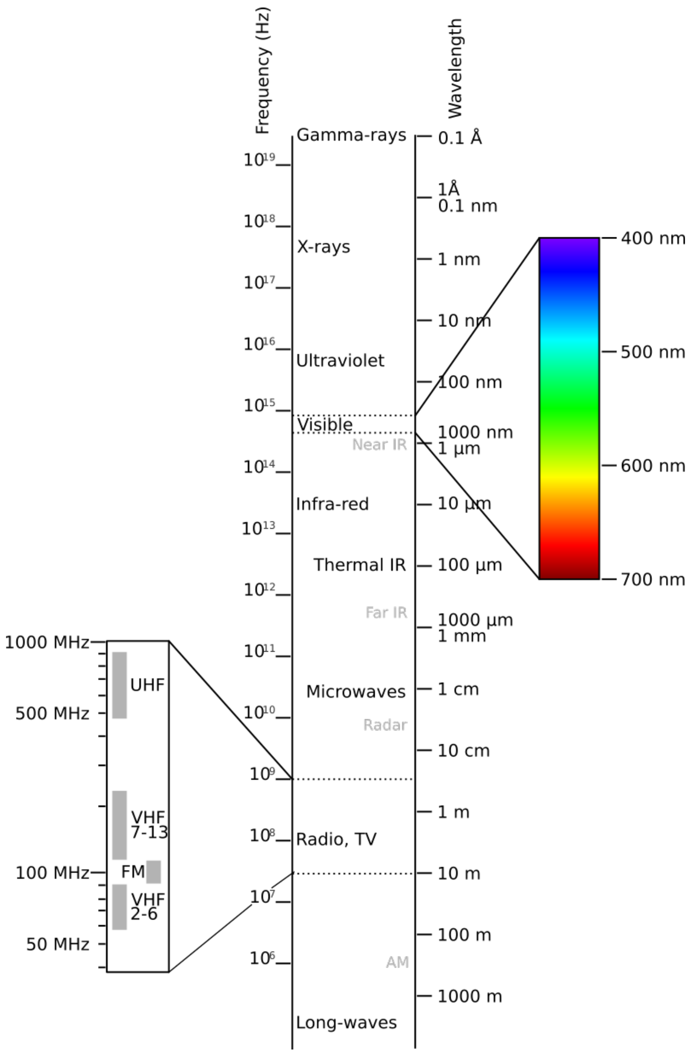

Fig. 3.12 The electromagnetic spectrum indicating the normal terms used in literature.

> "Practical laser communications is impeded by the inherent strict requirements on agile and accurate steering of the laser beam over a wide angular range that is addressed by the pointing, acquisition and tracking systems of Laser Communications Platforms [170]".

WiFi is cost effective because it also uses one of the ISM band. Using a COTS solution operating in one of the ISM bands, would eventually reduce the cost of development. But then the question arises, would the WiFi physical layer specifications be able to meet the dynamics and scintillation observed in LEO. The commonly used frequency bands in Amateur satellites and their proposed operations in the context of IMM is stated in Table 3.6, based on the available COTS in the two frequency bands.

3.7.3 Selection of Components

The ISL is divided in to three functional systems. The beacon signal generator, a high data rate sub-system, and a low data rate sub-system. Although one can implement all three in one system, but, with separate hardware, redundancy is achieved, and single point of failure is reduced.

For the beacon signal generator after extensive survey and many options, a simple Microchip RFPic is selected. It houses a complete analogue and digital part, in a single chip. It is easily programmable and provides a clean interface to other bus especially the OBC. The purpose is to generate continuous wave Morse coded words, sending the name, number and brief state of the systems as an audible message.

Since the data rate support is directly linked to the bandwidth used, therefore the bandwidth of the filters used in several stages determines the ideal data rates. Due to relative motion of satellites, significant Doppler shifts are anticipated, which add to the RF bandwidth and baseband bandwidth agility requirements (use of wide band adaptable filters). This is one of the reasons, to use two separate interfaces to support low and high data rates. Secondly for high data rate supports, the processing capabilities should be fast, as compared to low data rates. Fast processors in turn demand fast analogy to digital and digital to analogy converters. Typically the high end processors and ADC or DAC are power hungry components, which justifies our architecture to keep separate high data rate and low data rate paths. When high data rate is not being used, it can be powered down, reducing the consumption of power.

To overcome impairments due to channels, strong processing capabilities are required. The modem processing could be on an FPGA, or a DSP. As reconfigurability is foreseen, if the platform could afford

Table 3.6 ISM frequency available for use in Amateur satellite ground links, proposed for IMM.

Frequency	Band	Proposed Use in IMM
130.0000 - 139.9999 MHz	VHF	For beacon signal.
430.0000 - 439.9999 MHz	UHF	Ground link and Inter-Satellite sink.
2400.0000 - 2499.9999 MHz	UHF (S-Band)	Inter-Satellite link.

extra resources, both the FPGA and DSP could be employed. Since implementation is faster on DSP, but parallel execution is best handled by FPGAs. Ultimately, it boils down to the design, development and testing tools, and the skill set of developers, to select any of the two hardware for digital processing. However, FPGA is preferable for its complete design freedom. For instance, in a DSP the bus is either 32 or 64 bit, whereas, the bus width in FPGA is at our discretion. The precision of registers is similarly at our discretion, which allows flexibility, where higher precision or accuracy in numerical results is required. In this way, the FPGA circuits can be optimised to custom tailored designs.

Several COTS solutions were surveyed.This exercise was carried out several times, and is documented in the PDR for CubeSat design for Surrey University [171]. One of the possible set of components to go about preliminary design of the module is depicted in Figure 3.13. For budgetary purposes, available components such as the TriCore processor, and FPGA (Xilinx Spartan 3) were preferred over others. The power consumption, ease of implementation, size and availability was taken as the criterion for selecting devices.

The High Data rate Mode utilises the 20 MHz bandwidth, which is supported by Maxim Inc. product named MAX2830 [172]; a monolithic transceiver IC conforming to IEEE 802.11 g/b standard. It has a built in power amplifier which can generate an RF transmit power of 17.1 dBm, and several configurable parameters which would be useful during integration with baseband modem, and system OBC.

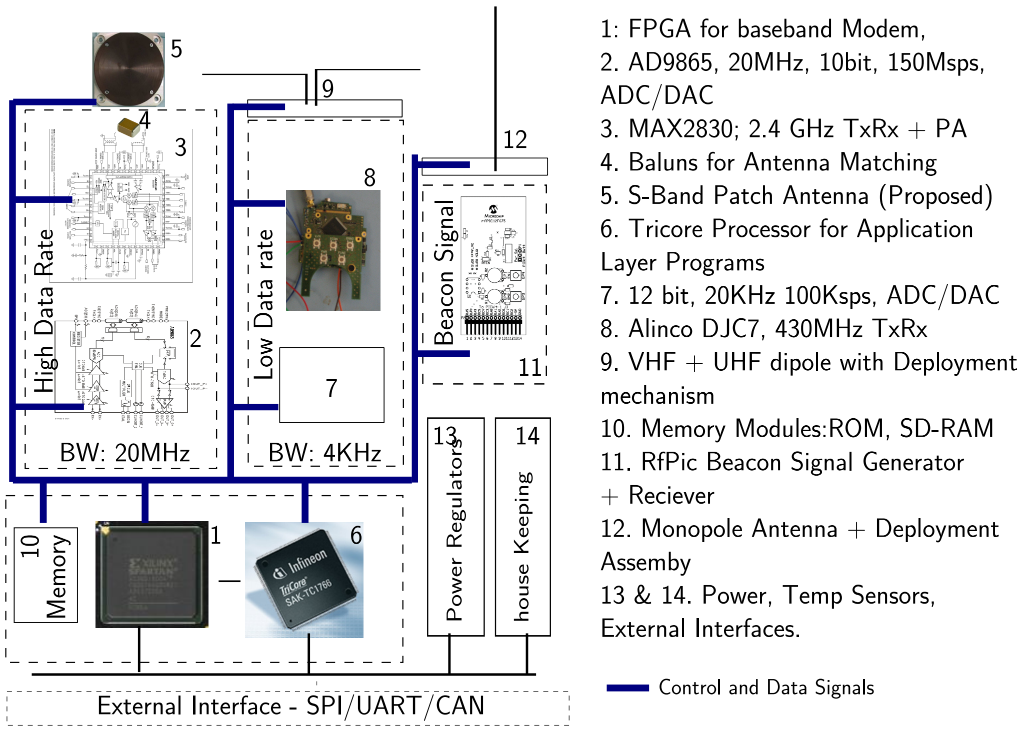

Fig. 3.13 ISL Communications Module hardware based on COTS. There are two operational modes, high Data rate on a directional antenna, low data rate on Dipole antenna. Beacon Signal generator and receiver is separate from main ISL transceivers.

An ADC/DAC from Analog Devices, for the interface between the radio and the DSPU. For the DSPU, both an FPGA or TriCore Infineon processor has been evaluated. The power consumption and a rough power budget is tabulated in Table (3.7). It is evident that, the power consumption of ISL module is about 3 W. Which means, that additional solar panels must be employed.

The maximum power that is consumed when either of the modes are operational, is 3.2 Watts, with an additional 30% for unaccounted passive components, line losses and such. In low data rate mode 2.1 Watts is expected to be consumed. The reason for keeping two different hardware components, and a third for the beacon signal, is to ensure as much basic redundancy as possible, and to cope with uncertain / unknown channel characteristics after deployment.

3.7.4 Antenna Selection

The requirement is to have an Effective Isotropic Radiated Power (EIRP) of 1 Watt, to comply with the regulatory. As for the directivity of the antenna is concerned, we also require networking with other satellites in the vicinity. This is not a point to point link, but in fact point to multi-point link. In IEEE 802.11 based networks, handshaking signals are sent to acquire the channel for communications, since a single frequency of operation is being used. Once the channel is acquired, then the rest of the transceivers are required to be quiet till the transmission is completed. Therefore all transceivers should be able to listen to any communication which is being carried out. Therefore omni-directional radiation pattern is a requirement, which is easily filled by a simple wire dipole. Other options require a configuration of patch antenna array configured to provide a rough isotropic radiation pattern.

Say if we use a configuration of antennas that generate circularly polarised waves isotropically, then the sense of polarisation matters. If the receiving antenna is not matched to receive the right sense of

Table 3.7 Power Consumption (worst case) one case of in house available hardware for ISL.

Component	Standby	Transmit	Receive	Comments
MAX2830	0.1155W	1.5471W	0.2122W	RF transceiver with built in amplifier complying IEEE 802.11 physical layer standard. Consumption at 85°C.
AD9861	0.0429W	0.592W	0.963W	Analogue to Digital Converter , Freq 80 Msps; Absolute max power dissipation 1.66 W at 85°C
TriCore	0.55mW	1W	1W	Processor, Maximum power when all peripherals are used, although much lower is anticipated during operations.
MAX9850	0.27μW	0.291mW	-	Digital to analogue converter
DJC7	0.0703W	1.11W	0.259W	Handheld FM Radio for point to point links. Maximum power consumption when display has been stripped off.

polarisation, effectively it would not be able to pick up the signal. This is considered in the scenario, that one sense of polarisation is generated then the same sense type antenna should be used in conjunction at the receiver. However, due to the nature of ionosphere plasma, wave propagating along the Earth's magnetic field would tend to have one sense of polarisation clockwise (CW) or counter clockwise (CCW). Different antennas would therefore be required at the receiving end to capture any one of the possible polarised wave.

A directional patch antenna operating in the S-band is perceived for experimentation of link at higher frequencies.

As for the antenna on the ReSat, it has to be high gain, and preferably steerable directional antenna, so that the link between the SenSat could be closed. ReSat is also required to be able to communicate with Geo Satellites. Therefore its antenna needs to be well defined, with the capability of generating circularly polarised waves of both senses (right hand and left hand). The gain of the antennas is not selected here, but is expected to be at least 5 to 10 dBi.

We leave the design of antenna and their mechanical interface to spacecraft in the hands of experts[173, 174], and proceed with the orbit selection.

3.8 Orbit Selection

The orbital elements are used extensively in the relative motion simulation in this section and in the study of relative motion therefore, they are defined here. There are several ways in which an orbit can be defined, we use Keplerian elements in our simulation based studies (see [175, 176, 177] for details and analytical approaches).

The orbit of a satellite around Earth is uniquely identified by six parameters called "orbital elements", "Keplerian elements" or "osculating elements". An arbitrary orbit around Earth is shown in Figure 3.14a. The shape of orbit can be any conic section, but for Earth based orbits it is generally an ellipse, whose one focal point is the centre of Earth. The orientation of the ellipse in space is defined with respect to Earth centred inertial (ECI) frame of reference denoted by $\hat{\mathrm{I}}$,$\hat{\mathrm{J}}$, and $\hat{\mathrm{K}}$ as shown in Figure 3.14a. The orientation of orbit with in this frame is defined by the following;

- i the inclination angle between the orbital plane with respect to Earth's equatorial plane.
- Ω the right ascension of the ascending node indicates the angle between vernal equinox and the point on orbit at which satellite crosses equator from south to north.
- ω the argument of perigee angle between the ascending node to the line of perigee.

The elliptical orbit is defined by its parameters as shown in Figure 3.14b. The extreme points of an elliptical orbit are apoapsis and periapses. The geometry of the ellipse is defined by the semi-major axis

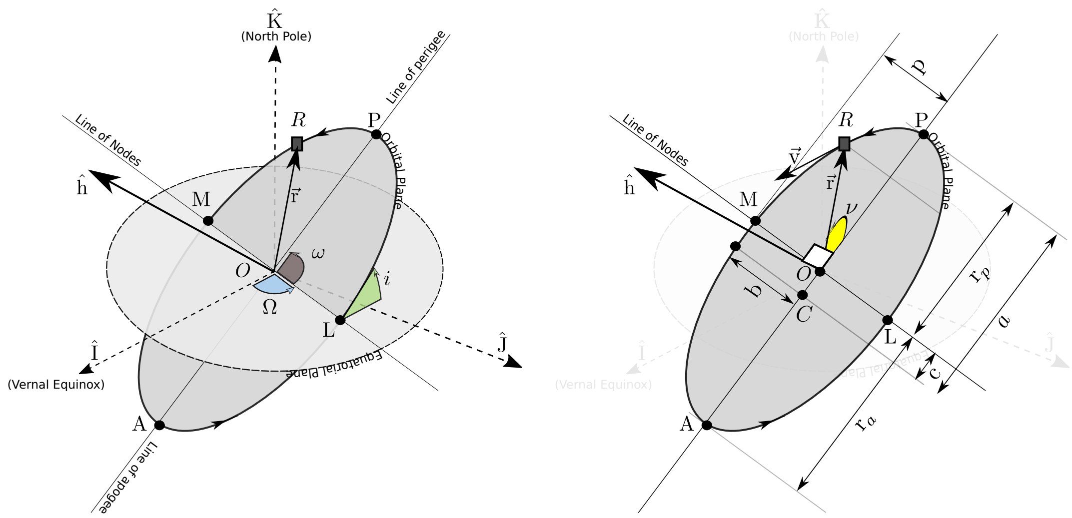

(a) Orbit in space **(b)** Perifocal orbital plane.

Fig. 3.14 Orbital elements defining the orbit, the unique position in orbit, and the orientation of orbit in space.

a, semi-minor axis b, and the eccentricity of the ellipse e defined as $e = c/a$. The "semiparameter", p is the perpendicular distance from the primary focus O to the orbit. The semiparameter is also called "semilatus rectum" or simply the "parameter". The semiparameter is related to eccentricity according to Eq. (3.1).

$$p = \frac{b^2}{a} = a(1 - e^2) \tag{3.1}$$

where eccentricity is defined as in eq. (3.2).

$$e^2 = \frac{a^2 - b^2}{a^2} \tag{3.2}$$

Throughout the orbit, the position of satellite is represented by the position vector $\vec{r}$, which is the radius from O. The "altitude" is measured from the surface of Earth to a location on orbit. In a circular orbit $e = 0$, therefore altitude appears unchanged for the orbit, whereas in elliptical orbits altitude varies. For very small eccentricities, often the terms are used interchangeably in literature which is sometime confusing.

The position of a satellite within the orbit is defined by the angular displacement $\angle \text{ROP} = \nu$, called the true anomaly, taken in the direction of satellite velocity $\vec{v}$. P is called perigee, which is the closest point to the focal point O, where as the farthest point A is called apogee. The point L is called the ascending node defined as the point where the satellite cuts the equatorial plane when moving from south to north. Similarly the point M is defined as the descending node. The angular momentum of the orbit is represented by $\hat{h}$, which defines the energy of the orbit.

3.8.1 Special Orbit Types

Table 3.8 describes special orbits used in Earth bound missions. Since COTS based small satellites are to be used, and ionosphere monitoring is the intended objective, LEO is the region of interest. Other orbits of significance are described for the sake of completion and reference for other missions.

Table 3.8 Characteristics of Special orbits commonly used in Literature. (For details see Vallado [175]).

Orbit Type	Description	Application
GEO[a]	Earth centric orbit, altitude≈38000 km with a period same as Earth's sidereal day. Manifested by direct radiation dosage.	Communications satellites broadcasting video services with no impact on propagation delay, appearing to be stationary in the sky.
LEO[b]	Earth centric orbits, altitude between 160 & 1100 km. Safe from high radiation dosage but, manifested with atmospheric drag pulling satellites to Earth	Earth observation missions and Global Communications service by satellite constellations, supporting lesser end to end propagation delays.
MEO[c] or ICO[d]	Earth centric orbits between LEO and GEO, avoiding Van-Allen Belts of charged particles. Almost no atmospheric drag.	Constellation of satellites providing Global Positioning (GPS) service, Global Communications service
Molnya	Highly elliptical orbits	Communications satellite spend major chunk of their time over a region of Earth. Russia uses Molnya orbits to harbour its communications satellites, since GEO satellite signals are severely disrupted due to low inclined antenna picking up ground noise. Science missions to cover a specific region more than others in the magnetosphere, ionosphere study.
Polar Orbits	Nearly circular orbits passing over the poles of Earth, inclined at $\pm 90°$.	Earth observation, surveillance.
Sun Synchronous	A nearly polar orbit around a planet, in which the satellite passes over any given point of the planet's surface at the same local mean solar time	Missions requiring same lighting conditions[e] over target region on Earth.
Halo	Special regions in inter-planetary space where "n-body forces of attraction" cancel out e.g. Sun, Earth and Moon.	Lagrange points (liberation points) e.g. L1 on Sun-Earth line ISEE-1 mission monitored solar wind.
Frozen Orbits	an orbit for an artificial satellite in which natural drifting due to the central body's shape has been minimised by careful selection of the orbital parameters	Applications requiring repeating ground tracks useful in Earth imaging.

[a]Geostationary, geosynchronous Earth orbits
[b]Lower Earth orbits
[c]Medium Earth Orbits
[d]Intermediate Circular Orbits
[e]Shadow of object at each pass of satellite is consistent with earlier pass.

3.8.2 Proposed Mission Orbits

Of the many types of orbits, the most feasible for our case would be near polar orbit, retrograde with respect to Earth's motion. In reality a small eccentricity is always present, meaning, true circular orbits are not practically viable. For the sake of discussion, and ease of estimation, assume circular orbits where the average speed is about 7 km/s at altitude of 600 km. In one second the sensor has moved 7000 meters. So a second sensor placed at say 1000 meters from the first, would be following the first, would enable the desired spatial resolution. The revisit time of the same spot is after about 24 hours; note that revisit times depend on the actual orbital elements. Each sensor is capable of taking a measurement in 1 sec, repeating measurement every 1 min.

Now the next measurement takes place after 60 seconds. Then the spacecraft have travelled a distance of 420000 meters. This is a disadvantage in LEO where orbit mean speeds are high. Now to be able to cover this area we need to place a satellite every 1000 meters. To cover 420000 meters there are going to be 420 sensors. Placing that many sensors is an overkill, however, if done, would yield unprecedented information about the ionosphere.

The alternative is to place sensors in a cluster of small groups. Each group spans a space of radius 1 km, with 10 sensors, then a resolution of 100 m is achieved.

The alternative is to relax the spatial and temporal resolution so that, one sensor satellite carries two or more daughter satellites with it. They are tethered to the mother sensor satellite and revolve around it. Tethering allows the mother to retrieve the daughter satellite, and can deploy again later when needed. Alternatively, if tether is not used, the daughter is released once.

The angular momentum of the satellites is aligned with the orbital energy. Say the tether length is about 100 m or less, then the separation of the two daughter probes is 200 m. As the mother satellite moves with the same 7000 m/s speed, taking measurements every 1 min, the daughter satellites take the measurements around the mother satellite, thus improving spatial coverage.

Another mother satellite also need to be placed about 2000 m behind the first. The tethered satellites are a proposal, however, the physical length depends on how the reel is made, and the density of the tether.

It is apparent from this simple discussion, there are several ways the sensors can be placed, and their placement is restricted to their mode of deployment, their ability to maintain their orbit. Since CubeSats inherently are free flying objects, they have difficulty maintaining the orbits. So a resolution just figured out would not last for long, however the number of satellites still increase the spatial resolution.

3.8.2.1 Retrograde Polar Orbits

The near polar retrograde orbit has a property that it revolves opposite the motion of the Earth's angular motion. In this way the satellite traverses almost all of the longitudes (with a gap between the ground track). To illustrate this point, a record of the locations satellite traversed over 10 hours from the start of its orbit are recorded, and marked for illustration in Figure 3.15. Another snapshot of the coverage area is after 24 hours.

3.8.2.2 Three Proposed Orbital Configurations

There are three known regions which exhibit distinct characteristics in Earth's ionosphere namely the equatorial, mid-latitude and the two poles [178]. All of these are of considerable interest and need to be monitored. So the purpose is to set the orbital parameters such that these regions are covered.

For the interested regions the associated type of orbits would be as follows;

1. When the region of interest is mid latitude (30 to 70 deg), avoiding the poles (70 - 90 deg), then inclined orbits are preferred.
2. When the region of interest is the pole, then strictly polar orbits of about 90-97 deg inclination are preferred. The polar orbits have the advantage that they enable satellites to actually traverse almost all latitude and longitudes above Earth. The poles at lower altitude exhibit dense charged particles with high energy, which can be harmful to the satellite electronics.
3. Where as for the equatorial region only, then less inclined orbits are more preferable.

The Figure 3.16 illustrates three distinct orbital configurations using several satellites. The dotted lines are the footprint of satellites on ground, illustrating the region being covered as they move in orbit. Dots also represent that measurements are discrete, not continuous. A Walker constellation is used, simulated for a couple of days. Illustrations are prepared by using Savi and its constellation design tool [179].

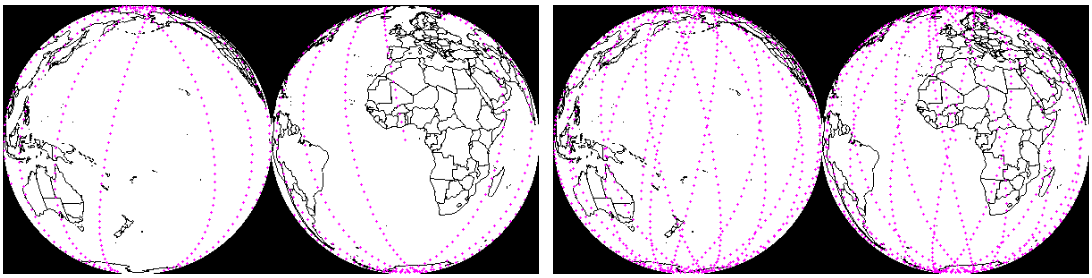

(a) Coverage area after 10 hr. **(b)** Coverage area after 24 hr.

Fig. 3.15 Illustrating the coverage of satellites in near polar circular orbits after 12 and 24 hrs, using the spherical projected Earth.

Relative motion assessment and Doppler shift is the topic of Chapter 4, in which selected cases are discussed in detail.

3.9 End of Life Estimations

The death of a satellite can be from any of the following reasons

1. loss of a communications link with the satellite especially telemetry and telecommand,
2. loss of on-board fuel or loss of on-board capability to conduct orbital manoeuvres
3. when the mission is successfully completed i.e. the main objectives have been met.

In the case of a successful mission, the satellite is shifted to a different orbit, vacating space for other satellites. In the case of GEO, the graveyard is at higher altitudes, whereas, in the case of LEO, satellites are allowed to fall towards Earth to burn themselves as they enter the neutral denser atmosphere below 100 km altitude. The high frictional force generates enough heat to disintegrate the metal structure, burning the satellite in air.

In estimating EOL for free falling satellites such as CubeSats, their orbit needs to be assessed under the influence of perturbations other than the gravitational pull, particularly the atmospheric drag. The drag is proportional to the orientation of satellite's surface area relative to the velocity vector. As the satellite lose its angular momentum, it loses its altitude, eventually falling back to Earth. The spacecraft disintegrates on entering the denser neutral atmosphere at altitudes less than 100 km. The satellite in LEO is thus considered to have reached its End of Life (EOL).

The small satellites whose characteristics are given in Table 3.9, are potential members of IMM, thus are selected for determining EOL. The surface area, mass and overall dimensions of the member satellites are stated in Table 3.10. The orbits of each of the satellite is simulated using the numerical orbit propagator by [176]. Each one of the satellite is assumed to be deployed at an altitude of 600 km (see Table 3.9 for other orbital parameters), and allowed to fall freely under the effects of perturbing forces

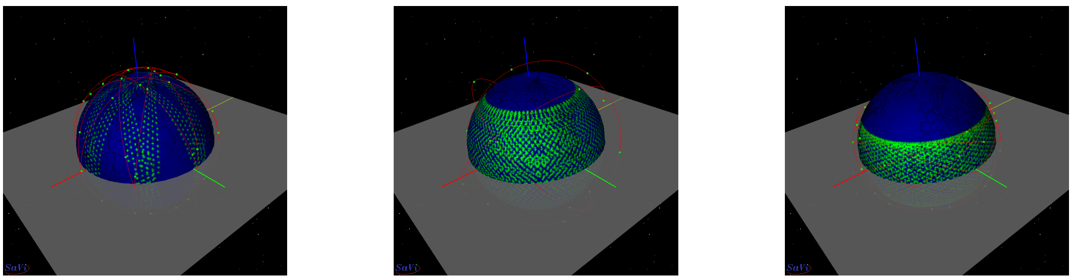

(a) Poles. $i = 97°$ **(b)** Mid-latitude $i = 70°$. **(c)** Equatorial $i = 10°$.

Fig. 3.16 Placement of satellites in orbit to cover three distinct regions of Earth, the poles, the mid-latitude and the equator.

listed in Table 3.11. The EOL is determined at the time when the altitude drops below 150 km (see Figure 3.17 as an example).

Table 3.9 Orbital elements used for LEO orbit decay for satellites in Table 3.10.

Parameter	Value	Comments
Semi-major Axis	6978.173 km	Altitude 600 km
Inclination	98.57°	Polar orbit
Eccentricity	1×10^{-6}	Near circular orbit
Right Ascension of the Ascending Node	0.0	
Argument of Periapses	0.0	
Mean Anomaly	0.0	

Table 3.10 Satellites mass, surface area and area to mass ratio, used in orbit propagation to study decay.

Satellite Name	Mass kg	Surface Area m^2	Area/Mass m^2/kg	Comments
PCBSat [23]	0.02	0.01	1/2	10x10x2 cm
CubeSat 1U [168]	1	0.01	1/100	10x10x10 cm
CubeSat 1U	2	0.01	1/200	
CubeSat 3U	3	0.03	1/100	10x10x30 cm
CubeSat 3U	5	0.06	3/250	10x10x60 cm extra Solar panel
MicroSat	50	0.25	1/200	50x50x50 cm (hypothetical assumption)
UoSAT [164]	50	0.11	1/250	33x33x53 cm + Gravity Gradient Boom

Table 3.11 Perturbation force and their configurations used in the orbit propagator from Montenbruck [176].

Parameter	Settings
Epoch time	00:00:00, 01 March 1999
Gravitational Field Model	Joint Gravitational Model (JGM) No.3, 20x20
Atmospheric Drag	Modified Harris Priester Model (Ballistic Coefficient: Cd=2.3)
Other Perturbing Forces	Third body effects, Solar radiation pressure
Propagation time step	120 s

The simulated satellites are PCBSat, CubeSat 1U and MicroSat (Table 3.10). All satellites are assumed to be free falling, therefore, the natural decay of orbit is simulated. PCBSat has the shortest lifespan since it's mass is least of all the considered satellites. In Figure 3.18c the EoL is achieved at about 16000 min equivalent to 266.67 hrs or ≈11 solar days in orbit. Even if large number of PCBSats are deployed in the order of hundreds, they would not be a hazard nor a source of space debris. On the other hand, a significant increase in spatial resolution in measured data can be achieved.

CubeSat 1U with mass 1 kg can live up to about 84000 min i.e. 1400 hrs or 58 solar days as shown in Figure 3.18a. Whereas, MicroSat in Figure 3.18b can stay in orbit for about 170000 min equivalent of 118 solar days. A CubeSat 1U with 2 kg mass was simulated to study the effect of area to mass ratio, which turns out to be similar to MicroSat in Figure 3.18d.

In the above simulations, it has been assumed, that the satellite surface is always facing the velocity vector. Whereas, in reality, in free flight mode, the satellites would be tumbling initially till their

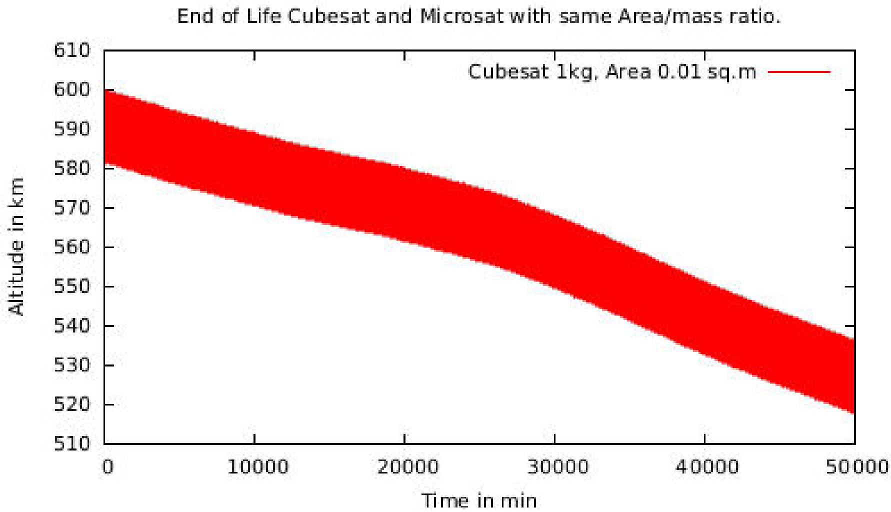

Fig. 3.17 CubeSat orbit decay from an altitude of 600 km. The wide line shows the variation between apogee and perigee. Decay rate is (590-530)/(50000) =0.0012 km/min.

attitude is stabilised. Spin stabilised for sensors whereas relay satellite which would be 3-axis stabilised. Therefore, the actual decay would be slower than the simulated extreme values.

It has been concluded, that if the lifespan of the sensor satellites needs to be increased, their area to mass ratio, be reduced, in the free flight mode (without on-board orbit control facility). It is observed that with the same area to mass ratio, irrespective of the size of satellites, the orbit decay rate remains the same as illustrated in Figure 3.18d.

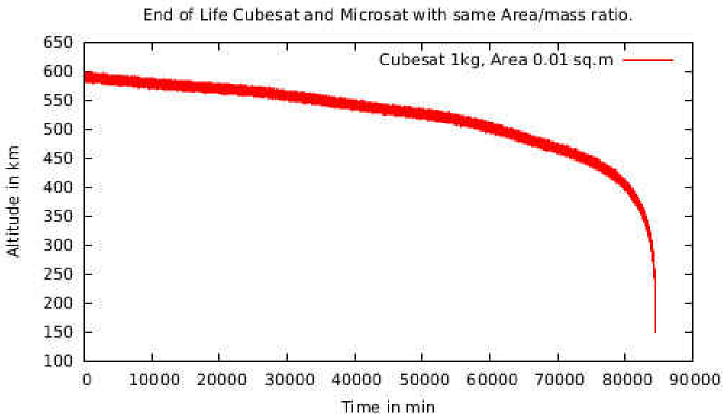

(a) 1U CubeSat 1 kg

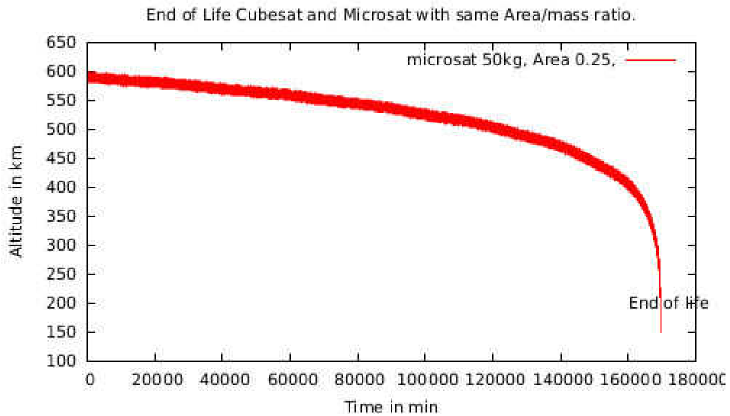

(b) MicroSat 50 kg

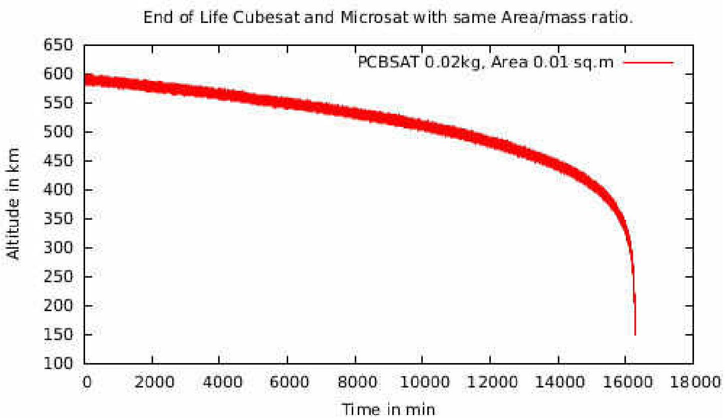

(c) PCBSat 0.02 kg

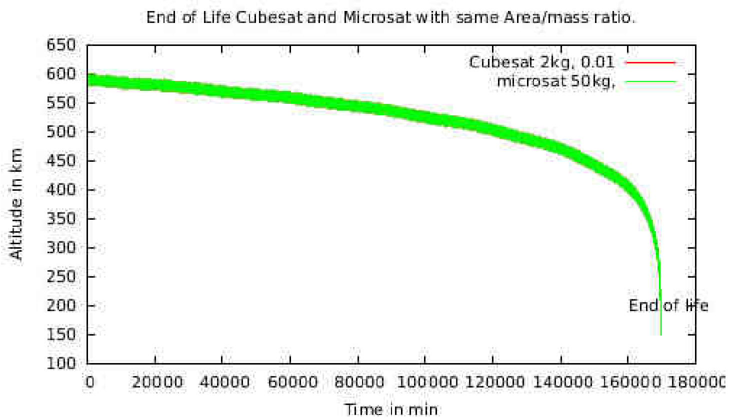

(d) 1U CubeSat 2 kg (hypothetical) and MicroSat 50 kg

Fig. 3.18 End of Life (EoL) estimates of pico/nano class of satellites in free flight mode. PCBSat de-orbits within a month, CubeSat 1 kg takes 2 months whereas MicroSat takes 4 months.

3.10 Link Budget Estimates

This section calculates estimates of the communications RF power requirements by carrying out link budget calculations, based on the assumptions and perceived operations of sensors and relays in the SBWSN deployed in LEO. The link budget is calculated for three frequencies and various link ranges, where no fading is assumed. Fading is the topic discussed separately in section 5.4.1.

The Link Budget depicted graphically (Figure 3.19) is calculated on the basis of self explanatory parameters whose values are given in Table 3.12 Table 3.13 and Table 3.14. The carrier to noise power ratio for expected data rates at 430 MHz are calculated while shown in Figure 3.19(a), for 900 MHz in Figure 3.19(b) and for 2400 MHz in Figure 3.19(c). The evaluation is done for separations in the range from 200 to 1000 km in steps of 100 km.

Links between relay satellite and geostationary satellites are not discussed here, although they follow the same evaluation method.

Link Budget Tables

The link budget tables are stated here which give us a rough estimate of the requirements the modem has to achieve. Three frequencies have been selected and three bandwidths have been selected for preliminary analysis. The tables calculate the carrier to noise ratio for different bandwidths.

To read the link budget calculation consider Table 3.12. There are three sub-sections, which compute the link budgets for 430, 900 and 2400 MHz (top to bottom). The vertical line separates the link budget parameters (left hand side) from the link calculations (right hand side) for the listed distances in the top most row of each section. For 430 MHz carrier frequency, at 200 km, the available C/N is 17.6 dB (read second column after the vertical line); at 600 km C/N is 8.13 dB and so on. The anticipated losses used in the link budget calculuations are, path loss, polarization loss, plasma loss and pointing loss (see Maral[115] or Evans[78] for standard definitions). Since there is no neutral atmosphere nor rain in the inter-satellite link, therefore, these losses are not considered*.

*The same format is used in calculating satellite to ground links, that is why unused parameters are kept in the tables.

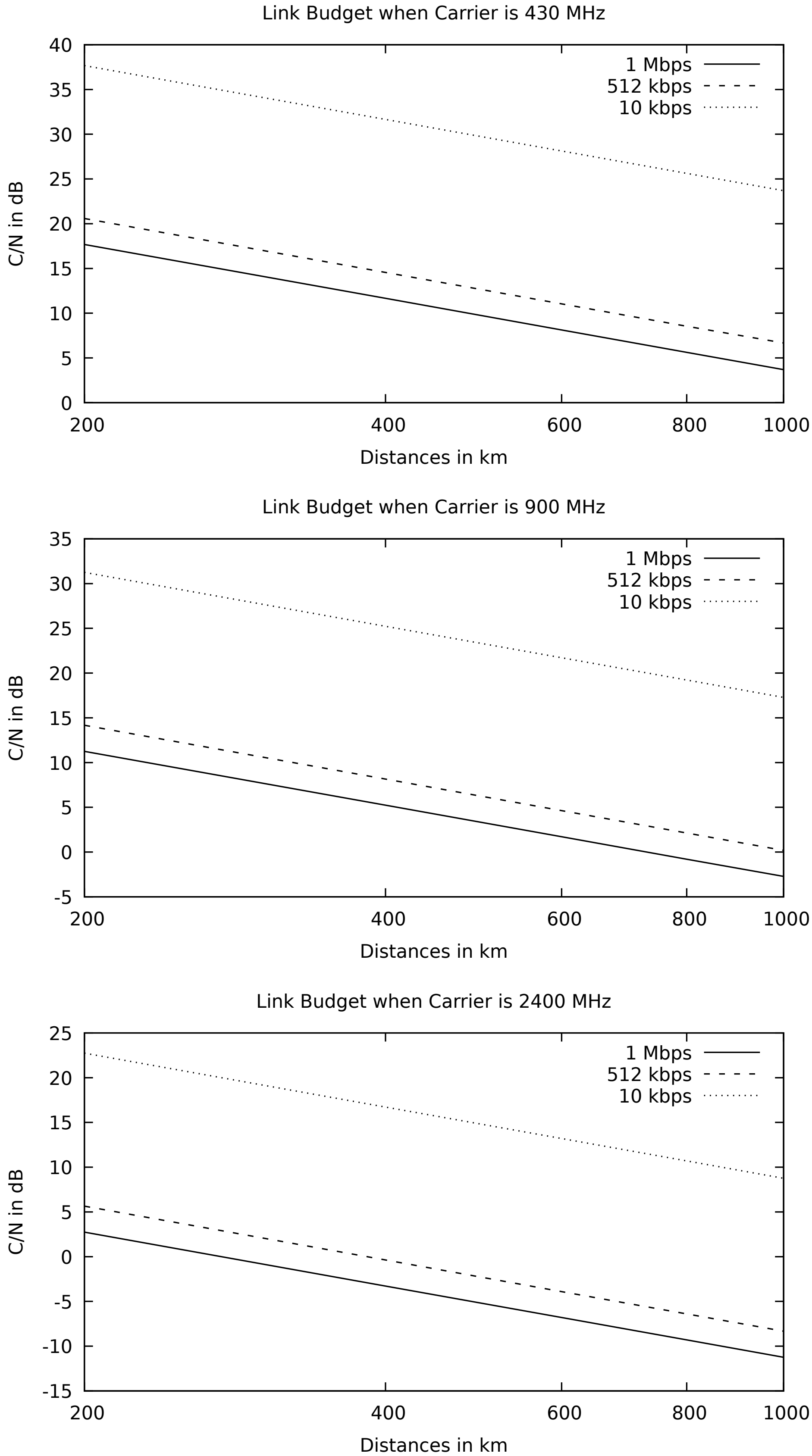

Fig. 3.19 C/N for data rates 1 Mbps, 512 kbps, 10 kbps (a) 430 MHz using Table 3.12, (b) 900 MHz using Table 3.13 and (c) 2400 MHz using Table 3.14.

Table 3.12 Link Budget Calculations for datarate of 1 Mbps

		Operating Freq 430 MHz					
		Distance (km)	200	400	600	800	1000
Wavelength (m)	0.70	EIRP (dBm)	30	30	30	30	30
Bandwidth (dBHz)	60	Lpath (dB)	131.13	137.15	140.67	143.17	145.11
Bandwidth (MHz)	1	Lpol (dB)	3	3	3	3	3
Required C/N (dB)	14	Lplasma (dB)	3	3	3	3	3
Boltzmann's Constant (dBW/HzK)	-228.60	Lpointing (dB)	3	3	3	3	3
T (dBK)	40.80	Latm+rain (dB)	0	0	0	0	0
Noise Temperature (K)	12000	Rx gain (dB)	0	0	0	0	0
		Noise (dB)	-127.81	-127.81	-127.81	-127.81	-127.81
		Available C/N (dB)	**17.68**	**11.66**	**8.13**	**5.63**	**3.70**
		Operating Freq 900 MHz					
		Distance (km)	200	400	600	800	1000
Wavelength (m)	0.33	EIRP (dBm)	30	30	30	30	30
Bandwidth (dBHz)	60	Lpath (dB)	137.55	143.57	147.10	149.59	151.53
Bandwidth (MHz)	1	Lpol (dB)	3	3	3	3	3
Required C/N (dB)	14	Lplasma (dB)	3	3	3	3	3
Boltzmann's Constant (dBW/HzK)	-228.60	Lpointing (dB)	3	3	3	3	3
T (dBK)	40.80	Latm+rain (dB)	0	0	0	0	0
Noise Temperature (K)	12000	Rx gain (dB)	0	0	0	0	0
		Noise (dB)	-127.81	-127.81	-127.81	-127.81	-127.81
		Available C/N (dB)	**11.26**	**5.24**	**1.72**	**-0.80**	**-2.72**
		Operating Freq 2.4 GHz					
		Distance (km)	200	400	600	800	1000
Wavelength (m)	0.125	EIRP (dBm)	30	30	30	30	30
Bandwidth (dBHz)	60	Lpath (dB)	146.07	152.09	155.61	158.11	160.05
Bandwidth (MHz)	1	Lpol (dB)	3	3	3	3	3
Required C/N (dB)	14	Lplasma (dB)	3	3	3	3	3
Boltzmann's Constant (dBW/HzK)	-228.60	Lpointing (dB)	3	3	3	3	3
T (dBK)	40.80	Latm+rain (dB)	0	0	0	0	0
Noise Temperature (K)	12000	Rx gain (dB)	0	0	0	0	0
		Noise (dB)	-127.81	-127.81	-127.81	-127.81	-127.81
		Available C/N (dB)	**2.74**	**-3.28**	**-6.80**	**-9.30**	**-11.24**

Table 3.13 Link Budget Calculations datarate 512 kbps

		Operating Freq 430 MHz					
		Distance (km)	200	400	600	800	1000
Wavelength (m)	**0.70**	EIRP (dBm)	30	30	30	30	30
Bandwidth (dBHz)	**57.10**	Lpath (dB)	131.13	137.15	140.67	143.17	145.11
Bandwidth (Hz)	**512000**	Lpol (dB)	3	3	3	3	3
Required C/N (dB)	14	Lplasma (dB)	3	3	3	3	3
Boltzmann's Constant (dBW/HzK)	-228.60	Lpointing (dB)	3	3	3	3	3
T (dBK)	40.80	Latm+rain (dB)	0	0	0	0	0
Noise Temperature (K)	12000	Rx gain (dB)	0	0	0	0	0
		Noise (dB)	-130.71	-130.71	-130.71	-130.71	-130.71
		Available C/N (dB)	**20.58**	**14.56**	**11.04**	**8.54**	**6.60**

		Operating Freq 900 MHz					
		Distance (km)	200	400	600	800	1000
Wavelength (m)	**0.33**	EIRP (dBm)	30	30	30	30	30
Bandwidth (dBHz)	**57.10**	Lpath (dB)	137.55	143.57	147.10	149.60	151.53
Bandwidth (Hz)	**512000**	Lpol (dB)	3	3	3	3	3
Required C/N (dB)	14	Lplasma (dB)	3	3	3	3	3
Boltzmann's Constant (dBW/HzK)	-228.60	Lpointing (dB)	3	3	3	3	3
T (dBK)	40.80	Latm+rain (dB)	0	0	0	0	0
Noise Temperature (K)	12000	Rx gain (dB)	0	0	0	0	0
		Noise (dB)	-130.71	-130.71	-130.71	-130.71	-130.71
		Available C/N (dB)	**14.17**	**8.15**	**4.63**	**2.13**	**0.19**

		Operating Freq 2.4 GHz					
		Distance (km)	200	400	600	800	1000
Wavelength (m)	**0.125**	EIRP (dBm)	30	30	30	30	30
Bandwidth (dBHz)	**57.10**	Lpath (dB)	146.07	152.09	155.61	158.11	160.05
Bandwidth (Hz)	**512000**	Lpol (dB)	3	3	3	3	3
Required C/N (dB)	14	Lplasma (dB)	3	3	3	3	3
Boltzmann's Constant (dBW/HzK)	-228.60	Lpointing (dB)	3	3	3	3	3
T (dBK)	40.80	Latm+rain (dB)	0	0	0	0	0
Noise Temperature (K)	12000	Rx gain (dB)	0	0	0	0	0
		Noise (dB)	-130.71	-130.71	-130.71	-130.71	-130.71
		Available C/N (dB)	**5.65**	**-0.37**	**-3.90**	**-6.39**	**-8.33**

Table 3.14 Link Budget Calculations datarate 10 kbps

		Operating Freq 430 MHz					
		Distance (km)	200	400	600	800	1000
Wavelength (m)	**0.70**	EIRP (dBm)	30	30	30	30	30
Bandwidth (dBHz)	**40**	Lpath (dB)	131.13	137.15	140.67	143.17	145.11
Bandwidth (Hz)	**10000**	Lpol (dB)	3	3	3	3	3
Required C/N (dB)	14	Lplasma (dB)	3	3	3	3	3
Boltzmann's Constant (dBW/HzK)	-228.60	Lpointing (dB)	3	3	3	3	3
T (dBK)	40.80	Latm+rain (dB)	0	0	0	0	0
Noise Temperature (K)	12000	Rx gain (dB)	0	0	0	0	0
		Noise (dB)	-147.81	-147.81	-147.81	-147.81	-147.81
		Available C/N (dB)	**37.67**	**31.65**	**28.13**	**25.63**	**23.70**
		Operating Freq 900 MHz					
		Distance (km)	200	400	600	800	1000
Wavelength (m)	**0.33**	EIRP (dBm)	30	30	30	30	30
Bandwidth (dBHz)	**40**	Lpath (dB)	137.55	143.57	147.10	149.60	151.53
Bandwidth (Hz)	**10000**	Lpol (dB)	3	3	3	3	3
Required C/N (dB)	14	Lplasma (dB)	3	3	3	3	3
Boltzmann's Constant (dBW/HzK)	-228.60	Lpointing (dB)	3	3	3	3	3
T (dBK)	40.80	Latm+rain (dB)	0	0	0	0	0
Noise Temperature (K)	12000	Rx gain (dB)	0	0	0	0	0
		Noise (dB)	-147.81	-147.81	-147.81	-147.81	-147.81
		Available C/N (dB)	**31.26**	**25.23**	**21.72**	**19.22**	**17.28**
		Operating Freq 2.4 GHz					
		Distance (km)	200	400	600	800	1000
Wavelength (m)	**0.125**	EIRP (dBm)	30	30	30	30	30
Bandwidth (dBHz)	**40**	Lpath (dB)	146.07	152.09	155.61	158.11	160.04
Bandwidth (Hz)	**10000**	Lpol (dB)	3	3	3	3	3
Required C/N (dB)	14	Lplasma (dB)	3	3	3	3	3
Boltzmann's Constant (dBW/HzK)	-228.60	Lpointing (dB)	3	3	3	3	3
T (dBK)	40.80	Latm+rain (dB)	0	0	0	0	0
Noise Temperature (K)	12000	Rx gain (dB)	0	0	0	0	0
		Noise (dB)	-147.81	-147.81	-147.81	-147.81	-147.81
		Available C/N (dB)	**22.74**	**16.72**	**13.20**	**10.70**	**8.76**

3.11 Discussion

Although the primary purpose of the proposed mission is to set the background scene based on which further investigations of inter-satellite communications system could be carried out, which not only confines the scope of investigations, but the results / findings are practically useful.

A secondary outcome of the exercise has led to the proposal of a novel ionosphere monitoring mission which is of great importance not only to the science community, but serves the needs of community associated with radio based services. The low cost of pico/nano satellites ensures that the overall cost of mission remains feasible, and the use of commercially available components to develop the satellites reduces the time of development, therefore rapid deployment is possible. The proposed mission validates the novel space based wireless sensor network concept feasibility based on the metric defined in Table 3.15.

The plasma bulk density monitoring within the ionosphere is a current requirement which has been addressed in this chapter by evaluating feasibility of using very small satellites i.e. CubeSats and PCBSats along with microsatellites such as UoSat acting as a relay. A basic set of instruments i.e. Langmuir probe and 3-axis magnetometer, keeps the design of sensor satellites simple, low cost and mass producible. The science payload can fit in the small confines of a 1U CubeSat or PCBSat with an extra engineering, and without extra effort in a 3U CubeSat structure. Several sensors deployed in large numbers improve the spatial and temporal resolution, illustrated in Figure 3.20. Adding a PCBSat to the 3U CubeSat, as a mother daughter configuration, allows finer scale measurements near the mother satellite. The mother daughter configuration suggested, assumes, daughter to drift away from the mother, and released at a predefined time or at a designated location. Tethers can also be used to keep the daughter tied to the mother, and if possible to retrieve the daughter back. The tethered mother-daughter configuration is not the primary objective of the research and has been left (see related works [187, 188]).

Table 3.15 Feasibility metric for the proposed SBWSN Mission i.e. the Ionosphere monitoring mission.

Parameter	Value	Comments / Justification
Financial Viability	Yes	Extensive use of COTS, reduced unit cost of satellite implies reduced overall mission cost.
Scientific Feasibility	Yes	Achieved multi point sensing with much higher spatial and temporal resolution to provide for the needs of; space plasma physicist [161]; precise navigation and guidance control [180]; and updating ionosphere models [181]
Technical Feasibility	Yes	Small science instruments identified are practically realisable, along with necessary supporting bus-systems all fit with in small confines of pico/nano class of satellites. Launch vehicles support cluster deployment see [182, 183].

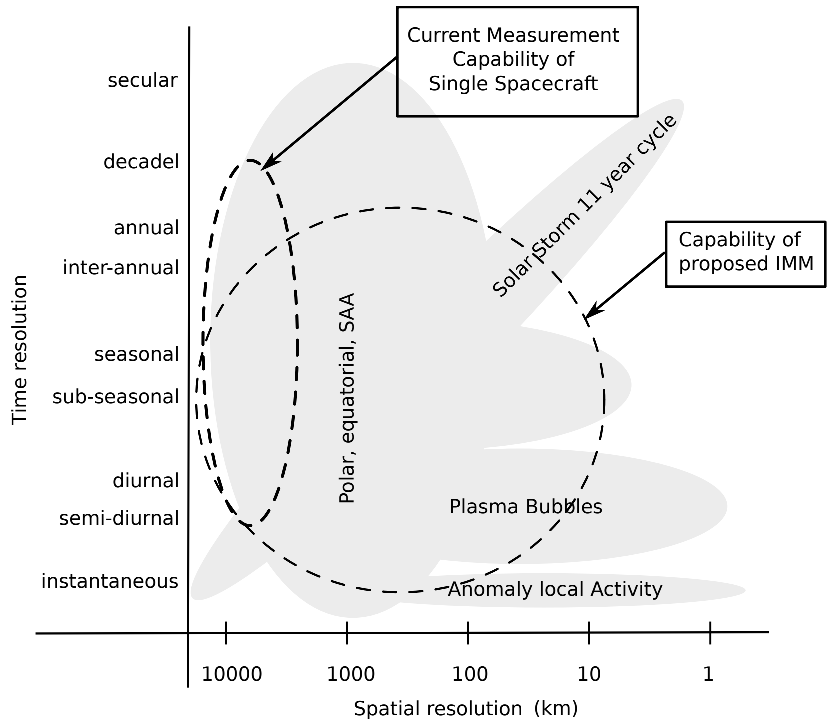

Fig. 3.20 The variation in the ionosphere plasma density in terms of spatial resolution and time resolution, indicating current capability and proposed improvement by IMM. Illustration developed from indicators published by Aarons [178], studies conducted by [153, 152, 184, 185, 186], and existing missions to study ionosphere as given in section 3.2.1.

3.12 Conclusion

Earth's ionosphere has a significant impact on radio based services used in our daily life. The disturbances are generated by events from "above" as well as "below" the ionosphere. Multipoint sensing is desired to improve our understanding of the generated disturbances. In this chapter, the purpose has been to apply the concept of SBWSN to monitor Earth's ionosphere, so as to improve the spatial and temporal resolution of measurements, not possible with current single platform missions.

The mission design revolves around the use of low cost mass producible platforms, equipped with a minimal set of identical instruments. The proposed mission scenario aims at deploying large number of sensor satellites, so that fine scale turbulence could be captured. A mother-daughter sensor satellite configuration is proposed, in which the daughter could be ejected out of the mother. The daughter may or may not be retrieved, but it would allow a much finer measurement. These measurements are anticipated to provide a much better understanding of the complex processes involved in the dynamics of turbulent plasma.

If a relationship is found between the disturbances in ionosphere prior to the actual occurrence of an earthquake, then the proposed mission would act as an early warning system. Inter-Satellite links allow assimilating the data from sensors and relaying it back to Earth, so that the disturbance could be monitored and a precursor to a solar storm detected. However, for a true predictor for solar storms, a network of sensors at much higher altitudes is also required.

It has also been discussed in the chapter, that in addition to the deployment of multiple sensors, the measuring capabilities and quick response time of the instrument is also important. A satellite deployed in LEO traverses 7 km in one second. Though LP is a tried and tested method, the time to take a measurement depends on the underlying design of sweep generator, sampling frequency of current measurement, and settling times involved. Therefore, by the time one sweep is completed, satellite has traversed a large distance. The mother-daughter sensor satellite concept introduced in this chapter, allows further control over deployment of a sensor where and when desired. The deployment of CubeSat from a larger satellite or PCBSat from CubeSat, is conceptually similar. The deployment mechanism is investigated in the next chapter.

In the context of inter-satellite communications links, the chapter identifies, the possible orbits in the region of interest and type of platform. The orbital configurations proposed in this chapter are not sufficient for detailed relative motion studies. Selected well defined orbits are needed to study the impact of relative motion, therefore, the next chapter The impact of relative motion on more is thus studied in the next chapter.

CHAPTER 4

IMPACT OF RELATIVE MOTION ON INTER-SATELLITE LINK DESIGN

The outlined mission scenario in Chapter 3 is an example SBWSN, which comprises of smaller sensor satellites, whereas, slightly larger satellites act as relays. The motion of the sensor satellites with respect to each other as well as with respect to the relay satellites is markedly important

4.1 Introduction

The relative motion of orbiting satellites is unavoidable and has a twofold impact on ISL design: (a) the communications range becomes dynamic, and (b) the Doppler frequency shift is observed. The first requires the data transfer rate to be fast enough to exchange acceptable volume(s) of data between members of the network in the time when the satellites are within a communications range. The second factor must be compensated for, in the first stage of the communications receiver, and any residual frequency shifts be adjusted in the baseband modem. In the previous Chapter 3, mission scenario identified possible regions of deployment but the orbits were not defined in terms of orbital parameters.

In order to study relative motion specific orbits must be defined. The satellites can be deployed in many ways*, of which, a few selected cases are investigated in depth. The three cases selected for studying relative motion, are:

(a) relative motion of three 1U CubeSats (depicting sensor to sensor motion in a free flight mode),
(b) sensor satellites with respect to a relay satellite (depicting relative motion at different altitude) and
(c) relay satellite with respect to a relay satellite (depicting motion in the same orbits using a "string-of-pearl" configuration).

*It is for this reason, that physical layer issues are not discussed in literature, since they are mission specific and require detailed analysis.

The topics pertinent to the relative motion i.e. (a) Doppler frequency shift, (b) Relative motion vectors, and (c) Orbital dynamics. are discussed in the subsections to follow.

4.1.1 Doppler Frequency Shift

In this section we make use of the commonly employed terms i.e. the observer denoted by subscript $(\,)_o$ and source by $(\,)_s$. The source is the transmitter and the observer is the receiver. The speeds are measured by magnitude of the relative velocity vectors.

Consider a source transmitting a sinusoidal wave generated at a frequency f_s. When both the source and observer are moving with respect to each other with certain velocities $\vec{v}_s$, and $\vec{v}_o$, then due to the Doppler Effect the observed frequency by the receiver is different from the source, thus denoted by f_o. The observed frequency f_o and the source frequency f_s are related by Eq. (4.1), where c is the speed of sinusoidal wave in the medium. The Doppler shift in frequency is then computed by $f_0 - f_s$, where +ve sign shows increased frequency and -ve means decreased frequency.

$$f_o = f_s \quad \frac{c \pm v_{os}}{c \pm v_{so}} \tag{4.1}$$

In the eq. (4.1), there are four cases that are incorporated with the $\pm$ sign. The speed considered is the magnitude of velocity vector from the source to the observer represented by v_{so} and from observer to source represented by v_{os}. The actual magnitude (speed) of velocity vectors (v_o or v_s) cannot be used, because in eq (4.1) the component of velocity in the direction of observer or source is used, whose impact causes Doppler shift.

From eq (4.1) there are four possible sign configurations. Which are based on the apparent movement with respect to each other. In selecting the sign, care must be taken:

- When the observer moves towards the source, then the sign in the numerator is taken positive, else negative.
- When the source is moving towards the observer, then sign in the denominator is considered negative, else positive.

In the case of two or more satellites in orbit, the relative velocity vectors need to be determined, so that by using eq. (4.1) the observed frequency could be assessed, then Doppler frequency shift and shift rates be determined.

4.1.2 Relative Velocity Vector

Consider the source satellite S (transmitting satellite generating the carrier wave) and the receiver satellite R. The position and velocity vectors and the associated relative motion vector (rate of change of relative distance) is illustrated in Figure 4.1. The position of satellites is represented by $\vec{r}$ and the velocity by $\vec{v}$. Say S_0 link with R_0 is being evaluated for Doppler frequency, then the relative position vector is $\vec{r_{21}} = \vec{r_1} - \vec{r_2}$, and its magnitude represents the distance d.

The problem is to determine the component of velocity vector $\vec{v_1}$ in the direction of R_0, and vice versa. The component of velocity vector v_1 towards R_0 can be determined from the vector dot product of v_1 and $\vec{r_{21}}$. The projection of a vector on another vector is the basic definition of dot product in vector algebra [175, Appendix-C]. It is the magnitude of this dot product that is the speed required in eq. (4.1).

The second part of the problem is to assess the direction of motion, so that correct sign is used in the numerator and denominator of the eq. (4.1). When the angle from dot product is less that 90° the direction is towards each other, whereas, for greater angle values, the satellites are moving away. With this condition the sign is selected.

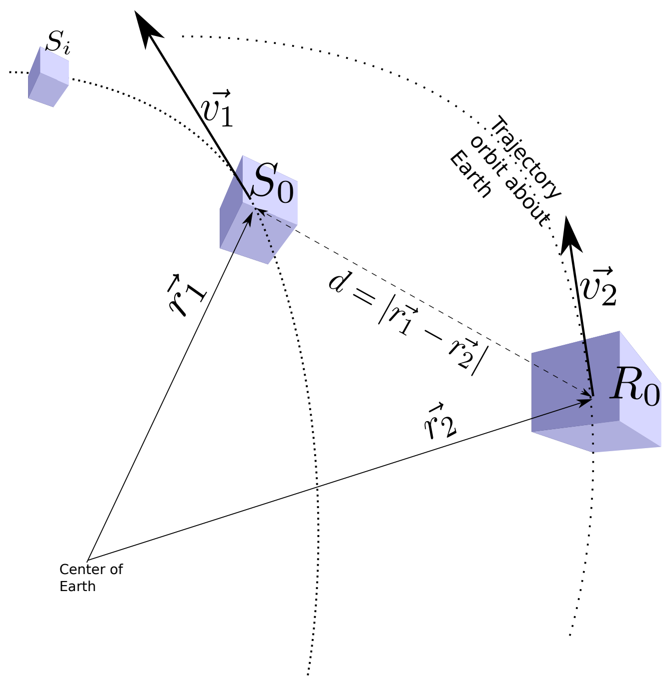

Fig. 4.1 Illustration of the relative motion problem. The velocity vector and the relative motion required to determine the Doppler Frequency shift, observed by a satellite when other transmits and vice versa.

4.1.3 Perturbing Forces in Orbital Dynamics

The motion of satellites in orbit (orbital dynamics) is governed by Newton's law of gravitation, which were refined from Kepler's laws of planetary motion, stated as follows:

- the planets move in a plane, the orbits described are ellipses with sun at one of its focus
- the vector from the sun to planets sweeps equal areas in equal times,
- the ratio of the square of the period (T) of revolution of a planet around the sum to the cube of the semi-major axis (a) of the ellipse is the same for all planets.

Newton extended the work of Kepler, by stating the law of gravitation;

> "two bodies of mass m and M attract each other with the force which is proportional to their masses, and inversely proportional to the square of the distance r between them."

He also modified these laws by introducing the concept of **orbital perturbations** [125] to account for actual movements*

$$F_g = G\frac{mM}{r^2} = \mu\frac{m}{r^2} \tag{4.2}$$

where G is the constant called universal gravitation constant $6.672 \times 10^{-11}\ m^3kg^{-1}s^{-2}$. Consider the constant values of the mass of Earth, $M = 5.974 \times 10^{24}$ kg, and G, the product $GM = \mu = 3.986 \times 10^{14}\ m^3/s^2$. In eq. (4.2), the Keplerian hypothesis assumes, that the gravitational field of the central mass acts on the smaller mass, which can be considered an ideal case. Whereas, the force of attraction from the moon, and the sun also plays its role. Furthermore, when the satellites are orbiting the Earth, the thin atmosphere generates a resistance to the motion, the effect is called atmospheric drag. These additional forces also effect the motion of satellite in orbit, which needs to be accounted for in the equations of motion.

With the Keplerian hypothesis there is only the attraction of central body which is assumed to be homogeneous and spherical, which generates a conservative field of gravitational force. The trajectory thus obtained is plane, fixed in space, and characterised by a set of constant orbital parameters. These orbital parameters, can be obtained from the observation of position and velocity vector of the satellite. In the case of actual orbits, additional forces perturb the above mentioned ideal orbital trajectory. The orbital parameters are not constant, but are a function of several variables representing the forces governing the motion of satellites. Extrapolation of the next position from an initial position and velocity is called **orbit propagation**. The precision and accuracy of orbit propagation depends on the forces being considered, the accuracy of the numerical models of the considered forces, and the numerical

*For details on numerical methods used in orbital mechanics refer to [176, 175] and for analytical derivation of the method of perturbations see [177].

methods used in solving the integrals involved in calculation. Other than the gravitational force, all other forces which affect the motion, are called **perturbing forces** or **perturbations**.

Major perturbations that must be considered are;

- Asymmetry of the Earth's gravitational potential; the terrestrial potential at a point in space depends not only on the distance from the centre of Earth, but also on the latitude and longitude of the point concerned and the time. This is due to the irregularities in the rotation of the Earth, irregular mass distribution (ocean tides, Earth's crust) and internal geophysical phenomenon. The zonal and tesseral harmonics which define the potential function, depend on the data collected via satellite tracking, surface gravimetery and altimeter data. This data is referred to as Geopotential Coefficients. Common Earth gravity model derived from satellite tracking data are; Joint Gravity Model (JGM) and Earth Gravity Model (EGM). JGM-1 of order and degree 70 was issued in 1994 which was a prelaunch model for TOPEX/POSEIDON. JGM-2 included 6 months postlaunch data of TOPEX/POSEIDEN [189]. An increased accuracy was achieved in JGM-3 [190]. New models are continuously being developed e.g. EGM96S (Earth Gravity Model) of order and degree 70, and EGM96 of order and degree 360 [191]. For precise orbit propagation, numerical methods employ higher order and degree models for the Earth's geopotential. JGM-3 is used in the numerical orbit propagator employed with order and degree 20.
- Attraction of the moon and the sun;
- Solar radiation pressure;
- Aerodynamic drag; the satellite face significant change in velocity vector due to the considerable upper atmospheric drag force, only negligible above 3000 km. The drag force depends on the density of the atmosphere, which in turn depends on the time of day, latitude, longitude, sun spot number and various physical and chemical processing occurring in the ionosphere. For LEO orbit propagation, accurately modelling the drag force is crucial. The reference model is the well known Jachia-Roberts model introduced in 1965, then revised in 1971 i.e. J71 model [192], revised again in 1977 (J77) [193] and in 1981 (J81) [194]. These models are based on measurements of satellite acceleration and incorporate mass spectrometer data. Jachia-Mueller model or the series of MSIS (Mass Spectrometer and Incoherent Scatter) models are often used in numerical simulations. For a succinct comparison of well known models and their computational complexity see [176, Sec 3.5.4].

The actual satellite motion is due to the equilibrium formed between the forces, namely;

- the inward pulling forces of attraction by Earth's gravitational field and the outward pushing forces by satellite momentum,
- the well understood perturbing forces (atmospheric drag, solar radiation pressure, third body effects and such), and
- the non conservative perturbing forces (firing of thrusters, internal momentum wheel and such).

It is thus possible to determine the position of the satellite at each instance, by integrating equation of motions, in a geocentric reference frame. Hence on any given day, the six orbital parameters can be estimated.

4.1.4 Orbit Simulation

The orbit propagator requires initial conditions in terms of position and velocity vectors, or in terms of orbital elements. The simulation determines the position and velocity at defined time instances, i.e. at 1 second in our case. The position and velocity vectors for individual satellites are saved in a file for the duration of the simulation, which are used in determining the relative velocity vectors required in eq. (4.1)

There are four options to propagate orbit from the initial position and velocity vectors of a satellite which involve the use of: a) a simple two body formulation employed in preliminary analysis of orbit dynamics; b) numerical methods to propagate the orbit trajectory under the influence of disturbing forces also known as perturbation forces; c) linearised forms of analytical solutions called the Hill's equations [195, 196]; or d) analytical expressions for absolute motion [197]. We opt for the second method (b), since we can achieve representative values for our intended application that is the study of short and long term relative motion evolution from the point of deployment, for which simulation code exists. Options (c) and (d) give a better insight into the evolving dynamics of orbital parameters and are more suitable for advance orbit dynamics work, which is beyond the scope of this thesis.

The orbit propagator used in this thesis is provided by Prof. Gill from Delft University of Technology [176], which simulated orbits with the appropriate perturbation forces.

To incorporate a real world problem, ejection of CubeSat from DNEPR is used as a case study. The initial conditions of the CubeSat are determined, which are used in the numerical orbit propagator. Since CubeSats come is various sizes, the simplest case is that of a 3U being ejected from P-POD. The initial conditions are simply the position and velocity vector at the point of ejection with the ejection velocity subtracted, in the local body frame of reference. The position and velocity vectors are in local body frame of reference, which are then converted to ECI frame of reference, which are then used in orbit propagation. However, when a cluster of 1U CubeSats is ejected, then the resulting velocity changes must incorporate the push by separation springs attached to each CubeSat. Again care must be taken, that the position and velocity vectors determined in this manner is in the local body frame of reference, and needs to be transformed to ECI frame, before using it as input to the numerical orbit propagator.

In the following section, we estimate the initial conditions of three 1U CubeSats when ejected in orbit.

4.2 Case Study : Deployment of CubeSats from DNEPR

A satellite is deployed in space with the help of a launch vehicle (LV) [198]. One of the launch vehicle commonly used to deploy more than one satellite in low Earth orbits is considered for further investigations, namely, the Russian DNEPR. The selection of the DNEPR launch vehicle is motivated by the fact, that most small satellites being launched in polar orbits, use this vehicle. In addition, DNEPR has the necessary interfaces and heritage to allow simultaneous ejection of very small satellites, successfully in LEO as "piggy back ride".

4.2.1 Cluster Deployment in Orbit via DNEPR

DNEPR launch vehicle (LV) is based on the SS-18, liquid fuelled, inter-continental, ballistic missile technology, which has been re-engineered for use in commercial purposes, after its retirement from military service [182]. There are three stages of rocket and an additional stage called the Space Head Module (SHM). The three stages are in "line configuration" i.e. one on top of the other, with SHM being the tip of LV, which carries the satellite as its payload (shown in Figure 4.3).

There are three SHM configurations that can be used to meet launch requirements. They are called, and respectively shown in Figure 4.2

- Standard length SHM for accommodation of a mid-size satellite (Type-1),
- Standard length SHM for accommodation of a group of small satellites (Type-2),
- Extended length SHM for accommodation of a large-size satellite (Type-3).

The launcher can deploy at altitudes of 300, 500, 600 and 800 km at an inclination of 98°. It should be noted, that the Type-2 SHM supports cluster deployment at the desired polar orbits.

4.2.1.1 Launch Sequence

A launch sequence for the Nov 2013 cluster deployment by DNEPR is taken as the basis for studying deployment of CubeSats. The stages in which several satellites are deployed by a LV is illustrated in Figure 4.3, called the **cluster deployment** by DNEPR standards [182]. Each satellite is ejected from upper stage of LV i.e. the SHM at a specified time with reference to the lift off time. This separation changes the velocity of satellite with respect to the SHM, thus defining its trajectory in orbit, which is stated as "SC Nominal Orbit Parameters" located at bottom right in Figure 4.3. Larger satellites carry on-board fuel, which is used to adjust their orbit and attitude as desired e.g. change inclination or altitude. This is part of the commissioning process, which takes some time often several weeks [7], before the spacecraft is ready for conducting normal operations. It should be observed that very small satellites such as CubeSats, do not carry on-board fuel as per the CubeSat specifications [168], thus they

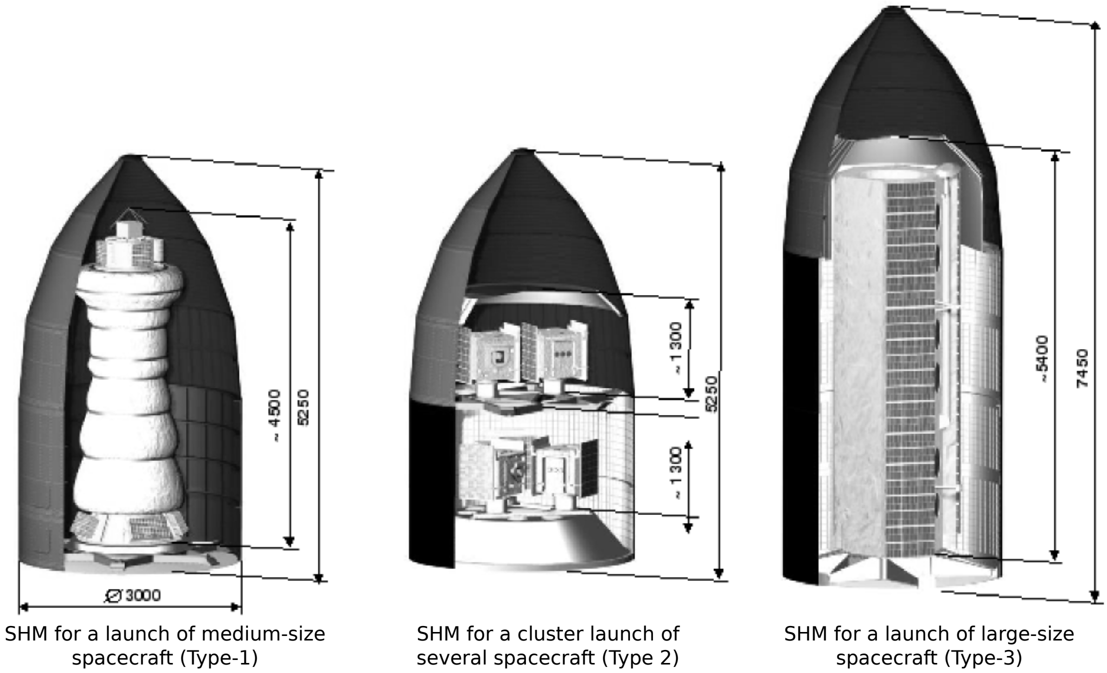

Fig. 4.2 SHM of DNEPR in three configurations [182].

are called free flying objects. The manner they are ejected, determines their final trajectories. However, on-board attitude controller (if any), would take some time to orientate the spacecraft.

A dedicated interface is required which controls the timely ejection of satellites. For CubeSats, a dedicated deployer has been developed, which keep the CubeSats from being accidentally deployed and interfere with deployment of main payload, known as P-POD [22]. P-POD can be attached to another satellite or the SHM directly. P-POD gets a deployment signal i.e. a signal which opens its hatch, ejecting the CubeSats in orbit. Generally, each CubeSat within the P-POD is from a different user, therefore, they are required to separate as soon as they are ejected in orbit, so that, they could be identified uniquely, after confirmed communications links are established.

We are interested in (a) the separation of CubeSats and (b) the evolution of their orbits from the point of deployment. Both depend on the initial velocity given to each of the CubeSats, relative to the SHM. Therefore, deployer mechanism and CubeSat design specifications are briefly described next.

4.2.1.2 Deployer and Separation Springs

The Polytechnic Pico-Orbital Deployer (P-POD) is specifically designed to deploy CubeSats in orbit [22]. A rectangular tube like structure with a plunger spring at one end, while the other end is covered by a lid. It can house one 3U CubeSat, or three 1U CubeSats, or a combination of 2U, 1U or 0.5Us.

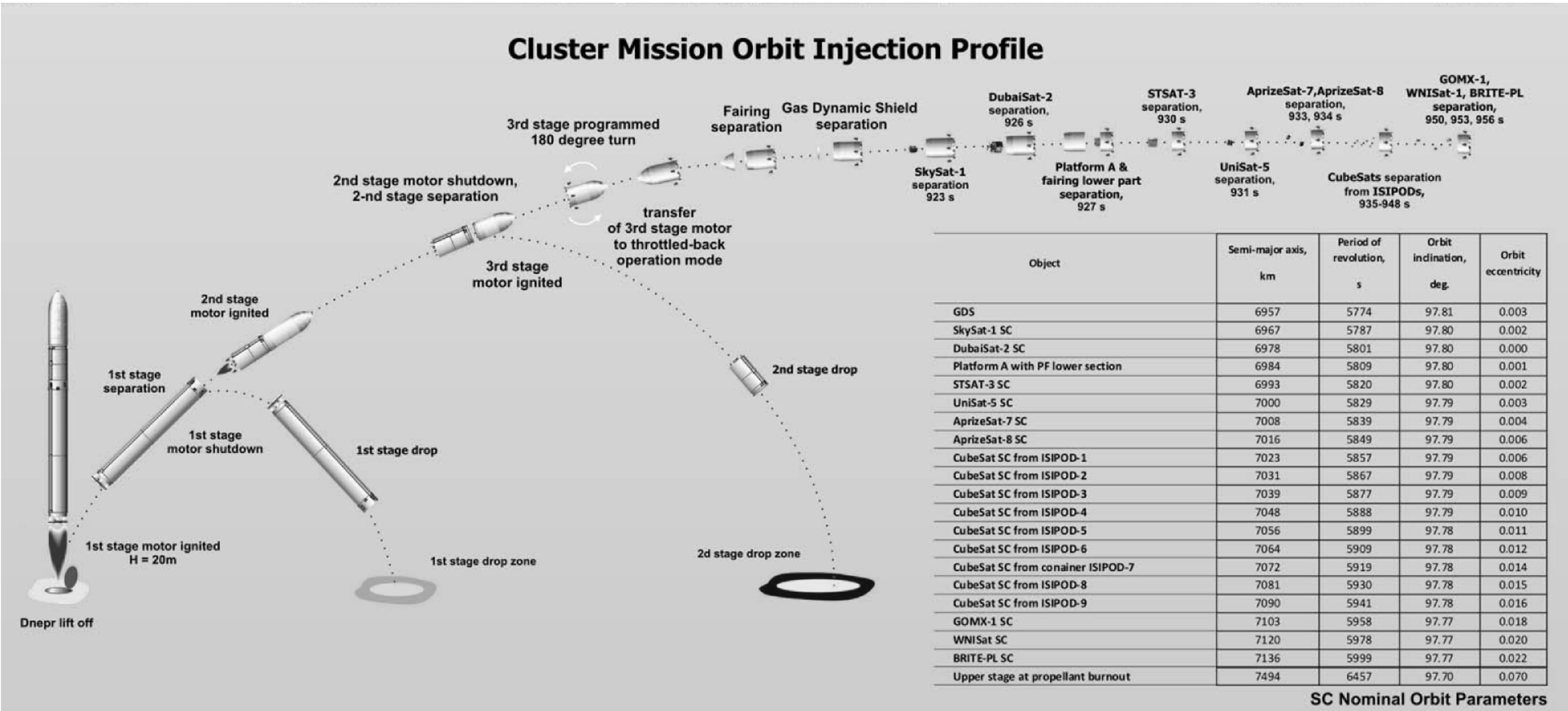

Object	Semi-major axis, km	Period of revolution, s	Orbit inclination, deg.	Orbit eccentricity
GDS	6957	5774	97.81	0.003
SkySat-1 SC	6967	5787	97.80	0.002
DubaiSat-2 SC	6978	5801	97.80	0.000
Platform A with PF lower section	6984	5809	97.80	0.001
STSAT-3 SC	6993	5820	97.80	0.002
UniSat-5 SC	7000	5829	97.79	0.003
AprizeSat-7 SC	7008	5839	97.79	0.004
AprizeSat-8 SC	7016	5849	97.79	0.006
CubeSat SC from ISIPOD-1	7023	5857	97.79	0.006
CubeSat SC from ISIPOD-2	7031	5867	97.79	0.008
CubeSat SC from ISIPOD-3	7039	5877	97.79	0.009
CubeSat SC from ISIPOD-4	7048	5888	97.79	0.010
CubeSat SC from ISIPOD-5	7056	5899	97.78	0.011
CubeSat SC from ISIPOD-6	7064	5909	97.78	0.012
CubeSat SC from conainer ISIPOD-7	7072	5919	97.78	0.014
CubeSat SC from ISIPOD-8	7081	5930	97.78	0.015
CubeSat SC from ISIPOD-9	7090	5941	97.78	0.016
GOMX-1 SC	7103	5958	97.77	0.018
WNISat SC	7120	5978	97.77	0.020
BRITE-PL SC	7136	5999	97.77	0.022
Upper stage at propellant burnout	7494	6457	97.70	0.070

SC Nominal Orbit Parameters

Fig. 4.3 DNEPR cluster mission profile launched in Nov 2013. (courtesy of ISC Kosmostros [183]).

The following method can be used to determine the initial conditions for any CubeSat configuration within the deployer.

The CubeSats are plunged out with a mean speed* of 2 m/s less than the speed of upper stage of DNEPR [199]. The P-POD baseplate spring is much stiffer than the separation springs attached to the legs of CubeSats. The CubeSats at this stage can be considered one packed cluster. The CubeSats start separating from each other with the force exerted by separation springs i.e. the springs attached at the bottom side of CubeSat legs as shown in Figure 4.4. The separation springs push away the adjacent CubeSats changing their velocity vector thus changing the orbital elements.

Orbital parameters are stated for the satellite on which P-PODs are attached, however, for each of the CubeSats, the position and velocity needs to be determined. By determining the acceleration imparted by each separation spring, the change in velocity and position vectors are determined. In the following section, the characteristics of the spring are described.

4.2.2 Motion of CubeSats at the Moment of Ejection

In order to determine the position and velocity of each CubeSat at the instance the plunger pushes all three of them out of the P-POD, the motion of the CubeSats can be formulated as a coupled spring-mass problem as illustrated in Figure 4.5. The plunger spring refers to the stiffer spring attached to the base of P-POD, whereas, lesser stiffer pre-compressed springs attached to the legs of CubeSats are referred to as separation springs. In this section the motion induced by the separation springs is modelled. Since the springs are attached to CubeSats and lose contact as soon as the two CubeSats move away the distance the length of the separation springs, therefore, the the motion of each CubeSat is a coupled effect of the respective influencing springs for the duration, the springs do not lose contact.

Each CubeSat can be considered a mass m_i with $i = 1,2,3$ representing CubeSat 1, CubeSat 2 and CubeSat 3 respectively. Two springs are attached to one side of the mass representing the two separation springs attached to the legs of CubeSat (Figure). In formulating the problem, two springs of equal length and same type, are replaced by a single spring having a spring constant k_i where $i = 1,2,3$. The separation spring is connected to one side of the mass represented by a dot in Figure 4.5, whereas, it is not connected to the other side. Thus, when the compressed spring has de-sprung, the mass lose contact with the adjacent surface, no longer exerting any force. At this instance the position and velocity of each CubeSat is determined. This position and velocity is with reference to body frame attached to P-POD.

All three CubeSats are pushed inside the P-POD, and the lid is closed, thus compressing all the springs. For our problem CubeSat 1 is at the bottom of the cluster, CubeSat 2 is in the middle, and CubeSat 3 at the top. On opening the lid, the baseplate quickly throws all the CubeSats out of P-POD before the separation springs are allowed to de-sprung. At this instance, CubeSat 1 is merely in contact with

*This speed is variable and can be modified as per the launch vehicle (LV) requirements.

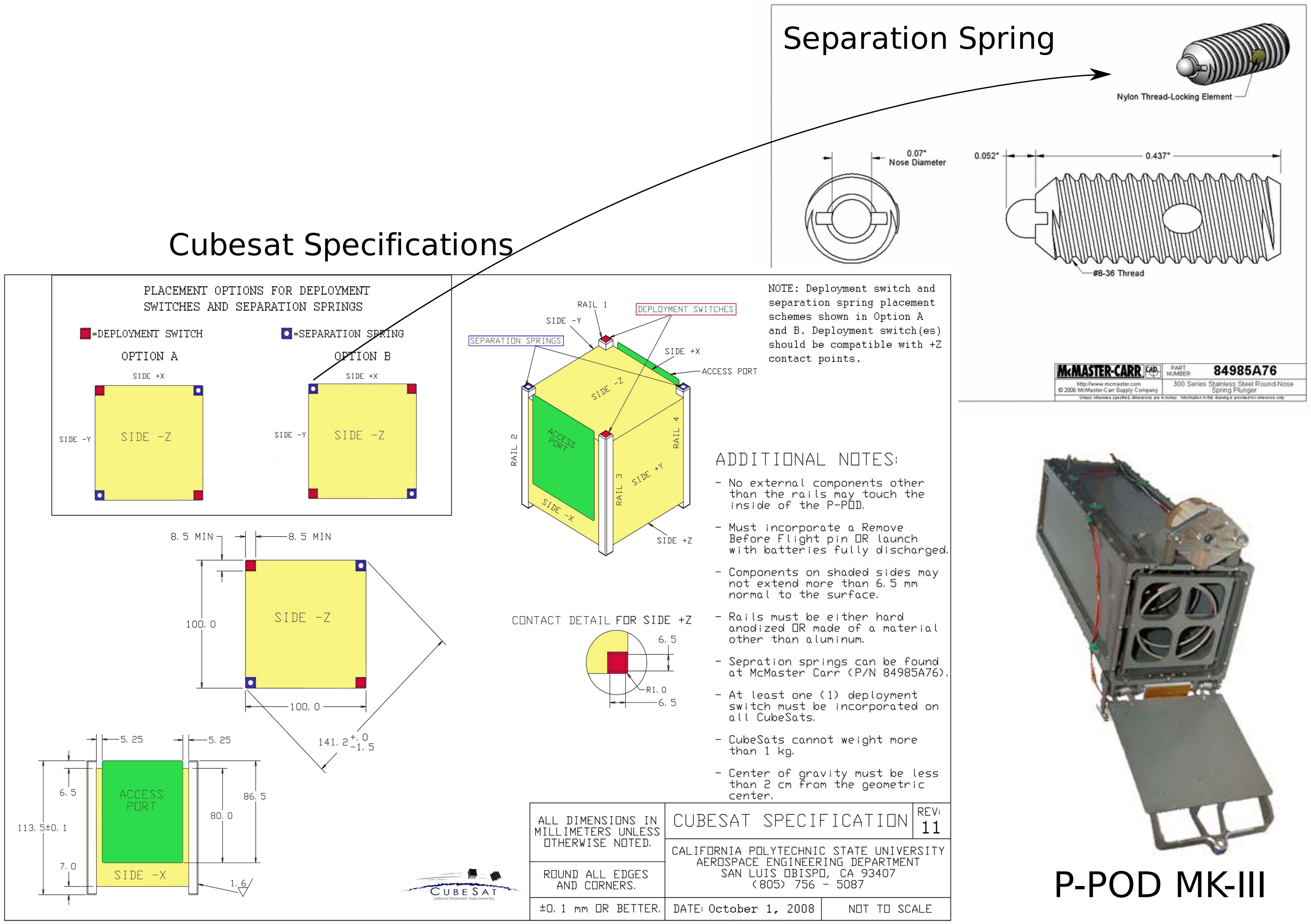

Fig. 4.4 CubeSat Design Specifications [168], highlighting the placement of small separation springs. P-POD (Type MK-III) the CubeSat deployer is also shown in bottom right corner, with lid open, and visible baseplate attached to mush stiffer (plunger) spring.

baseplate, however, at the next time instance the contact is lost. The governing equations of motion for each m_i due to the separation springs is formulated and numerically solved, at this instance.

Referring to Figure 4.5, each spring mass position is r_i for $i = 1,2,3$ where index i indicates the respective mass. The dotted line represents the state of equilibrium, when no force is being exerted by the springs. After compressing each separation spring, when allowed to desiring, the acceleration of each mass is governed by the coupled forces of adjacent springs in contact with the mass. For the motion of m_1, spring k_2 of m_2 is also effective, in addition to its own spring k_1. For m_2, spring k_3 of m_3 is also effective in addition to its own spring k_2. Whereas, for m_3, only k_3 is effective. The motion of each mass must be incorporated in the equations of motion.

Firstly, we formulate the problem assuming that m_1 has a contact with the baseplate (which is lost immediately i.e. k_1 becomes ineffective). The spring 1 with spring constant k_1 exerts a force on the baseplate when compressed by a length l_c (see Figure 4.6 for definition of l_c), whereas spring of mass m_2 exerts a force on m_1, when compressed by length l_c. L is the length of one side of the CubeSat. The coupled effect is an acceleration, which is captured by the equation of motion eq. (4.3) for m_1. The position is measured from the baseplate of P-POD.

$$m_1\ddot{r}_1 = -k_1(r_1 - 0 - l_c) + k_2(r_2 - (r_1 + L) - l_c) \tag{4.3}$$

where $\ddot{r}_i$ is the acceleration in terms of position r_i.

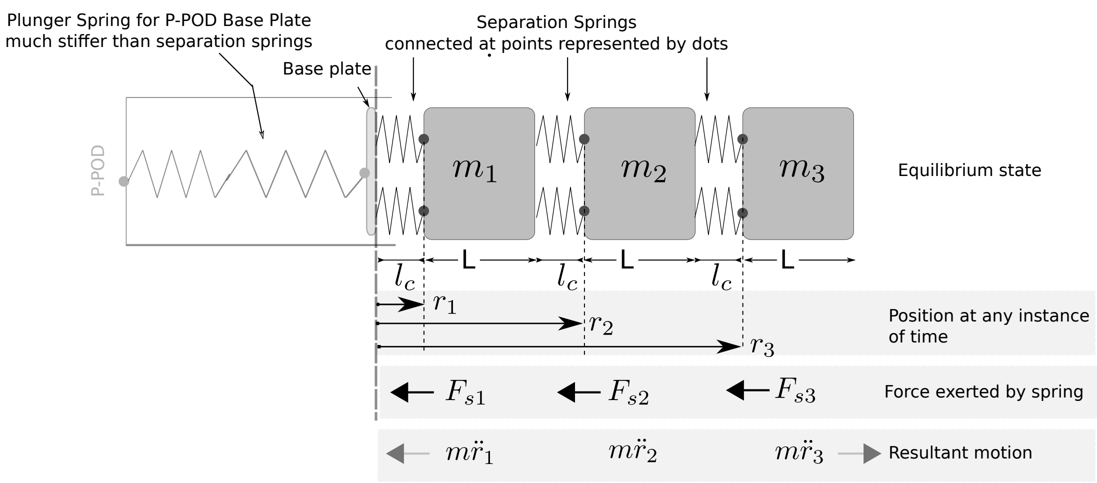

Fig. 4.5 Reference frame and displacement directions of a coupled system of three masses with attached springs, inside a tube.

Similarly, motion of m_2 is governed by its own spring exerting force F_{s2}, coupled to the force exerted by spring attached to m_3. Furthermore, the motion of m_1 and m_3 must be incorporated. Thus m_2 movement is governed by:

$$m_2\ddot{r}_2 = -k_2(r_2 - (r_1 + L) - l_c) + k_3(r_3 - (r_2 + L) - l_c) \tag{4.4}$$

Similarly m_3 is governed by the equation of motion;

$$m_3\ddot{r}_3 = -k_3(r_3 - (r_2 + L) - l_c) \tag{4.5}$$

The initial conditions i.e. at t=0, for the equations of motion for all three masses, are stated as follows;

$$r_1(0) = 0 \tag{4.6}$$
$$r_2(0) = r_1 + L \tag{4.7}$$
$$r_3(0) = r_2 + L \tag{4.8}$$
$$\dot{r}_i(0) = 0 \qquad i = 1, 2, 3 \tag{4.9}$$

where L is the length of 1U CubeSat taken as 3.937 inch (10 cm).

It must be noted, that the above governing equations are also bound by the conditions when spring lose contact with the adjacent surfaces;

- k_1 becomes zero, at the very first instance, because it has no surface to push on (P-POD has moved away already).
- k_2 becomes ineffective as soon as m_2 moves a distance $(r_2(t) - (r_1(t) + L) - l_c) \geq l_c$.
- k_3 cannot exert any force as soon as m_3 moves $(r_3(t) - (r_2(t) + L) - l_c) \geq l_c$.

The coupled equations of motion given by eq. (4.3), eq. (4.4) and eq. (4.5) are second order Ordinary Differential Equations (ODE), which can be solved by converting them in to a system of first order ODEs by methods outlined in [200]. However, in this formulation, we require k called the spring constant as defined in Hooke's law, which is determined as follows.

4.2.2.1 Separation Spring Characterisation

The McMaster (p/n 84985A76) spring used in CubeSats, is pre-compressed with the specifications stated in Table 4.1. The nominal length of the spring is the length when the spring is neither compressed nor stretched, also called the natural length in equilibrium. When Hooke's law is employed in determining the coupled motion of the mass attached to spring, then the formulation requires extension or compression of spring in terms of the nominal length. Therefore, nominal length of the precompressed spring is determined in this section.

The force F_s exerted by the spring is related to the length by which the spring is compressed (or stretched) by a factor called the spring's constant k. Let the nominal length be defined as l_{nom}. With reference to the notation in Figure 4.6, and assuming a linear relationship of force and length of spring, then by Hooke's law, the force exerted by spring when it is pre-compressed by a length $k_s l_x$ inch is 0.5 lbs. Whereas, when the spring is further compressed to allowable length of $k_s(l_x + l_c)$ inch, then the spring exerts 1.5 lbs. The value of spring constant k_s can be found by solving the following two equations;

$$1.5 = k_s(l_x + l_c) \tag{4.10}$$

$$0.5 = k_s(l_x) \tag{4.11}$$

Since the data sheet gives all values in Foot Pound Second (FPS) system of units, therefore, all calculations are carried out using FPS units. End results are converted into SI units.

The nominal length of spring is determined by solving the relationships that $l_{nom} - l_x = 0.437$ inch and $l_c = 0.052$ inch, whereas when further compressed $l_{nom} - (l_x + l_c) = 0.385$ inch. Solving the relationship in eq (4.10), we find the value of spring constant of a single spring $k_s = \frac{250}{13}$.

It is important to define the nominal length of the spring, if it is calculated wrongly we will end up using the wrong force, and the wrong value of spring constant, leading to incorrect results.

Line (a) in Figure 4.6 gives the correct nominal length for the Vlier Spring used, where as for Line (b) it is clear that the force is not zero at the state of equilibrium. In the numerical solution, the springs are compressed by a length of 0.078 inch which is equal to the sum of the precompressed length and the compressed length.

Table 4.1 Spring Properties McMaster (p/n 84985A76)

Name	Value	Units	Value	SI Units	Label	Comments
Force	1.5	lbs	6.67	N	F_s	compressed to $l_x + l_c$ (Fig. 4.6)
Force	0.5	lbs	2.22	N	F_s	compressed to l_x (Fig. 4.6)
Nominal Length	0.463	inch	0.012	m	l_{nom}	Calculated
Spring's Constant	19.23	lb/inch	3367.69	N/m	k	Calculated
Pre-compressed Length	0.026	inch	0.0006604	m	l_x	Given data sheet

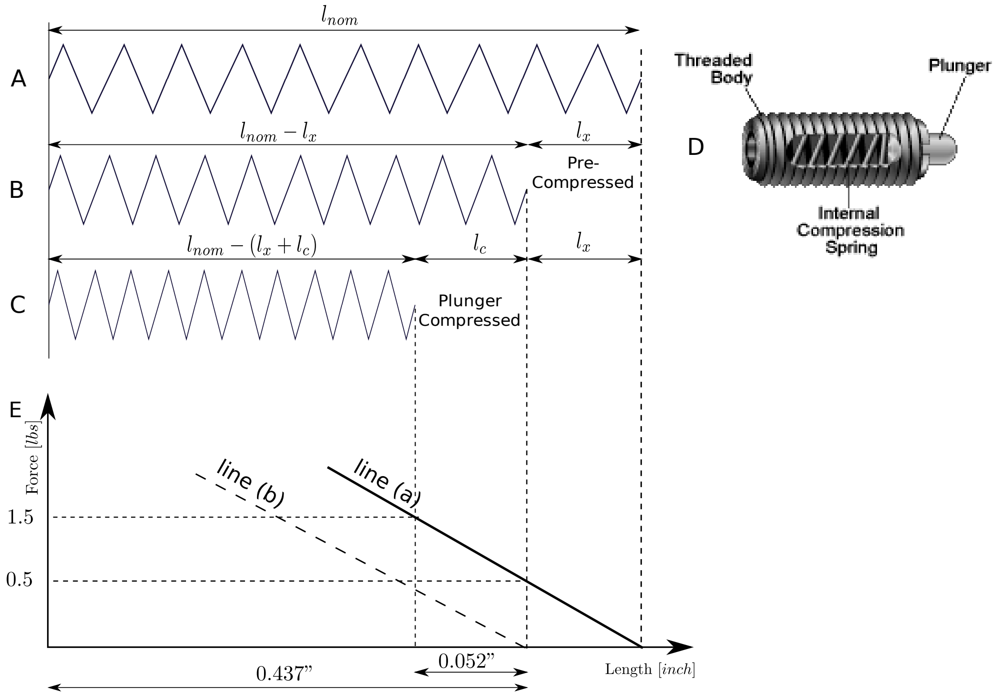

Fig. 4.6 Nominal length, compressed length and the pre-compressed length, to determine the true value of springs constant.

4.2.2.2 Velocity Changes due to Separation Springs

Matlab also provides a mechanism to solve the system of first order ODEs, numerically. To solve the above stated equations, a script was written using MATLAB which is presented in given in Appendix C.1.

In finding the position and velocity of the CubeSats, the model is kept simple, and the following assumptions are used, which can be modified in future studies.

- There is no frictional force between the sides of the P-POD and CubeSats,
- The separation springs are balanced and exert equal force simultaneously; note this assumption is practically not possible, a slight change in the separation spring lengths would impart a slight difference in force on each leg, adding direction to the otherwise tangential velocity assumed. That is why satellites come out tumbling in reality.
- The formulation is done at the instance when the base plate of P-POD has just lost contact with the cluster of masses (i.e. the three CubeSats). That means plunger spring is much more powerful than the separation springs, and separation springs are not able to expand till the time plunger has expanded.
- The separation springs apply the force tangent to the orbit curve along the velocity vector of SHM.

At the instance when the cluster is pushed out, it is intact i.e. separation springs are still compressed. CubeSat 1 separation spring could not exert any force since its spring has nothing to push onto i.e. the

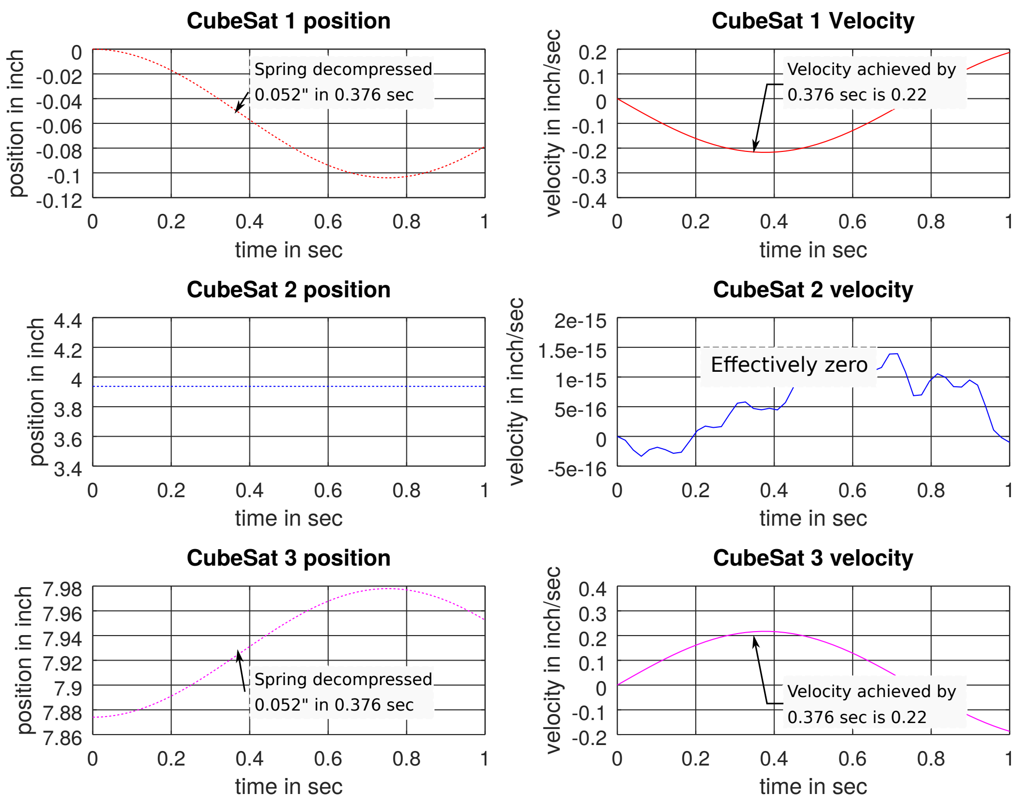

Fig. 4.7 Changes in position and velocity of CubeSats when referenced from the P-POD baseplate. CubeSat1 has lose contact with P-POD baseplate (thus k1=0). The position and velocity after the marked locations should be read as constant values. The numerical solver assumes all springs are attached.

P-POD has moved away at the rate of 2 m/s from the cluster of CubeSats. However, CubeSat 2 can push on CubeSat 1 and CubeSat 3 can push on CubeSat 2. The net result is that CubeSat 1 and CubeSat 2 are pushed away from CubeSat 2, with equal accelerations, but in opposite directions. CubeSat 3 direction is considered positive, whereas, CubeSat 1 direction is considered negative, with respect to CubeSat 2. In Figure 4.7, the resulting position and velocities are plotted. In the Figure, no additional condition has been incorporated within the numerical script, rather, the code assumes that the springs are all attached to each mass, therefore, oscillatory solution is observed (it also acts as a necessary condition to check the numerical solution). However, in our case, the spring lose contact which is highlighted in the Figure 4.7.

It is found from evaluating the resultant position and velocity (see Figure 4.7) that the CubeSat 1 moves 0.052 inch (0.00132 m) in 0.3761 sec. The velocity of CubeSat 1 after 0.3761 sec is -0.22 inch/sec (-0.0056 m/s). The same is found for CubeSat 3, but the direction of motion is opposite, thus the velocity is +0.22 inch/sec (+0.0056 m/s). Now we can find the change in velocity with respect to the SHM.

The P-POD plunger spring pushes the cluster of CubeSats out of P-POD away from SHM in the opposite direction of SHM motion with the velocity difference of 2 m/s [22].

Therefore the resultant change in velocity ΔV_T for CubeSat 1 is -1.944 m/s, whereas for CubeSat 2 is -2.00 m/s and for CubeSat 3 is 2.0056 m/s. The small difference in position has been ignored in determining the osculating elements, which is the topic of next subsection.

4.2.3 The Orbital Parameters of CubeSats

Now that we know how P-POD ejects CubeSats, we can simulate orbits, provided, a reference orbit for the P-POD is known. From DNEPR launch vehicle, a P-POD is assigned an orbit, whose parameters are listed in Table 4.2.

Where $R_\oplus = 6378.137$ km is the mean Radius of Earth as defined under JGM-3 [176]. The value of semi-major axis a in (km) can be calculated using the equation

$$a = \left(\frac{\mu T_{rev}^2}{4\pi^2}\right)^{1/3} \tag{4.12}$$

$$= \left(\frac{398600.4415 \times 5946.9^2}{4\pi^2}\right)^{1/3}$$

$$= 7094.46 \tag{4.13}$$

where μ is the Earth's gravitational parameter, T_{rev} is the orbit period in sec. From the value of a in km, it is easy to find the value of orbit parameter $p = a(1-e^2) = 7094.10$ km. Using the *vis-viva* equation of orbital energy [201, Chap 6,9]), the velocity can be stated as:

$$V^2 = \mu\left(\frac{2}{r} - \frac{1}{a}\right) \tag{4.14}$$

Table 4.2 P-POD A on DNEPR deployment information [199]

Apogee (km)	Perigee (km)	Period (sec)	Eccentricity
$R_\oplus + 772.1$	$R_\oplus + 660.6$	5946.9	0.0071

we can substitute r which is the instantaneous radius (km), with the value of perigee altitude and find the value of velocity at perigee. Also with a little manipulation, in terms of eccentricities, the velocity at perigee, can be calculated;

$$V_p = \sqrt{\left(\frac{\mu}{a}\right)}\sqrt{\frac{1+e}{1-e}} \tag{4.15}$$

giving the value of $V_p = 7549.055$ m/s.

For the rest of the analysis the point of ejection of the CubeSat cluster can be considered as the point of perigee, since it has been assumed that the velocity vector is tangential to the radial vector of the orbit. It must be noted here, that the radial vector is with reference to the centre of Earth as defined in ECI frame.

The Keplerian elements (orbital parameters or osculating elements) for the P-POD A ejecting the cluster from SHM are given in the Table 4.3.

Using the relationships derived from the variation of parameters in osculating elements as detailed in [201], we can determine the change in osculating elements due to change in velocity i.e V_T calculated earlier. The relationships define the change in osculating elements due to a perturbing acceleration in the $S: radial$, $T: tangential$ and $W: Normal$ direction of the satellite, aligned to the radial, velocity and orbital specific energy vectors; then the rate of change in each parameter is given as follows;

Table 4.3 Keplerian Elements derived from DNEPR information for P-POD (A) example.

Parameter	Symbol	Units	Value	Comments
Gravitational Coefficient	$GM_{\oplus} = \mu$	km^3/s^2	398600.4415	JGM-3
Mean Earth Radius	R_{oplus}	km	6378.137	JGM-3
Perigee radius	r_p	km	7038.737	given in Table 4.2
Apogee radius	r_a	km	7150.237	given in Table 4.2
Eccentricity	e	unit less	0.0071	given in Table 4.2
Semi-major Axis	a	km	7094.46	Calculated from eq (4.12)
Orbit Parameter	$p = a(1-e^2)$	km	7094.10	Calculated
Inclination	i	rad	1.7104	DNEPR LV specs (98°)
RAAN	Ω	rad	0	Assumed
Argument of Perigee	ω	rad	0	Assumed
Mean Anomaly	M	rad	0	Assumed

$$\dot{\Omega} = \frac{r}{\sqrt{\mu p}} \frac{\sin u}{\sin i} \quad W \tag{4.16}$$

$$\dot{i} = \frac{r}{\sqrt{\mu p}} \cos u \quad W \tag{4.17}$$

$$\dot{p} = 2\sqrt{\frac{p}{\mu}} \quad T \tag{4.18}$$

$$\dot{e} = \sqrt{\frac{p}{\mu}} S \sin v + \sqrt{\frac{p}{\mu}} T \left(1 + \frac{r}{p}\right) \cos v + e \frac{r}{\sqrt{\mu p}} T \tag{4.19}$$

$$\dot{w} = \frac{1}{e} \left[\sqrt{\frac{p}{\mu}} S \cos v + \sqrt{\frac{p}{\mu}} T \sin i - e \frac{r}{\sqrt{\mu p}} W \sin u \cot i \right] \tag{4.20}$$

$$\dot{\tau} = \frac{r^2}{e\mu} \left[-(\cos v - eN \sin v) S + \frac{p}{r} NT \right] \tag{4.21}$$

where $N(v)$ is given as

$$N(v) = 2\frac{p^2}{r^2} \int_0^v \frac{\cos v}{(1 + e\cos v)^3} dv \tag{4.22}$$

Where r is the position vector of satellite at any given instance of time t, v is the true anomaly calculated positive from periapses (point of perigee), $u = \omega + v$ is the argument of latitude, and rest are the familiar terms in orbital mechanics [201].

With the assumption of a change in velocity in a very small duration of time (as compared to orbital period), then the change in parameters is not gradual but can be considered abrupt, and denoted by the symbol Δ. Since the change in acceleration is in a very small duration of time t_n, then the velocity vector associated with the acceleration can be stated as;

$$\Delta V_T = \int_0^{t_n} T dt \tag{4.23}$$

$$\Delta V_S = \int_0^{t_n} S dt \tag{4.24}$$

$$\Delta V_W = \int_0^{t_n} W dt \tag{4.25}$$

Further more the derivative symbol in eq. (4.16) to (4.21) changes to Δ, to denote the linear increment.

Since we are considering only tangential velocity changes, therefore $V_s = V_W = 0$. Thus from the value of tangential velocities found earlier, and using the eq. (4.16) to (4.21), we can find the change in orbital parameters for each of the three CubeSats due to separation springs.

The Table 4.4 fills in the values calculated for each of the CubeSat. CubeSat 1 is the one which was first in the P-POD, then CubeSat 2, and last in is CubeSat 3. However since there is no change in velocity of CubeSat 2 we consider its orbit as the reference orbit and find the changed parameters for CubeSat 1 and CubeSat 3. The difference in orbital parameters with respect to CubeSat 2 are listed in Table 4.4.

Table 4.4 Change in Osculating Elements due to impulsive change in tangential velocity.

Parameter	Expression	CubeSat 1	CubeSat 2	CubeSat 3
Δp	eq.(4.18)	-5.3512×10^{-4}	-5.3363×10^{-4}	-5.3214×10^{-4}
Δe	eq.(4.19)	-5.3704×10^{-4}	-5.3554×10^{-4}	-5.3404×10^{-4}
Δa	$a = \frac{\Delta p}{1-\Delta e^2}$	-5.3512×10^{-4}	-5.3363×10^{-4}	-5.3214×10^{-4}

The rest of the parameters do not change because true anomaly v is zero at point of perigee r_p and tangential velocity has changed only. Therefore we get a new set of Keplerian elements for the three deployed CubeSats given in Table 4.5. See Annex C.1.2 for a MATLAB (OCTAVE) script which computes change in a, e, i due to change in tangential velocity.

Table 4.5 Final orbital elements for CubeSats deployed via P-POD used for simulation.

Osculating Element	**CubeSat 1**	**CubeSat 2**	**CubeSat 3**
a (km)	7094.459464876	7094.459466370	7094.459467865
e	0.006562963	0.006564463	0.006565962
i (deg)	98	98	98
Ω (deg)	0	0	0
ω (deg)	0	0	0
M (deg)	0	0	0

4.2.4 Resulting Relative Motion of CubeSats

The values determined in Table 4.5 are used in the numerical orbit propagator. The orbit for each CubeSat is propagated with a time step of 120 sec. The simulated orbits are assessed for inter-satellite distance for initial 700 min in orbit, the results are shown in Figure 4.8.

It is observed from the relative motion, that the satellites are relatively close to each other during the initial period of deployment. The satellites come closer and move away from each other, therefore, Doppler frequency increase and decrease is expected. However, due to a slow drift, the Doppler frequency shift is low. It is noted that CubeSat 1 and CubeSat 3 move away from CubeSat 2, with the same rate about 100 m in 100 min. The relative distance between CubeSat 1 and CubeSat 3 increases at a rate of 200 m in 100 min. The separation distance increases beyond 1 km within the first eight orbits. So for the sensor to sensor communications link experimentation, separation springs need to be removed. Then the drift rate would be only due to differential drag as discussed by Barnhart [29].

The Doppler frequency shift is calculated by subtracting the actual frequency from the observed frequency. The Doppler shift observed over the simulated period is plotted for 430 MHz in Figure 4.9 and for 900 MHz in Figure 4.10. CubeSat 2 is considered the source, while the other two CubeSats act as observers, so the Doppler shift observed by CubeSat 2 and CubeSat 3 are calculated from the relative distance.

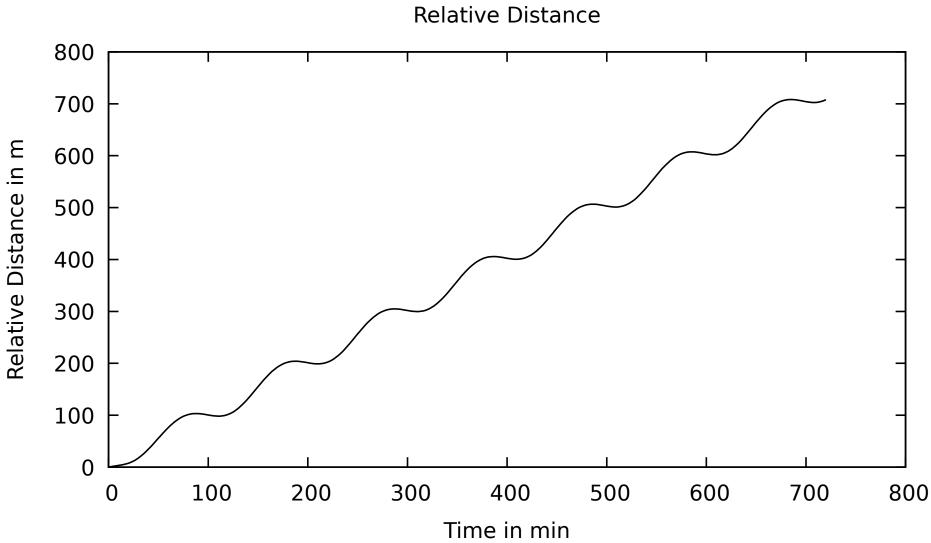

(a) CubeSat 2 and 1 same as CubeSat 2 and 3

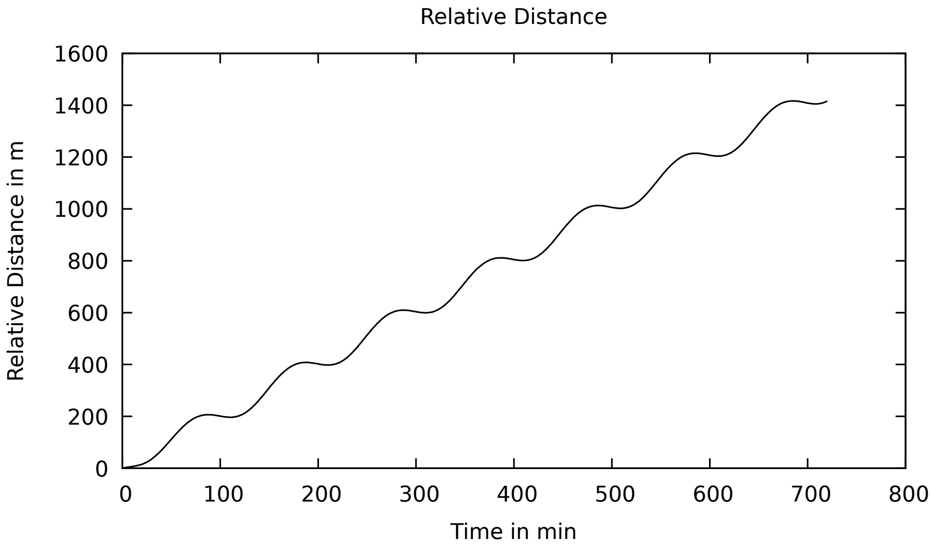

(b) CubeSat 1 and 3

Fig. 4.8 Relative distance of each CubeSat.

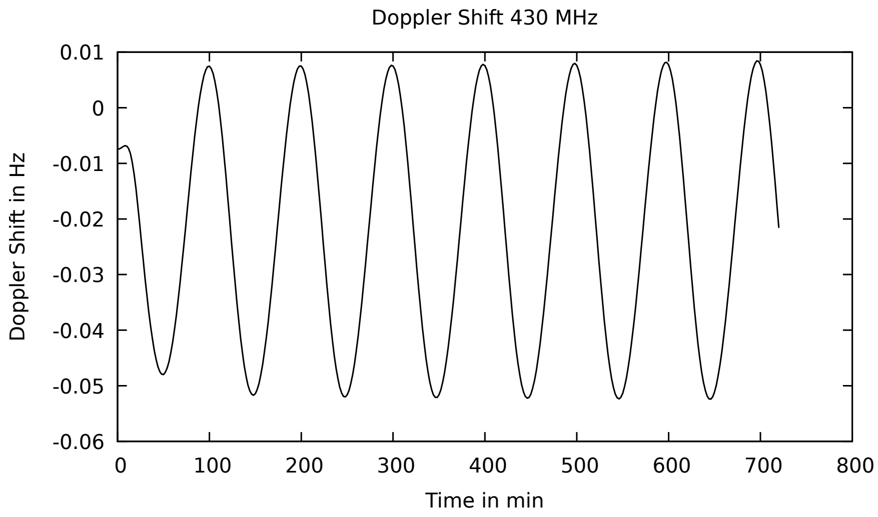

(a) CubeSat 2 and 1 and 3

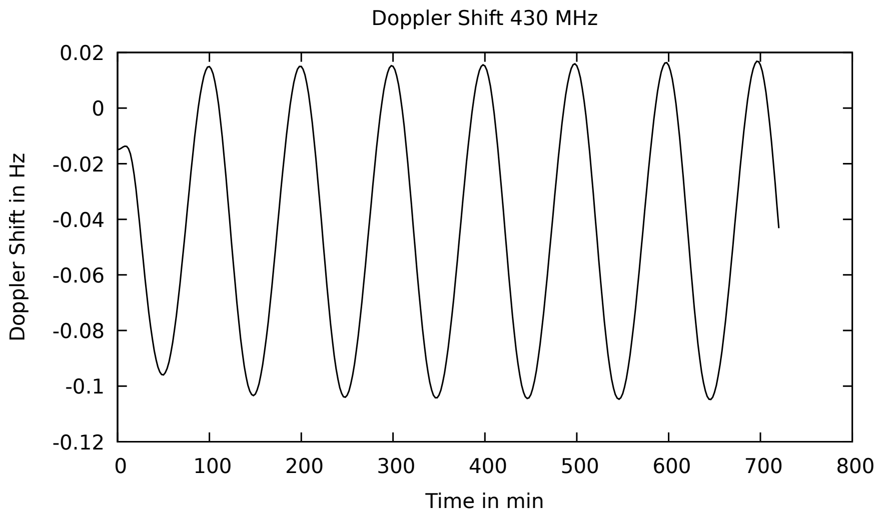

(b) CubeSat 1 wrt 3

Fig. 4.9 Doppler Shift due to relative motion.

4.3 Case Study : Sensor Satellite with respect to a Relay Satellite

Orbital configurations are possible in many ways. Therefore the Doppler Frequency shifts are determined from simulating selected orbits in the following cases:

- The first is a Relay satellite at a higher altitude and sensor satellites at a lower altitude, both in LEO. The relative motion of the relay and sensor satellite is studied.
- The second is a "string of pearls" configuration, in which several satellites are in the same orbit but separated e.g. Disaster Monitoring Constellation (DMC) [114].

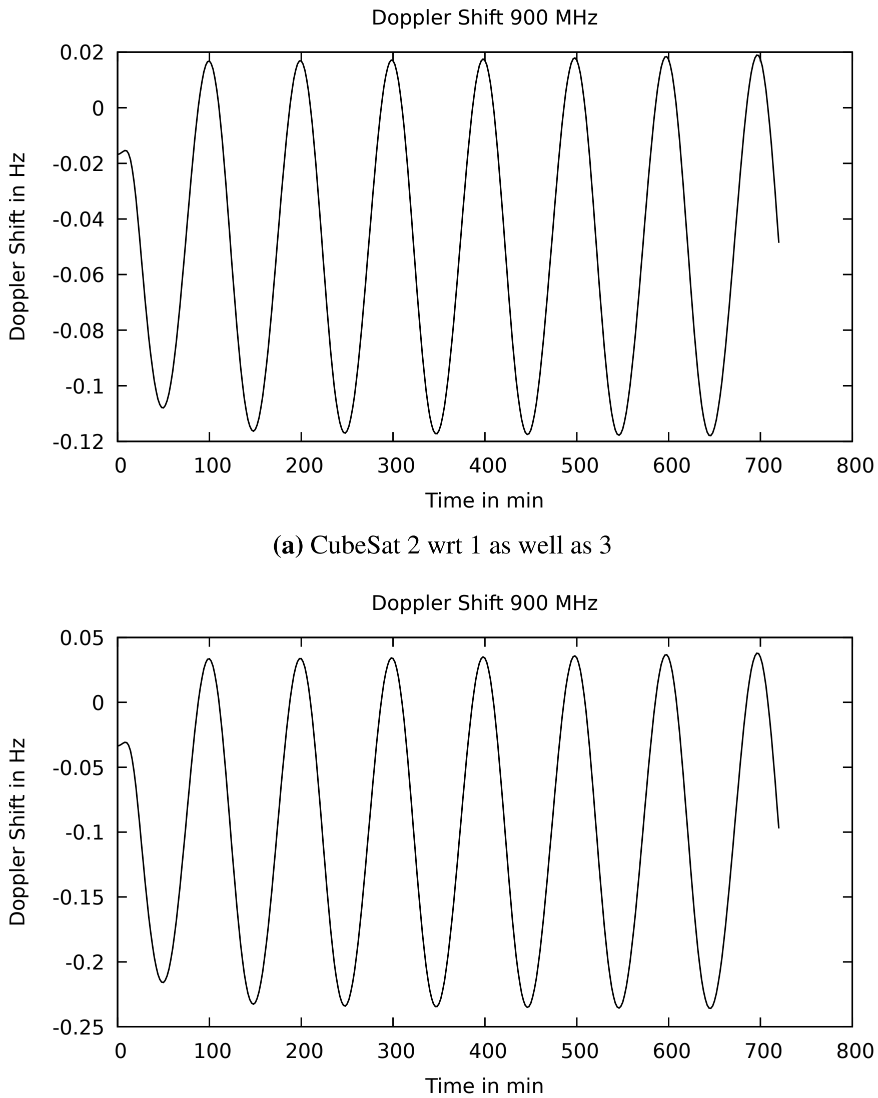

(a) CubeSat 2 wrt 1 as well as 3

(b) CubeSat 1 wrt 3

Fig. 4.10 Doppler Shift for 900 MHz due to relative motion.

A scenario is selected, in which a ReSat is placed at a higher altitude say about 800 km in a polar orbit. The SenSats are placed at an initial altitude of 500 km, and their orbit decays.

We assume that the antenna on the ReSat has a beam width of 40 deg. The projected coverage area on the surface of a sphere can be simulated in Savi using Geomview at the back end. However, the sphere typically represent the Earth of radius 6378.14 km. If we do not change this radius to incorporate the altitude of the SenSat, the visible coverage area is incorrect. In the settings the radius is corrected to include 500 km altitude, and then the projection is observed. In this manner, we can visibly assess link availability time for our preliminary design, which allows the selection of antenna parameters easier.

4.3.1 Link opportunity window for ReSat and SenSat

Simulating the orbits with Savi, for a constellation of ionosphere monitoring mission, with only two orbital planes selected, and a relay satellite placed in between them is illustrated in the Figure 4.11. In the illustration, the coverage area by the Relay Satellite is based on its projection on Earth. A wider area of coverage is visible. In reality, the SenSat is at about 500km altitude, and is much nearer the ReSat. Therefore the coverage area of the antenna radiation cone is reduced equivalent to the ratio of 800/500.

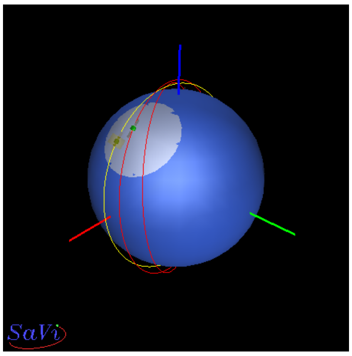

(a) SenSat1 Link opportunity start.

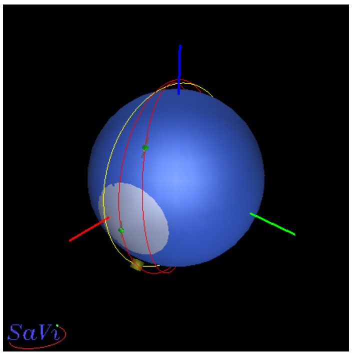

(b) SenSat1 Link opportunity end.

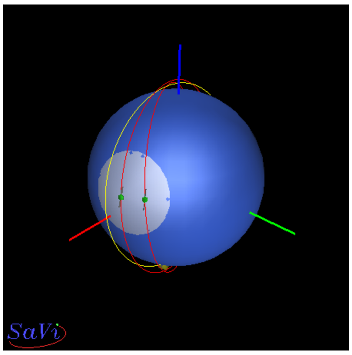

(c) SenSat2 Link opportunity start.

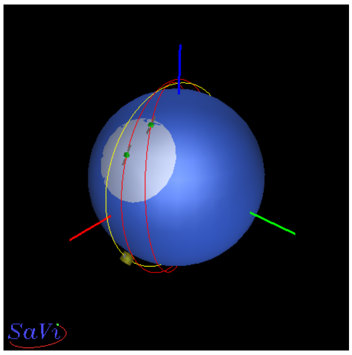

(d) SenSat2 Link opportunity end.

Fig. 4.11 ISL opportunity window for ReSat with SenSat1 and SenSat2, simulated with J2 perturbations only using SaVi. The cones depict the coverage zone of the antenna field of view on Earth (about 40 deg beam width).

4.3.2 Relative motion of Relay Satellite and Sensor Satellite

For the relay satellite and the sensor satellite set, relative motion assessment shows interesting results. The relative distance and Doppler shift for 430 MHz between the Relay Satellite (Sat 1) to the sensor satellites (Sat 2 and Sat 3) is illustrated in Figure 4.12. The satellites tend to move very far as they traverse other side of the Earth, that is why large relative distances are observed in the plotted data. Although it is not clearly visible, but the SenSats gradually lose attitude in free flight, so does ReSat in free flight mode. In reality, ReSat are assumed to have on-board fuel to maintain their orbits. Thus, SenSats fall back to Earth as free flying objects, whereas ReSat maintains its orbit till its expected EoL and then forced to lose altitude.

The small oscillations in Doppler Shift indicate one orbit of SenSats with respect to ReSat. The sharp edges indicate the times when ReSat and SenSat approach from opposite sides, because of the different precession rates of the orbits at different altitudes. That is why abrupt change of relative distance and Doppler shift is observed. Since the relative velocity is significantly high, therefore, high Doppler shift is observed in this case.

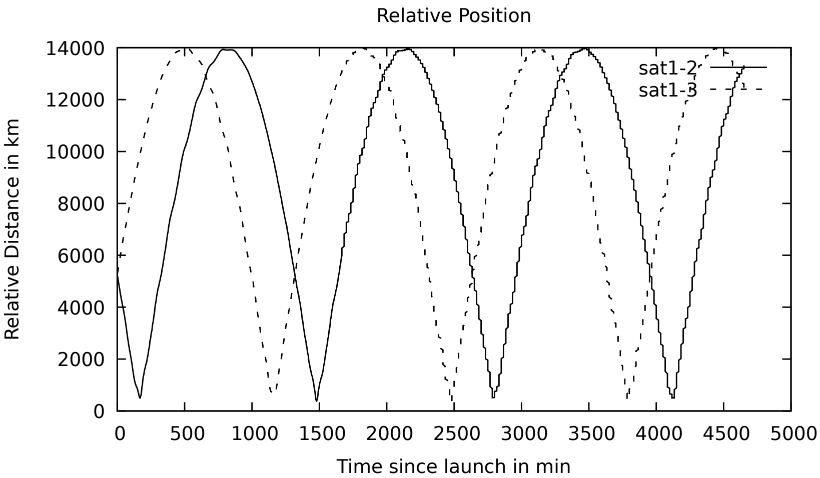

(a) Relay Sat Distance with respect to SenSats

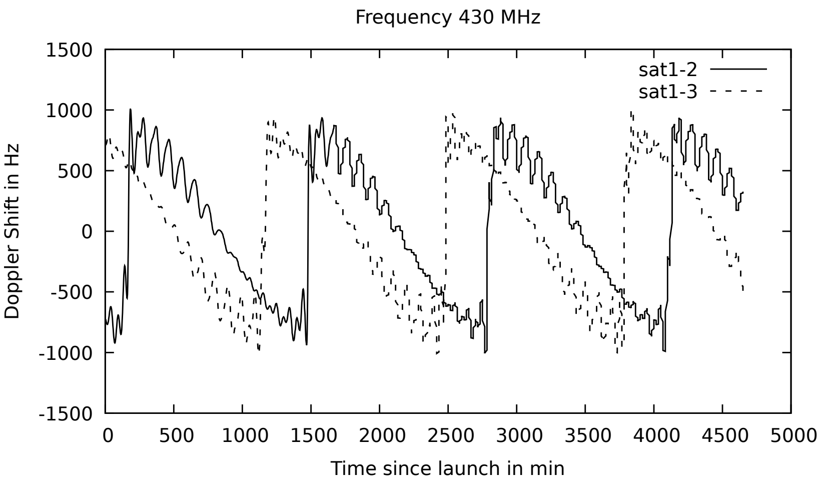

(b) Relay Sat Doppler frequency with respect to SenSats

Fig. 4.12 Relative motion and Doppler Frequency shift observed after simulation using numerical orbit propagator.

4.3.3 Discussion of relative motion between ReSat and SenSat

Doppler frequency shifts computed over several orbits, are illustrated in Figure 4.13 for carrier frequency of 430 MHz. The high shift rate is evident when the satellite approach each other and also with higher operational frequencies. Optimal link availability would be few minutes before and after the maximum shift rate.

Taking the numerical derivative of the Doppler shift, results in shift rate. The Doppler shift rate is maximum at two occasions, (a) when the satellites are moving closer to each other, and (b) when the satellites are moving away from each other. This behaviour is observed in ground stations tracking LEO satellite passes, which endorses the results obtained.

At high Doppler shift rates, the PLL design is a critical factor in successful communications link (for details referred to [202]). The opportunity window to establish the link is between the times, when Doppler shift and its rate of change is in the acceptable levels of PLL design. Assuming PLL is correctly designed, then the link opportunity windows is less than 20 min.

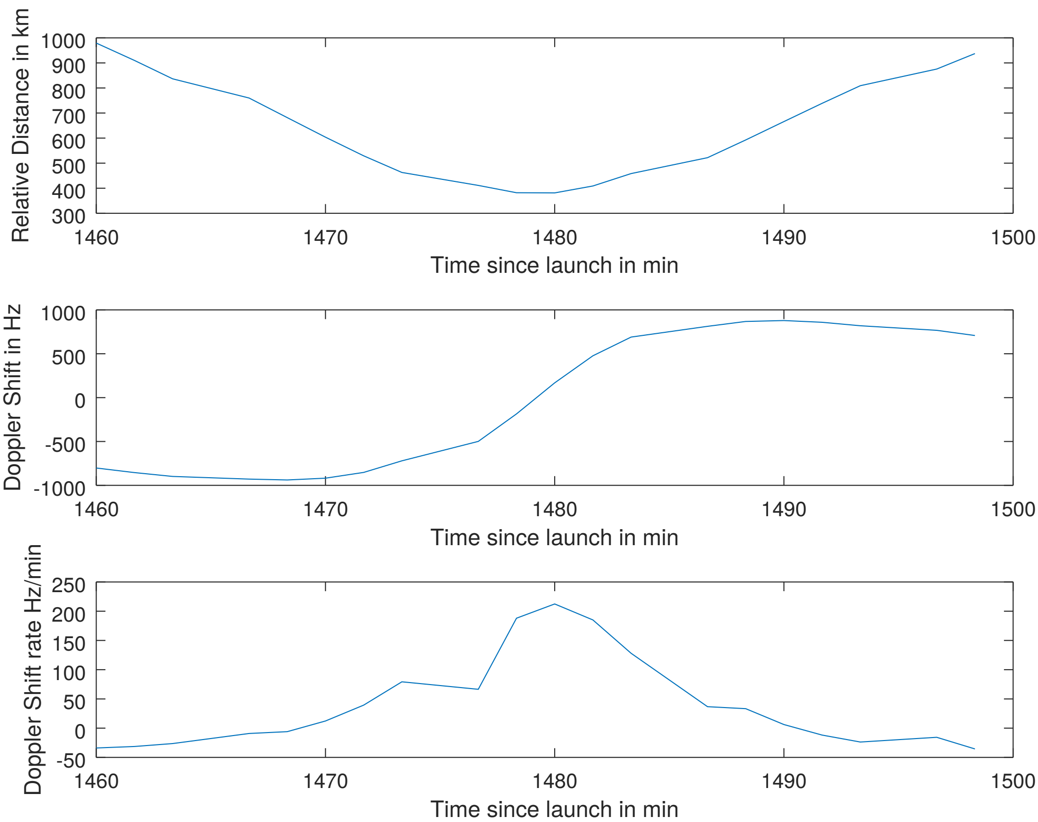

Fig. 4.13 Relative motion, Doppler shift and Doppler shift rate at closest approach for ReSat with respect to SenSat1 430 MHz.

4.4 Relative Motion of a Relay Satellite with respect to a Relay Satellite in the Same Orbit

Inter-satellite links between two ReSats is considered here. For the ReSat, a **string-of-pearls** type orbit is perceived. Satellites move in the same orbit (path), but spaced out, therefore each satellite follows the other in the same orbit. In this way they resemble pearls on a string, where each pearl can move along the path defined by the string.

The Rapid Eye constellation (also known as Disaster Monitoring Constellation (DMC)), is selected for preliminary evaluation purposes, depicting ReSats.. It comprises of 5 equally spaced similar satellites in polar orbit at 650 km launched in 2008, from a single launch. Visuals of the constellation are shown in Figure 4.14. The yellow colour in Figure 4.14b is the footprint of antenna radiation pattern, whereas, the greenish dots represent the ground tracks and the blue represents the region yet to be traversed by the satellites.

It is clear, that although the constellation is at the same altitude as is desired for IMM, however, they are unable to establish a clear line of sight for ReSat to ReSat inter-satellite link. The first observation is to increase the number of satellites per orbital plane. The second observation is that, in these simulations, the ReSat are being assumed to be in free flight mode as well. That is why the relative distance is changing, and there is a Doppler shift.

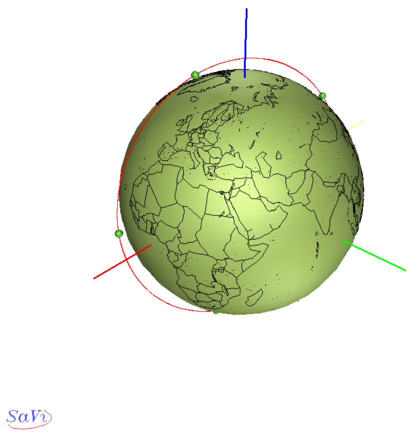

(a) Constellation of 5 equally spaced satellites.

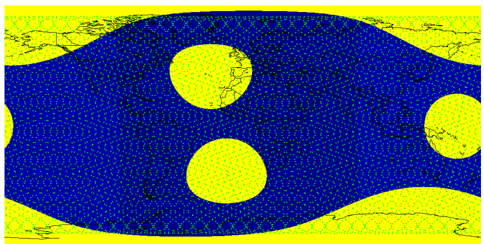

(b) Ground Coverage (green dots) after a few hours of simulation. Radio coverage represented by yellow circles.

Fig. 4.14 Rapid Eye constellation of 5 equally spaced similar Earth observatory satellites (650 km Sun Synchronous orbit).

However, it is being perceived, that ReSat being a larger satellite, shall be carrying on-board fuel, and would be able to maintain its orbit. Of course, then the relative distance would also be maintained, not as precisely as is required in FF missions. Therefore, the Doppler shift would be low.

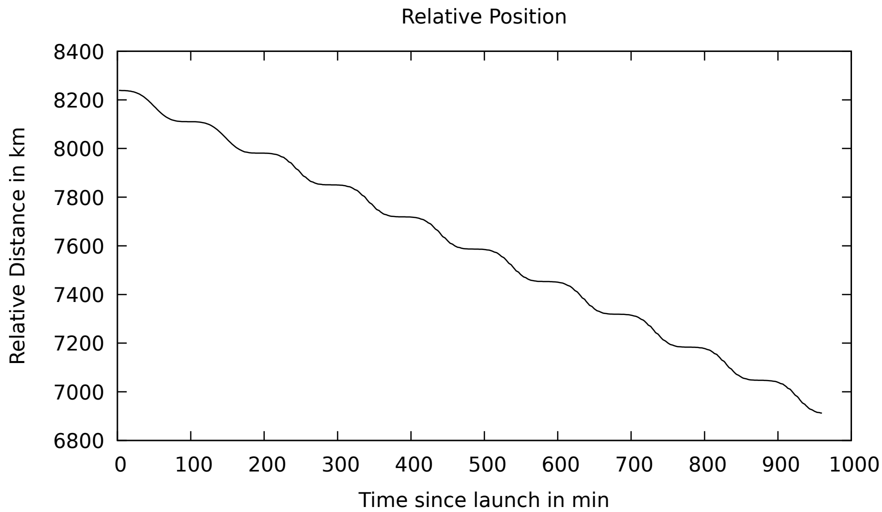

(a) Sat 1-2 Relative Distance

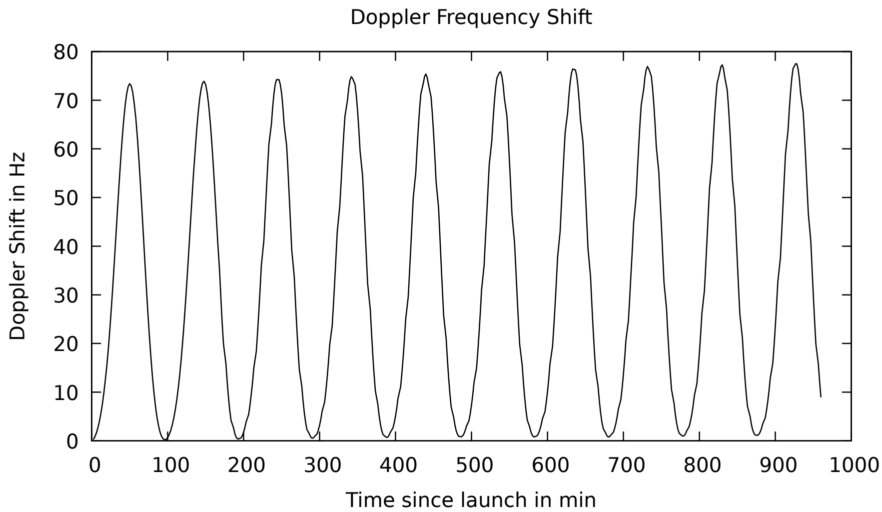

(b) Sat 1-2 Doppler

Fig. 4.15 Relative motion and Doppler shift 430 MHz of two adjacent satellites in a "String-of-Pearl" orbital configuration.

The relative displacement and the associated Doppler shift at 430 MHz for only two adjacent satellites is given in Figure 4.15. To assess the Doppler shifts, it is being assumed, that the satellites are in free fall. Although, in reality, these larger satellites would have orbit control, and 3-axis stabilised attitude controllers. Point to point links between relay satellites would require directional antennas, with nominal beamwidth, which may not need fine pointing, since the relative motion over the orbits is not significant.

4.5 Summary and Conclusion

In this Chapter the relative motion is studied with the help of numerical methods projecting the motion of a satellite from initial conditions, under the influence of 20×20 gravitational model, high precision atmospheric model (modified Jachia 71 model), third body effects and solar radiation pressure. Unlike analytical methods where close proximity approximations are assumed to be under the influence of same force fields, a high precision numerical orbit propagator incorporates variation of force fields, thus providing a better insight to the evolution of satellite orbits.

The following three cases have been investigated for evaluating the Doppler Frequency shift arising from the relative motion of communicating satellites.

- The case of free flying sensor satellites is studied by evaluating in-depth the deployment of 1U CubeSats by DNEPR in LEO polar orbits.
- The case of satellites in the same orbit i.e. the position in orbits is similar to a "string of pearls ", is studied emulating the effects on relative motion of Relay Satellites in the same orbit (Disaster Monitoring Constellation uses these orbits, which are perceived to act as orbits for Relay satellites).
- Relative motion of Relay satellite and Sensor Satellites is also simulated for a simple case.

In conducting the study, the launch sequence has been studied in depth, the deployment mechanism commonly employed for pico/nano class of satellites has been investigated, and in the process a numerical orbit propagator suitable for high precision / accuracy studies utilised, unlike similar studies where focus is on the use of analytical methods. Although analytical methods do provide an insight to the expected trajectories of satellites, they are unable to cater to the minor differences arising due to use of simple Earth's gravitational field models (commonly J_2 term of the harmonic potential function representing gravitational field is used, where as we have used 20×20 terms with the capability of using 70×70 or higher terms in the numerical code).

In the second case, since the satellites are in the same direction therefore the relative motion of the satellite is slow, and the Doppler frequency shift observed is tens of Hz. However, for the third case, where SenSat approaches ReSat high Doppler shift in kHz is observed. The Doppler shift is low, when the satellites communicate within the orbital plane, however, it is high, for intra-orbit links as observed in ReSat and SenSats. For, satellites in GEO, the case would be of a very high Doppler shift, exceeding that which is observed at the ground station for passing LEO satellites. A second and third order PLL based design would be required, in the first stage of radio, which should be checked during preliminary evaluation of COTS.

In order to technically evaluate SBWSN enabling technologies, an alternative controlled method of deploying CubeSats in orbit needs to be determined. The satellites be deployed in a manner, that the separation does not exceed a certain limit. CubeSats may be deployed from international space station (ISS) using its robotic arm.

Relative motion plays a critical role in the design and development of ISL hardware, and selection of the transmission schemes. The most important factors, that need to be addressed are the following **dynamic factors**:

- the link opportunity window
- the Doppler shift and shift rates

Mission design can be optimised on the basis of the above two factors. Constellation design tools, such as Walker Constellation are available, however, a new tool for free flying objects is deemed necessary for optimised mission orbit designs.

In the next chapter, the environment and its impact on propagating waves is investigated.

CHAPTER 5

WAVEFORM CHANNEL MODEL FOR INTER-SATELLITE LINKS IN LOW EARTH ORBITS

The purpose of this Chapter is to study the effects of the environment in Low Earth Orbits (LEO) on the propagation of the electromagnetic waves and determine the inter-satellite communications channel characteristics. The investigation is aimed at: (i) identifying possible causes of electromagnetic wave reflection, refraction, or scattering by studying in-orbit environment and (ii) identifying appropriate waveform channel model depicting the impairments caused due to interaction of in-orbit constituents during wave propagation. Based on the outcome of the study, an appropriate waveform channel model is defined.

5.1 Introduction

A wireless digital communications systems comprises a transmitter and receiver. The transmitter signal undergoes distortions as it interacts with the circuits making up the transceiver (hardware). After radiation, the propagating waves interact with the environment, further distorting the transmitted signal, and at reception after passing through the receiver circuit a similar set of hardware processes cause distortions before the baseband signal is available for message extraction. The impairments thus caused due to circuit effects are named **hardware impairments**, whereas, impairments caused by environment interactions with propagating wave, are called **channel impairments**. Both types of impairments distort the signal, for which the mitigation techniques are accordingly devised.

Hardware impairments are due to the signal processing circuits such as filters, amplifiers, multipliers, transistors, diodes and such, which are used for analogue signal processing. Some of the impairments are briefly discussed as follows. In analogue to digital conversion, quantisation losses are a major concern in analogue to digital conversion, whereas, fixed point representation in digital signal processes is also one of the concern. The nonlinear effects due to the use of power amplifier (prior to radiation), operating close to its saturation mode distorts signals with non-constant envelopes. Therefore signals with constant envelopes such as phase and frequency modulation are preferred. In processes other than the power amplification, the local carrier frequency offsets, phase changes, imbalances in the two paths being followed in I/Q architecture, offsets in local sampling clock, all contribute to distorting the signal. This operational mode is common in satellite operations, and the distortion is simulated using Saleh model [203]. Each impairment and its effect are well addressed in literature, unfortunately they are not within the scope defined for this thesis, however, interested readers can begin investigations by referring to the references provided in books [66, 75, 204].

The channel impairments are caused by several factors. In the wireless channel, the first impact on signal as it propagates away from the source is the loss of signal strength as a function of distance, wavelength and the properties of media. Same is true for wired medium, its attenuation factor depends on the make and type of the wire (different for copper wires, twisted pairs, coaxial wires). In its simplest form the media is considered void of any other particle i.e. free space, Friis devised a simple means of detecting this loss known as Friis transmission model [52] or free space path loss. However, for a medium with constituent molecules and particles, the attenuation tends to vary again as a function of the time, space and frequency of the signal, a phenomenon called **fading** in land-mobile communications [205] and **scintillation** in radio astronomy as well as in satellite to ground communications [206, 207].

The known sources of impairments can thus be modelled in baseband, for computer simulation based study, as depicted in Figure 5.1 (moving from transmitter to receiver). The identified blocks of the channel model can all be used in simulation based studies, or where possible, impairments caused by hardware can be eliminated reducing the simulation complexity and simulation run-time. Where hardware is available, and the simulation environment can be interfaced to the hardware, a hardware-in-the-loop (HIL) co-simulation method is fruitful. The code actually runs on the hardware, thus removing the need for hardware effect simulation, reducing the complexity of channel model to only propagation impairment modelling. Hardware impairments thus can be ignored in the preliminary design evaluation of baseband modem.

In evaluating the channel characteristics, the environment needs to be studied, for each path that is followed by the signal from the transmitter and receiver, must be identified. In wireless transmissions, the analysis of the received signal simplifies significantly, by identifying a path the wave takes from the transmitter to the receiver. The environment in its path can then be studied to identify the possible sources distorting the wave. The nature of distortion can then be ascertained with the help of existing knowledge accumulated over the years. The nature of medium or any other physical object present along the path can then be studied individually for its impact on the propagating wave. In wireless transmissions the wave can propagate taking one of the possible paths from transmitter to receiver, namely; (i) a single direct path, (ii) a single indirect path, (iii) multiple paths including a direct line of

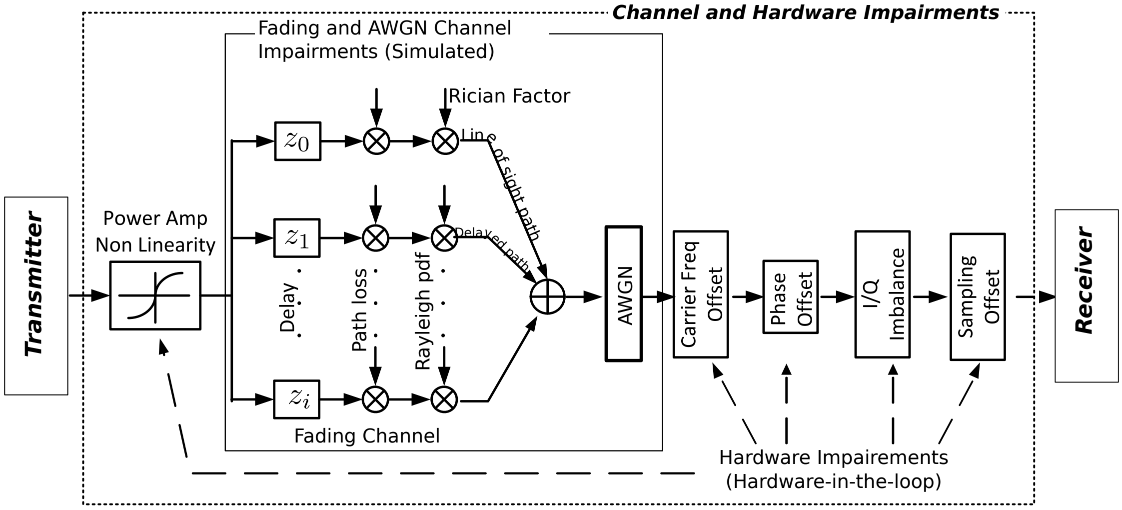

Fig. 5.1 Types of hardware and channel impairment from [208].

sight path (from transmitter to receiver), or (iv) multiple paths without a direct line of sight path, signals reach while passing through indirect paths. When ascertained that there are multiple paths, then each path is characterised for its propagation delay, the attenuation type (static or dynamic) and sources of interference on that path. For several paths, a path profile is thus formed, where each path characteristics are described.

While undertaking computer based simulation studies, the digital communications system is broken down in to manageable sub-systems. A complete end-to-end system simulation is possible provided a resourceful computer is available. Depending on the need of the sub-system analysis, the communications channel can be modelled either as a **discrete channel**, or **waveform channel**, following the definition of Meyr [209]. The outer receiver works on the bits identified by the inner receiver working on the electrical waveform demodulated by the analogue front end of the receiver side. The functional blocks of both receivers and the type of channel model requirements are depicted in Figure 5.2. The discrete channel is used when channel encoding performance is being studied i.e. the performance of error correction codes (number of errors detected and corrected in bit sequence). The need is to randomly flip the bit sequence to test the performance of error correction codes. Whereas, when baseband modem performance is to be studied, the need is to distort the electrical waveform by changing its time and frequency domain characteristics depicting the changes as would be observed in real world.

The demodulator estimates the sent message from the distorted waveform. The performance metric for a demodulator is the bit error rate. When the message is correctly received, with in acceptable BER, then its performance is acceptable. The acceptable BER depends on the type of message and the channel. For example commands being uploaded to satellites, cannot tolerate a single bit error, whereas, bulky images or science data downloaded from satellites can tolerate a certain amount of error. The certain

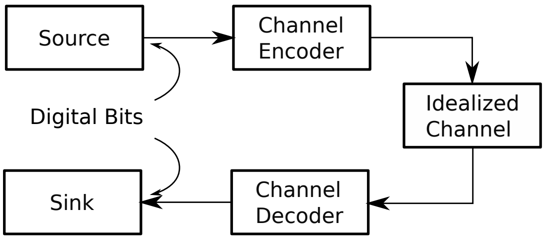

(a) Idealized communication model studied in information theory. Assuming digital sources.

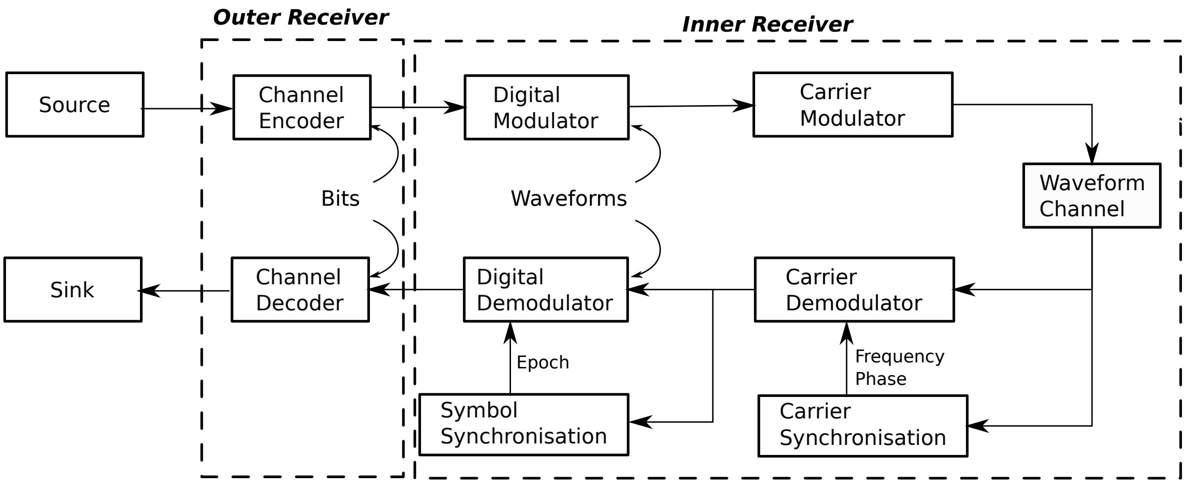

(b) Physical communications model. Assuming digital sources generating bits.

Fig. 5.2 Inner and Outer receiver definitions by Meyr [209] and the associated digital channel models.

amount of error is defined. Therefore, performance of the receiver is based strictly on the channel under which the type of service is being provided*.

In subsequent discussions, the terms waveform channel and channel are used interchangeably, referring to waveform channel. The baseband modem performance would vary according to the channel model employed, whereby, the channel model should correctly depict the propagation environment in which the modem is to operate. Hence, the knowledge of channel is critical to the design of modem. Particular care must be given to deriving the channel model. Waveform channel is the topic of this chapter.

The waveform channel model is derived either from measurements or is based on the theory of physical propagation, latter approach is followed in this thesis, since in-orbit experiments are outside the scope of the research. Published literature sources are studied first to determine the channel model. The characterisation of the channel in time or frequency domain often involves statistical descriptions (random processes defined by probability distribution functions first published as a uniform theory of stochastic process to model random time varying channel behaviour by Bello [55]). The parameters

*Further information on the availability of telephony circuits can be found in ITU-T Recommendation G.821. In general data service cannot tolerate BER < 10^{-2}, recommended is to achieve BER > 10^{-6}. Again it depends on the type of channel being used, see [210, 211] for detailed discussion on performance i.e. BER in fading type channels vs AWGN type channels.

of the underlying distributions and power spectral densities are usually estimated from measured data. Developing mathematical models for the propagation of signals in space environment requires a good understanding of the underlying physical phenomenon. To develop a model for an ionospheric radio channel, one must understand the physics of radio wave propagation (magneto-ionic theory [212, 213] governing propagation of radio waves). "One of the challenges in channel modelling is the translation of a detailed physical propagation model into a form that is suitable for simulation. Communication engineers rely on experts in the physical sciences to provide the fundamental models for different types of physical channels. For example, the mathematical model of a radio channel may take the form of the Maxwell's equations (as is the case in magneto-ionic theories). While accurate, this model must be simplified and converted to a convenient form, prior to its use in simulation" [66].

When converting into a "convenient form", one of the important consideration is the accuracy vs performance. Non-linear functions require time consuming numerical methods, whereas, linear functions are easier to solve numerically. The first decision is to assume that channel can be characterised in terms of linear functions, for the sake of simplicity. The second is the variation of channel properties with time and space; time varying functions are more complicated than time-invariant functions, whereas, variation with space means incorporating spatial dependency in functions as well. A simpler approach is to evaluate the performance for a space for its characteristics at one instance at a time, selecting the worst case scenario in this regards is the right approach, since the system can perform better in other scenarios if it can sustain the worst case.

5.1.1 Assumptions and Considerations for Channel Characterisation

The channel is evaluated for its characteristics in the light of the following assumptions;

1. The sensor satellites use isotropic antennas, therefore, signals can be received from any direction about the antennas i.e. the field of view can be considered a 4π sr sphere (Figure 5.3).
2. The relay satellites may use directional antennas.
3. Several sensor satellites may be in close proximity of each other.
4. There is a possibility that several clusters of sensor satellites may operate in proximity not necessarily very close but at a reasonable communications range.
5. The sensors would gradually lose their altitude till they reach 150 km, below which the satellites rapidly enter Earth's atmosphere. The region of interest is therefore, between 150 km and 1000 km.

The factors which must be considered in the context of the antenna radiation pattern i.e. the field of view, are:-

- The antenna types at both the transmitter and receiver dictate the maximum communications range; that is the distance in which acceptable communications (message) takes place.

- The significance of objects present within the communications coverage area is important when the radiation pattern is isotropic, since they influence channel by becoming sources of multiple reflectors, causing multipath effects. Whereas, in the case of directional antennas, their presence may be ignored, depending on the number of objects and their location within the radiation pattern, distance between the transmitter and receiver.
- The type of antenna being used also dictate the role of attitude and orbit control design of satellite. In other words, when the satellite is tumbling without any attitude control mechanism, isotropic antenna is preferred, which is used for engineering data acquisition during the initial commissioning phase.

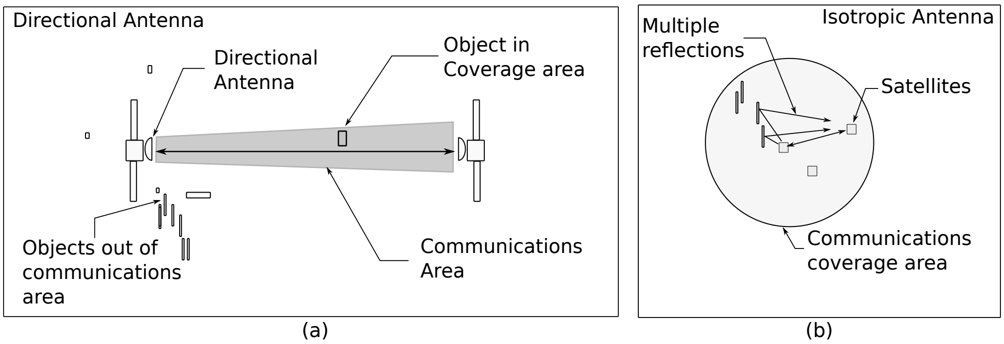

Fig. 5.3 Considerations for radiation pattern. (a) Directional antenna, narrow beam width, objects cause little effect. (b) Isotropic radiation pattern, limited range, objects cause multiple reflections (scattering) causing multipath fading.

5.1.2 Channel Transfer Function Definition

For the purposes of analysis and study, the communications system for the transmitter receiver pair can be modelled as illustrated in Figure 5.4. The message from the source is converted to a time domain signal x(t) which is the input to the channel represented by h(t), and the receiver extracts the message from the distorted received signal y(t).

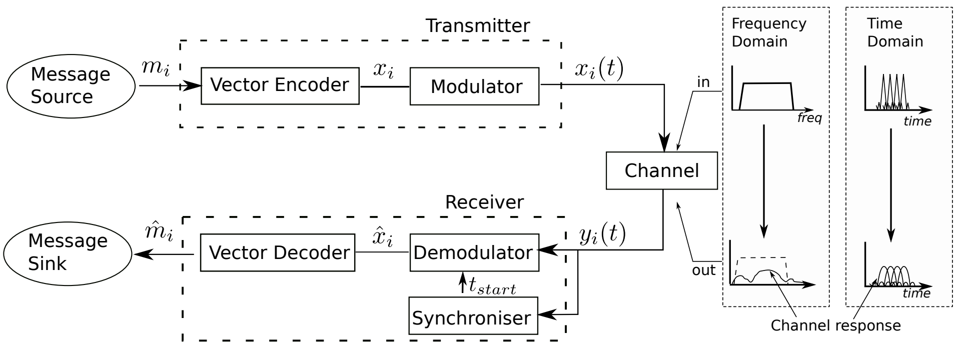

Fig. 5.4 Notation of the input and output signal through the channel.

Consider the channel as a system of signal processes (amplification, filtering, sampling, transformations, interference, impedance mismatching and such) which change the incoming signal properties in an undesirable manner. The undesirable effects are captured in mathematical expressions called channel transfer functions; h(t) when time domain analysis is being carried out, and H(f) for frequency domain analysis; where H(f) is Fourier transform of h(t).

The received signal y(t) is outcome of the convolution ($\star$) of channel transfer function h(t) and transmitted signal x(t), expressed as:

$$\mathrm{y(t) = h(t) \star x(t)} \tag{5.1}$$

The intrinsic noise w(t) is added to Eq. (5.1), resulting in a generic representation of received signal as:

$$\mathrm{y(t) = h(t) \star x(t) + w(t)} \tag{5.2}$$

In computer based simulations, time domain signals are discrete forms of the signal, stated as:

$$\mathrm{y[n] = h[n] \star x[n] + w[n]} \tag{5.3}$$

When the transmitter and receiver are non-stationary then the surrounding environment may change as is the case in land mobile communications [214] or satellite to mobile communications [215]. In both cases the deteriorating effects are incorporated within the channel transfer function applicable to the coverage area. In this manner, the transfer function becomes simpler to implement. The temporal and spatial dependence of channel transfer function is generated stochastically (see Annex B.2 for examples of fading channel transfer functions).

The objective of this chapter is to determine the form of h(t).

The simplest and well known form is described first, to illustrate the over all process of channel modelling.

5.2 Signal Attenuation

Consider the transmitted signal x has an amplitude A, then how does the channel attenuate this amplitude as it reaches the receiver. In this case the channel response h only attenuates A which can be modelled as an attenuation factor α, then the received signal can be stated as;

$$y[n] = \alpha\, A\, x[n] + w[n] \tag{5.4}$$

The nature of attenuation function α in eq (5.4), is determined after further investigations.

When the signal has a constant level A representing the mean voltage level, then the power in the signal over that time duration is $P = V^2/R$, where R is the resistance across which the voltage is being measured, generally 50 ohms for antenna interface.

For a given distance, when the received signal strength measured remains same irrespective of the time, or place, then the environment can be considered ideal. Such an environment would only exhibit loss of energy due to propagation from the source to the receiver.

5.2.1 Free Space Path Loss

To determine the attenuation when a transmitter and receiver are a distance d apart, consider the antennas being isotropic i.e. the radiation pattern is uniform all about the antenna, then the power radiated per unit solid angle when P_t is fed to the antenna is

$$\frac{P_t}{4\pi} \qquad \text{(Watt/steradian)} \tag{5.5}$$

In the case when an antenna amplifies the radiated power by a factor called the gain of the antenna G_t, then the effective isotropic radiated power (EIRP) is

$$EIRP = (P_t G_t)/4\pi \tag{5.6}$$

An antenna with the surface area A_{aper} situated at a distance d from the transmitter subtends a solid angle A_{aper}/d^2 at the transmitting antenna. It receives a power equal to

$$P_r = \frac{P_t G_t}{4\pi} \frac{A_{aper}}{d^2} = \Phi\, A_{aper} \qquad \text{(W)} \tag{5.7}$$

The magnitude Φ is called the power flux density expressed in $\mathrm{W/m^2}$, which are used in determining the power captured by the antenna.

The receiving antenna captures the radiated power on an effective surface area $A_{r_{eff}}$ expressed in terms of the gain as

$$A_{r_{eff}} = \frac{G_r}{4\pi/\lambda^2} \qquad (\mathrm{m}^2) \tag{5.8}$$

Hence the received power using eq. (5.7) and eq. (5.8) gives;

$$P_r = P_t G_t G_r \left(\frac{\lambda}{4\pi d}\right)^2 \tag{5.9}$$

Separating the terms not associated with the antenna or assuming that the gains of the antenna are unity, a relationship of the loss of signal power can be stated as;

$$L_{free} = \frac{P_r}{P_t} = \left(\frac{\lambda}{4\pi d}\right)^2 \tag{5.10}$$

where L_{free} is the free space path loss, and the simplest form describing the attenuation function α, relating transmitted power and received power by the distance and the operational frequency. The dependent factors are distance and wavelength. Note this is a time invariant function i.e. there is no relationship with time.

In eq. (5.10), the medium is assumed to be vacuum, therefore, any cause of attenuation due to medium can be incorporated.

In the next section, attenuation of wave due to ionised gas in Earth's magnetic field is considered.

5.2.2 Loss of Power in Plasma

In inter-satellite links, the medium is ionised gas comprising of electrons and ions moving freely. When the satellite transmits, the electromagnetic wave interacts with the free moving charged particles. This interaction is complex, and a full wave theory is required to describe the interaction with a single particle, which is then simplified to describe multiple phenomenon. The propagation of wave through the ionised gas is well described in magneto-ionic theory see for instance a treatise by Ratcliffe [213] and Budden [216, 212]. We shall follow the treatise by Ratcliffe to describe the fundamental expressions.

The EM propagation depends on the density of electrons and ions, the collision of electrons with ions, whose motion is governed by the imposed magnetic fields. To investigate the absorption, the complex refractive index is written as

$$\eta = \mu - i\,\chi \tag{5.11}$$

so that the wave propagating in z-direction in the medium is represented by:

$$E = \mathrm{A}\ \exp\{\mathrm{i}\ \omega\ (t - \eta\ z/c)\} \tag{5.12}$$

and written with the complex refractive index

$$E = \mathrm{A}\ \exp(-\omega\chi z/c)\ \exp(\mathrm{i}\omega(t-\mu z/c)) \tag{5.13}$$

This wave is attenuated to $\exp(-\chi)$ within a distance of $z = c/\omega = \lambda/2\ \pi$, while travelling with a velocity c/μ. The absorption coefficient κ is stated as

$$\kappa = \omega\chi/c \tag{5.14}$$

Where the relationship of absorption coefficient is determined from the complex refractive index.

5.2.2.1 The Appleton-Hartree Equations

The complex refractive index η of a magneto-ionic medium was derived from the works of Lorentz by Appleton [213, pg.5]. Considering the effects of particle collisions (which cause attenuation), the refractive index takes the form as follows;

$$\begin{aligned} \eta^2 &= (\mu - i\chi)^2 \\ &= 1 - \frac{X}{1 - iZ - \dfrac{Y_T^2}{2(1-X-iZ)} \pm \left(\dfrac{Y_T^4}{4(1-X-iZ)^2} + Y_L^2\right)^{\frac{1}{2}}} \end{aligned} \tag{5.15}$$

Simplified nomenclature commonly used in magneto-ionic studies is used:

$$\omega_N^2 = 4\pi N e^2/\varepsilon_0 m_e \tag{5.16}$$

$$\omega_H = \mu_0 B_\oplus |e|/m_e \tag{5.17}$$

$$\omega_L = (\mu_0 B_\oplus e/m)\cos\Theta \tag{5.18}$$

$$\omega_T = (\mu_0 B_\oplus e/m)\sin\Theta \tag{5.19}$$

$$X = \frac{\omega_N^2}{\omega^2} \tag{5.20}$$

$$Y = \frac{\omega_H}{\omega} \tag{5.21}$$

$$Y_L = \frac{\omega_L}{\omega} \tag{5.22}$$

$$Y_T = \frac{\omega_T}{\omega} \tag{5.23}$$

$$Z = \frac{\nu}{\omega} \tag{5.24}$$

where N is the electron concentration along the path of observed EM wave propagation. e and m_e are the charge and mass of electron. ε_o is the permittivity of free space; ν is the electron collision frequency; Θ is the angle between $\mathbf{B}_{\oplus}$ and Oz; Oz is the direction of propagation of wavefront; $\pm$ sign refers to the ordinary mode and the extraordinary mode. When a linearly polarised wave passes through an assembly of charged particles in the presence of a magnetic field, it causes electrons to move round in circles. If the composite wave (addition of re-radiated wavelets from electrons) whose field also rotates in the original way, then the polarisation has not changed, hence is a characteristic ordinary wave. If the polarisation of the composite wave is opposite to the original wave's polarisation, its the characteristic extraordinary wave.

The velocities, the absorption, and the wave polarisation depends amongst other parameters on the quantities Y_L and Y_T i.e. on the angle between the direction of propagation and the direction of the imposed Geomagnetic field $\mathbf{B}_{\oplus}$, the density of charged particles, the number of electrons along the wave path, the collision of electrons with heavy ions and the irregular structures of plasma.

In order to deduce a relationship of attenuation factor, simplify the relationship. It is convenient to consider the magnitude of χ in the special case when the wave propagates along the direction of Earth's magnetic field, i.e. $Y_T = 0$, then eq. (5.15) becomes

$$(\mu - \mathrm{i}\chi)^2 = 1 - \frac{X}{(1 \pm |Y_L| - \mathrm{i}\, Z)} \tag{5.25}$$

Expanding the left hand side and equating the real and imaginary parts with right hand side in eq. (5.25), the following relations

$$\mu^2 - \chi^2 = 1 - \frac{X(1 \pm |Y_L|)}{(1 \pm |Y_L|)^2 + Z^2} \tag{5.26}$$

$$2\mu\chi = \frac{XZ}{(1 \pm |Y_L|)^2 + Z^2} \tag{5.27}$$

A useful expression is obtained for the absorption coefficient κ;

$$\kappa = \frac{\nu}{2c} \frac{I}{(1 \pm |Y_L|)} \left\{ \frac{1 - \mu^2 - \chi^2}{\mu} \right\} \tag{5.28}$$

Ratcliffe elaborates, “that at places where μ departs appreciably from unity*, it is feasible for practical applications to assume that $\chi^2 \ll 1-\mu^2$, otherwise the wave would become so heavily attenuated in a distance of one or two wavelengths that it can not be detected.”. Therefore eq.(5.28) is reduced to

$$\kappa = \frac{\nu}{2c}\frac{I}{(1 \pm |Y_L|)}\left\{\frac{1}{\mu} - \mu\right\} \tag{5.29}$$

It is evident from eq. (5.29) that the attenuation function depends on several variables which vary with the time and location. The dynamic relationship indicates that the loss of a signal is not constant which is an observed fact in satellite to ground links, as well as long distance HF radio links.

5.2.2.2 Simplified Forms for Absorption

There is little published literature regarding the absorption factor for inter-satellite links. A relevant paper is from Middlestead [145]. He studied the impact of man made disturbance in ionosphere, on ISL for a network of satellites operating at an altitude of 700 km. His network operates in the extremely high frequency (EHF) band, much higher than the gyro-frequency of plasma. The attenuation factor in decibels per meter (dB/m) at EHF is given as a good approximation as;

$$\alpha(z) = 1.16 \times 10^{-19}\,\frac{N_e(z)}{f_g^2} \qquad \text{(dB/m)} \tag{5.30}$$

where z is the direction of propagation, f_g is frequency in GHz and the total attenuation is calculated over the path length d. He concludes that the attenuation at these high frequencies is negligible even when a high intensity nuclear blast occurs. Davies [150] follows the same approximation as by Ratcliffe and Budden.

Nathan [184] uses a similar set of approximations in their studies. The absorption of radio waves in the regular ionosphere is defined in terms of intensity of radio wave as;

$$I(k) = I_0\ \exp(-2\frac{\omega}{c}\int \alpha dz) \tag{5.31}$$

where I_0 is the intensity of incident wave. For frequencies of interest, $\omega \gg \omega_N$ and $\omega > \omega_H$, the coefficient of absorption can be presented as;

$$\alpha = \frac{1}{2}\,\frac{\omega_H^2(\nu)}{\omega(\omega^2+(\nu)^2)} \tag{5.32}$$

*The real part of refractive index is unity outside the plasma depicting free space, whereas the complex part is zero.

where ν is the collision frequency having both electron with ions and neutrals. The magnitude of absorption over the path other than the F region* is given by

$$\alpha = 10\log_{10}\frac{I_0}{I(k)} = \frac{4.3}{c}\int\frac{\omega_H^2(\nu)}{\omega[\omega^2+(\nu)^2]}dz \tag{5.33}$$

Furthermore, for the ionosphere at altitudes greater than the altitudes of D and E layers, the absorption of radio waves in the irregular ionosphere, is stated as follows;

$$\alpha \approx \frac{4.58\cdot 10^{-5}}{\omega^2}\int N_e\,\mu dz \tag{5.34}$$

"It is further noticed, that absorption usually cannot exceed values of about 0.2-0.3 dB on days without magnetic disturbances, sometimes increasing up to 0.5 dB during small magnetic disturbances, whereas for strong magnetic storms the value can reach up to several dB" [184, pg.405]. The above statement assumes satellite to ground links.

To the best of the author's knowledge no details were available in the literature at the time of the writing of the thesis regarding absorption values related to inter-satellite links. There might be a substantial difference between attenuation for an ISL and a space to ground link (or sensor to relay link which is mostly vertical) as a limb viewing payload sees about 50 times as much atmosphere as a nadir viewing imager†.

Therefore, these values must be considered in the link budgets being calculated for inter-satellite links, especially operating over polar and equatorial regions, to determine worst case scenarios. But the absorption of energy by plasma is not the type of impairment. Other forms of transmission impairments due to plasma are described in the following section.

5.3 General Transmission Impairments due to Plasma

The plasma is not an isotropic medium but is anisotropic i.e. the wave properties when travelling in a direction may differ when travelling in the opposite direction. It is particularly observed in satellite to ground links for frequencies less than 10 GHz [53, 217, 218]. Inter-satellite links in LEO would be affected, whereas, ISL for Geo to Geo satellites, would not be concerned, because plasma density and Earth's magnetic field reduces its strength farther away from the Earth.

*The distinct density of ionised gas allows us to distinguish Earth's ionosphere into regions called the D (60 - 90 km (during the day only)), E (90 - 150 km (during the day)) and F (150 to $\geq$ 500 km) layers, see section 5.4.1.1.

†Dr S.E. Hobbs, private correspondence, March 2019.

"The radio wave suffers both large-scale changes due to variations in electron density and small-scale irregularities. The effects include the scintillation, absorption, variations in the direction of arrival, group path delay, dispersion, Doppler shift, polarisation rotation, refraction and phase advances.All of the effects are proportional to the total electron content (TEC)" [219].

The Total Electron content (TEC) is the total number of electrons in a column of unit area along the path from the transmitter to the receiver, and is measured in TEC $= \int \mathrm{Ndl}$, having units of electrons$/\mathrm{m}^2$, along the traversed path length l. Nominal values of electron densities for concerned altitudes are quoted for reference in Table 5.1.

Table 5.1 Electron Density for concerned altitudes on a typical day and night [219, ch.2].

Altitude [km]	N-day $electrons/m^3$	N-night $electrons/m^3$
400	10^{12}	3×10^{10}
600	10^{10}	5×10^{9}
800	10^{9}	9×10^{8}

For frequencies well above the critical frequencies of plasma, the following simple relationships are applicable, useful in preliminary system design.

RF Carrier Phase Advance: Delaying the arrival of a signal is similar to advancing the phase of the received signal; i.e. it appears to have travelled further than it actually has. The phase advance $\Delta\phi$ is given as

$$\Delta\phi = \frac{8.44 \times 10^{-7}}{f} \times TEC \qquad \text{(radians)} \tag{5.35}$$

where f is measured in Hertz.

For a 600 km altitude, using value of TEC = 1×10^{15}, the phase advances for relevant frequencies at 0.5, 10 and 100 km inter-satellite distances are stated in Table 5.2.

Table 5.2 RF Phase advance on relevant frequencies for a 600 km altitude, during day time, for selected inter-satellite distances.

Frequency	$\Delta\phi$ (rad) for distance		
(MHz)	0.5 km	10 km	100 km
130	0.032	0.65	6.49
430	0.0098	0.20	1.96
2400	0.00176	0.0352	0.352

Group Path Delay: The phase path length through a medium does not equal the true path length. Since the phase path length is directly proportional to the refractive index, which in turn is a function of frequency, a transmitted signal having a bandwidth will suffer a group delay. So when the signal bandwidth is wide, the delay within the spectrum is significant. The group delay acting on a single frequency (pulse) will cause the signal to arrive later than it would have done if transmitted in vacuo. The excess time delay over the vacuo transit time is given as

$$\Delta t = \frac{40.3}{cf^2}\,\text{TEC} \qquad \text{(sec)} \tag{5.36}$$

where c is velocity of light.

Distortion of Pulse Waveforms: The ionospheric dispersion causes pulse broadening by virtue of the differential time delay across the signal bandwidth, Δf according to the following relation.

$$\Delta t = \frac{80.6 \times 10^6}{cf^3}\,\Delta f\ \text{TEC} \qquad \text{(sec)} \tag{5.37}$$

Faraday Rotation: At operational frequencies above 100 MHz the approximate rotation in the polarisation is given as

$$\Omega = \frac{2.365 \times 10^{-5}}{f^2}\,B_L\ \text{TEC} \qquad \text{(radians)} \tag{5.38}$$

where B_L is the Geo magnetic field (nT) component parallel to the wave direction taken at the mean ionospheric height.

Doppler frequency: The rate of change of phase is defined as frequency, therefore

$$f = \frac{1}{2\pi}\frac{d\phi}{dt} \qquad \text{(Hz)} \tag{5.39}$$

Then the approximate Doppler frequency shift [219] as

$$f_D = \frac{1.34 \times 10^{-7}}{f}\frac{d(TEC)}{dt} \qquad \text{(Hz)} \tag{5.40}$$

A simple discussion highlights the propagation effects of ionised gas on wave at three different frequencies. Increasing the frequency has an advantage that distorting propagation effects due to interaction with ionised gas reduce. For the same antenna gains, more RF power is required to achieve the same BER (digital transmission) when using a higher frequency when compared to a lower frequency. Increasing operational frequency means, improving the pointing accuracy of directional antennas used. Mechanical structures or electrical beam forming is required to direct the main beam towards the target. Therefore, a tradeoff has to be made in actual link design.

Smaller satellites (pico class) have less on-board resources as compared to larger satellites (nano class) in terms of electrical power and on-board space and/or volume. However, if the effective area of antenna be increased by some means, then more transmitted power can be captured. It must be noted, that for IEEE 802.11 based networking protocols, the radiation pattern of transmitter and receiver has to be close to isotropic, since a single frequency is shared amongst the network.

Table 5.3 Summary of ionospheric effects for frequencies from 100 MHz to 10 GHz, for a one-way link at a 30° elevation angle [217] based on the data collected over several years for Geostationary satellite ground links.

Effect	Freq. Depend.	100 MHz	250 MHz	500 MHz	1 GHz	3 GHz	10 GHz
Faraday rotation	$1/f^2$	30 rotations	4.8 rotations	1.2 rotations	108°	12°	1.1°
Propagation delay	$1/f^2$	$25\mu s$	$4\mu s$	$1\mu s$	$0.25\mu s$	$0.028\mu s$	$0.0025\mu s$
Refraction	$1/f^2$	$< 1°$	$< 0.16°$	$< 2.4'$	$< 0.6'$	$< 4.2''$	$< 0.36''$
Variation in the direction of arrival (r.m.s)	$1/f^2$	$20'$	$3.2'$	$48''$	$12''$	$1.32''$	$0.12''$
Absorption (auroral and/or polar cap)	$\approx 1/f^2$	5 dB	0.8 dB	0.2 dB	0.05 dB	6×10^{-3} dB	5×10^{-4} dB
Absorption (mid-latitude)	$1/f^2$	< 1 dB	0.16 dB	< 0.04 dB	< 0.01 dB	< 0.001 dB	$< 10^{-4}$ dB
Dispersion (ps/Hz)	$1/f^3$	0.4	0.026	0.0032	0.0004	1.5×10^{-5}	4×10^{-7}
Scintillation[a]					$>$ 20dB pk-pk	$\approx$ 10 dB pk-pk	$\approx$ 4 dB pk-pk

[a] Values observed near the Geo magnetic equator during early night time hours at equinox under conditions of maximum sunspot number.

5.4 The Fading Phenomenon

Fading is a well known phenomenon whose root cause is either microscopic changes in the medium or multiple replicas of the same signal reaching the receiver (either due to reflections from objects or refraction due to turbulent medium such as neutral atmosphere, water, and ionised gas in ionosphere).

The channels which exhibit fading as a function of time are called time varying channels, and the stochastic theory presented by Bello [55] is the basis of modelling such channels [220, 221, 222, 223, 224, 225]. To model fading effects, means determining the requisite probability distribution functions which govern the dynamic attenuation of the signal at any given time. When multiple paths are observed, then each path has its own dynamic attenuation. The dynamics of the attenuation factor is therefore governed by the auto-correlation properties of the probability distribution function representing dynamic attenuation. These functions are referred to as "power spectrum functions" in the literature studying the scintillation effects due to turbulent media.

Mason [226] developed an mathematical expression to determine the error probability of a Differential BPSK modem, used in satellite to ground and satellite to aircraft links. The fading channel is simulated by adding a fading component after the transmitted signal x(t), of the following form:

$$s_r(t) = \mathrm{Re}\{\zeta(a)a(t-t_D)\exp[j2\pi(f_c+f_D)(t-t_d)] \tag{5.41}$$

where t_D is the time delay, and f_D is the Doppler shift of $s_r(t)$ relative to the direct component. The function $\zeta(t)$ is a complex, stationary, zero mean, Gaussian, random process. Since the channel is being considered Rician, therefore this component being added to the direct line of sight component, has a Rayleigh amplitude distribution and uniformly distributed phase. Mason assumes that the $\zeta(t)$ is assumed to have the auto-correlation function

$$\begin{aligned} R_\zeta(\tau) &= \frac{1}{2}\langle\zeta^*(t)\zeta(t+\tau)\rangle \\ &= D\rho_\zeta(\tau) \end{aligned} \tag{5.42}$$

where D is a constant and $\rho_\zeta(\tau)$ is the normalised correlation function of $\zeta(t)$ with $\rho_\zeta(0) = 1$. The average power in the fading component is D. An important parameter in comparing system performance in fading environment is the ratio of the direct component to the multipath power D, often referred to as the k-factor [227]. Various forms of the auto-correlation function has been assumed in the literature. Five of them are stated along with their spectra. All of these forms involve a parameter B_D which is called "fading bandwidth" [226] since it is a measure of the width of the spectrum $S_\zeta(f)$.

These forms are pre-programmed functions in the Communications Tool Box of MATLAB, using it is a matter of identifying the average power in the fading component, the path delays expected and the auto-correlation function (spectrum).

Table 5.4 Spectra and Auto-correlation function of Fading Process $\zeta(t)$ [226].

Denotation	Spectrum $S_\zeta(f)$	Auto-correlation Function $R_\zeta(\tau)$	Comments
Rectangular	$D/(2B_D)$ for $\lvert f\rvert < B_D$, 0 elsewhere	$D\dfrac{\sin(2\pi B_D\tau)}{2\pi B_D\tau}$	Simplest form of Fading used by Hummels and Ratcliffe [228] while studying coherent MSK and OQPSK detection.
Gaussian	$D\exp\left(\dfrac{-f^2}{B_D^2}\right)$	$D\exp(-(\pi B_D\tau))$	Discussed by Bello [229], Miyagaki et.al. [230]
Land Mobile	$D/\left(\pi B_D(a+f^2/B_D^2)\right)$	$D\,J_0\,(2\pi B_D\tau)$	J_0 is zero-order Bessel Function of the first kind. Well known model see Jakes [205]
First-order Butterworth	$D/\left(\pi B_D\left(1+\dfrac{f^2}{B_D^2}\right)\right)$	$D\exp[-2\pi B_D\lvert\tau\rvert]$	Bello and Nelin [231] discussed this spectrum.
Second-order Butterworth	$D/\left(1+\frac{16f^4}{B_D^4}\right)$	$D\exp(-\beta\lvert\tau\rvert)[\cos(\beta\tau)+\sin(\beta\lvert\tau\rvert)]$	Where $\beta=\pi\dfrac{B_D}{\sqrt{2}}$. Salwen [232] used it to define time-varying channels (fast fading).

In the following section, scintillation i.e. rapid changes in amplitude and phase is discussed, which is similar to fading in communications channel.

5.4.1 Scintillation Due to Turbulent Plasma

Fading can be called a time varying attenuation, as the signal strength varies with time and space.

Two causes of fading have been identified in inter-satellite links. The first being multiple reflections due to reflectors in the vicinity, and the second is the changes in refractive indices due to disturbances in plasma density.

When the electromagnetic wave (radio) traverses drifting ionospheric irregularities, the radio wave experiences fading i.e. enhancement of amplitude, angle of arrival variations and phase fluctuations; collectively the effect is called ionospheric scintillation. The scintillation effects vary widely with frequency, magnetic solar activity, time of day, season and latitude. The irregularities producing scintillation are predominantly in the F layer at altitudes ranging from 200 to 1000 km with the primary disturbance observed at high latitude and equatorial regions.

A survey of the morphology of irregularities by regional division by Aarons [178] divides the globe into three major sectors of scintillation activity (Figure 5.5); (i) the **equatorial regions** an area with in $\pm 20°$ of the magnetic equator; (ii) the high latitude region comprises the area from the **high-latitude** edge of the trapped charged particle boundary in to the polar region. (iii) all other regions are termed as **middle latitude**.

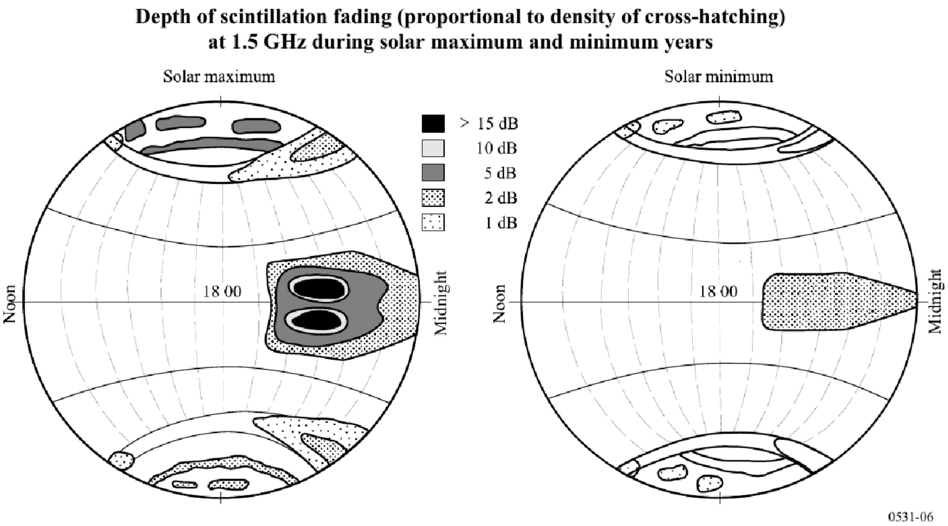

Fig. 5.5 Depth of scintillation fading at 1.5 GHz during solar maximum and minimum years [233].

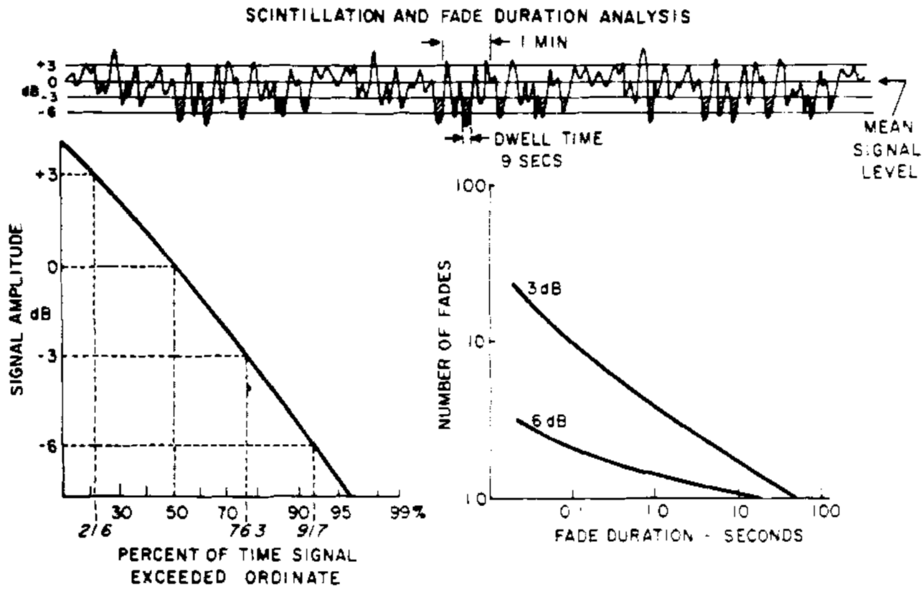

Fig. 5.6 At the top, the envelope of received signal is plotted. Intensity of signal undergoes fading due to its passage through the ionosphere irregularities. The lower left plot is the percent of time signal that exceed mean signal value. The lower right plot is the number of fades for the fade duration in seconds for 3 dB and 6 dB fade (from [178]).

The intensity fading and its characteristics can be best discussed with the help of an illustration e.g. Figure 5.6. The root mean square (RMS) also known as the envelope of the received signal is plotted in dB over a time interval. Suppose the receiver cannot lock on the signal when the received signal strength is 5 dB less than the average value i.e. 0 dB. Therefore it is important to estimate the frequency when signal fades below fade margin called the number of fades. In addition, the time for which the fade persist is called the fade duration or "dwell time". The impact is loss of signal tracking and the acquisition of signal starts again, disrupting the communications link. The result is a loss of data throughput rate. Even when the signal is above 0 dB line, it can cause saturation at the receiver, which also result in erroneous reception. Therefore, estimating the signal fade, fade rate and fade duration is particularly significant in the case of high data rate transfer.

5.4.1.1 Irregular Structures in Ionosphere

The form or structure of ionosphere plasma is of great interest to researchers [178, 234] and operators alike [150, 184].

Ionosphere can be divided in to distinct regions distributed spatially, as well as with altitude. Distinct dense regions of charged particles form the D, E, F layers and Van-Allen belts. The D, E, F layers are part of the Earth‘s ionosphere and is within the low Earth orbit region. Furthermore, it is known that irregular propagation effects are observed at the poles (auroral regions), magnetic equator (equatorial region) and the South Atlantic Anomaly (SAA), illustrated in Figure 5.5. Severe fading is shown in darker shades where as lighter shades depict fading of about 1 dB.

Aarons declares that “in their intensity and their effect on trans-ionospheric propagation, **equatorial F layer irregularities** dwarf those of the high latitude regions. Fluctuations from ionospheric irregularities in the F layer have been reported at frequencies as high as 7 GHz.”

A plume like equatorial irregularity develops after sunset, which result in a orange segment like shape. The patch expands in east-westward dimension of 100 to several hundred kilometres. It comprises field aligned elongated rod or sheet like irregularities. The vertical thickness of the patch is 50 to several hundred kilometres. The patch has maximum intensity irregularities in a height region from 225 to 450 km with irregularities to over 1000 km. Its north-south dimensions are of the order of 2000 km. Once formed the patch drifts eastward with a drift velocity of 100 to 200 m/s. The patch duration is greater than $2\frac{1}{2}$ hours, whereby effects have been observed for 8 hours [178].

Middle-latitude scintillation activity is not as intense as that encountered at equatorial, auroral or polar latitudes. The activity observed at mid-latitude is generally an extension of phenomenon at equatorial or auroral latitudes in general, however, sporadic E is considered the cause of intense scintillation during day time resulting in a second maximum of scintillation [178].

It is evident that the irregular structures in ionosphere are the main cause of fading which grow to altitude up to 1000 km and are effective to frequency less than 10 GHz in severe cases. The experimental facts have enforced our understanding of the theory behind the structures and the fading in the waves.

5.4.1.2 Scintillation Index

The scintillation is characterised by the variance in received power with the S_4 index commonly used for intensity scintillation and defined as the square root of the variance of received power divided by the mean value of the received power. An alternative less rigorous but simple measure of scintillation index has been adopted by workers in the field defined as follows, from [178]

$$SI = \frac{P_{max} - P_{min}}{P_{max} + P_{min}} \tag{5.43}$$

where P_{max} is the power level of the third peak down from the maximum excursion of the scintillation and P_{min} is the level of the third peak up from the minimum excursion measured in dB. The equivalence of selected values of these indices is indicated in Table 5.5.

Table 5.5 Equivalence of scintillation indices with peak to peak variation.

S_4	dB
0.075	1
0.17	3
0.3	6
0.45	10

The parameter *fade coherence time* is pertinent to digital communications see section 5.5.2.2 for more details. If coherence time is long compared to the time interval corresponding to one bit, the average bit error can be computed in terms of S_4. The knowledge of coherence time, the coherence bandwidth and the scintillation index S_4 is sufficient for evaluating the performance of digital transmission scheme in transionospheric propagation [53, pg.1-52].

5.4.1.3 Altitude of Turbulent Ionosphere

Recent studies [29] have shown that turbulence does travel upward, as shown in Figure 5.7, where the plasma bubbles cause disturbances observed as high as 800 km and beyond, lasting several hours after local sunset. The plasma turbulence at the altitude of the satellite is significant enough to cause scintillation in ISL as well.

Increasing interest in the accuracy of global positioning system based on satellites (GPS), has instigated research in simulating the ionospheric scintillation to determine the performance evaluation of ground based GPS receivers, particularly important when solar storms are expected every 11 years.

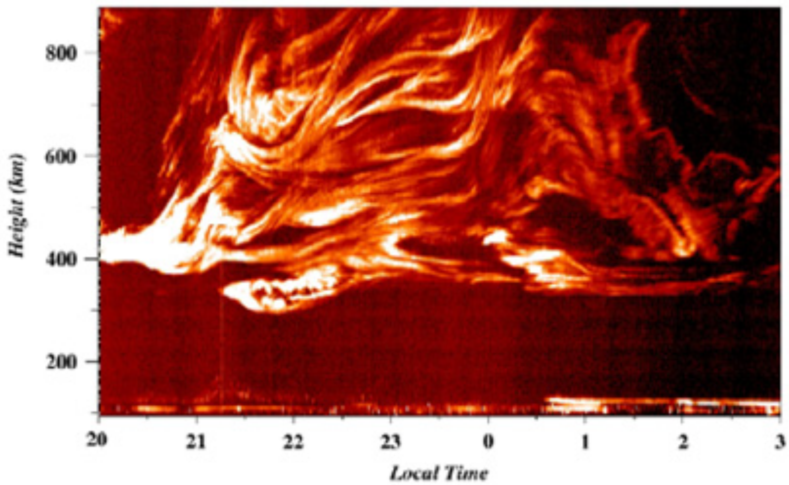

Fig. 5.7 Plasma depletion as high as 800 km altitude, starting right after sunset, observed over Jicarmarca, Peru, by backscatter RADAR 1996 [29].

Humphrey et.al [180] presents a method of simulating the ionospheric scintillation for computer studies. When S_4 is less than 1, then it can be related to the Rician K factor, by the following relationship;

$$K = \frac{\sqrt{1-S_4^2}}{1-\sqrt{1-S_4^2}}, \qquad \text{for} \quad S_4 \leq 1 \tag{5.44}$$

which means that Rician p.d.f. can be used in the simulation modelling.

However, Humphrey simulated scintillation using the Butterworth filter Type-II as the spectrum function(Table 5.4) to generate the tap weights for amplitude changes, which when compared with the data generated using phase screen models [59, 56, 57, 58], showed good match.

5.4.1.4 Discussion

The channel coherence time and coherence bandwidth can be obtained via measurements,analytical analysis or numerical methods to propagate wave through the turbulent medium. Unfortunately, in this thesis, these values could not be ascertained. However, an educated guess is being made, that is, to take into consideration fading from multiple reflected signals as the base for determining channel model and further modem evaluation. The determination of such parameters for satellite to ground have been known, but not published for satellite to satellite links.

Based on this assumption, a simple channel model is derived using geometrical methods assuming that multiple waves either due to refraction or reflection reach the receiver, from all sides, in the next section, keeping in view the presence of physical objects which are strong candidates for the above assumption.

5.4.2 Fading Due to Physical Objects In-Orbit

From the perspective of inter-satellite communications, the in-orbit objects other than the ionised gas can act as a source of electromagnetic wave reflections and/or scattering the wave energy, directly causing severe distortion to the received signal. . The presence of space debris, meteors and the fellow satellites in the close proximity are considered.

5.4.2.1 In-orbit Debris

Space debris is a mixture of various size and shape objects. They include man made metal and non metal objects as well as small to medium sized natural objects. Examples of orbital debris includes spent rockets, clamps, de-spun cables, metallic fragments, paint, rocket exhausts, and remnants of launch vehicles and exploded spacecraft.

The debris as a source of reflection can be assessed by their presence in the orbit. The average density of orbit debris of size 1 m and 10 cm is very low as shown in Figure 5.9 and Figure 5.8. Such a low average density of these objects does not qualify them as significant contributors as wave reflectors.

However, the average does not mean that their contribution be ignored completely. A worst case scenario can be when two or more pieces of significant dimensions find themselves in the vicinity of spacecraft. The only time they would be a cause of interference or multiple reflections, when the debris orbit and the free flying satellites move in the same direction. This scenario is highly unlikely, unless a rendezvous is attempted. Therefore, we can ignore the presence of debris as a source of interference.

Interested reader is referred to the details and its predictive modelling covered elsewhere [236, chap 11]. Meteors leaving a large tail of highly charged particles falling on Earth, are not part of this data, therefore, they are included in the next section.

5.4.2.2 Meteors

Meteor trails have been used in Meteor Burst Communications systems [237], their presence cannot be ignored in the case of ISL, if they are within the communications range of ISL.

Davies [238] refers to the term "meteor" as particles that are completely burned up by frictional heating upon entering the Earth's atmosphere. They are composed of metallic atoms (predominantly sodium,

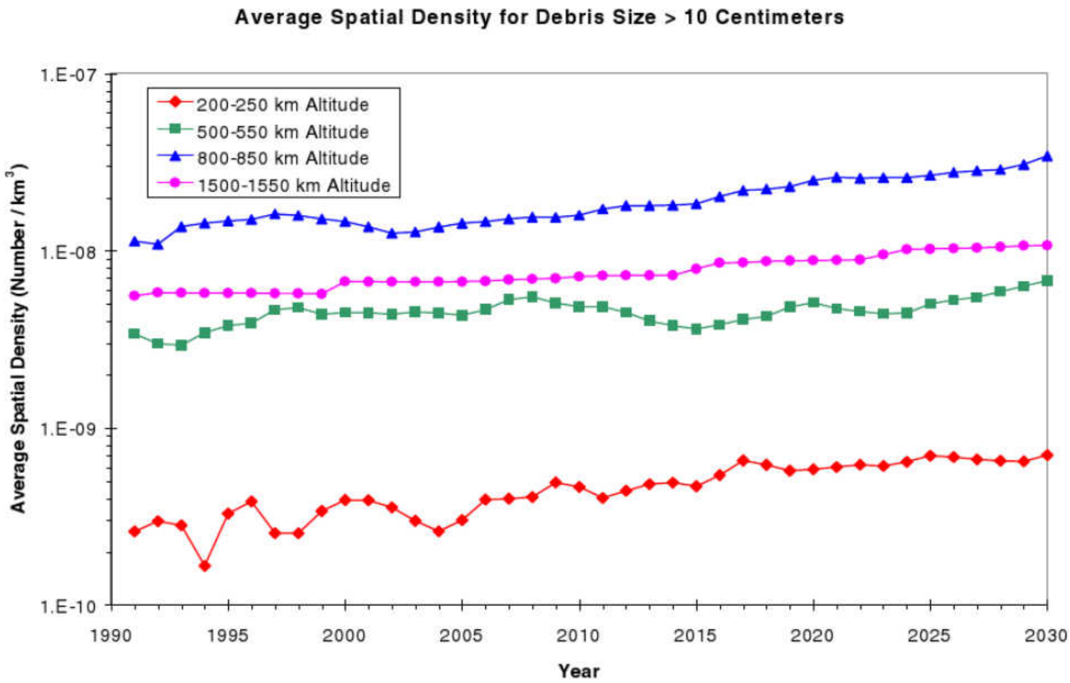

Fig. 5.8 Spatial Density variation between 1991 and 2010 for debris size > 10 cm . The densities are benchmarked from U.S. Space Command Data and the future projections are estimated from EVOLVE [235].

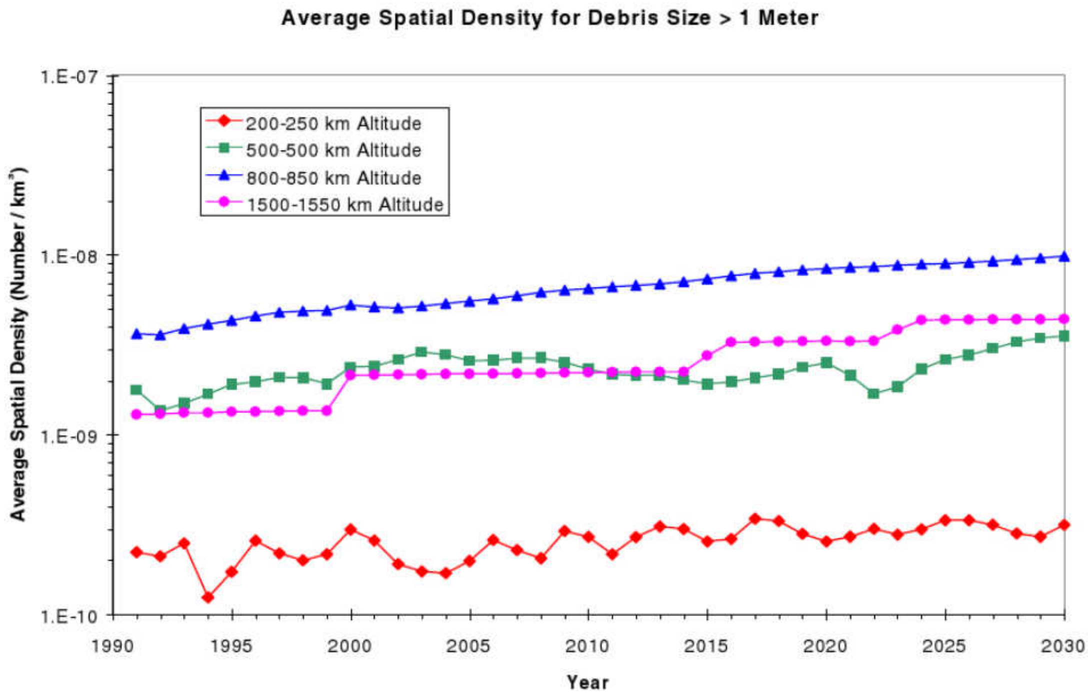

Fig. 5.9 Spatial Density variation between 1991 and 2010 for debris size > 1 m . The densities are benchmarked from U.S. Space Command Data and the future projections are estimated from EVOLVE [235].

calcium, silicon and iron) [239]. Particles in the mass range of 10^{-7} and 10^{3} g with dimensions in the range of 40 μm to 8 cm are primarily responsible for radio reflections. Before being swept up by the Earth's atmosphere these meteors are in elliptical orbits around the Sun and their origins are thought to be from comets.

Meteor presence can be divided into two classes:

- **Meteor showers** are collections of particles whose occurrence is predictable. They are all moving with the same velocity in fairly well-defined orbits around the Sun, and are observed when the Earth cut their path. These meteors account for only a small fraction of the total incidence of meteors.
- **Sporadic meteors** are those which are not predictable, and can be spotted when they enter Earth's upper atmosphere. These meteors seem to move in random orbits, and their origin is assumed to be beyond our solar system. Therefore, in contrast to the meteor showers which appear to come from a specific radiant point in the sky, sporadic meteors have radiant that appear to be randomly distributed. This distribution is not uniform but are for the most part concentrated toward the ecliptic plane and move in the same direction around the Sun as the Earth moves.

The mass distribution of sporadic meteors is such that, there are approximately equal total masses of each size of particle. The approximate relation between particle mass and number is given in Table 5.6. The mass distribution of shower meteors is somewhat similar to that for the sporadic meteors with the important difference that there are more large particles relative to the number of smaller ones than for the sporadic meteors.

Mention has been made in the literature to the fact that in VHF forward scatter strong bursts of signal are frequently superimposed on the background signal reflected from turbulent irregularities. These bursts are due to the reflections from ionised "trails" produced by meteors mostly in the height range of 80 to 120 km [150] but trails have been observed as high as 246.9 km [240].

The ionised trail in the 80-120 km altitude is the result of conversion of the kinetic energy of meteor into potential energy of ionisation as the meteor is slowed down by collisions with the neutral molecules. Whereas, the atmospheric density above 120 km is too low for drag heating to sufficiently heat the surface temperature of the meteor. The possibility that the high-altitude meteor phenomena are produced by physical sputtering is accepted in the meteor research community [240]. The ionisation is distributed in the form of a long, thin paraboloid of revolution with the particle at the head [238], which for practical modelling perspectives can be considered as long tubular structures. It can be inferred that re-entering satellites or debris could also cause plasma trails.

The electron density per unit length of the trail is proportional to the mass of the particle. A VHF echo at the monitoring frequency of 224 MHz becomes observable when the generated plasma reaches the critical density of 6×10^{14} m^{-3}. At the UHF frequency of 931 MHz a critical density of 10^{16} m^{-3} is reached where the echoes become observable [240]. Brosch implies that the high-altitude ($>$ 150 km)

Table 5.6 Order of magnitude estimates of the properties of sporadic meteors [238].

	Mass (grams)	Visual magnitude	Radius	Number of this mass or greater swept up by the earth each day	Electron line density (electrons per meter of trail length)
Particles pass through the atmosphere and fall to the ground	10^4	-12.5	8 cm	10	–
Particles totally disintegrated in the upper atmosphere	10^3	-10	4 cm	10^2	–
	10^2	-7.5	2 cm	10^3	–
	10	-5	0.8 cm	10^4	10^{18}
	1	-2.5	0.4 cm	10^5	10^{17}
	10^{-1}	0	0.2 cm	10^6	10^{16}
	10^{-2}	2.5	0.08 cm	10^7	10^{15}
	10^{-3}	5	0.04 cm	10^8	10^{14}
	10^{-4}	7.5	0.02 cm	10^9	10^{13}
	10^{-5}	10	80 μm	10^{10}	10^{12}
Approximate limit	10^{-6}	12.5	40μm	10^{11}	10^{11}
of radar	10^{-7}	15	20μm	10^{12}	10^{10}
measurement$\rightarrow$	10^{-8}	17.5	8μm	?	?
Micrometeorites (Particles float down unchanged by atmospheric collisions)	10^{-9}	20	4μm	Total for this group estimated as high as 10^{20}	Practically none
	10^{-10}	22.5	2μm		
	10^{-11}	25	0.8μm		
	10^{-12}	27.5	0.4μm		
Particles removed from the solar system by radiation pressure	10^{-13}	30	0.2μm	–	–
	–	–	–	–	–

meteor population may be 0.05% of the total meteor detected which implies that a significant number is present in LEO. Whereas, as the altitude decreases the meteor trails become significant.

First row of Table 5.6 indicates that out of the many meteors which would eventually fall, indirectly means, that rest remain in orbit, where the SBWSN is to operate. This implies that when the wavelength of propagating EM wave is comparable with the size of the meteors, the meteors may reflect or scatter the energy of the wave fields. Therefore their impact on the propagating waves depends on their probability of occurrence at the time of propagation as well as at the actual frequency (wavelength) of the carrier in use.

5.4.2.3 NanoSats in Close Proximity as Reflectors

It is envisioned that when several pico/nano/femto class of satellites are deployed in a controlled manner, so that the sensors are in close proximity, say less than a km, then there is a possibility that NanoSats may act as reflectors. This is particularly true when the operational frequency is higher than 10 GHz.

the deployment in the form of clusters operating in close proximity that is less than 1 km radius, then the satellite structures themselves may act as reflectors of electromagnetic signals. The cluster may be formed either by the use of tethers attached to each sensor satellite, or by the use of on-board propellant to maintain relative distances in orbit.

5.5 Fading Channel Model

It has been established in the previous discussions, that the received signal will exhibit fading type phenomenon, during the life of the IMM mission. Be it when the ionosphere gets disturbed after sunset, and the turbulence moves upward from 400 km towards 800 km altitude; or be it the presence of in-orbit debris, or be it the presence of other satellites in close proximity. The phenomenon of scintillation is similar to the concept of fading type channels extensively studied in terrestrial mobile communications. Scintillation is being investigated anew, for degradation of GPS signals [241], as well as for precise inter-satellite distance control [87]. Scintillation observed in the satellite to ground links have also been extensively studied where it has been concluded, that the received signal statistics follow Rayleigh probability distribution functions in extreme cases or Nakagami-m distribution for less extreme cases [242, 180, 243, 241, 206, 61, 244].

MATLAB has an extensive library that can model a fading channel using both Rician and Rayleigh fading channels taking the mathematical forms described by [245]. A general description for the channel model is given in [246].

Therefore, in this section, the fading channel models used by Matlab are studied, so that they could be altered to our needs.

5.5.1 Brief Description of Channel Models used in MATLAB

"The Rayleigh and Rician multipath fading channel simulators used in MATLAB use the band-limited discrete multipath channel model described in [247, ch.9]."* The assumption that the delay power profile and the Doppler Spectrum of the channel are separable, allows the model to take the form of an FIR filter (with a linear impulse response).

*Taken from the online help of MATLAB 2008 on fading channel simulation setup.

For the sampled input signal s_i the output of the filter is a recursive relationship, given as

$$y_i = \sum_{n=-N_1}^{N_2} s_{i-n}\, g_n \tag{5.45}$$

where g_n is the set of tap weights given by

$$g_n = \sum_{k=1}^{K} a_k \operatorname{sinc}\left[\frac{\tau_k}{T_s} - n\right], \qquad -N_1 \leq n \leq N_2 \tag{5.46}$$

In the set of equations above

T_s is the input sample period to the channel,

τ_k where $1 \leq k \leq K$ is the set of path delays, and K is the total number of paths in the multipath fading channel,

a_k is the set of complex path gains* of the multipath fading channel,

N_1 **and** N_2 are chosen so that $|g_n|$ is small when n is less than $-N_1$ or greater than N_2.

Each path gain a_k is subsequently generated by the following process;

1. A complex uncorrelated (white) Gaussian process with zero mean and unit variance is generated in discrete time.
2. The complex Gaussian process is filtered by a Doppler Filter with frequency response $H(f) = \sqrt{S(f)}$ where $S(f)$ denotes the desired Doppler power spectrum (selected by user).
3. The filtered complex Gaussian process is interpolated so that its sample period is consistent with that of the input signal. A combination of linear and polyphase interpolation is used.
4. The resulting complex process z_k is scaled to obtain the correct average path gain.
   a) In the case of Rayleigh channel the fading process is generated using

$$a_k = \sqrt{\Omega_k} z_k \tag{5.47}$$

   where $\Omega_k = E[|a_k|^2]$ (expected value defined in stochastic process).
   b) In the case of Rician channel, the fading process is obtained as

$$a_k = \sqrt{\Omega_k}\left[\frac{z_k}{\sqrt{K_{r,k}+1}} + \sqrt{\frac{K_{r,k}}{K_{r,k}+1}}\; e^{j\,(2\pi f_{d_{LOS}} + \Theta_{k_{LOS}})}\right] \tag{5.48}$$

*The path gains are not correlated with each other.

where $K_{r,k}$ is the Rician K-factor of the k^{th} path, $f_{d_{LOS}}$ is the Doppler shift of the line of sight component in Hertz (Hz), and $\Theta_{k_{LOS}}$ is the initial phase of the line of sight component in radians (rad).

5. At the input to the band-limited multipath channel model, the transmitted symbols must be oversampled by a factor at least equal to the bandwidth expansion factor introduced by pulse shaping.
   - For example, if sinc pulse shaping is used, for which the bandwidth of the pulse-shaped signal is equal to the symbol rate, then the bandwidth expansion factor is 1, and, in the ideal case, at least one sample-per-symbol is required at the input to the channel.
   - If a raised cosine (RC) filter with a factor in excess of 1 is used, for which the bandwidth of the pulse-shaped signal is equal to twice the symbol rate, then the bandwidth expansion factor is 2, and, in the ideal case, at least two samples-per-symbol are required at the input to the channel.

Assuming that reflectors are present in the vicinity of transmitter and receiver, channel model is presented. To characterise the parameters we shall follow the definitions as given by Sklar [210, 211].

5.5.2 Multipath Intensity Profile

Knowledge of multipath-intensity profile $S(\tau)$ answers the question; "For a transmitted impulse how does the average received power vary as a function of time delay τ?". The maximum delay is τ_{max}. The relationship of symbol time T_s and τ_{max} is such that, when $\tau_{max} > T_s$ then the channel exhibits frequency selective fading, otherwise the frequency response is flat.

If multiple copies of the transmitted signals reach the receiver, a sum of time-delayed signals result in a faded signal, whose amplitude and phase varies with time. The faded signal can then be generated with the help of a path profile given as input to communications channel model implemented as a function in Matlab.

Path profile can be generated using many assumptions. The distribution of scatterers / reflectors is the main consideration. A simple geometry for the problem takes the form of a circle or an ellipse [221]. The reflectors can be assumed to be distributed about a transmitter (or a receiver) or both. Lets assume the reflectors are all gathered about the transmitter, as is in the case of multiple sensors deployed in close proximity. To simplify the problem, all reflectors are assumed to be point reflectors, and are distributed in the form of a circle about the transmitter. The transmitter is assumed at the centre of the circle and reflectors on the perimeter of the circle, equally spaced out. The receiver is also placed on the perimeter of the circle (for simplification). So when the sensors move away from each other, the radius of the circle increases. It is being assumed, that the communications range is more than 1 km. Therefore this simple case * assist in determining a path profile which can be used in channel models. The direct

*The above stated scenario is just one possibility amongst many physical topologies. Path profiles for each possible topology is left for future works.

and indirect paths are shown in Figure 5.10. The wave directly reaching the receiver (Rx) is the direct path. The waves reaching after reflecting from other objects are the reflected waves. The path profile is calculated in the following section.

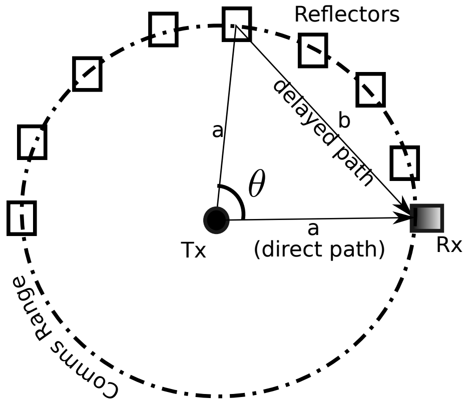

Fig. 5.10 Geometry used in calculating path profile delay.

5.5.2.1 Path Profile

A channel is referred to as frequency-selective if $B_0 < 1/T_{sym}$ (B_0 coherence bandwidth), where the symbol rate $1/T_{sym}$ and the signal bandwidth W depends on the baseband modulation type (BPSK, M-ary PSK, M-ary QAM, MSK etc.).

With reference to the Figure 5.10, the delay profile for each path is calculated assuming free space, for respective carrier frequency e.g. 430 MHz in this case. The shortest distance between the Tx and Rx is taken as the reference path called path 0. Signal reaching the receiver over other paths is delayed with respect to the reference path, that is why, 0 delay is shown in path 0 in Table 5.7. For the 0.1 km radius of circle, the signal reaching the Rx is delayed by 0.14 μsec over path 1, similarly another copy of signal reaches Rx delayed by 0.28 μsec and so on. Similarly the delay path profile for radius of 0.5 km, 1 km and so on are also stated. A complete list of the simulated multipath profile and their coherence band width is stated in Table 5.7. The path profile for paths 1 km and less are illustrated in Figure 5.11.

Say for the low data rate corresponding to bandwidth less than 20 kHz, the channel is flat fading for Case 1 but frequency selective fading for Case2. However, as data rate is increased to say 1 MHz, both cases become frequency selective fading. Appropriate mitigation is thus required in the design of communications systems. Hence B_0 sets an upper limit on the transmission rate that can be used without incorporating a channel equaliser.

Using basic trigonometric relationship the following values are found for τ_{max};

- Case1 : when the reflectors are close together at 1 km (circle radius), $\tau_{max} = 6.67$ μsec,

Table 5.7 430 MHz ISL channel delay path profile in LEO. Path 0 is the direct path, and other paths with respective excess delay, delay spread r.m.s and coherence bandwidth.

			Delay at various ranges				
Path No.	Angle (rad)	Gain (dB)	0.1 km (μsec)	0.5 km (μsec)	1 km (μsec)	100 km (μsec)	400 km (msec)
0	0	0	0.00	0.00	0.00	0.00	0.0
1	0.4488	-6.39	0.14	0.74	1.48	148	0.5934
2	0.8976	-10.85	0.28	1.45	2.89	289	1.1570
3	1.3464	-14.06	0.41	2.08	4.16	416	1.6626
4	1.7952	-16.35	0.52	2.61	5.21	521	2.0849
5	2.24399	-17.89	0.60	3.00	6.01	601	2.4026
6	2.69279	-18.79	0.65	3.25	6.50	650	2.5998
7	3.14159	-19.08	0.66	3.33	6.67	667	2.6667
Delay Spread RMS σ_τ (μsec)			0.47150	2.357	4.715	471.5	2000
Coherence Bandwidth B_0 (kHz)			381.67	67.524	33.755	0.337	0.079

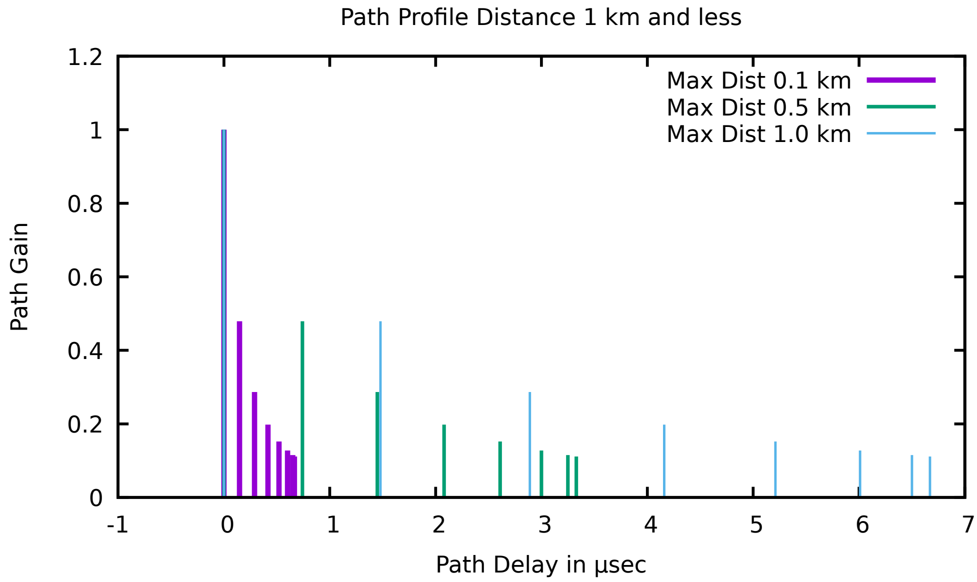

Fig. 5.11 Path profile for Tx-Rx direct distances of 0.1, 0.5 and 1 km. Direct path has gain 1, all delayed path gains are less than 1. 8 paths are plotted based on data in columns 5 to 7 Table 5.7.

- Case2 : when the reflectors are far at a range of 400 km (circle radius), τ_{max} =2.67 msec.

5.5.2.2 Coherence Bandwidth

Coherence Bandwidth B_0 is a statistical measure of the range of frequencies over which the channel passes all spectral components with approximately equal gain and linear phase. As an approximation

$B_0 \approx \frac{1}{\tau_{max}}$. The delay spread is often characterised in terms of root mean squared (RMS) delay spread σ_τ, which is the square root of the second central moment of $S(\tau)$ [210], where

$$\sigma_\tau = \sqrt{\bar{\tau^2} - (\bar{\tau})^2} \tag{5.49}$$

An exact relationship between coherence bandwidth and delay spread does not exist, and must be derived empirically from received signals in respective channels. Bogusch [61] uses the following relationship for investigating the frequency selective fading effects on digital communications in ionosphere channel;

$$B_0 = \frac{1}{2\pi\sigma_\tau} \tag{5.50}$$

From eq. (5.50) the coherence bandwidth for the two cases are;

- Case1, $B_0 = 33.755$ kHz
- Case2, $B_0 = 79.577$ Hz

5.5.2.3 Motion Induced Channel Time Variance

The time varying nature of the channel is caused by the relative motion between the transmitter and receiver, or by movement of the medium or the objects within the channel. The relative motion causes an apparent change in all path lengths, which result in variation in signal's amplitude and phase. This is prominent when multi-paths are present.

The spaced-time correlation function specifies the extent to which there is correlation between the channel's response to a continuous wave (CW) sent at time t_1 and the response to signal sent at t_2. The **coherence time** T_0 is a measure of the expected time duration over which the channel's response is essentially invariant.

Doppler frequency shifts measured of the signal can be employed to determine the time-variant nature of the channel. The coherence time can be inversely related to the Doppler shift f_d within a multiplicative factor. A popular rule when the correlation function of the channel's response to sinusoids is not available [210] is;

$$T_0 = \frac{0.5}{2f_d} \tag{5.51}$$

The literature defines the width of the Doppler power spectrum as Doppler spread, fading rate, fading bandwidth or spectral broadening, and is essentially twice the maximum Doppler shift about the carrier [74].

Using the estimates of Doppler frequency shifts from the relative motion assessments, we deduce the coherence time of the channel given in Table 5.8.

The channel is said to be fast fading if the symbol rate $1/T_{sym}$ is less than the fading rate $1/T_0$ i.e. $T_{sym} > T_0$. Conversely the channel is referred to as slow fading if the signalling rate is greater than the fading rate. The Doppler spreading, the channel fading rate, sets a lower limit on the signalling rate that can be used without suffering fast-fading distortion. To mitigate the effects of fast fading would be that we desire $T_{sym} << T_0$. If this condition is not satisfied, the random frequency modulation (FM) due to varying Doppler shifts will degrade system performance significantly. The effect yields an irreducible error rate that cannot be overcome by simply increasing E_b/N_0 [210, 211].

5.5.3 Channel Model Simulation

With the basic parameters in hand, now we are able to use them in MATLAB [68]. Using the parameters deduced for two cases in the previous section, we use them in the inbuilt system functions, and take snapshots of the time varying behaviour of the stochastic channel.

There are two bandwidths used in simulation to visualise the effect of the anticipated channel, narrow band and wide band. The channel impulse response and the frequency response snapshots are shown for illustrative purposes in Figure 5.12 for Case 1 (close proximity satellites) and Figure 5.13 for Case 2 (far distant satellites). The frequency response of the channels Figure 5.12b shows that channel behaves as flat fading over the 20 kHz bandwidth. Although in the Figure 5.12 and Figure 5.13 empirical result is plotted, it refers to the channel response simulated in Matlab.

In Figure 5.13b deep fades are observed which means that the channel exhibits frequency selective fading. Another interesting point to note is that the Doppler Spectrum is not a close match to the Jake's Doppler spectrum, as shown in Figure 5.12c, and Figure 5.13c.

Table 5.8 Coherence Time from Doppler Shifts estimated from relative motion of satellites in various scenarios at 430 MHz.

Doppler Shift f_d (Hz)	Doppler Spread $2f_d$	Coherence Time T_0 (msec)	Comments
1	2	250	Close proximity cluster
5	10	50	Close proximity cluster (Free flying)
10	20	25	ReSat to SenSat (Long Distance)
20	40	12.5	Twice the value of ReSat to SenSat

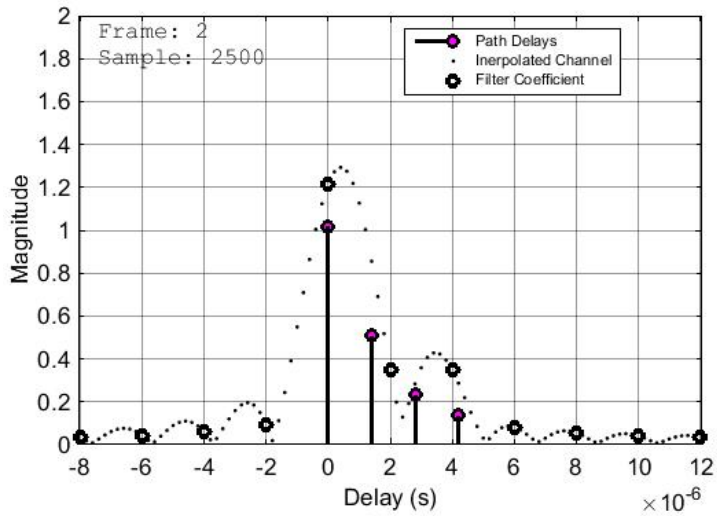

(a) Case1 Channel Impulse Response (IR).

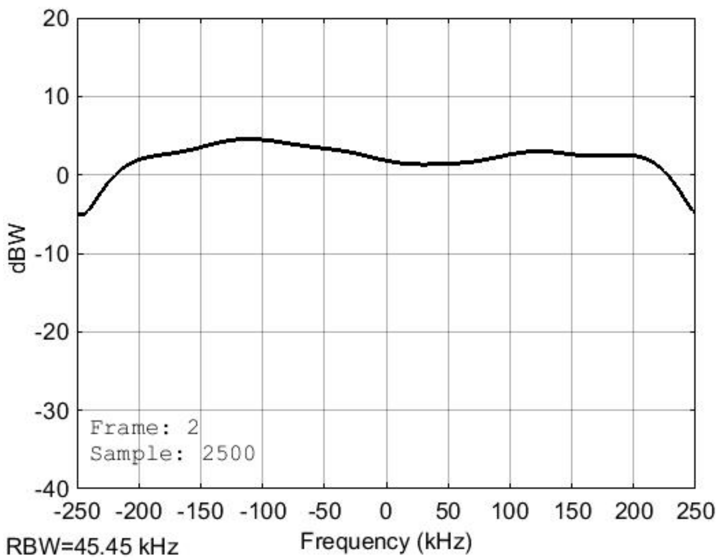

(b) Case1 Channel Frequency Response (FR).

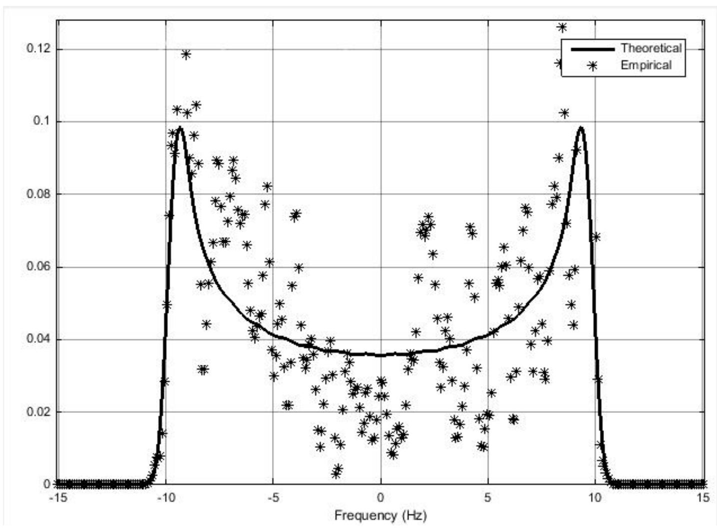

(c) Case1 Channel Doppler Spectrum.

Fig. 5.12 Channel Impulse Response, Frequency Response and Doppler Spectrum for Case 1.

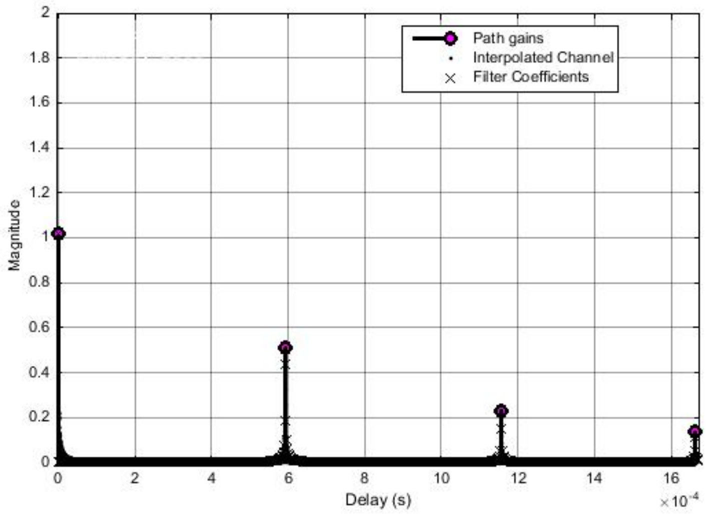

(a) Case2 Channel Impulse Response (IR).

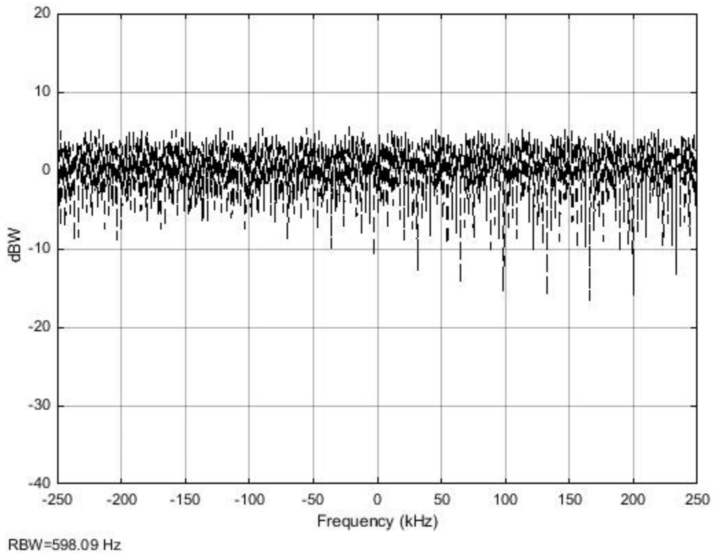

(b) Case2 Channel Frequency Response (FR).

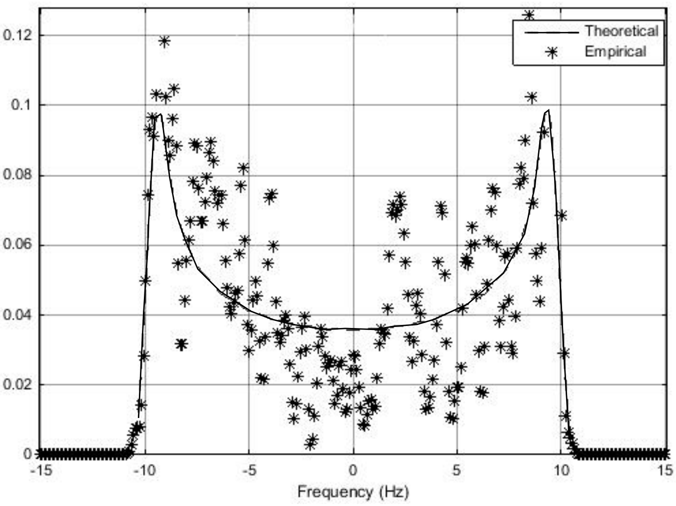

(c) Case2 Doppler Spectrum.

Fig. 5.13 Channel Impulse Response, Frequency Response and Doppler Spectrum for Case 2.

5.5.4 Channel Model for MODEM Testing

We consider two extreme cases of the channel model, to be used by modem simulations. The two channels are designated as Chan1 and Chan2. The characteristics are summarised in Table 5.9 and coherence time defined in Table 5.10. The path loss for both channels is normalised, by dividing the path loss by the max path loss.

These gains are the absolute maximum, whereas the channel exhibits random behaviour, which is simulated by changing the gains governed by the Rayleigh or Rician probability distribution functions. Since there is a Doppler spread associated with the mobility, it is assumed to be following Jake's Doppler Spectrum, bound by the maximum frequency shift of 20 Hz and 10 Hz for the specular (direct line of sight) path.

The Rician factor is set to 10 because of the strong line of sight component as compared to weak non line of sight. The gain of the other paths is a random variable governed by Rayleigh probability density functions, whereas initial values are stated.

Since the digital modulation scheme is mostly affected by the small scale fading manifests, therefore only these characteristics are used in simulation. The bit to noise energy ratio is varied between 0 to 20 dB.

Table 5.9 Channel path delays and r.m.s delay spread and coherence frequency Chan1 (1 km range), Chan2 (400 km range) operating at 430 MHz.

Path No.	Normalised Path Gains		Path Delays in (μsec)	
	(dB)	linear	Chan 1	Chan 2
Direct	0	1	0.00	0.0
1	-6.39	0.47889	1.48	593.4
2	-10.85	0.28665	2.89	1157.0
3	-14.06	0.19806	4.16	1662.6
4	-16.35	0.15215	5.21	2084.9
5	-17.89	0.12737	6.01	2402.6
6	-18.79	0.11492	6.50	2599.8
7	-19.08	0.11111	6.67	2666.7
		RMS Delay spread :	4.7 μsec	200 μsec
		Coherence Frequency :	33.8 kHz	79.6 Hz

The said channels shall be used in performance measures for the modem. It is important to note here, that these are one set of several possible path profiles, so as the scenario changes so does the path profiles. However, since the channel behaviour is a stochastic process, therefore, the fading remains random. But the coherence bandwidth and coherence time may change with new path profiles as well as the region of operation (where spacecraft are deployed).

Table 5.10 Coherence Time from Doppler Shifts estimated from relative motion of satellites in various scenarios at 430 MHz.

Doppler Shift f_d (Hz)	Doppler Spread $2f_d$ (Hz)	Coherence Time $T_0 = 1/(2f_d)$ (msec)	Comments
1	2	250	Close proximity cluster
5	10	50	Chan1
10	20	25	(Long Distance)
20	40	12.5	Chan 2

The fading is simulated for 9 path interference causing fading at the receiver. Although Doppler frequency shifts have been selected based on selected orbits, as soon as the orbital configuration changes, the Doppler shift need to be reassessed. Since there is no published data about coherence time and coherence bandwidths for inter-satellite links, therefore the values determined in this chapter can be used as a starting channel model for further investigations.

5.6 Noise Simulation

All electrical circuits generate random fluctuations due to the intrinsic movements at the atomic level, generally called thermal noise. The resistance in electrical circuits which have intrinsic thermal agitation observed as random fluctuations, even when there is no signal being generated. Noise is an unwanted but unavoidable signal, and it rides the wanted signal in a manner exhibiting additive properties.

In frequency domain, the noise power is observed over all frequencies, therefore it is called white noise.

In our simulation studies the thermal noise is a fundamental parameter, since the wanted signal should be distinguishable from intrinsic noise, which is only possible, when the signal to noise energy or power ratio is significantly high.

The simulation of noise involves two basic ideas:

- the first is the generation of the time series of random variables, and,
- the second is shaping the spectrum of the time series to produce the desired correlation properties.

Consider the first problem – that of generating the time series, i.e. a sequence of random variables. The randomness of the variables is assumed to be identically distributed, and that the generation is independent of each other. Such sequences are referred to as “iid” — independent, identically distributed. Therefore for a “iid” sequence, it is assumed that each random number is drawn independently from a population having a probability density function.

The noise $w[n]$ is a random variable described by Gaussian or normal probability density function (p.d.f.) stated as,

$$\text{p.d.f}(w[n]) = \frac{1}{\sqrt{2\pi\sigma^2}} \exp\left(-\frac{1}{2\sigma^2} w^2[n]\right) \tag{5.52}$$

The random variable has a zero mean value and a spread about the mean with a variance σ^2. The square brackets indicate that the sequence is made up of discrete samples.

Since noise is observed as random fluctuations "riding the signal envelope", it is modelled as additive, therefore the received signal takes the form;

$$y[0] = h[0] \star x[0] + w[0] \tag{5.53}$$

A single sample at $n = 0$ is used as an example.

Thermal noise is modelled as a zero-mean, stationary, Gaussian random process, with the power spectral density that is flat over a very wide range of frequencies. The process is called white noise in analogy to white light, whose spectral density is broad and uniform over a wide frequency range. The power spectral density of thermal noise is [115, ch. 3] kT, where $k =$ Boltzmann Constant and T is the temperature in Kelvin. The Gaussian distribution function cannot be integrated in closed form, therefore numerical methods are used.

Uniform random number generators are available in high-level computing languages such as C, and scripting languages such as MATLAB. Ziemer shows, that a uniform random number can be generated of arbitrary probability density function provided an invertible transformation can be found [204, pg 119]. The analytical expression eq. (5.52) is directly used in simulation. In MATLAB, the function *randn()* and *awgn()* are extensively used for generating random noise.

5.7 Conclusion

In this Chapter, it is identified, that ionised gas causes fading which is due to rapid changes in the refractive index of the ionised gas; particularly in turbulent regions in orbit. The signal may fade as deep as 20 dB from the mean signal strength being received at times of extreme turbulence, causing the communications link to disrupt. It has been highlighted, that the turbulent nature of plasma is observed as high as 1000 km altitude, the same altitude where the satellites are to operate. Therefore necessitating the need to incorporate fading type channel in performance evaluation of digital transmission schemes and modem testing.

It is revealed that space debris and in-orbit meteors can be a cause of concern when the carrier frequency is above 10 GHz, because, of the small wavelengths, they can act as a scatterer or a reflector. Meteor trails are of concern when the SBWSN operates at altitudes of 300 km or less, because at this altitude they are known to leave long trails of highly ionised trails. The size of satellites itself is also of concern which can act as reflectors depending on the frequency used in ISL. 3U CubeSat is of concern for frequency of operation of 10 GHz whereas, its if of little concern for frequencies at 2.4 GHz or below.

The channel characteristics are found to be a subject of attenuation, exhibiting both fast and slow fading, due to the relative motion of the satellites with respect to the dynamic nature of plasma in ionosphere, as well as due to possible reflectors in the vicinity of communications range. Therefore, as is generally assumed in literature, inter-satellite communications links below 10 GHz cannot be modelled as simple free space path loss models, rather, the fading effects both fast and slow must be incorporated in the evaluation of modem design and performance.

Time varying fading channels are easily modelled using Tapped Delay Line (TDL) structure, in which the tap gains and delays, depict the real world scenario. TDL is a general structure, it is the determination of number of taps, and the probability function which governs the tap gains, and tap delays, which make it environment specific. In the context of SBWSN, where inter-satellite links are observed as inter-orbit and intra-orbit, the path profile is determined on two extreme cases. Firstly when the satellites are in close proximity of each other and there are multiple path effects due to reflectors in the vicinity are considered. Secondly, for inter-orbit links, where several scatterers or plasma refraction causes multipath effects.

To the best of the knowledge, this is the first time, inter-satellite links have been evaluated by considering the fading effects, for which channel model has been described. The channel model would allow the design engineer to better select the digital modulation scheme and its design parameters, so that a robust digital modem be designed / selected for the mission scenario.

This chapter also contributes to the state of the art, by elaborating the steps involved in assessing the environment effects, which are useful for evaluating mission scenarios where deployment is carried out in other regions. It is also pertinent to note here, that the operational frequency plays an important role when considering the fading effects either due to refractive index changes in plasma or due to reflections due to space debris / meteors within the communications range. The role of antenna radiation pattern is also critical, since isotropic antenna is considered purely for the reason, that wireless networking protocols such as IEEE 802.11, LTE are designed for such operations.

OFDM based modem which is the primary modulation scheme in most wireless technologies supporting networking such as IEEE 802.11 and LTE, is evaluated in the next Chapter for its design and performance in the light of the channel characteristics identified and modelled in this Chapter.

CHAPTER 6

EVALUATION OF A BASEBAND MODEM FOR INTER-SATELLITE LINKS IN LEO

This chapter evaluates the impact of the channel modelled in Chapter 5 on a baseband design using orthogonal frequency division multiplexing (OFDM). OFDM is one of the physical layer specified for data transmission over wireless links in the IEEE 802.11 protocol, being considered for use in SBWSN.

The OFDM design is studied in depth to address the following two objectives: (i) investigate if the OFDM design can be modified "on-the-fly", so that the link remains operational even when the channel behaviour changes severely, i.e. in the presence of variations in the channel coherence time and coherence bandwidth; (ii) evaluate the performance of the OFDM modem under the anticipated influence of the channel characteristics, modelled in Chapter 5. The term "on-the-fly" refers to an electronic system which can be updated or reconfigured, without disrupting on-going operations in the event of a system restart (either soft or hard). The modem and channel are both modelled in MATLAB.

6.1 Introduction

Communications channel characteristics have been identified to be changing both with time and space, therefore, the communications system must be adaptable or reconfigurable — the cause of which is not channel fading rather poor design, to incorporate an unforeseen channel behaviour. Reconfigurability can be achieved at each level of the communications system, however it results in costly and bulky system designs. A hybrid software defined radio (SDR) architecture reduces the cost by fixing the analogue part and allowing changes in the baseband digital modem, which is relevant to the purpose of this research. Therefore, in this thesis, it has been assumed that the physical transmission scheme suggested by IEEE 802.11 (modified) shall be implemented in the form of a hybrid software defined radio. IEEE 802.11 suggests using two transmission schemes, (a) OFDM and (b) DSSS. The former is selected in this investigation, since a considerable in-house know-how had been developed, including an OFDM implementation on an FPGA interfaced to SpaceWire.

In this Chapter the design parameters that govern the generated waveform are the primary topic of discussion, rather than the implementation aspects. The waveform has to be generated within the limitations posed by the physical communications channel identified earlier (section 5.5.4), i.e. the coherence bandwidth and coherence time should be met. Otherwise, a severe fading would be observed resulting in a link disruption that would be caused by an inadequate design of the underlying modulation scheme, and not the channel fading.

6.2 Overview of OFDM Design

Traditionally, a single carrier is employed in modulation and transmission of data. When more than one carrier is used, then the modem is referred to as a multi-carrier modulator with a corresponding demodulator. The modulator - demodulator pair referred to as **modem**, is not inter-operable between different modulation schemes. However, with the use of a software defined radio (SDR) architecture, the modem can be implemented in a soft form, which can be upgraded to support other modulation schemes.

When the OFDM concept was floated initially, the implementation was analogue, consisting of several oscillators working in phase, which was not only costly but technically cumbersome. However, the same effect could be realised easily using a Discrete Fourier Transform pair the idea first proposed by Chang [248, 249]. However, at that time, signal processors were neither powerful enough nor cheap, which resulted in a limited use of OFDM mostly confined to military or defence projects. The advances in the micro-electronics and very large scale integrated circuits (VLSI) technology produced powerful but cheap digital signal processors in the mid 90s, and efficient discrete Fourier transform algorithms rejuvenated the interest in utilising OFDM as a main-stream transmission scheme.

In the following section the design concept is described in depth, as it is essential to addressing the research questions posed in this chapter.

6.2.1 Theoretical Background

Fundamentally, the available bandwidth for data transmission is divided into $\tilde{N}$ independent sub-bands called sub-channels (Figure 6.1). The transmit signal is the sum of $\tilde{N}$ independent sub-signals, each of equal bandwidth and with centre frequency f_i, $i = 1, \ldots, \tilde{N}$. Each of these sub-channels are considered to be either of M-ary PSK[*] modulated signal or M-ary QAM modulated sub-symbols. In all cases $\tilde{N}$ is a power of two so that efficient versions of the Fast Fourier Transform (FFT) can be used and the size of

[*]M-ary refers to 2,4,8,16... 2^n integers which can be used to define the constellation diagram.

FFT is $N = 2\tilde{N}$. The $\tilde{N}$ depends on how rapidly the transfer function of band-limited channel varies with frequency.

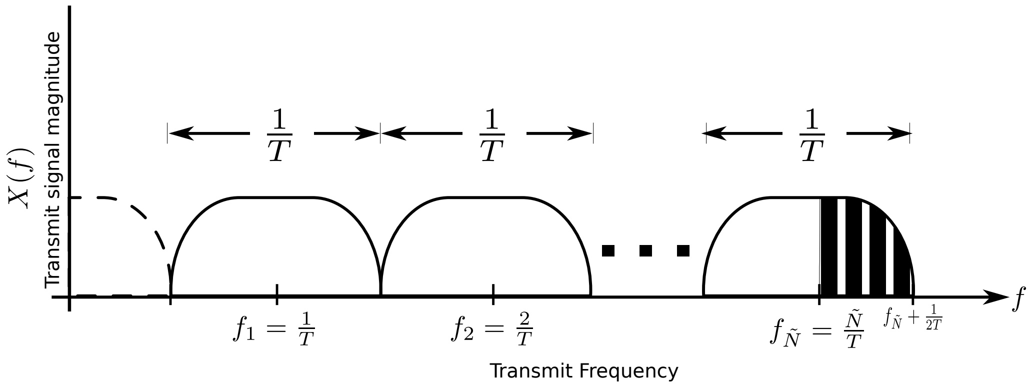

Fig. 6.1 Sub-bands in frequency bandwidth [250] .

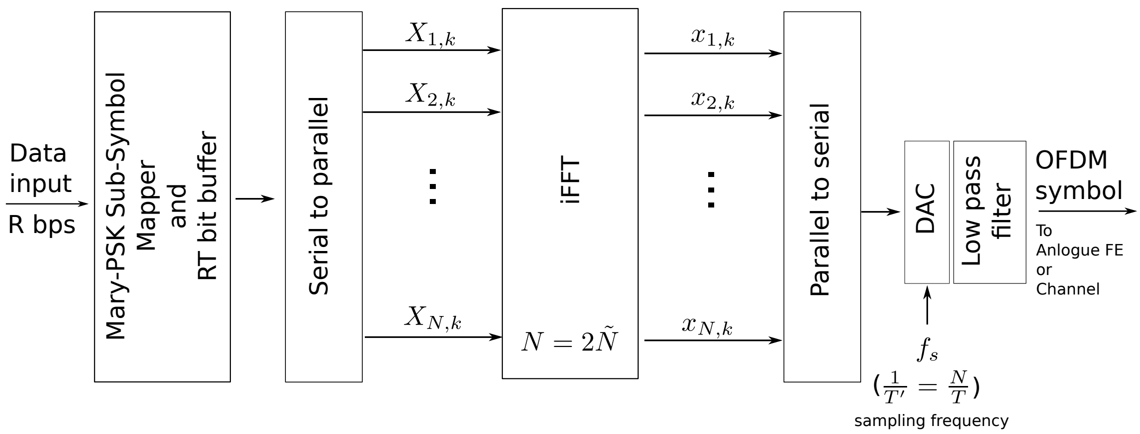

Fig. 6.2 OFDM Transmitter functional block based on the use of iFFT proposed by Chang.

Figure 6.2 illustrates the transmitter path. An input bit stream* of data rate R bps is buffered into blocks of $b = RT$ bits, where T is called the symbol† period in seconds, and $1/T$ is the symbol rate. Of these b bits, b_i $(i = 1, \ldots, \tilde{N})$ are intended for use in the i^{th} sub-channel for transmission.

$$b = \sum_{i=1}^{\tilde{N}} b_i \tag{6.1}$$

These b_i bits are translated into complex (PSK) sub-symbols $X_{i,k}$ which are sent over the k^{th} transmitted symbol. The mean-square value of X_i is called the sub-symbol energy E_i, and the sub-symbol power

*We shall follow the notation of Cioffi [250] in the rest of the section to describe the system.
†The symbol here after refers to the OFDM symbol. M-ary PSK output is referred to as sub-symbol.

is defined as $P_i = E_i/T$. The $N = 2\tilde{N}$ point inverse Fast Fourier Transform (iFFT) combines the $\tilde{N}$ sub-symbols into a set of N real valued time-domain samples, $x_{n,k}$, where $(n = 0,...,N-1)$. The set of N successive time domain samples is the k^{th} transmitted symbol (OFDM symbol). These N samples are converted from parallel to serial format and pass through a digital to analogue converter (DAC). DAC samples at sampling frequency $f_s = 1/T' = N/T$, and the output is a continuous time modulated signal $x(t)$. This is passed to the analogue front end or the channel as appropriate.

At the receiving end, the reverse process takes place. The transmitted symbol $x(t)$ after passing through the channel is distorted, therefore the received symbol is denoted by $y(t)$. The analogue to digital converter (ADC) takes samples of $y(t)$ in digital form, which is fed to Fast Fourier Transform (FFT). The output of FFT is N complex sub-symbols of which $\tilde{N}$ are used in decoder. The memory less decoder as shown in Figure 6.3, determines the symbol, from which bits are extracted. In this manner, bits are received.

The inverse Fourier transform (iFFT) is an example of an orthogonal transformation that preserves the energy of the frequency-domain symbol. The energy of transmitted symbol [250] is the sum of each sub-symbol energies (eq.(6.2)).

$$\sum_{i=1}^{\tilde{N}} |X_{i,k}|^2 = \sum_{n=1}^{N} x_{n,k}^2 \tag{6.2}$$

The transmit power is deduced from sub-channel energies using eq.(6.3).

$$P = \frac{E}{T} = \frac{\sum_{i=1}^{\tilde{N}} E_i}{T} = \sum_{i=1}^{\tilde{N}} P_i \tag{6.3}$$

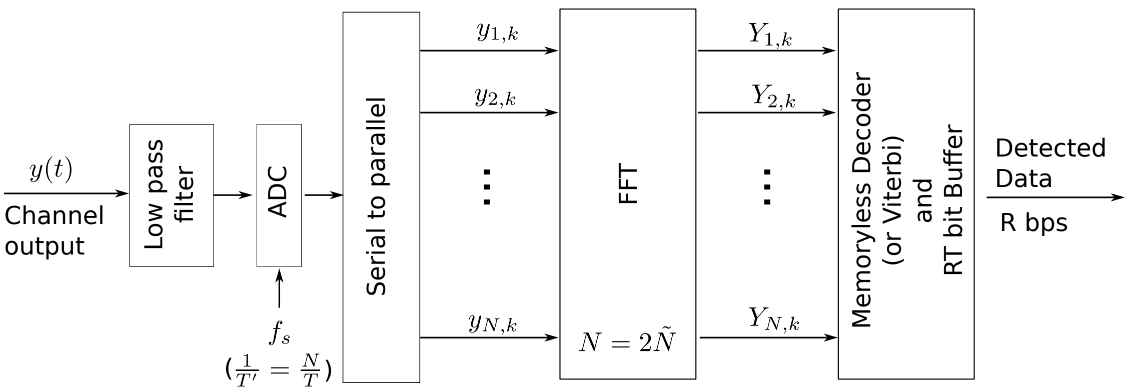

Fig. 6.3 OFDM Receiver functions as a reverse process of Transmitter. Functional blocks except Synchroniser based on the FFT transform proposed by Chang.

In the above treatise, the OFDM transmitter and receiver is assumed to be perfectly synchronised, which is not the case in practice. The "synchroniser" estimates the start of symbol, after which the demodulation and decoding takes place. OFDM is sensitive to timing offsets in the time domain and frequency offsets in sub-carriers in the frequency domain. Therefore, the synchroniser is considered an integral part of OFDM system performance evaluation, that is why it is discussed in a separate section 6.4.

6.2.2 The Significance of Sub-Channels

A channel with an impulse response $h(t)$ and additive (Gaussian) noise $u(t)$ is illustrated in the form of a block diagram in Figure 6.4. In the following analysis of the inter-symbol-interference (ISI) channel, the channel output is denoted as $y(t)$.

When $\tilde{N}$ is large, the continuous transfer function of the channel response $H(f)$ can be approximated by the discrete curve illustrated by rectangles in Figure 6.4. Each of the rectangles is a band of frequency $1/T$Hz wide. The value of the transfer function $H(f_i)$ is abbreviated as H_i at the centre frequency of sub-channel.

When $\tilde{N}$ is sufficiently large then the rectangles are very narrow, and it is mathematically correct to write

$$Y_{i,k} = H_i X_{i,k} + U_{i,k} \tag{6.4}$$

where $Y_{i,k}$ $i = 1, \ldots, \tilde{N}$ are the complex outputs of the N-point FFT and similarly $U_{i,k}$ denote the noise samples. When $\tilde{N}$ is large, the noise components can be shown to be independent when $u(t)$ is Gaussian.

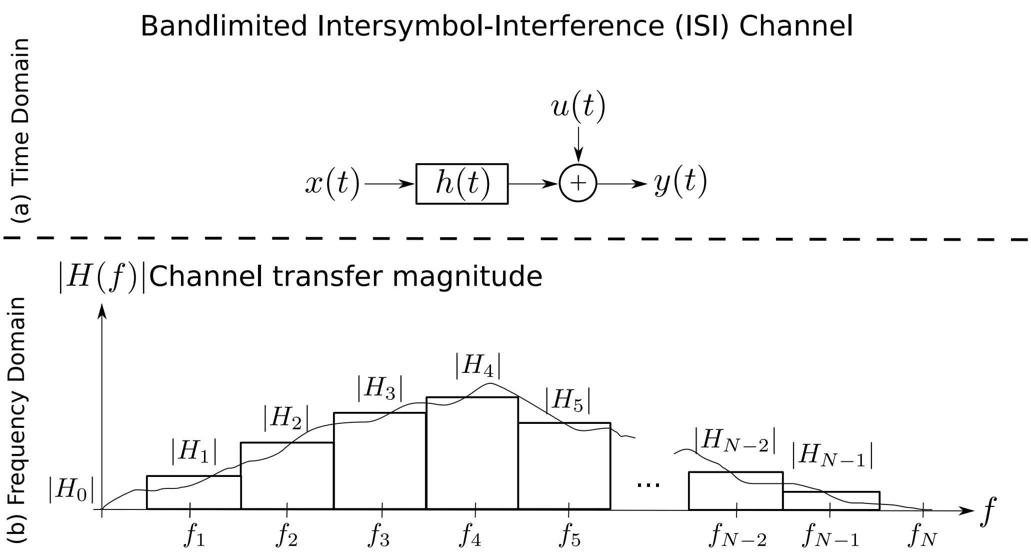

Fig. 6.4 Channel and multichannel decomposition of channel response [250].

We note that then, because the sub channels are independent, they can be individually decoded using a memory less detector for each. This set of memory less detectors is the optimum maximum-likelihood detector for the transmitted signal. Maximum-likelihood detection is then achieved with no equalisation nor any use of sequence detection. The price paid is the iFFT / FFT, which is often implemented at a small fraction of the cost of digital filtering or sequence detection for comparable situations [250].

6.2.3 Design Parameters

The important parameters which define an OFDM symbol are described in this section.

6.2.3.1 Sub-Carrier Spacing

The selection of N dictates the sub-carrier spacing. The selection is made on the basis of estimated frequency offsets observed by the system. Usually the extent of the channel coherence determines the maximum sub-carrier spacing. Due to parallel transmission, the OFDM symbol is longer than that of the single-carrier symbol. Unfortunately, time-selective fading compromises the long OFDM symbol, by introducing inter-channel-interference (ICI). Therefore the OFDM symbol is upper bound by the length of the interval that the channel stays stationary. As the symbol period is the inverse of the sub-carrier spacing, the minimum sub-carrier spacing is thus determined by rapid changes in channel impulse response.

6.2.3.2 Guard Interval

When many delayed replicas of the transmitted signal are received, then the signals may interfere with the original in a random manner. The phenomenon is called inter-symbol-interference (ISI) and is the primary cause of fading. The fading gets severe when transceivers are mobile.

To eliminate the ISI, guard interval of N_g samples is inserted at the beginning of each OFDM symbol as depicted in Figure 6.6. These are the last N_g samples of the OFDM symbol, making the transmitted symbol of $N+N_g$ sample length. This "cyclic prefix" enables the symbol to retain orthogonality of sub-carriers, when FFT is taken at the receiving end.

The guard interval depends on the channel's maximum excess delay.

6.2.3.3 Null Sub-Carriers

Some of the sub-carriers near the zero frequency (also called Direct Current (DC)) and the end $\tilde{N}$, are not used. This helps avoiding interference of unwanted frequency components generated by the analogue front end during the amplification and frequency up conversion. The DC component is a manifest in communications systems, since it can lead the amplifiers to operate in saturation region and clip the time domain signals. The unused sub-carriers are called null sub-carriers, which reduces data rate, but must be incorporated.

6.2.3.4 Spectrum Shaping

Wireless standards regulate the out of band signal power by specifying spectrum masks, which must be adhered to by the transmitting end. A time domain windowing is applied. A popular window applied is the raised cosine window of the form

$$w(t) = \begin{cases} 0.5 + 0.5\cos\left(\pi + \pi(t + N_g T)/(\beta T)\right) & -N_g T \leq t \leq (-N_g + \beta)T, \\ 1 & (-N_g + \beta)T \leq t \leq NT, \\ 0.5 + 0.5\cos\left((t - NT)/(\beta T)\right) & NT \leq t \leq (N + \beta)T \end{cases} \tag{6.5}$$

where βT is the length of the roll-off region and N and N_g are the number of OFDM symbol and guard interval samples, respectively. Windowing reduces the effective guard interval therefore extra samples in the guard be left for unwanted window effects.

6.2.3.5 Peak-to-Average Power Ratio

The peak-to-average power ratio (PAPR) is defined in eq (6.6).

$$PAPR = \frac{max|x(t)|^2}{E\{|x(t)|^2\}} \tag{6.6}$$

In the worst case, in which all the sub-carriers are coherently and equally summed up, the time-domain OFDM symbol can have a PAPR of about N. Say for 256 point FFT based sub-carriers, PAPR can be as high as 24 dB where as for 64 sub-carriers it can be about 18 dB.

The problem arises, when the peak causes the RF power amplifier to operate in its saturation mode, causing distortion not because of the channel, but due to clipping of the signal.

Several methods have been discussed to reduce the PAPR a summary can be found in [208]. We shall not consider any of the reduction techniques, to deduce raw performance evaluation.

6.2.4 Example Systems

A summary of the telecommunication services utilising MCM or OFDM is summarised in Table 6.1, which acts as a reference and guide for system designer. It also highlights the usage of OFDM in current and future telecommunications systems.

Consider the digital video broadcasting-terrestrial (DVB-T) system, operating in the 400-800 MHz bandwidth. It supports 2K and 8K FFT. In 2K mode, 1705 out of 2048 sub-carriers are used to carry data and pilot signals. As the symbol period is shorter, this mode tackles the fast-changing channel conditions. On the other hand, 8K mode has a longer guard interval, making it more capable of coping with multipath channels, with a long delay spread. Of all the 8192 sub-carriers, 6817 are used. With 64-QAM, highest data rate achieved is 31.67 Mbps with a code rate of 7/8.

The IEEE 802.11a/g operate in ISM band of 2.4-2.5 GHz. A total of 64 sub-carriers divide the whole 20MHz bandwidth. The guard band ratio and guard interval ratio are 0.1875 and 0.25 respectively supporting an adaptive modulation rate with a maximum data rate up to 54 Mbps.

The 3GPP-long-term evolution (3GPP-LTE) evolved universal terrestrial radio access (E-UTRA) project, intending to improve the UMT mobile phone standard to meet the so called fourth-generation (4G) requirements, adopts OFDMA with various FFT sizes in the downlink transmission. Its bandwidth caries from 1.25 to 20 MHz to provide flexible allocation. The sub-carrier spacing is fixed at 15 kHz, which results in possible FFT sizes ranging from 128 to 2048 points. The optimal cell size is 5 km so that 16.67 μsec is reserved for the guard interval. The target data rate is 100 Mbps in the 20 MHz bandwidth.

Table 6.1 OFDM design parameters used in wireless services provided by Digital Audio Broadcasting (DAB), Digital Video Broadcasting - Terrestrial (DVB-T), Wireless Local Area Network (WLAN), WMAN and Mobile Communications long term evolution networks [208].

	DAB				**DVB-T**		**802.11**	**802.16e-OFDM**	**3GPP-LTE EUTRA**					
Carrier Frequency (GHz)	0.375	1.5	1.5	3	0.4 0.8		2.5,5.8	2 – 11	2					
Sample Frequency (MHz)	2				6.8,8,9.14		20	8/7*B, 7/6*B	1.92	3.84	7.68	15.36	23.04	30.72
Bandwidth (MHz)	1.5				6,7,8		20	1.5 28	1.25	2.5	5	10	15	20
FFT size	2048	1024	512	256	8192	2048	64	256	128	256	512	1024	1536	2048
Used Sub-carriers	1536	768	384	192	6817	1705	52	200	76	151	301	601	901	1201
Guard band Ratio	0.25				0.1678	0.1675	0.1875	0.2185	0.41					
Sub-carrier Spacing (kHz)	1	2	4	8	1.116	4.464	312.5	125	15					
FFT Period (μsec)	1000	500	250	125	896	224	3.2	8/7*B, 7/6*B	66.7					
Guard Interval (μ sec)	246	123	62	31	224	56	0.8	2	4.67					
					112	28		1						
					56	14		0.5	16.67					
					28	7		0.25						
Guard Interval Ratio	¼				¼		¼	¼	9/128					
					1/8			1/8						
					1/(16)			1/(16)	¼					
					1/(32)			1/(32)						
Constellation	DQPSK				QPSK		BPSK	BPSK						
					16-QAM		QPSK	QPSK	QPSK					
					64-QAM		16-QAM	16-QAM	16-QAM					
							64-QAM	64-QAM	64-QAM					
Maximum Data Rate (Mbps)	1.8				31.67		54 M	104.7	> 100					

6.3 Reconfigurable OFDM System

Table 6.2 lists down the effect of increasing the bandwidth of the OFDM transmission scheme by increasing the sampling frequency, and keeping other OFDM parameters constant. This is the proposed method of changing the OFDM symbol time duration to match the channel characteristics. **With the channels defined earlier, the acceptable sampling frequency rate is 128 kHz and above.**

It is deduced, from the above observation, that since the sampling frequency is easily configurable in DSP, therefore, just by changing the sampling frequency also reconfigures the complete OFDM symbol, which can overcome the degradation effects of channel. This method is useful, since, without changing any other flow, or parameter in the implementation or design, OFDM symbol characteristics can be made to conform to the changing channel characteristics i.e. channel coherence bandwidth and channel coherence time.

It is highly desirable, that the reconfigurable feature should not add complexity to the existing design implementation of OFDM modem. The identified feature, meets the said desired features, and is considered a novel contribution to the ISL modem design.

Furthermore, it can easily be deduced, that commercially available IEEE 802.11 compliant devices cannot be used as it is in space application, rather, a DSP or FPGA implementation — already implemented in-house (SSC) by Paul [35].

Table 6.2 Dependence of OFDM Symbol duration and Guard Interval time on the selection of sampling frequency. Second part of the table indicates expected data rates with stated preambles, number of sub-carriers used, and bits per symbol.

DAC Sampling Freq (kHz)	**8.00**	**16.00**	**32.00**	**64.00**	**128.00**	**256.00**	**512.00**	**1024.00**	**20000.00**
N points	128	128	128	128	128	128	128	128	128
Usable BW (kHz)	4	8	16	32	64	128	256	512	10000
No of Sub Channels (N)	64	64	64	64	64	64	64	64	64
Sub Carrier Spacing (Hz)	62.5	125	250	500	1000	2000	4000	8000	156250
Samples per Guard ($N/4$)	32	32	32	32	32	32	32	32	32
Samples per Symbol	160	160	160	160	160	160	160	160	160
Symbol Duration (sec)	0.02	0.01	0.005	0.0025	0.00125	0.000625	0.0003125	0.00015625	0.000008
Guard Duration (Sec)	0.004	0.002	0.001	0.0005	0.00025	0.000125	0.0000625	0.00003125	0.0000016
No of Used Sub Carriers	36	36	36	36	36	36	36	36	36
Bits per Carrier	1	1	1	1	1	1	1	1	1
Bits per Symbol	36	36	36	36	36	36	36	36	36
Symbols per Second	50	100	200	400	800	1600	3200	6400	125000
Preamble Symbols	10	10	10	10	10	20	100	100	200
Data Carrying Symbols	40	90	190	390	790	1580	3100	6300	124800
Max Data Rate (bps)	**1440**	**3240**	**6840**	**14040**	**28440**	**56880**	**111600**	**226800**	**4492800**

6.4 The Synchroniser

In a communications system, the synchroniser is a critical functional block of the receiver. In the idle state, the receiver is waiting for a valid transmission, that is expected to be in bursts, in which a “packet” comprising several OFDM symbols would arrive. Several packets can be grouped together to form a “frame”. The purpose of the synchroniser is to first establish whether the transmission is valid or just noise. Then it must estimate the start time of the transmission, from which symbols are detected, based on their known time duration. Since each symbol has a particular time duration and repetition rate, the time synchronisation must keep track of the timing for the complete duration of transmission.

The power of each symbol is designed to be higher than the average noise power. To distinguish incoming symbols from noise, their power level is being measured, and compared with the average noise level. As soon as the average power increases a fixed threshold, it marks the start of a transmission. However a more complex processing is required for symbol start time estimation, which depends on the type of transmission.

When a distinct carrier is available at the baseband level, then the phase-lock loop (PLL) can lock on the carrier, and provide the necessary time synchronisation. This is used in “coherent” receiver architectures, such as BPSK, QPSK, FSK. However, when a carrier is not present, then “non-coherent” detection approaches are used utilising the “correlation” methods to determine the timing information. The theory of estimation and detection of parameters such as time offsets, frequency offsets and phase offsets is described well by Kay [251, 252].

There are two basic types of synchronisers, namely, data aided (DA) and non data aided (NDA). DA scheme requires a dedicated symbol transmitted, whose properties and content are known to the receiver, which is used for synchronisation purposes. NDA scheme exploits the repetition properties of a symbol. DA scheme outperforms NDA for all practical purposes, and is extensively used in wireless communications as recommended by standards such as IEEE 802.11, LTE and Cellular networks. The dedicated symbol is called “pilot”, which is easy to detect, and lock onto. A set of pilot symbols appended to the data carrying symbols is often called “preamble” in OFDM literature.

The existing techniques use extensive use of “phase-locked loop” (PLL) and “correlation” to establish a start of symbol. Take for instance the BPSK or QPSK receiver which uses “Costas Loop” an extension of PLL, to not only synchronise but also demodulate. For such devices to operate, a constant envelope of symbols is desirable, with a significant power in the carrier. The transition of phase from symbol to symbol establishes a local clock. However, for symbols with no constant envelope, nor any repetition of amplitude, or phase or frequency, the correlation technique is used. The known symbol is correlated with the incoming signal. When the two signals are aligned, the output of correlation function is maximum, often called “peak”. The peak establishes the start of symbol. The technique relies on the fact, that noise is uncorrelated, however the transmitted signals have a good correlation measured as its coefficient. So whenever a high correlation is found, above a threshold value, a valid symbol is detected, and the start of symbol is calculated from the location of peak. This method is used in OFDM and spread spectrum code division multiple access (CDMA) systems, where symbols do not have a distinctive time domain repetition.

PLL is useful for main RF carrier frequency offset estimation, but for fine N sub-carrier offsets within the OFDM symbol, it is not a viable option. Therefore, an alternate method for sub-carrier offset estimation is required. Today, joint timing and frequency offset estimation algorithms are reported in literature. We shall utilise one such algorithm, for our OFDM performance evaluation. It is not within the scope of this work to evaluate or improve existing algorithms.

The algorithms which could readily be implemented in MATLAB were from VanDeeBeek [253], Troya [254, 255] and Schmidl & Cox [256, 257]. Since Troya [255] implemented the algorithm in an FPGA, specifically for low powered devices, his synchroniser is modelled in MATLAB which forms the basis for our OFDM modem performance evaluation.

The synchroniser requires a predefined set of symbols, which are correlated with incoming symbols, to determine the start of symbol where the correlation is maximum. The predefined set of symbols is called pilot symbol which includes data required for data aided synchronisation and channel estimation purposes. The pilot symbol used in our studies is described in the following subsection.

6.4.1 Pilot Symbol

The objective of the pilot symbol is to provide information for the synchroniser to establish timing, and the sub-carrier to assist in frequency offsets. Furthermore, the pilot generated uses the same process as a normal OFDM symbol does. Using only three sub-carriers, equally spaced apart, pilot symbol with a constant envelope is formed. The sub-carriers provide crude frequency offset estimation. The pilot symbol can therefore provide a crude channel transfer function. A better channel response is possible by using all sub-carriers.

The advantage of such a pilot is that individual sub-carriers can be detected with the help of bandpass filters. The use of three bandpass filters tuned to the centre frequencies, can provide a simple solution to detection of valid symbol. It can then switch the rest of the digital signal processing circuitry on for further processing, saving power consumption.

The number of pilot symbols to be used as a preamble, is determined from field experiments using actual hardware. The radio based transmissions from a car, and with in the laboratory, we found that the first two to three pilot symbols got distorted beyond recognition, therefore twice of that and additional symbols for safer operations, we selected 10 pilot symbols for transmission. The alternate symbol is multiplied by -1, causing it to shift the phase by π rad. Two of the pilot symbols* in time domain illustrate this property in Figure 6.5.

The pilot uses sub-carriers $f_i = \{1,1,1\}$ where $i = \{8,16,32\}$, and rest of sub-carriers are multiplied by zero (unused sub-carriers). The subsequent pilot symbol is loaded with $f_i = \{-1,-1,-1\}$ where $i = \{8,16,32\}$. In addition to the pilot, 5 symbols to denote start of data and 5 symbols to denote end of data are used. These symbols use all the sub-carriers loaded with known bits, which allows channel estimation. So basically the burst of transmission starts with 10 pilot symbols, start of data, variable length data, and end of data, illustrated in packet form in Figure 6.6. Although for testing, the data length is set variable, but recommended practice is to set the number of data symbols. In this manner, the receiver can keep a count of data symbols, and can request for a resend, if for some reason, all data symbols are not received.

The power spectral density of the above mentioned symbols is shown in the Figure 6.7. It is noticed that the power of the OFDM symbol decreases significantly when only three sub-carriers are used as compared to 36 sub-carrier. This is due to the distribution of signal energy to subsequent frequency channels, as is known in Frequency Division Multiplexing (FDM). Single carrier modulated with 1 Watt, is divided into the number of sub-carriers in the same channel. So when 3 sub-carriers are used (Figure 6.7a, 6.7b) the power is divided by 3 hence the average is computed as 0.33 W; similarly for 36 sub-carriers (Figures 6.7c, 6.7d, 6.7e, 6.7f), it amounts to $1/36 \approx 0.02$W .

The average power is calculated using the definitions in eq. (6.3). The y-axis is the power density per Hz calculated by the area under the curve method used by "psd"†.

6.4.2 Joint Timing and Frequency Offset Estimator

The synchroniser must accomplish the following operations:

1. Distinguish start of transmission from noise.
2. Start of the OFDM symbol, so that cyclic prefix (guard samples) be extracted, and data symbols determined.
3. Sub-Carrier frequency offset estimation and correction. The inter-carrier-interference (ICI) is caused due to undue frequency offsets.
4. Channel estimation and correction.

There are several OFDM synchronisers reported in literature such as [258, 259, 260, 261, 253, 262, 263, 257, 264, 265, 266, 267, 268, 269, 225, 249]. Of the algorithms, Schmidl and Cox algorithm is implemented in GNURadio, and Troya [255, 254] is shown in Figure 6.8. The latter algorithm has been implemented in VLSI on FPGA, for low power wireless transceivers, which is desirable in our study.

*This pilot provides necessary transitions which can assist a PLL to be used as well, although not verified in this study.
†"psd" is an inbuilt MATLAB function.

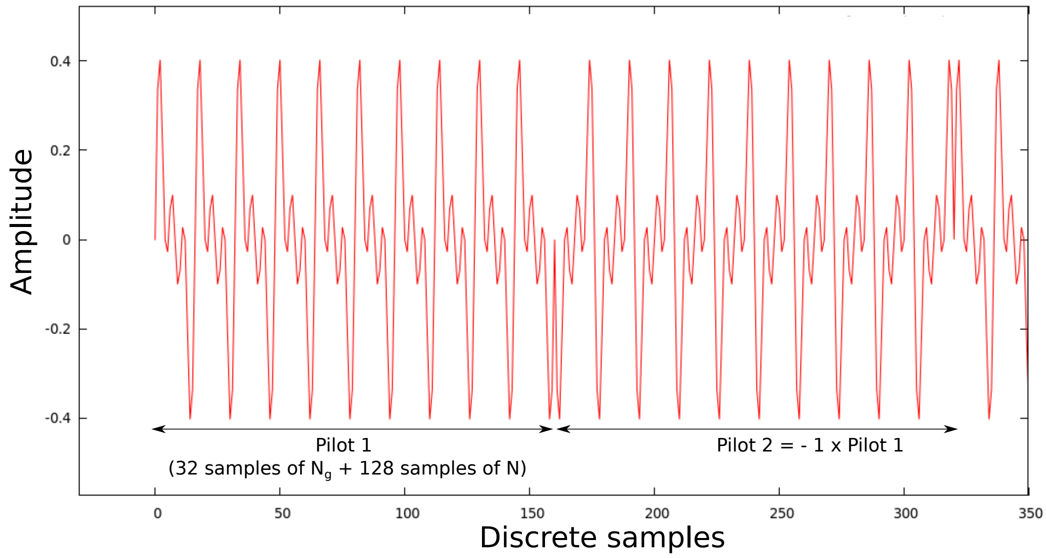

Fig. 6.5 Two Pilot symbols in time domain (32+128=160 samples), illustrating constant envelope, and phase shift between symbols. Ten pilots form the preamble of our burst.

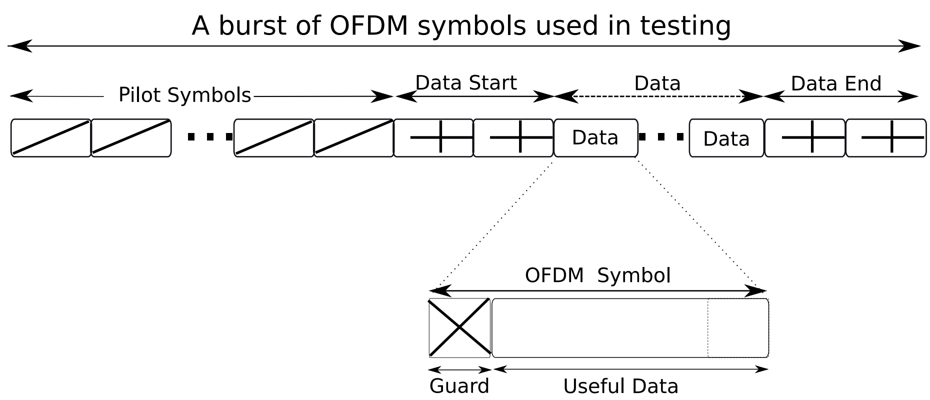

Fig. 6.6 A burst of OFDM symbols starting with pilot, data start, data and data end symbols, used in testing.

The joint symbol and frequency offset estimator has its own limitations, which are discussed following the analysis and description by Troya [255].

Let r represent the received signal from the radio, after ADC. If the In phase (I) and Quadrature phase (Q), is used then the I/Q combined form a complex signal. Other wise take Hilbert transform [75] of the real input. The samples at a sampling frequency f_s, have a residual frequency offset. To determine the frequency offset from the auto-correlation function, Troya proceeds as follows. Let the carrier frequency offset (CFO) be $f_\varepsilon = \varepsilon \delta f$, where ε is the normalised CFO , and δf is the sub carrier spacing. The symbols are made such that sub-channels see flat fading, then we can safely assume that the gain of

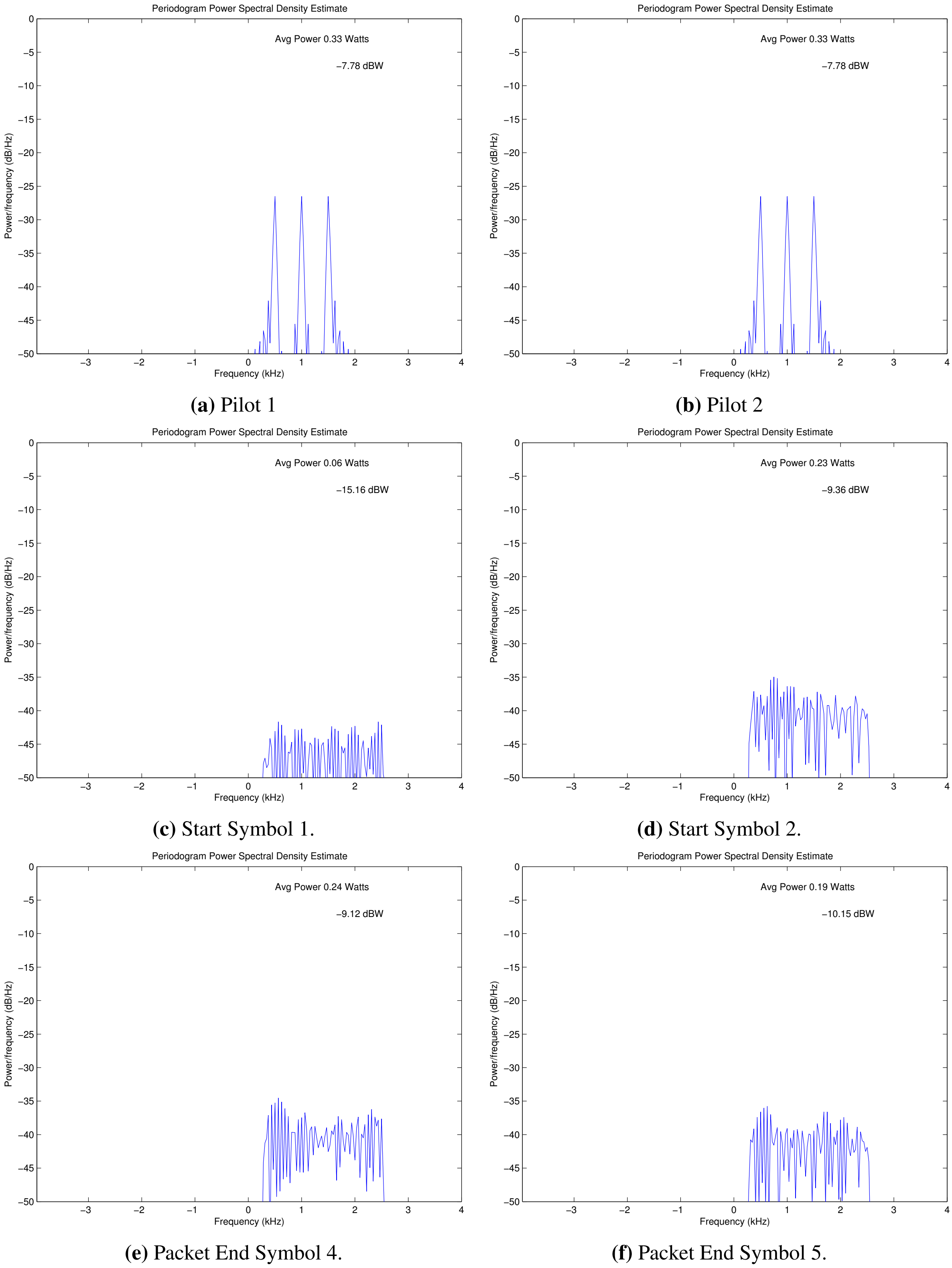

Fig. 6.7 Power Spectral Density Estimation known OFDM symbols.

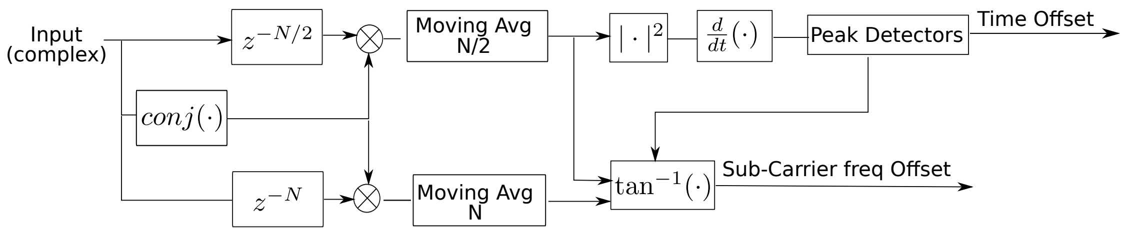

Fig. 6.8 Joint frequency and timing synchronisation algorithm as proposed by[254] implemented in this study.

channel response affects amplitude of the symbol. The AWGN noise distorts the symbol. The received signal samples can be written as [255];

$$r(m) = s(m) \cdot e^{j2\pi\varepsilon\frac{\delta f}{f_s}m} + n(m) \tag{6.7}$$

The auto correlation of r with its delayed version, $J_x(k)$ would be of the form [255];

$$J_x(k) = \sum_{l=0}^{N_{avg}-1} r^*(l-k) \cdot r(l-k-N_d) \tag{6.8}$$

N_d is the fixed delay, whose value is set for a specific pilot symbol, in our case the pilots repeat after N_d representing the periodicity of $s(m)$. N_{avg} is the value chosen in the moving sum average. More values in the average means more accuracy, however, it also means more time to establish a peak. When the symbol $s(m)$ is uncorrelated under the AWGN condition then eq. (6.8) can be approximated as [255],

$$J_x(k) \approx e^{j2\pi\varepsilon\frac{\delta f}{f_s}m} \cdot \sum_{l=0}^{N_{avg}-1} |s(l-k)|^2 \tag{6.9}$$

In eq. (6.9), it is evident that CFO error ε causes a phase shift in auto-correlator's output. Where $s(m) = s(m-N)$ the periodicity would cause the magnitude of auto-correlation highest, there the phase of $J_x(k)$ can be used to determine the frequency offset. To estimate the frequency offset ε, rearrange the terms in eq. (6.9) to get;

$$\varepsilon = \frac{f_s}{2\pi \cdot N_d \cdot \delta f} \cdot \arctan\left(J_x^*(k)\right) \tag{6.10}$$

The arctangent is bounded in the range $[-\pi, +\pi)$, which also bounds eq. (6.10) [255],

$$|\hat{\varepsilon}| \leq \frac{f_s}{2 \cdot N_d \cdot \delta f}. \tag{6.11}$$

The channel impulse response and the automatic gain controller settling time would affect the periodicity i.e. $s(m) \neq s(m-N_d)$. The noise also contributes, but by taking the average, its effects are compensated. The arctangent operation is restricted to the range $[-\pi, +\pi)$, hence the frequency can only be estimated within the range [255]

$$-\pi \leq 2 \cdot \pi \cdot \varepsilon \cdot N \cdot \frac{\delta f}{f_s} < \pi \tag{6.12}$$

or equivalently

$$|\varepsilon| < \frac{f_s}{2 \cdot N \cdot \delta f} \tag{6.13}$$

Since the ratio $f_s/\delta f$ is a fixed parameter, the range of possible estimated valued for ε only depends on the selected delay in the auto-correlator. When no oversampling is considered at the receiver, then for $f_s = 20$ MHz, and $\delta f = 312.5$ kHz (case of IEEE 802.11a), then the resulting $|\varepsilon| < 0.5$ for the delay $N_d = 64$ and $|\varepsilon| < 2.0$ for delay $N_d = 16$ samples.

6.4.3 Synchroniser Testing

The synchroniser was tested before the main end-to-end simulation was carried out. Although a thorough investigation was not carried out, but frequency offset of 1 kHz and phase offsets of 45 deg were detected and compensated for.

The power spectral density, the rotation in baseband signal space (constellation diagram of BPSK), and the corrected BPSK constellation after synchronisation is shown in Figure 6.9. Similarly a frequency offset is also detected, and compensated. The illustrations are captured when the synchroniser was being tested independent of a channel manifest, except manual frequency and phase offsets were being changed for the receiver input. The input to receiver was also manifested with AWGN. This baseband synchroniser is tested for functional adherence, keeping the frequency offsets deliberately low, because it is assumed that the first stage PLL will compensate for larger frequency shifts.

6.5 Baseband MODEM Performance

The end-to-end system for OFDM has been divided in to sub-systems at the functional level. As it is with any simulation based study, the depth or level of simulation is defined by the user. In this study, the functional blocks are simulated for functionality and not circuit level effects. The flow of transmission is

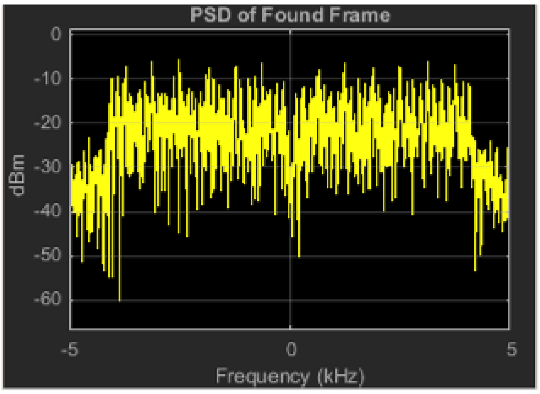

(a) Power Spectral Density of detected OFDM frame.

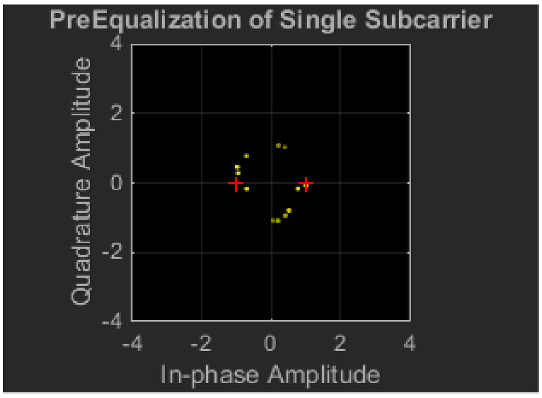

(b) Constellation diagram of BPSK before compensation.

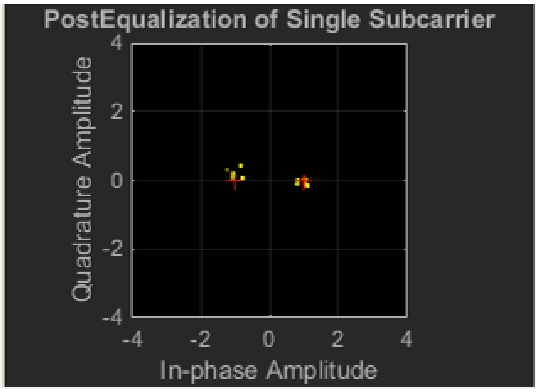

(c) Constellation diagram of BPSK after compensation.

Fig. 6.9 OFDM power spectral density, and compensation of the estimated phase and frequency for a single sub-carrier. Illustrates the correct detection of frame, and channel estimate after synchronisation.

thus . Furthermore, since the purpose had been to evaluated end to end system, therefore, the practical functions which are not considered in the theoretical concepts of OFDM have need to be incorporated.

To confine the scope of work, the performance evaluation is carried out for a baseband modem simulated in MATLAB, only. The Analogue Front End (AFE) components have not been considered in this evaluation study, however, the impairments have been considered, by conducting hardware-in-the-loop simulation studies, separately. The additional functional block i.e. the Synchroniser is also incorporated in the model, as documented in the section 6.6.

Therefore in a summarised form, it is being assumed, that the generated OFDM symbol, is modulated onto a carrier in AFE, which passes through the channel, getting distorted on its way to the receiver AFE, where it is demodulated to baseband signal. The baseband signal is then further processed to extract the OFDM symbols, from which the transmitted message is extracted.

The received message comprises bits, which are compared with the actual message bits, and the number of errored bits determined. The simulation is carried out by varying the SNR in a range of 0 to 20 dB. In this manner, the SNR for best performance can also be evaluated.

The performance tests begin with the effects of free space path loss.

6.5.1 Simulating Free Space Path Loss

In order to simulate the free space path loss an experimental setup has been developed consisting of two personal computers (PC). Each computer has the MATLAB package installed, and is equipped with a sound-card. MATLAB utilities required to interact with the sound-cards are also necessary (Data I/O toolbox). A stereo cable is used to connect both sound-cards. The speaker output is connected to an input line (or a microphone jack). One of the PCs acts as the transmitter, and the other one – as the receiver. Since the sound-cards can only be used for operating frequencies less than 20 kHz, therefore, this setup can serve the purposes of validating a low data rate communications system operating in space, when there are no sources of fading. The sound-cards are connected via a stereo audio cable. The speaker out is connected to line in (or mic if line in is not available). Thus, one of the PC acts as a transmitter, and the other receiver.

The audio output is first checked using an oscilloscope, to visually inspect the waveform being generated. If there is clipping, then th audio levels are reduced. Similarly, at the receiver side, audio signals are recorded and visually inspected within MATLAB for signs of clipping. An important point to highlight here is that the audio level of the sound card must be set so that the output on the oscilloscope is within 0.4V pk-pk , as to not cause clipping.

At the receiver side, AWGN channel is configured so that the received signal once captured can be further simulated at various SNR levels (0 to 10 dB)*. For each SNR level, the receiver is tested for its performance. The additive white Gaussian noise was generated in simulation, and added to the received signal prior to OFDM receiver.

The BER is calculated by sending OFDM symbols between the two PCs. The OFDM symbols are generated carefully, keeping the occupied bandwidth within the audio sampling frequency supported by the sound-cards. For each SNR level, the receiver is tested for its performance. The additive white Gaussian noise was generated via simulation, and added to the received signal prior to the OFDM receiver. Since the sound-cards can only be used for operating frequencies less than 20 kHz , therefore, this setup can be considered as a practical demonstration of a low data rate system operating in space, where there are no sources of fading.

*The MATLAB AWGN function is used with the parameters setting as ’measured’.

The transmission is configured in “Burst Mode”, i.e. the transmission is initiated after random time intervals in between transmissions. The configured OFDM baseband system parameters are defined in Table 6.3 and the results are tabulated in Table 6.4.

The synchroniser lose synchronisation for SNR lower than 3 dB.

6.5.2 Fading Channel Performance

In the previous section free space path loss was emulated. In this section, the channel is assumed to exhibit fading properties and their impact on the OFDM symbol design is discussed. The transmission scheme used for the simulation has the specifications given in Table 6.3. The simulation was carried out using Rician factor of 10, and maximum Doppler shift of 20 Hz.

Table 6.3 OFDM Parameters for Burst Communications Test

Parameter	value	Comments
N	128	N-point FFT, number of channels
Ng	32	Guard samples, cyclic prefix
f_s	8kHz	PC sound Card: Creative Sound blaster pro, 128 bit.
ix_f	[5:5+36-1]	Used sub carrier Index, rest are loaded with zero
ix_p	[8;8*2;8*3]	Pilot symbol carrier index
$M-PSK$	4, D-PSK	Differential phase shift keying, with Gray coding
Preamble	10	OFDM symbols for synchronisation
Data	63	Data OFDM symbols, generated using random numbers

Table 6.4 Symbol Errors for various Signal to Noise Ratio via sound-cards between two PCs. The Symbol Error Value is a mean of 50 runs.

SNR (dB)	Symbol Errors	Symbol Error Rate
3	404.3	0.1812
4	291.8	0.1307
5	197.3	0.0884
6	122.8	0.0550
7	70.7	0.0317
8	36.3	0.0163
9	16.2	0.0073
10	6.5	0.0029

The transmitted burst data is illustrated in Figure 6.10. It starts with a pilot symbol, and then the data symbols follow.

As it is known from theory, the channel manifests itself depending on the characteristics. The OFDM symbol bandwidth is directly linked to the sampling frequency so by increasing the sampling frequency, we increase the bandwidth. Therefore, the transmitted burst is affected differently for various sampling frequencies.

The smaller bandwidth is less than the coherence bandwidth, and is severely distorted as is observed in time domain. As the transmission bandwidth increases, the channel manifestation is less obvious in time domain (compare start of frame which is the pilot signal in Figure 6.10 with Figure 6.11a to Figure 6.11b).

As it can be observed from Figure 6.11a, transmission bandwidth, which is less than the channel coherence bandwidth, leads to severely distorted symbols in the time domain, respectively. Comparing the start of the frame in Figure 6.10, which is the pilot signal, with Figure 6.11a, Figure 6.11b, Figure 6.11c it can be seen that as the transmission bandwidth increases, the degrading effect is less obvious in the time domain.

It has also been observed, although not visible in the Figure 6.11, that long duration packets undergo deep fading occasionally, which leads to severely corrupted data frames.

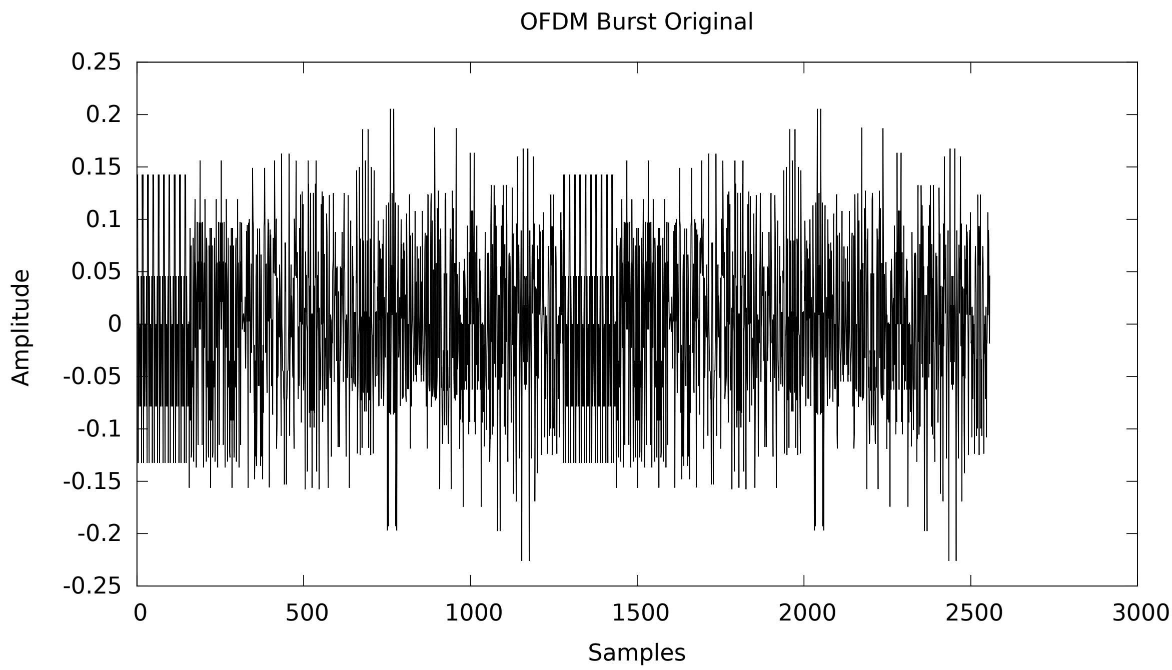

Fig. 6.10 OFDM Burst comprising of two frames, each frame consists of a header and data.

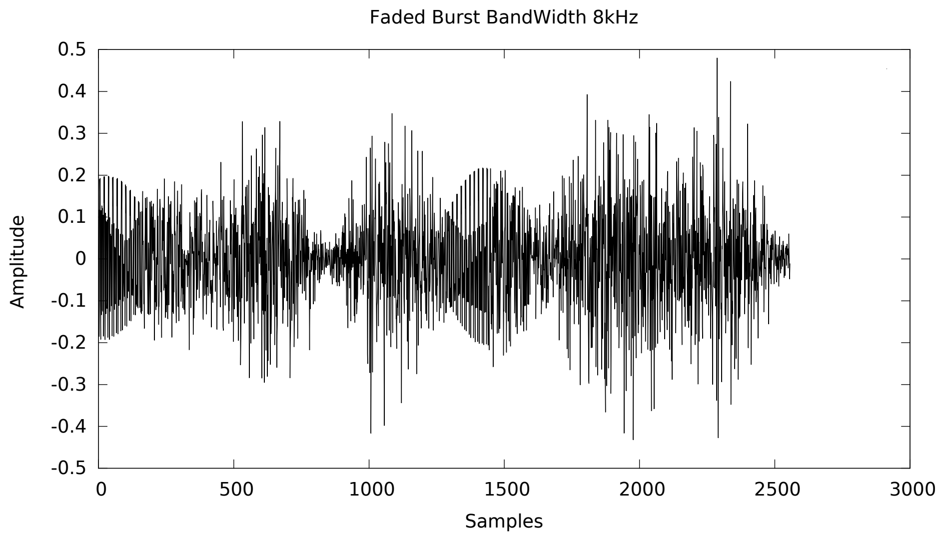

(a) Severely degraded symbols; transmission bandwidth less than channel coherence bandwidth.

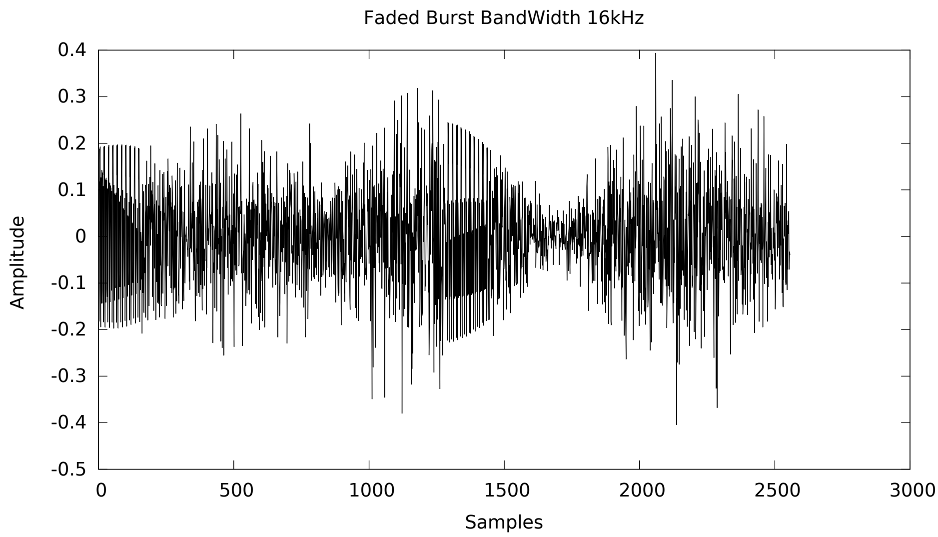

(b) Deterioration of symbols, transmission bandwidth close to channel coherence bandwidth.

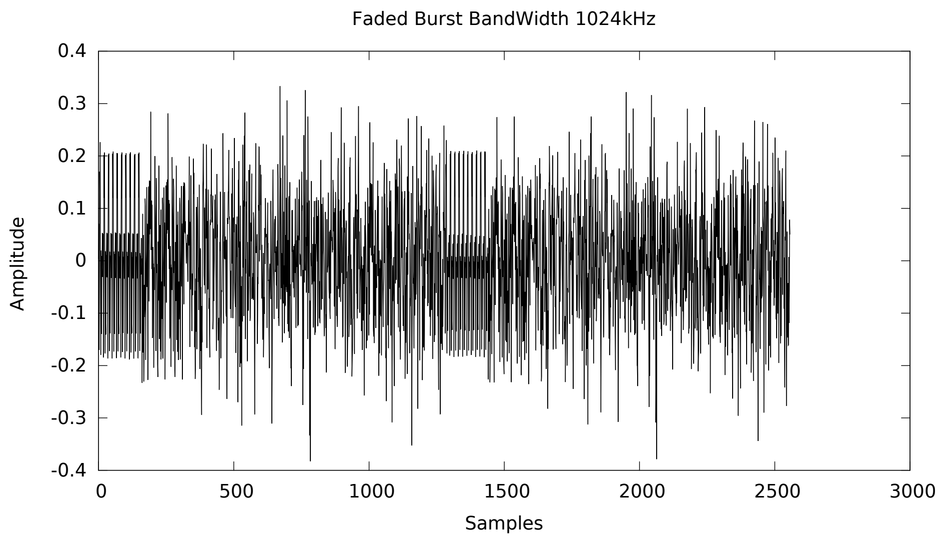

(c) Transmission bandwidth much greater than coherence bandwidth.

Fig. 6.11 Faded signal in time domain. Signal bandwidths (8,16 and 1024 kHz) under the influence of channel coherence bandwidth of 33 kHz.

Synchroniser Performance

The OFDM burst was transmitted 100 times and manifested with the Rician channel. The synchroniser performance was evaluated, based on the number of dropped frames out of the 100 transmitted. The number of dropped frames for the two channels are depicted as bar graph in Figure 6.12a and Figure 6.12b respectively. It can be seen in Figure 6.12a as the symbol energy increases, the number of detected frames also increases, however, for the bandwidth less than the coherence bandwidth, the performance is worse even when ample symbol energy is present e.g. for sampling frequencies 8 and 16 kHz). It can further be observed that about 100% frames are detected for sampling frequencies 128 kHz and 512 kHz. Whereas, for 1024 kHz, there are a few frames are dropped. A similar but slightly different performance is observed in the case of Chan2 in Figure 6.12b , where for all transmission bandwidths the receiver is able to detect the incoming transmission.

Bit Error Rate Calculations

The end-to-end performance of the transmission scheme is determined by the performance measure “bit error rate(BER)”. BER is plotted against E_b/N_0 varying from 0 to 20 dB, for the two fading channels.

Figure 6.13a plots the BER for the case of Chan1, for varying OFDM bandwidth. The worst case BER is for the OFDM symbol bandwidth 8 kHz, which is less than the coherence bandwidth of channel. Similar BER is found for 16 and 32 kHz, as well, that is why they are not plotted. It shows, practically there is no communications link, even though the pilots were detected, since the BER is 10^{-1}. Whereas, when OFDM bandwidth is higher than the channel coherence bandwidth for 64, 128, 512 and 1024 kHz OFDM symbols. It highlights our main point, that if OFDM symbol is not designed properly in accordance with the channel coherence bandwidth, the modem performance is poor, and generally not acceptable as is clearly visible for different OFDM bandwidths under the influence of Chan2.

It can also be deduced from here, that if the communications channel coherence bandwidth varies spatially or temporally, then, a reconfigurable OFDM modem is required, which could adjust its bandwidth accordingly. The algorithm required to adjust the OFDM bandwidth is out of the scope of this thesis.

When we consider 10^{-3} an acceptable minimum requirement for a highly fading case, then the OFDM performance is considered acceptable for $E_b/N_0 > 13$ dB in the case of Chan1, but its performance is not acceptable in the case of Chan2. An error correction and detection code would definitely improve the overall BER when compared to resulted stated here. Thus, these results act as the bare minimum level, which should be improved using additional techniques.

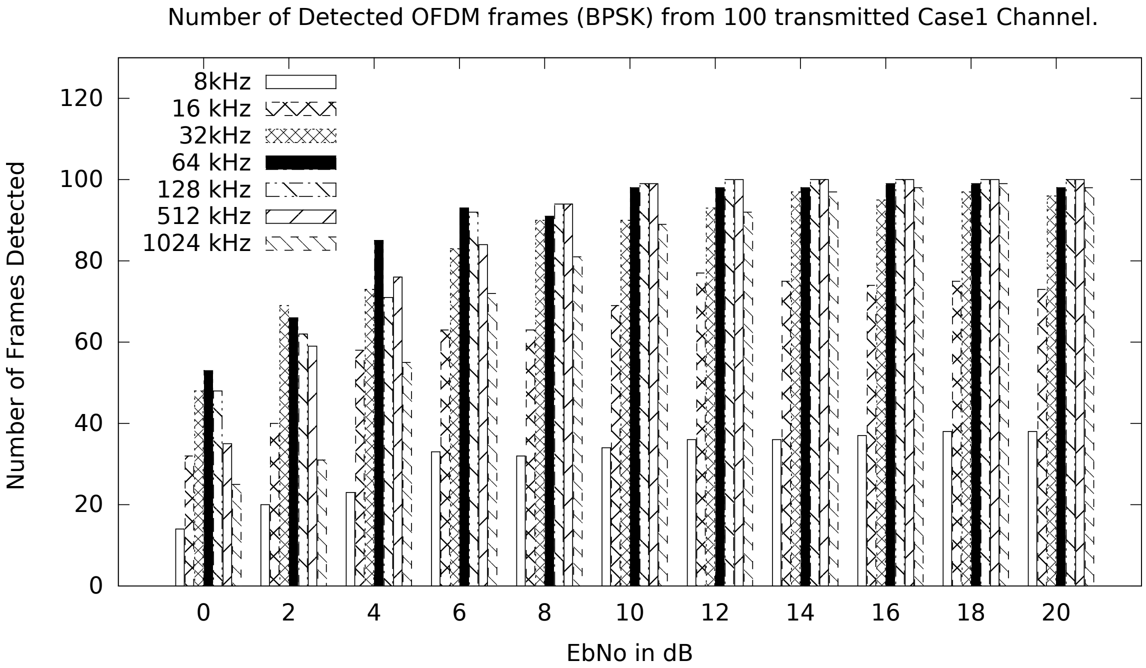

(a) Detected frames of the 100 frames, for the simulated symbol bandwidth, under varying E_b/N_0, for simulated Chan1.

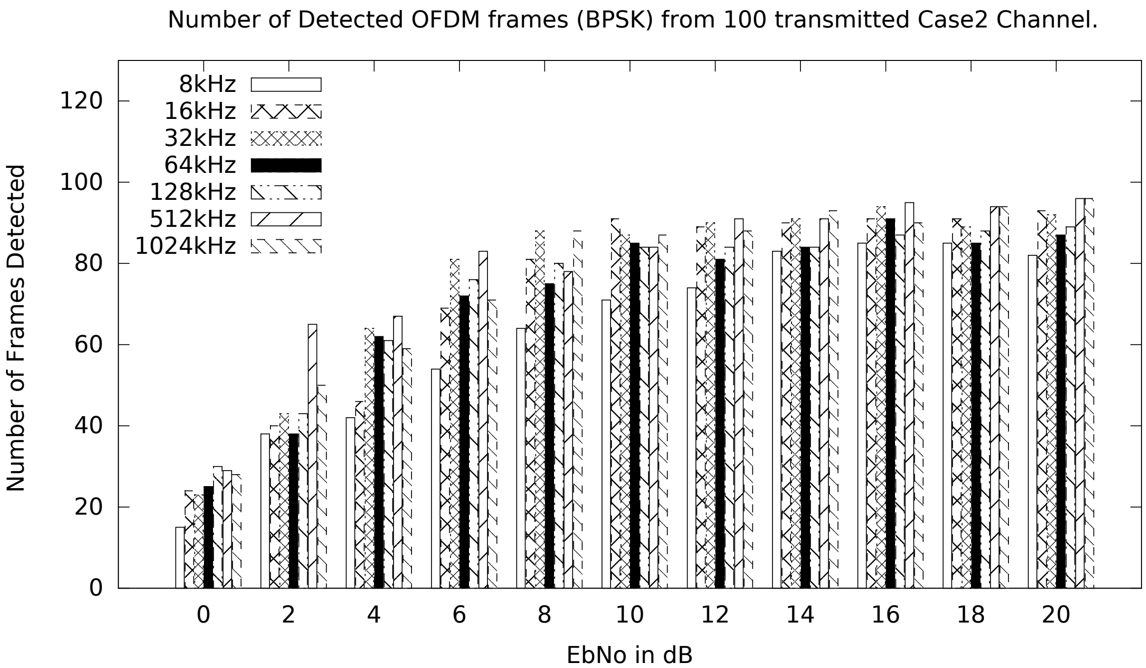

(b) Detected frames of the 100 frames, for the simulated symbol bandwidth, under varying E_b/N_0, for simulated Chan2.

Fig. 6.12 OFDM Synchronisation performance. Number of detected OFDM frames per 100 transmitted.

The above treatise also highlights the fact, that communications channel estimator, which is an inherent component of OFDM modem, plays a critical role in a dynamic channel such as anticipated in LEO inter-satellite links.

The performance evaluation reported in this section included only the fading channels, leaving out the hardware impairments. Rather than simulating the hardware impairments as models in MATLAB, a hardware-in-the-loop method is employed, the topic of discussion of the next section.

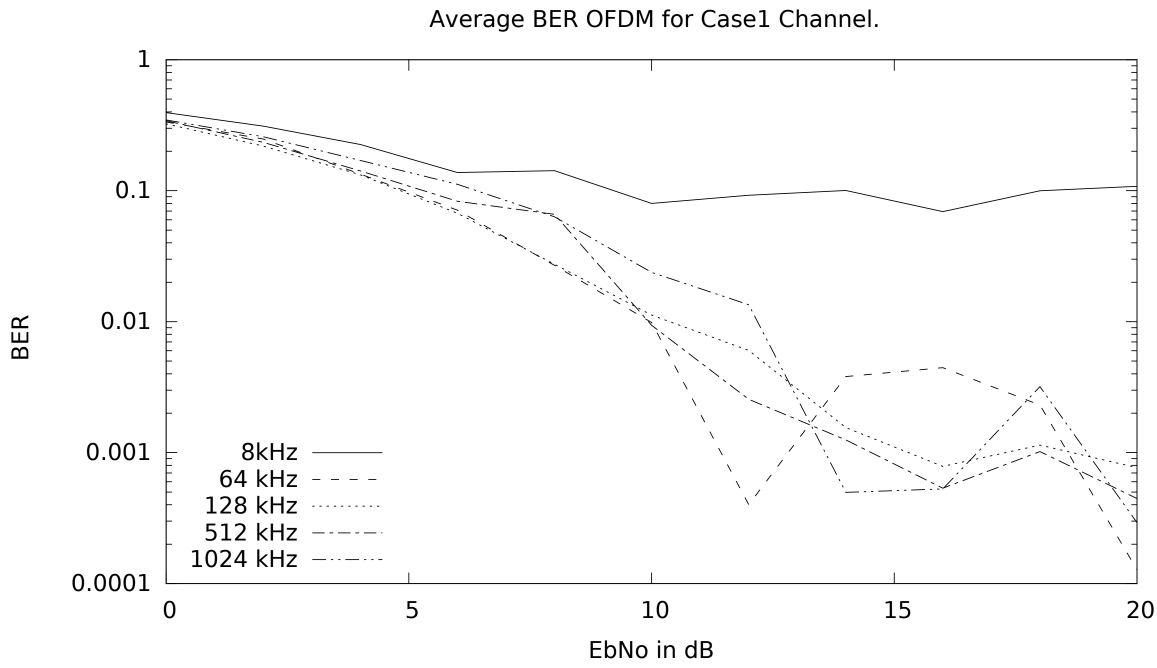

(a) Bit Error Rate estimates for simulated channel 1.

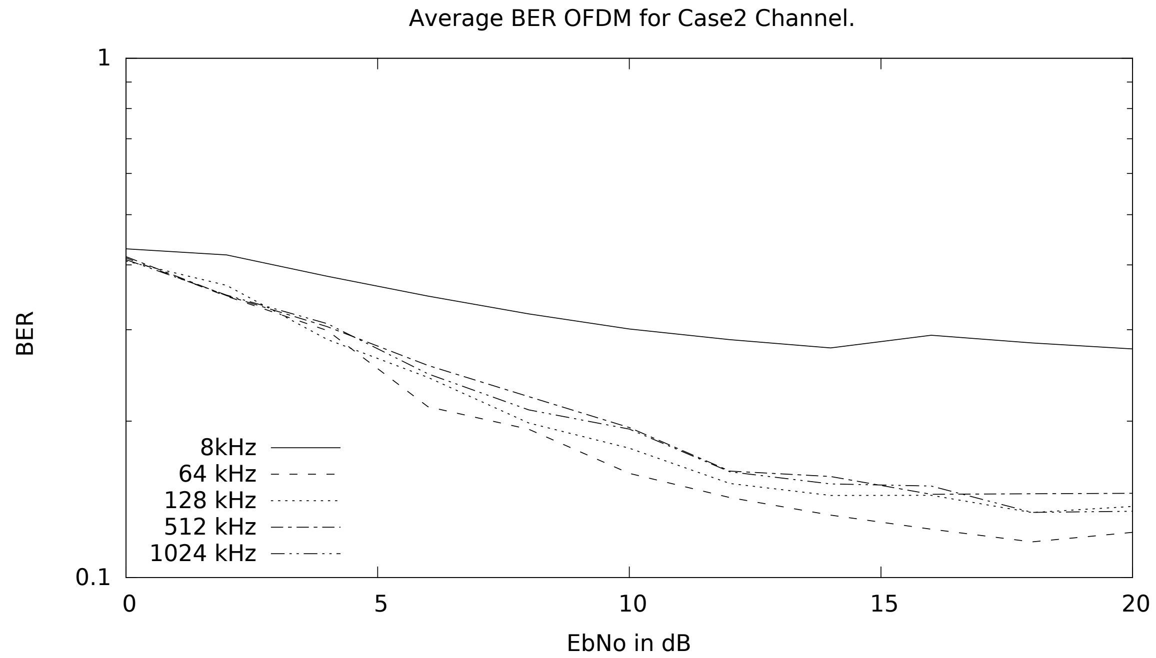

(b) Bit Error Rate estimates for simulated channel 2.

Fig. 6.13 End to end performance of OFDM transmission under the influence of two Channels defined in Section 5.5.4 (a) Case 1 and (b) Case 2.

6.6 Hardware-in-the-Loop Simulations

A method, referred to as hardware-in-the-loop (HIL), has been employed to incorporate the hardware impairments along with the simulated channel effects. The technique allows distributing the overall functionality to a selected hardware system supporting HIL, running all or part of the simulated functions.

Two cases were addressed. In the first case, only the baseband modem runs on an FPGA, whereas, in the second case, a complete system including the analogue to digital converters, analogue amplifiers, passband modulators, and antennas (complete analogue front end) is accomplished, with one unit acting as the transmitter, and the other unit acting as the receiver, emulating a complete end-to-end system performance.

6.6.1 Co-Simulation using Programmable Logic

The baseband modem is modelled in MATLAB [68] from where it has been converted to hardware blocks in the Simulink environment. The Xilinx System Generator (SysGen) tool [270] was used for the creation of the building blocks to be implemented on programmable logic in the form of Xilinx FPGAs. During the hardware in the loop simulation, the code runs on the FPGA and the output is fed back to MATLAB/Simulink. In particular, the Xilinx Spartan3S1500 FPGA device was used as part of the Nu Horizon FPGA board [271] which has been configured to support Hardware Co-Simulation. The board also houses a two channel 16 bit DAC supporting 100 ksps, Linear Technologies DAC LT-1654, which can be linked to analogue front ends for simulating low data rate modem configuration.

6.6.1.1 OFDM Transmitter

The block diagram of the OFDM transmitter implemented in Matlab/Simulink using Xilinx FPGA supported intellectual property (IP) cores via SysGen, is shown in Figure 6.14.

The blocks with a Σ sign in the middle are SysGen blocks, whereas, rest of the blocks in the Figure 6.14, are Simulink standard library components. To control the operations of the FFT block from SysGen, extra control signals had to be generated such as enable, start, and FFT number configuration. The FFT block by SysGen has an additional feature that it is reconfigurable for N values. If it is implemented for $N = 1024$, then it can be configured to operate in lower divisors of power of 2 e.g. 64, 128, 256 etc. This is a handy feature which can be used to increase or decrease the sub-channels i.e. increase of decrease the sub-carrier spacing. The significance of sub-carrier spacing is discussed in section 6.2.3.1.

The system was tested by passing the code for generating a pilot symbol to both the Simulink model and the FPGA implementation, and compared. The top two subplots in Figure 6.15 are the output of iFFT using MATLAB/SIMULINK, for both the real and imaginary parts (consecutively), and the bottom two

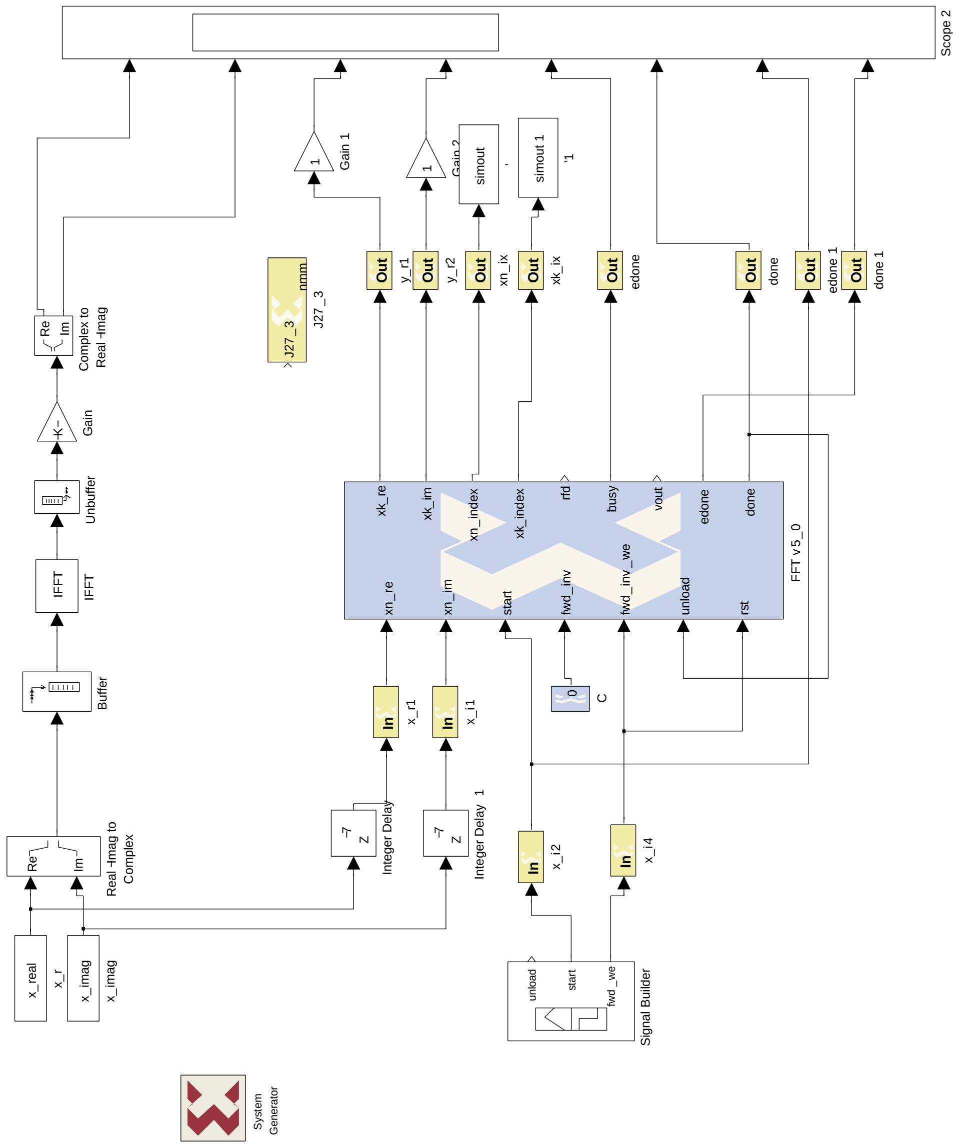

Fig. 6.14 OFDM Transmitter implemented in MATLAB/SIMULINK plus SysGen blocks, using Hardware in the loop simulation method.

figures are the output of FPGA. Note there is a delay between the two outputs, which is one time only, and does not affect the output. Another point to note is the output of iFFT from SysGen is inverted as compared to the output of iFFT.

All data is represented in fixed point notation in FPGA, therefore, when compared to floating point representation used by Matlab models, there is a reduced precision. This introduces a slight distortion in the waveform similar to quantisation noise (conversion of analogue continuous signal to discrete sampled signal). The result of HIL is shown in Figure 6.15. When the waveform was sent to a receiver modelled in MATLAB, the receiver was able to synchronise and decode OFDM (fading channel is not used). The fixed point implementation is thus considered acceptable.

6.6.1.2 OFDM Receiver

The model of synchroniser using both MATLAB/SIMULINK and Xilinx SysGen is shown in Figure 6.16. The synchronisation algorithm is described earlier in section 6.5.2.

The receiver takes input from the transmitted OFDM Burst Data which requires real and imaginary parts. Since MATLAB/SIMULINK supports complex number notation, therefore its blocks can take in complex numbers. Whereas the hardware treats and manages real and imaginary parts of the complex number separately. Therefore, there is an additional conversion of complex numbers into real and imaginary parts, and vice-versa (to and from Simulink to FPGA).

Since there was only one hardware, therefore, it could either be used as a transmitter or a receiver. So to test the receiver, the OFDM burst is generated on another PC, linked to a receiver PC setup for HIL interfaced to FPGA. The transmitter and receiver side were linked via sound-cards using a stereo cable. OFDM symbols being transmitted via sound-cards, captured by MATLAB, but tested for demodulation via FPGA. No fading type channel was used, since only the impairments caused by hardware was to be studied. Since the receiver was able to correctly demodulate the OFDM symbols, means that, the impairments caused by sound-cards and FPGA implementation, were not severe enough to disrupt the receiver functionality.

For the purpose of verifying the correctness of the decoded output, the received signals were co-simulated in a batch processing mode.

6.6.2 Wireless Link over a Software Defined Radio

In addition to the MATLAB / FPGA HIL scheme described above, a software defined radio based implementation was also carried out using GNURadio with the USRP N210 hardware. It is a software defined radio architecture type, with both the OFDM transmitter and receiver implemented in C++ code, running as an application under the Linux operating system (OS). The USRP N210 alongwith a wide

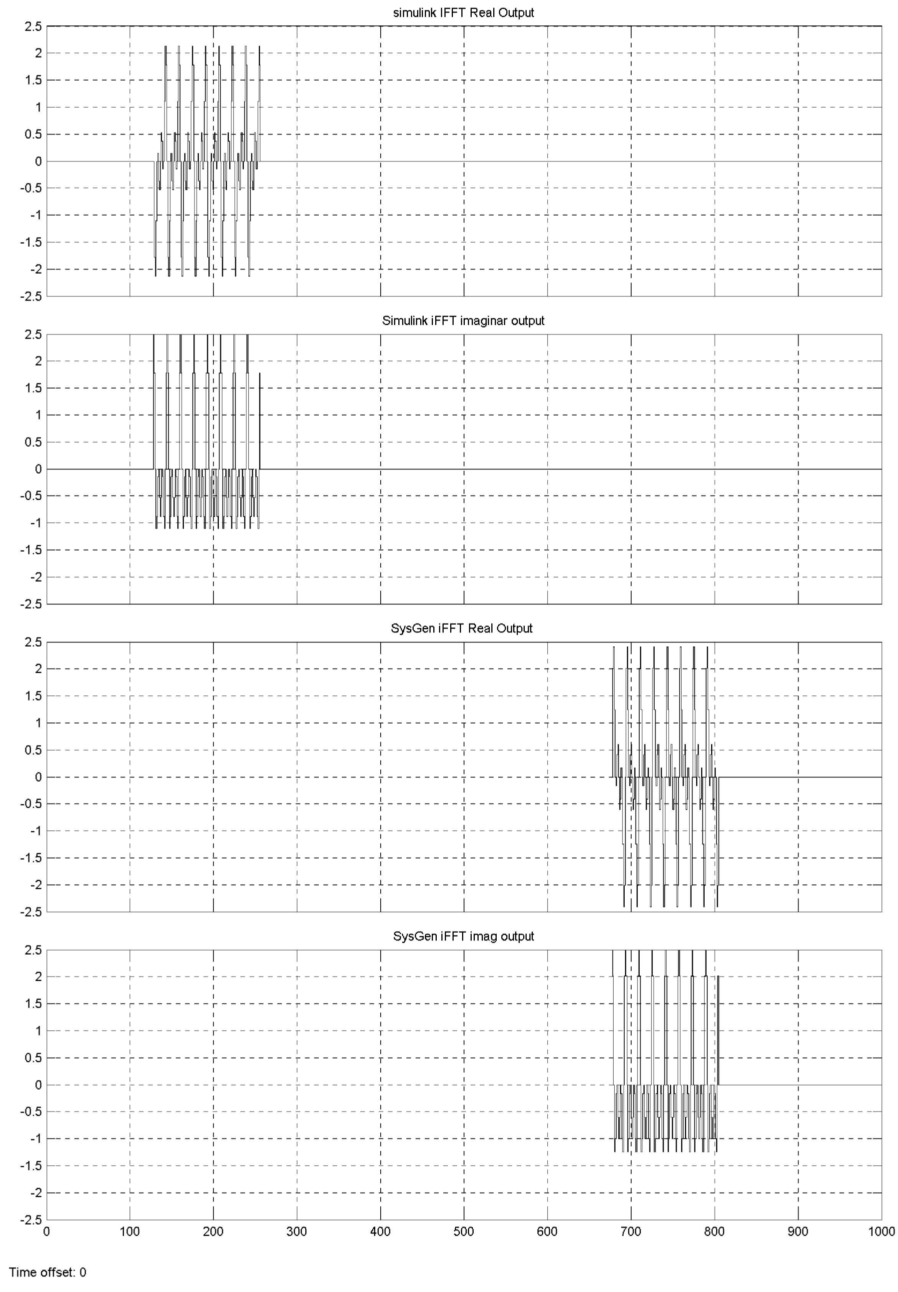

Fig. 6.15 OFDM transmitter pilot tone generation from FPGA.

band radio front end from Ettus Research [272, 273] is used as the AFE in the radio based end-to-end hardware based system performance evaluation.

GNURadio [274] is an open source software defined radio whose modules have been written in C++ for optimal performance. It can be interfaced to a hardware such as USRP N210 from Ettus Research Inc.

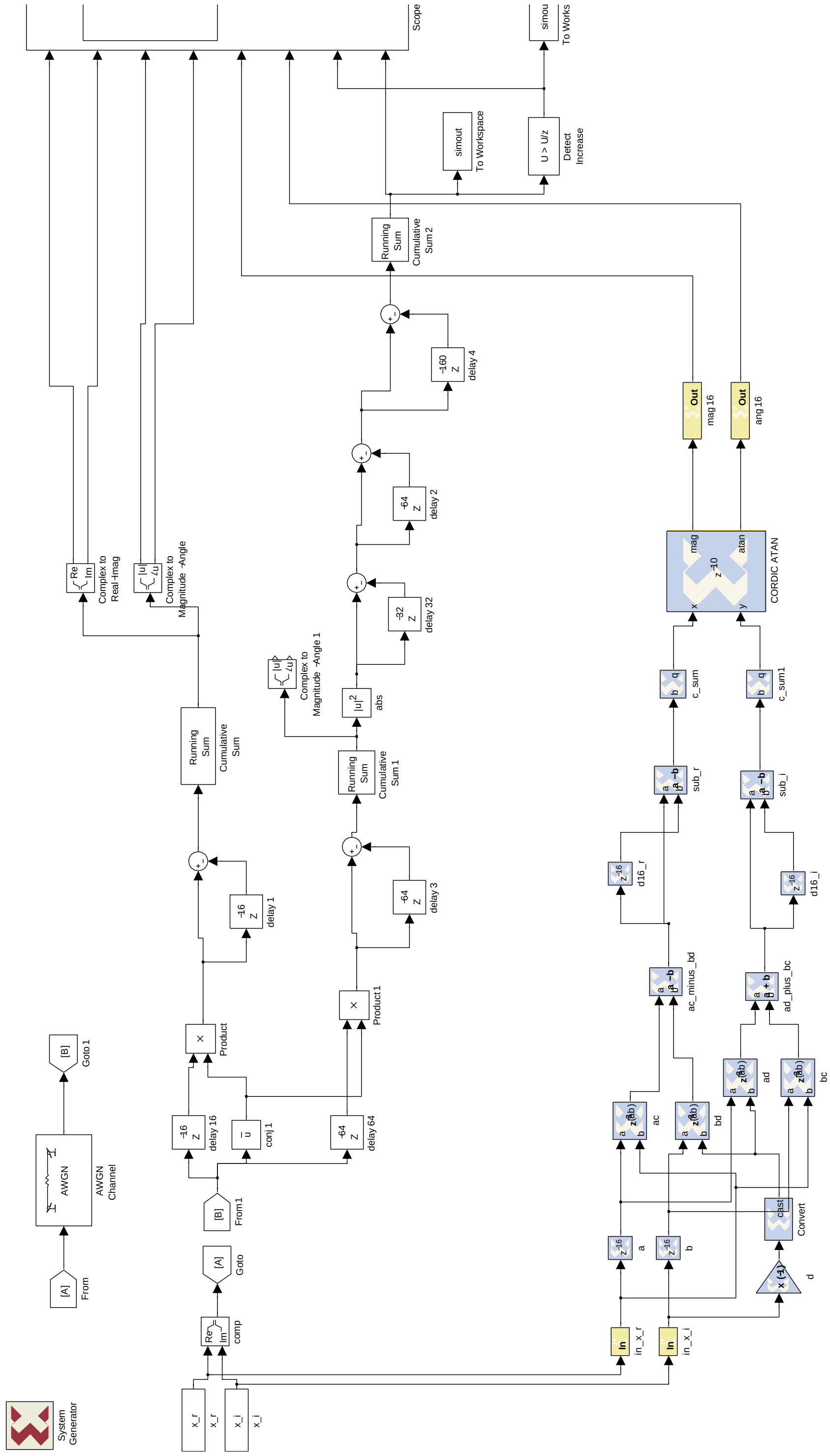

Fig. 6.16 OFDM Synchroniser modelled in MATLAB/SIMULINK and implemented in FPGA using SysGen.

USRP N210 supports several AFE available as RF daughter cards. One of the daughter cards called SBX [273], can transmit from 400 to 4000 MHz, which have been used.

Since GNURadio is implemented as software, running all its modules written in C++, while operating on the underlying operating system (OS), its processing speed is inherently limited by the OS support for real-time operations. GNURadio on Linux (e.g. Ubuntu or Debian based Linux) is not real-time. Therefore, while running an OFDM modem directly with hardware, there were visible glitches, dropped packets which generated an ambiguity whether, it was the problem of OS or the problem in modem, or the interface.

To systematically test, we changed the OS first. To overcome the issues of long delays in processes within the operating system, a small foot print and efficient (still non real-time) operating system was required, so that most of the system resources be made available to GNURadio, particularly the processing and memory. In GNU Radio we can set parameters on the fly, however, when the OS does not pass control to the input devices, then the application becomes unresponsive. After a significant search, a Linux distribution called Puppy [275] Linux (TahrPup) not only allowed easy installation of GNURadio, but an easy interface to the Ethernet based interface to USRP N210 as well. No previously observed issues such as dropped packets, non-responsive GNURadio modules, were observed after using the new OS.

6.6.2.1 GNU Radio Based Implementation

The experimental setup is shown in the Figure 6.17. The cart was made of LEGO blocks, to allow the movement of the transceiver. This experimental work fulfilled successfully the purpose of verifying the basic functionality of the hardware based transmitter and receiver.

However, the movement was not fast enough to cause an observable deterioration. The relative motion can be emulated using a mobile platform carrying this hardware. This detailed testing has been left for future work.

GNU Radio comes with a basic implementation of a configurable OFDM transmitter (Figure 6.18), complete with synchroniser at the receiving end (Figure 6.19). The synchroniser used the Schmidl and Cox [257, 264] method of peak detection. We hardly tweaked the code, and it operated very well not only over the air, but also when simulated for our case channels (Figure 6.20).

The packets were sent at a sampling frequency of 1 MHz with the radio configured to operate at the frequency of 900 MHz. The receiver was turned on first, and then the transmitter, and the log displayed the number of packet being received and any invalid packets.

The same code was simulated to run with the Chan1 using a multipath fading block. The receiver worked just as it was simulated, working flawlessly for a decent signal to noise ratio.

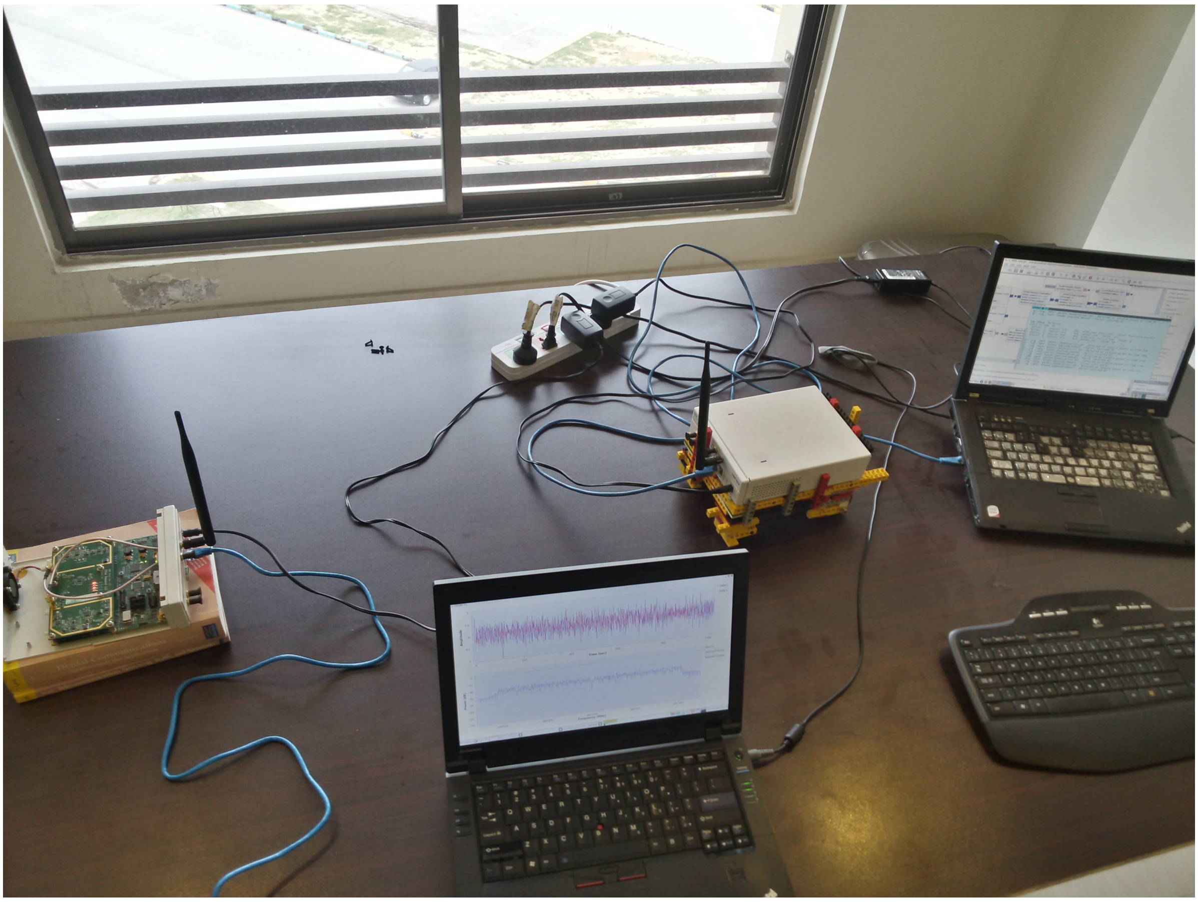

Fig. 6.17 GNU Radio with USRP N210 software defined radio implemented in Linux, to test OFDM transmission.

6.6.2.2 Frequency / Phase-Locked Loop

So far we have considered the frequency shifts in the OFDM receiver, which assumes that the major frequency shift is catered to by an external frequency lock loop or phase lock loop, which keeps a track of the carrier frequency whose major shift is due to relative motion called Doppler Frequency Shift. The impact of the frequency shift on the carrier system is that the receiver is unable to tune in to the transmitter frequency, and thus it seems as no transmission has been detected.

A Phase-Locked Loop (PLL) or the Frequency-Locked Loop (FLL) is able to lock on to the frequency even if the carrier is shifted. The main functional block diagram of the PLL is a comparator which discriminates the phase, gives the error signal to a filter which acts as the controller smoothing out the comparator output to be given to a frequency generator which updates its frequency according to the error signal. The generated frequency is again compared with the incoming signal an error signal is generated, whose magnitude controls the frequency shift of the local generator, and this carries on and on in the loop. The loop bandwidth essentially defines the working of the PLL [202].

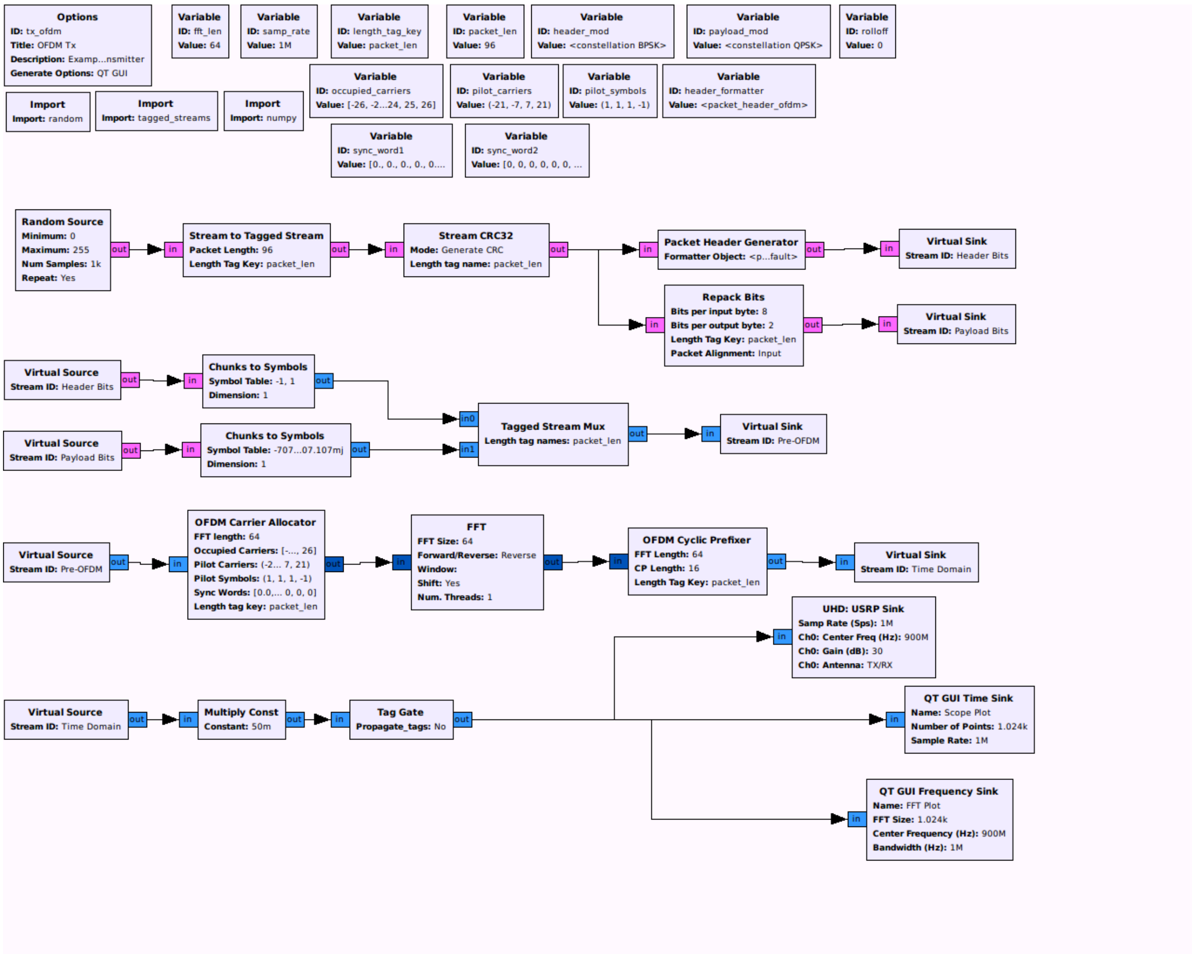

Fig. 6.18 GNURadio: Transmit side OFDM blocks

GnuRadio comes with many built in modules, particularly a functional phase-locked loop (PLL) which not only operated very well over 15 kHz frequency shift range, its reconfigurable loop bandwidth can be tuned to desired properties.

The functional block diagram in the GnuRadio Companion(a graphical front end to GNU Radio) is shown in Figure 6.21. This particular implementation is given in detail by the author on his web page [274]. While testing it for PSK data, it worked very well. Testing it was by changing the frequency and it would still lock on the frequency. By tweaking the bandwidth of the loop filter it would lock and retain the shifted frequency within the range of 15 kHz. When PLL achieves a lock on the receiver frequency even when it is shifted is shown in Figure 6.22a and Figure 6.22b displays the PLL unable to lock on the shifted frequency.

Thus by adding all the functional blocks of a radio and baseband modem in our testing, we complete our end-to-end performance evaluation of the proposed OFDM to operate in LEO environments for members of SBWSN to form inter-satellite communications links.

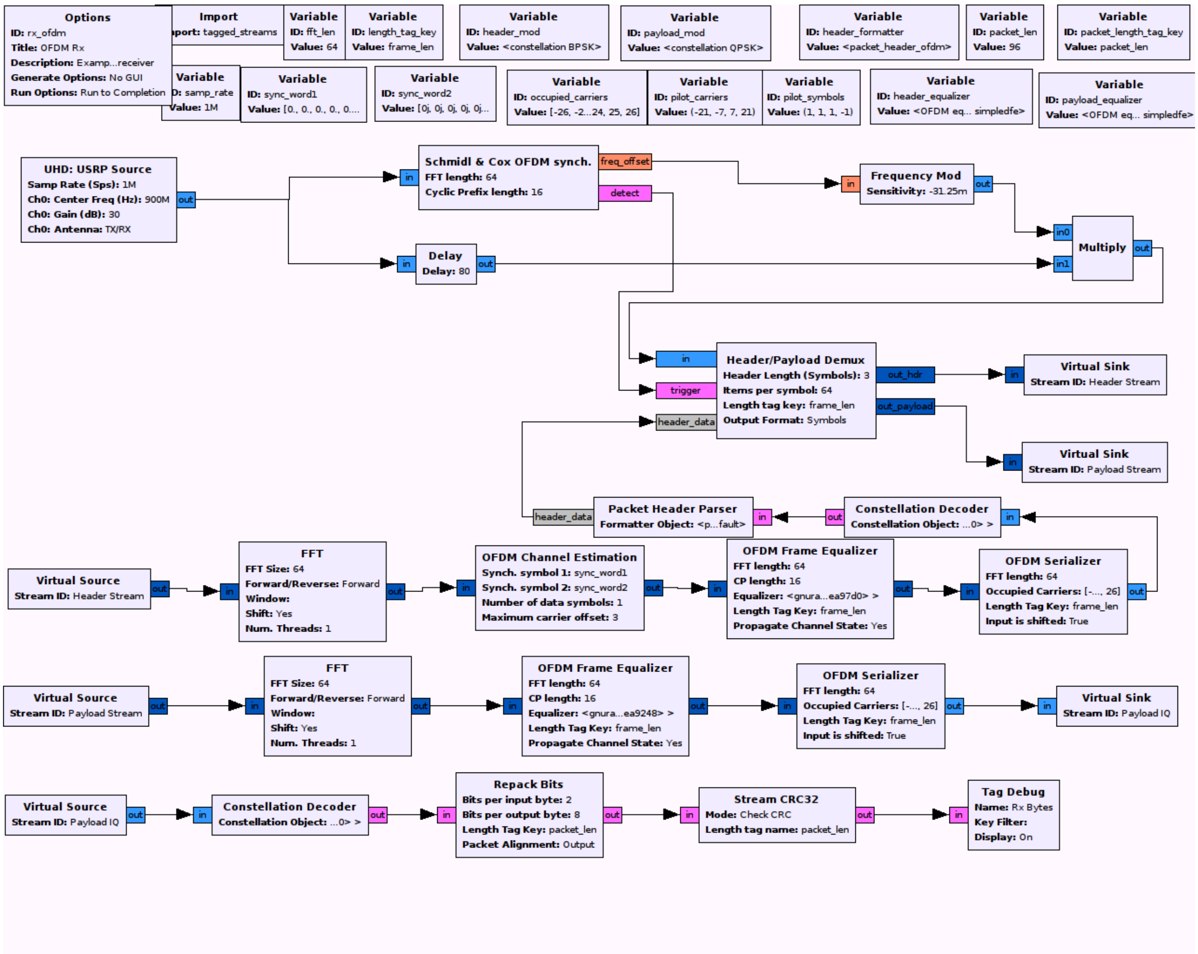

Fig. 6.19 GNURadio: Receive side OFDM blocks.

6.7 Discussion

OFDM has been previously proposed by Sidibeh [31] as part of IEEE 802.11 physical layer transmission scheme, and Paul [35] implemented an IEEE 802.11 compliant OFDM on FPGA. This chapter actually goes beyond that analysing the design of the OFDM, in the context of the communications channel characteristics, which are specific to the LEO space environment.

It has been shown that a dedicated OFDM modem needs to be properly designed as per the channel characteristics, otherwise severe degradation is observed in the simulation results. The OFDM timing synchronisation shows robust behaviour. Two hardware in the loop simulations, helped in incorporating issues arising from the actual hardware, which also showed promising results. Xilinx FPGA supports a configurable FFT core, which makes the module configurable. The second hardware-in-the-loop simulation is based on a GNU Radio interfaced with USRP N210. Over-the-air duplex transmissions

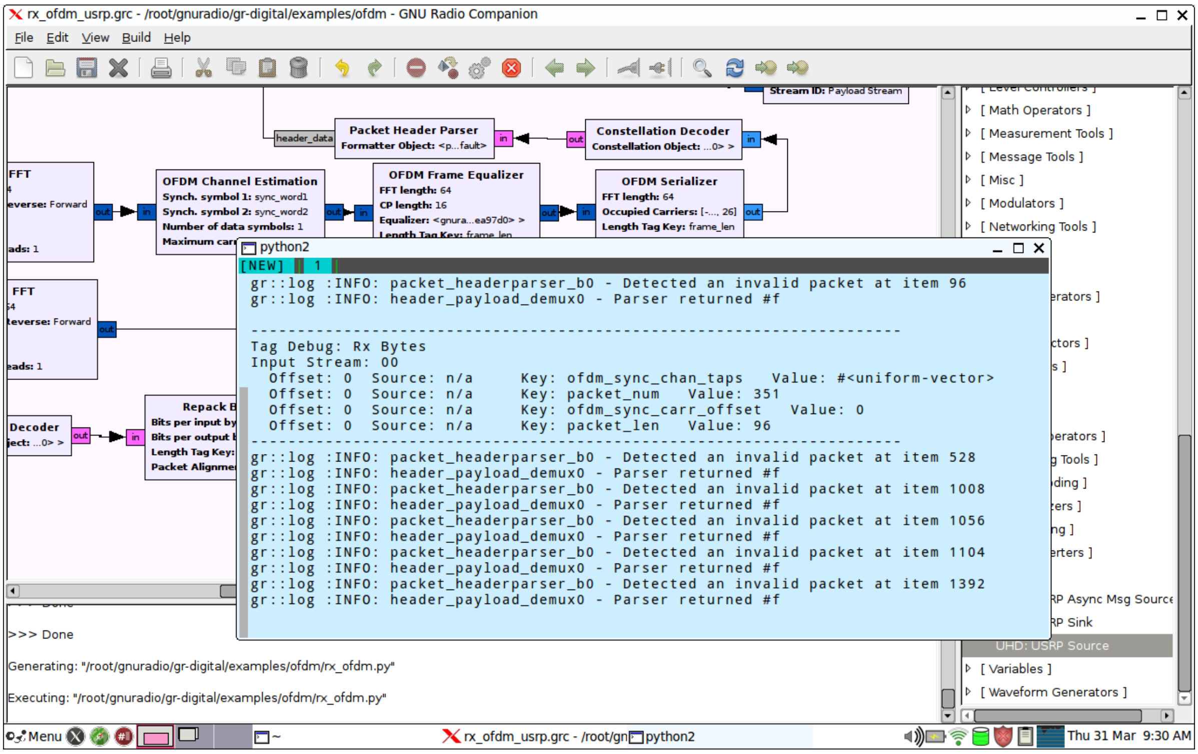

Fig. 6.20 Receive packets for the OFDM symbol.

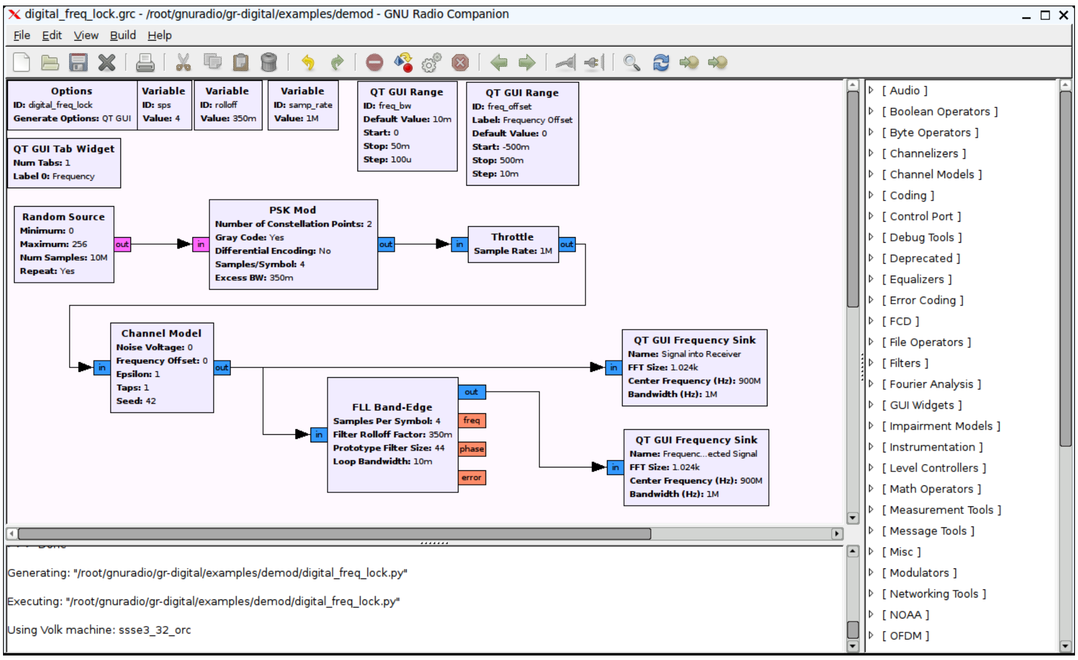

Fig. 6.21 GNU Radio frequency lock loop functional block.

were tested. Even one unit was placed on a cart which was moved about the receiver, but no substantial errors observed.

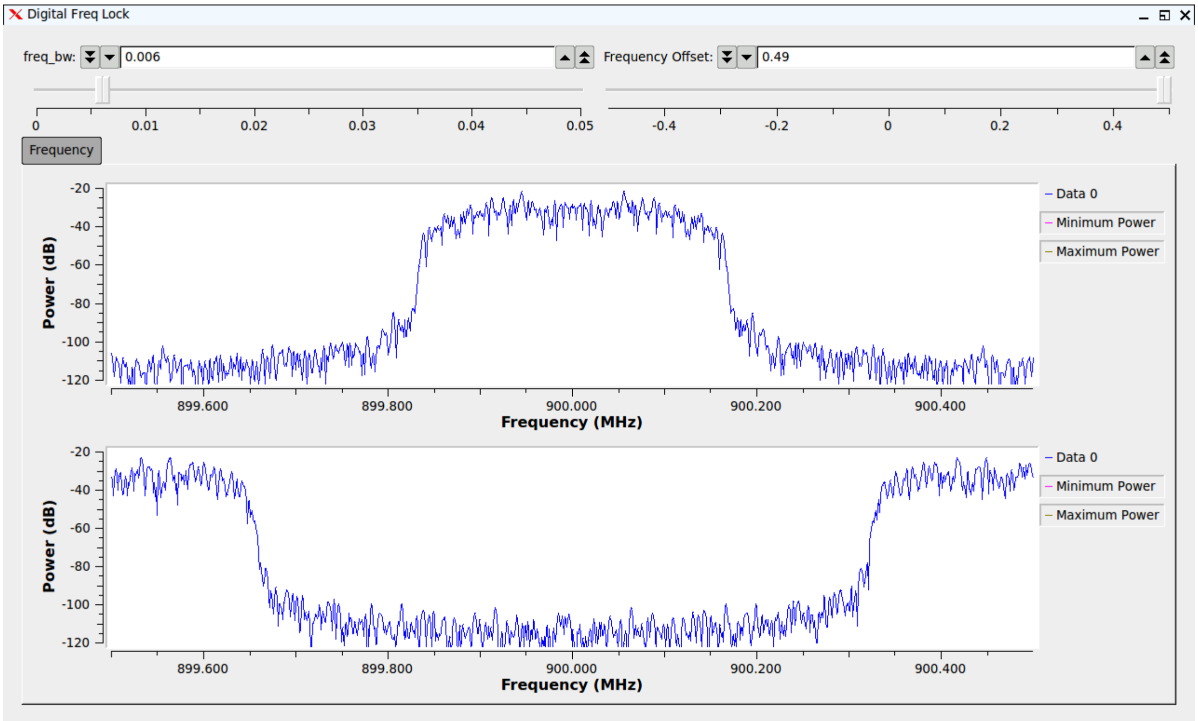

(a) FLL locked to the frequency.

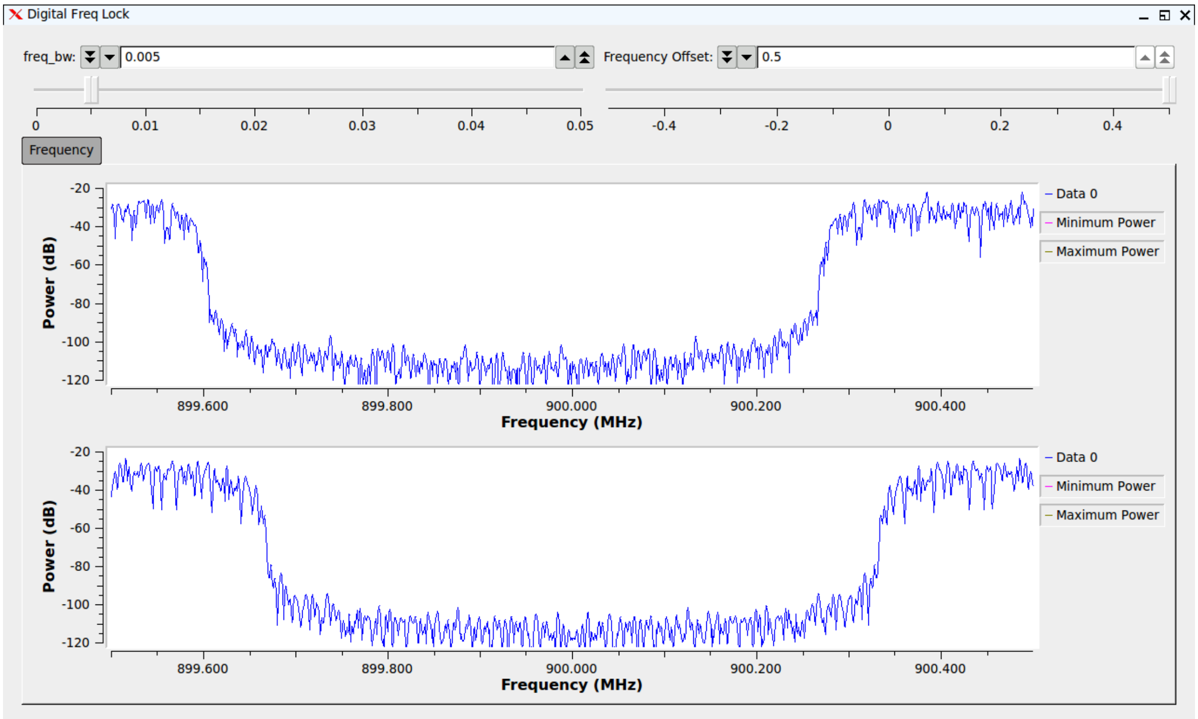

(b) FLL not locked on the frequency.

Fig. 6.22 Operations of GNU Radio FLL.

With the current implementation the OFDM baseband receiver had a requirement of E_b/N_0 of at least 10 dB, for operations without an error correction scheme. Lower requirements can be achieved by further improving the receiver. This chapter does not attempt to build the receiver algorithm, which has been done extensively for reference [255, 256, 208, 276, 253, 262, 277, 257, 264, 265, 267, 269, 268]. One method is to reduce the threshold value used in detecting the occurrence of peak correlation value also known as peak detection in literature. However, this increases the probability of false detection, therefore, the threshold is kept at 0.6, for a normalised correlation coefficient.

For converting to carrier to noise ratio, we can relate the bit energy E_b to carrier power C by the data rate R, occupying bandwidth B using the following relationships [115]:

$$\frac{C}{N} = \frac{E_b}{N_0} \times \frac{R}{B} \tag{6.14}$$

$$\frac{C}{N} = 10\ \log_{10}\left(\frac{E_b}{N_0}\right) + 10\ \log_{10}\left(\frac{R}{B}\right) \quad \text{(dB)} \tag{6.15}$$

When normalised noise power density is used, then the relationship becomes:

$$\frac{C}{N_0} = \frac{E_b}{N_0} \times R \tag{6.16}$$

6.8 Conclusions

This chapter justifies the use of OFDM as a strong candidate amongst the many possible physical layer transmission schemes existent today in terrestrial wireless technologies such as LTE, WiFi and such. Although OFDM has been proposed previously it has not been evaluated and characterised. In this chapter the OFDM design is analysed in the context of communications channel characteristics as perceived in LEO. It is the first study, which incorporates channel fading in inter-satellite links design for the LEO environment. The main novelty of this work is that it considers the coherence time and coherence bandwidth of the communications channel in the OFDM design, which were not taken into account previously and illustrates the deteriorating effects in case if the channel characteristic parameters are not incorporated in the OFDM design. In addition, by presenting the complete design process and demonstrating the effectiveness of the hardware-in-the-loop simulation methods, the first building blocks of an inter-satellite link testbed are proposed. This is a significant contribution to the emerging space based wireless sensor networks comprising pico/nano forms of satellites, and more generally to the area of inter-satellite links design.

CHAPTER 7

CONCLUSION AND FUTURE WORK

In the final chapter, after a summary of research, novel contributions are outlined, and a future research works extending the depth of investigations carried out in this thesis are indicated.

7.1 Summary of Research

Although the concept of wireless sensor networks for space (SBWSN) is appealing and several concurrent developments have enhanced the current state of the art of enabling technologies for SBWSN, but the physical aspects of the communications links between the satellites are generally left out on the grounds that they are considered mission specific. The communications channel characteristics for such ISL, depend on the in-orbit environment, the type of antenna used for ISL, and the operational frequency of the carrier wave. No suitable testing mechanism existed at the time of writing the thesis, which would allow performance evaluation of networking protocols for SBWSN, taking into account the ISL channel impairments caused by the relative motion and the interaction of the propagating waves with the in-orbit environment.

Therefore, based on the proposed ISL evaluation methodology in Chapter 2, a SBWSN testbed was suggested consisting of an environment generator, an orbit propagator, and a channel emulator, whose purpose is to generate impairments for the ISL. It is envisioned that the testbed would operate in the following sequence. First a SBWSN mission scenario would be identified, and the relative motion of the orbiting bodies would be evaluated based on that, then the environment in the identified orbit would be assessed, and the communications channel characteristics would be determined.

In Chapter 3, the SBWSN concept is applied to monitoring the Earth's ionosphere, so as to improve the spatial and temporal resolution of measurements, not possible with current single platform missions. The mission design revolves around the use of low cost mass producible satellite platforms, equipped with a minimal set of identical instruments. The proposed mission scenario aims at deploying a large number of sensor satellites, so that fine scale turbulence could be captured. A mother-daughter sensor satellite configuration is proposed, in which the daughter satellite could be ejected out of the mother satellite, allowing for finer measurements that could provide a considerably better understanding of the dynamics of turbulent plasma. The mission scenario identifies highly possible physical topologies in orbit for ISL.

In Chapter 4 the impact of relative motion on inter-satellite link design is studied with the help of numerical methods projecting the motion of a satellite from initial conditions, under the influence of 20×20 JGM-3 gravitational model, high precision atmospheric model (Harris-Priester), incorporating third body effects and solar radiation pressure. Three cases are investigated to determine the Doppler frequency shift experienced between the two communicating member satellites of a SBWSN: (a) relative motion of free flying CubeSats in LEO deployed at the same altitude, (b) relative motion of a sensor satellite with respect to a relay satellite in different altitudes in LEO and (c) relative motion of a relay satellite with respect to a relay satellite in the same orbit (string of pearl configuration in orbit).

Since the orbits have been selected where the motion of satellites was in the same direction, therefore the Doppler frequency shift observed in the first and third case is tens of Hz. Whereas, in the third case, it is tens of kHz, with high shift rate. Therefore, a third order PLL be used in the first stage of the receiver. Where possible, a second order PLL be also incorporated where nominal Doppler shifts are anticipated. Therefore, a flexible design of PLL is anticipated in SBWSN ISL communications receiver design.

The effects of the LEO environment on the propagation of the electromagnetic waves and the inter-satellite communications channel characteristics are investigated in Chapter 5. The effects are studied separately for interaction with ionised gas, space debris, meteors, and the presence of member satellites in close proximity. It is identified, that the ionised gas causes fading which is not because of multiple paths, but due to rapid changes in the refractive index of ionised gas during turbulent periods. The disturbances have been observed at 1000 km altitude, the same altitude where satellites are to operate. The space debris can be a cause of concern when the carrier frequency is above 10 GHz, because it is of the same size as the wavelength, therefore, it can act as an EM wave scatterer or reflector. The meteors and their trails are a cause of concern as they act as reflectors when SBWSN operates near 300 km altitude. The size of member satellites e.g. 3U CubeSat is again a cause of concern when the carrier wave frequency is about 10 GHz and above.

The communications channel has been found to exhibit dynamic attenuation, showing signs of both fast and slow fading, due to the relative motion of the satellites with respect to the dynamic nature of plasma in ionosphere, as well as due to possible reflectors in the vicinity of communications range. At times fading depth of 20 dB for short spans of time are anticipated, which may lead to communications outage. Therefore, as is generally assumed in literature, inter-satellite communications links using 5 GHz of less carrier waves cannot be modelled as simple free space path loss models, rather, the fading effects both fast and slow must be incorporated in the evaluation of modem design and performance.

Time varying fading channels are easily modelled using Tapped Delay Line (TDL) structure, in which the tap gains and path delays are selected such that the resulting impaired signal, depict the real world communications channel behaviour. TDL is a general structure, it is the determination of number of taps, and the probability function which governs the tap gains, and tap delays, which make it environment specific. In the context of SBWSN, where inter-satellite links are observed as inter-orbit and intra-orbit, the path profile is determined on two extreme cases. Firstly when the satellites are in close proximity of each other and when there are multiple paths due to reflectors in the vicinity. Secondly, for inter-orbit links, where several scatterers or plasma refraction cause a faded signal.

The impact of the waveform channel model on the baseband design using orthogonal frequency division multiplexing (OFDM) is evaluated in Chapter 6. OFDM is one of the physical layers specified for data transmission over wireless links in the IEEE 802.11 b protocol, being considered for use in SBWSN. The modem and channel both are modelled firstly in MATLAB, and the performance of the modem is assessed.

Performance evaluation was carried out not only in the MATLAB simulation environment, but where possible hardware impairments were also included in the design stage. Two hardware in the loop simulations, helped in incorporating issues arising from the actual hardware, which also showed promising results. A Xilinx FPGA supports a configurable FFT core, which makes the module configurable. The second hardware-in-the-loop simulation is based on a GNU Radio interfaced with USRP N210. Over-the-air duplex transmissions were tested. Even one unit was placed on a cart which was moved about the receiver, but no substantial errors observed.

It has been shown that a dedicated OFDM modem needs to be properly designed as per the channel characteristics, otherwise severe degradation is observed in the simulation results. The OFDM timing synchronisation shows robust behaviour, when the OFDM symbol is appropriately designed taking into account the channel coherence time and coherence bandwidth.

Although extensive work has been done during the course of this study, however, owing to the many possibilities arising in physical topologies, which govern the channel characteristics, the channel model presented in this thesis is only applicable for the following conditions:

- when isotropic radiation pattern is being used as is required for using IEEE 802.11 based network protocol,
- when the SBWSN operates in Earth's ionosphere in LEO, for the said physical topologies, when the carrier frequency is less than 5 GHz.

At carrier frequencies above 10 GHz, space debris as well as member satellites in close proximity may act as reflectors or scatterers, so care should be taken to incorporate the multipath effects at such high frequencies, provided isotropic radiation pattern is used.

7.2 Novelty Contribution

The following contributions to the current state-of-the-art have resulted from the research:

1. A novel study has been conducted in which the environment is evaluated for possible fading scenarios either caused by multiple paths or ionised gas scintillation. The following new findings have been established:
   - The communications channel is identified as a time varying “fading channel”, as opposed to the simple free space path loss model commonly used in the literature for ISL.
   - The channel is also found to exhibit multi-path effects at locations in orbit where space debris and meteor trails are present within communications range.

   This is the first work in which channel fading is incorporated in inter-satellite links design for the LEO environment.
2. In addition, for the first time, the performance of inter-satellite links has been evaluated using a fading type channel model. According to the open literature, until now only free space path loss models have been employed and physical layer issues have not been taken into account.
3. By presenting the complete design process and demonstrating the effectiveness of the hardware-in-the-loop simulation methods, the first building blocks of an inter-satellite link testbed are proposed. This is a significant contribution to the emerging space based wireless sensor networks comprising pico/nano satellites, and more generally to the area of communications system design using software defined radio architectures.
4. The OFDM has been justified as a strong candidate amongst the many possible physical layer transmission schemes existent today in terrestrial wireless technologies such as LTE, WiFi and such like. Although OFDM has been proposed previously, it has not been evaluated and characterised. In this thesis the OFDM design is analysed in the context of communications channel characteristics as perceived in LEO.
   - The main novelty of this work is that it considers the coherence time and coherence bandwidth of the communications channel in the OFDM design, which were not taken into account previously and illustrates the deteriorating effects in case if the channel characteristic parameters are not incorporated in the OFDM design.
   - A simple but robust reconfiguration method is proposed, which allows OFDM symbol to meet the changing channel conditions.

7.3 Future Work

This research addresses the multidisciplinary field of inter-satellite communications for SBWSN applications. Although several aspects of ISL have been covered, further work is needed to increase the depth of investigation at various levels.

1. **SBWSN mission scenarios**: Although a mission scenario has been presented in this thesis, however, more elaborate mission scenarios based on the SBWSN concept would improve understanding of the requisite platforms, types of on-board instruments, and possible physical topologies. LEO has been used as a basis for further investigations of inter-satellite channel characteristics, however, in the same manner, investigations should be extended for MEO, GEO, interplanetary space and planetary surface sensor networks.
   - In doing so, a software tool should be developed, in which mission scenarios could be developed with ease, and interfaced to SBWSN testbed.
   - In particular, the impact of tumbling satellites on the measurements taken by DC and AC instruments be studied in depth.
   - A graphical user interface, in which inter-satellite links could be visualised, would greatly assist mission scenario developers and ISL design engineers, for line of sight issues, and out of range estimations. In this regards, SAVI interfaced with GEOMview can be extended, or other third party libraries can be used.
2. **Relative Motion Assessments**: In addition to the polar orbits, non polar orbits should be evaluated in depth for LEO, MEO and GEO type orbits. Configurations like LEO to MEO, MEO to GEO to LEO, and LEO to GEO, be identified, and studied in depth for Doppler frequency shifts and shift rates. In the similar manner, planetary rover motion, inter-planetary orbital configurations can be further investigated.
3. **Controlled Deployment of Pico/Nano satellites**: Since for free flying satellites, the deployment mechanism plays a critical role, it should be studied in depth. A controlled mechanism to deploy several very small satellites in predefined orbits, while being ejected from SHM of a LV is interesting, and would prove to be very useful. The orbits could be predefined, so that the inter-satellite distances could be maintained even in free flight mode.

   The CubeSat deployment mechanism can be further improved to incorporate realistic friction forces, and study the ejection by incorporating uneven pressures on the two legs. A simulation tool, can be developed which could provide forces required to exert, so that a predetermined orbital trajectory is achieved.
4. **Channel Characteristics in LEO**: A simple TDL based channel model has been used in this thesis, which can be further elaborated by using ellipses to mark locations of members in SBWSN. A reverse problem identified during research, is to generate a channel model, which generates the requisite taps and path lengths in accordance to the desired fade depths, and fade duration, and link outages.

   On the same lines, channel characteristics for MEO, GEO and other planetary based orbits be carried out.
5. **MODEM for ISL**: OFDM has been described in detail, however, other MCM modulation schemes and single carrier modulation schemes should also be investigated on the same lines as described in this thesis. In particular energy efficient and continuous envelope modulation schemes be also tested.

6. **Channel Estimator for MODEM**: A robust channel estimation method for the dynamic channel behaviour would allow quick decisions for the onboard controller to change the OFDM modem configuration.
7. **Testbed** : An application interface be developed to pass the channel deterioration effects to network simulators such as NS-2 and NS-3 or any commercial tool of choice.

References

[1] M. N. Sweeting. “The University of Surrey UoSAT-2 spacecraft mission”. In: *Electronic and Radio Engineers, Journal of the Institution of* 57.5 (1987), S99–. ISSN: 0267-1689. DOI: 10.1049/jiere.1987.0077.

[2] Henry Helvajian. *Microengineering Aerospace Systems*. AIAA, 1999.

[3] Tor-Arne Grönland et al. “Miniaturization of components and systems for space using MEMS-technology”. In: *Acta Astronautica* 61.1–6 (2007). Bringing Space Closer to People, Selected Proceedings of the 57th {IAF} Congress, Valencia, Spain, 2-6 October, 2006, pp. 228 –233. ISSN: 0094-5765. DOI: http://dx.doi.org/10.1016/j.actaastro.2007.01.029. URL: http://www.sciencedirect.com/science/article/pii/S0094576507000410.

[4] Elizabeth Howell. *Elon Musk: Private Space Entrepreneur*. http://www.space.com/18849-elon-musk.html. Visited Jan 2017.

[5] Ilya Dashkovsky. *Russia's first private space company set to launch*. http://rbth.com/business/2013/10/19/russias_first_private_space_company_set_to_launch_30969.html. Visited Jan 2017. 2013.

[6] Tanya Vladimirova et al. “Enabling technologies for distributed picosatellite missions in LEO”. In: *Adaptive Hardware and Systems, 2006. AHS 2006. First NASA/ESA Conference on*. IEEE. 2006, pp. 330–337.

[7] Wiley J. Larson and James R. wertz. *Space Mission Analysis and Design*. Kluwer Academic Publisher, 2004.

[8] Tanya Vladimirova et al. “Characterising wireless sensor motes for space applications”. In: *Adaptive Hardware and Systems, 2007. AHS 2007. Second NASA/ESA Conference on*. IEEE. 2007, pp. 43–50.

[9] Loren P. Clare et al. “Space-based multi-hop networking”. In: *Comput. Netw. ISDN Syst.* 47.5 (2005), pp. 701–724. ISSN: 0169-7552. DOI: http://dx.doi.org/10.1016/j.comnet.2004.08.004.

[10] Philippe Dubois et al. “Adhoc wireless sensor networks for exploration of Solar-system bodies”. In: *Acta Astronautica* 64.5-6 (2009), pp. 626 –643. ISSN: 0094-5765. DOI: DOI:10.1016/j.actaastro.2008.11.012. URL: http://www.sciencedirect.com/science/article/B6V1N-4V8FF9T-1/2/0cdbf0b7f11b838c05e808ed99422580.

[11] Tanya Vladimirova et al. “Enabling Technologies for Distributed Picosatellite Missions in LEO”. In: *1st NASA/ESA Conference on Adaptive Hardware and Systems (AHS 2006)*. IEEE Computer Society. 2006, pp. 330–337.

[12] Tanya Vladimirova and Xiaofeng Wu. "On-board partial run-time reconfiguration for pico-satellite constellations". In: *Adaptive Hardware and Systems, 2006. AHS 2006. First NASA/ESA Conference on*. IEEE. 2006, pp. 262–269.

[13] *IEEE standard for Wireless LAN-Medium Access Control and Physical Layer Specification*. 1997.

[14] *IEEE 802.16 Standard for Local and Metropolitan Area Networks; Part16: Air interface for Broadband Wireless Access Systems*. IEEE Computer Society, Microwave Theory, and Techniques Society. 2009.

[15] *Zigbee Alliance*. https://www.zigbee.org/zigbee-for-developers/about-us/.

[16] T. Arslan et al. "ESPACENET: A Framework of Evolvable and Reconfigurable Sensor Networks for Aerospace Based Monitoring and Diagnostics". In: *Adaptive Hardware and Systems, 2006. AHS 2006. First NASA/ESA Conference on*. 2006, pp. 323 –329. DOI: 10.1109/AHS.2006.34.

[17] Richard T Lacoss. *Distributed Sensor Networks*. Tech. rep. ADA070455. Semiannual technical summary no. 3, 1 Apr-30 Sep 1978. Massachusetts Institute of Technology, Lexington Lincoln Lab, 1978.

[18] Brian Engberg, Jeff Ota, and Jason Suchman. "The OPAL Satellite Project: Continuing the Next Generation of Small Satellite Development". In: *Technical Session V*. Proceedings of the AIAA/USU Conference on Small Satellites. 1995.

[19] Koji Nakaya et al. "Titech Cansat Project 2000: Sub-Orbital Flight and Balloon Experiment". In: *The Journal of Space Technology and Science* 16.1 (2000), 1_9–1_18.

[20] C. I. Underwood, G. Richardson, and J. Savignol. "SNAP-I: A Low Cost Modular COTS-Based Nano-Satellite - Design, Construction, Launch and Early Operations Phase". In: *15th Annual AIAA/USU Conference on Small Satellites*. Logan, UT, 2001.

[21] J. Puig-Suari, C. Turner, and W. Ahlgren. "Development of the standard CubeSat deployer and a CubeSat class PicoSatellite". In: *Aerospace Conference, 2001, IEEE Proceedings.* Vol. 1. 2001, pp. 347–353. DOI: 10.1109/AERO.2001.931726.

[22] I. Nason, J. Puig-Suari, and R. Twiggs. "Development of a family of picosatellite deployers based on the CubeSat standard". In: *Aerospace Conference Proceedings, 2002. IEEE*. Vol. 1. 2002, pp. 457–464. DOI: 10.1109/AERO.2002.1036865.

[23] David J. Barnhart et al. "A low-cost femtosatellite to enable distributed space missions". In: *Acta Astronautica* 64.11-12 (2009), pp. 1123 –1143. ISSN: 0094-5765. DOI: DOI:10.1016/j.actaastro.2009.01.025. URL: http://www.sciencedirect.com/science/article/pii/S0094576509000198.

[24] David J Barnhart, Tanya Vladimirova, and Martin N Sweeting. "Very-small-satellite design for distributed space missions". In: *Journal of Spacecraft and Rockets* 44.6 (2007), pp. 1294–1306.

[25] David J Barnhart, Tanya Vladimirova, and Martin Sweeting. *Satellite-On-A-Chip Feasibility for Distributed Space Missions*. Tech. rep. DTIC Document, 2006.

[26] *CubesatKit : A development platform*. Last accessed 2018. Pumpkin Inc. URL: https://www.pumpkinspace.com/.

[27] Planet (previously PlanetLabs). *Monitor Earth, discover trends, deliver insights*. https://www.planet.com/. Last Accessed 2018.

[28] David J Barnhart, Tanya Vladimirova, and Martin Sweeting. "Satellite miniaturization techniques for space sensor networks". In: vol. 46. 2. 2009, pp. 469–472.

[29] R.L. Balthazor et al. “Distributed space-based Ionospheric Multiple Plasma Sensor networks”. In: *Aerospace conference, 2009 IEEE*. 2009, pp. 1–10. DOI: 10.1109/AERO.2009.4839357.

[30] N. Haridas, T. Arslan, and A.T. Erdogan. “Multiband Antenna for Space Based Reconfigurable Satellite Sensor Node”. In: *Wideband, Multiband Antennas and Arrays for Defence or Civil Applications, 2008 Institution of Engineering and Technology Seminar on* (2008), pp. 195 –202. ISSN: 0537-9989.

[31] Kawsu Sidibeh. “Adaptation of the IEEE 802.11 Protocol for Inter-Satellite Links in LEO Satellite Networks”. PhD thesis. University of Surrey, Surrey Space Centre, 2008.

[32] K. Sidibeh and T. Vladimirova. “Application of the IEEE 802.11 Protocol to Inter-Satellite Communications”. In: *International Review of Aerospace Engineering (IREASE)* 1.3 (2008), pp. 316–326.

[33] T. Vladimirova and K. Sidibeh. “WLAN for Earth Observation Satellite Formations in LEO”. In: *Bio-inspired Learning and Intelligent Systems for Security, 2008. BLISS ’08. ECSIS Symposium on*. 2008, pp. 119 –124. DOI: 10.1109/BLISS.2008.11.

[34] L. Kleinrock and F. Tobagi. “Packet Switching in Radio Channels: Part I - Carrier Sense Multiple-Access Modes and Their Throughput-Delay Characteristics”. In: *IEEE Transactions on Communications* 23.12 (1975), pp. 1400–1416. ISSN: 0090-6778. DOI: 10.1109/TCOM.1975.1092768.

[35] Jean Paul. “Communications Platform for Inter-Satellite Links in Distributed Satellite Systems”. PhD thesis. Surrey Space Centre, Faculty of Engineering and Physical Sciences, University of Surrey, UK, 2011.

[36] Xiaofeng Wu and Vladimirova T. “Hardware-in-Loop Simulation of a Satellite Sensor Network for Distributed Space Applications”. In: *Adaptive Hardware and Systems, 2008. AHS ’08. NASA/ESA Conference on*. 2008, pp. 424 –431. DOI: 10.1109/AHS.2008.55.

[37] X. Wu, T. Vladimirova, and K. Sidibeh. “Signal Routing in a Satellite Sensor Network Using Optimisation Algorithms”. In: *2008 IEEE Aerospace Conference*. 2008, pp. 1–9. DOI: 10.1109/AERO.2008.4526330.

[38] *The Network Simulator: NS-2*. Retreived on Feb2010. URL: http://www.isi.edu/nsnam/ns/.

[39] I. Lluch and A. Golkar. “Satellite-to-satellite coverage optimization approach for opportunistic inter-satellite links”. In: *2014 IEEE Aerospace Conference*. 2014, pp. 1–13. DOI: 10.1109/AERO.2014.6836307.

[40] J. Ma and R. Lu. “The Study on RF Inter-Satellite Links”. In: *Wireless Communications, Networking and Mobile Computing (WiCOM), 2011 7th International Conference on*. 2011, pp. 1–4. DOI: 10.1109/wicom.2011.6040269.

[41] W. G. Cowley and M. P. Lavenant. “Analysis of Uncoordinated ISL Networks”. In: *GLOBECOM 2009 - 2009 IEEE Global Telecommunications Conference*. 2009, pp. 1–6. DOI: 10.1109/GLOCOM.2009.5425413.

[42] Marina Ruggieri et al. *The Flower Constellation Set and its Possible Applications*. Final Report. European Space Agency, 2008. URL: "http://www.esa.int/gsp/ACT/doc/ARI/ARI%20Study%20Report/ACT-RPT-MAD-ARI-05-4108-FlowerConstellations-Rome.pdf".

[43] D. Mortari, O. Abdelkhalik, and C. Bruccoleri. “Relative flower Constellations with Applications for Planetary Explorations”. In: *15th AAS/AIAA Space Flight Mechanics Meeting* AAS 05-148 (2005).

[44] A. H. Ballard. “Rosette Constellations of Earth Satellites”. In: *IEEE Transactions on Aerospace and Electronic Systems* AES-16.5 (1980), pp. 656–673. ISSN: 0018-9251. DOI: 10.1109/TAES.1980.308932.

[45] CalPoly. *The Flower Constellation: home page*. http://flowerconstellations.tamu.edu/index.php. Last Visited Jan 2010.

[46] T. Dreischer et al. “Enhanced deep space data return by integrated RF Optical TT&C”. In: *Optical Fiber Communication - includes post deadline papers, 2009. OFC 2009. Conference on* (2009), pp. 1–3.

[47] H. Schweda et al. “Performance demonstration of the on-board active hydrogen maser for the ACES space mission of ESA”. In: *Frequency Control Symposium, 2007 Joint with the 21st European Frequency and Time Forum. IEEE International*. 2007, pp. 1116–1121. DOI: 10.1109/FREQ.2007.4319252.

[48] G.C. Baister and P.V. Gatenby. “Acquisition and Pointing Control for Inter-Satellite Laser Communications”. In: *What’s New in Satellite Communications, IEE Colloquium on* 40.4 (1996).

[49] Christopher Ward et al. “LEO satellite constellation performance analysis”. In: *Military Communications Conference, 1993. MILCOM’93. Conference record. Communications on the Move., IEEE*. Vol. 2. IEEE. 1993, pp. 742–747.

[50] D. Tomren et al. “Optical intersatellite links for the Celestri satellite communications system”. In: *Lasers and Electro-Optics, 1998. CLEO 98. Technical Digest. Summaries of papers presented at the Conference on*. 1998, pp. 347–. DOI: 10.1109/CLEO.1998.676275.

[51] D. W. Dreisewerd et al. “A high data rate LEO to GEO optical crosslink design”. In: *Military Communications Conference, 1992. MILCOM ’92, Conference Record. Communications - Fusing Command, Control and Intelligence., IEEE*. 1992, 1163–1169 vol.3. DOI: 10.1109/MILCOM.1992.244104.

[52] Harald T Friis. “A note on a simple transmission formula”. In: *Proceedings of the IRE* 34.5 (1946), pp. 254–256.

[53] Louis J. Ippolito. *Propagation Effects Handbook for Satellite Systems Design*. Tech. rep. Section 1 Background. Stanford Telecom ACS, 1999.

[54] Chun Loo. “A statistical model for a land mobile satellite link”. In: *IEEE Transactions on Vehicular Technology* 34.3 (1985), pp. 122–127. ISSN: 0018-9545. DOI: 10.1109/T-VT.1985.24048.

[55] P.A. Bello. “Characterization of randomly time variant linear channel”. In: *IEEE Transaction* CS-11(4) (1963), pp. 360–393.

[56] E. J. Fremouw and Akira Ishimaru. “Intensity scintillation index and mean apparent radar cross section on monostatic and bistatic paths”. In: *Radio Science* 27.4 (1992), pp. 539–543. ISSN: 1944-799X. DOI: 10.1029/92RS00293. URL: http://dx.doi.org/10.1029/92RS00293.

[57] EJ Fremouw et al. “Early results from the DNA Wideband satellite experiment—Complex-signal scintillation”. In: *Radio Science* 13.1 (1978), pp. 167–187.

[58] E. J. Fremouw and C. L. Rino. *Modeling of Transionospheric Radio Propagation*. Tech. rep. ARPA Order No. 2777. Stanford Research Institude, USA, 1975.

[59] E. J. Fremouw and H. F. Bates. “Worldwide behavior of average VHF-UHF scintillation”. In: *Radio science* 6.10 (1971), pp. 863–869.

[60] Roger A. Dana and Robert L. Bogusch. *Digital Communications in Fading Channels: Modulation and Codig*. Tech. rep. MRC-R-1043. Mission Research Corp. Santa Barbara, CA., Mar. 1987.

[61] R. L. Bogusch, F. W. Guigliano, and D. L. Knepp. “Frequency-selective scintillation effects and decision feedback equalization in high data-rate satellite links”. In: vol. 71. 6. 1983, pp. 754–767. DOI: 10.1109/PROC.1983.12662.

[62] *NASA CubeSat Initiative*. https://www.nasa.gov/directorates/heo/home/CubeSats_initiative. Last visited Dec 2016.

[63] *ESA CubeSat Technology*. http://m.esa.int/Our_Activities/Space_Engineering_Technology/Technology_CubeSats. Last visited Dec 2016.

[64] M.A. Calabrese et al. “NASA Sun-Earth Connection Program strategic planning and technology requirements (2000-2025)”. In: *Aerospace Conference Proceedings, 2000 IEEE*. Vol. 7. 2000, pp. 329–339. DOI: 10.1109/AERO.2000.879300.

[65] ESA. *Cosmic Vision: Space Science for Europe 2015 - 2025*. ESETEC, PO Box 299, 2200 AG Noordwijk The Netherlands, 2005.

[66] William Tranter et al. *Principles of communication systems simulation with wireless applications*. Prentice Hall Press, 2003.

[67] H. Harada and R. Prasad. *Simulation and Software Radio for Mobile Communications*. Artech House universal personal communications series v. 1. Artech House, 2002. ISBN: 9781580530446. URL: https://books.google.com.pk/books?id=amhNM01OKCUC.

[68] The Mathworks. *The Matrix Laboratory - MATLAB*. http://www.mathworks.co.uk/. ver 2007a. Last retrieved Jan 2010.

[69] *Advanced Design Systems (ADS)*. http://www.keysight.com/en/pc-1297113/advanced-design-system-ads?cc=PK&lc=eng. Formerly Agilent, now Keysight. Last Visited Nov 2016.

[70] ed. Markus Dillinger, Kamiz Madani, and Nancy Alonistioti. *Software Defined Radio: architectures, systems and functions*. Wiley, 2003.

[71] Charles D. Brown. *Elements of Spacecraft Design*. Reston, VA: AIAA Inc., 2002.

[72] *Consultative Committe for Space Data Systems Standards (Blue and Green Books)*. www.ccsds.org. Last Accessed 2016.

[73] *Recommendations for Space Data System Standards, Packet Telemetry (Blue Book)*. http://ccsds.cosmos.ru/publications/. Consultative Committe for Space Data Systems Standards. CCSDS Secreteriat, NASA Washington, DC.

[74] B. Sklar. *Digital Communications: Fundamentals & Applications, 2/E*. Pearson Education, 2009. ISBN: 9788131720929. URL: https://books.google.com.pk/books?id=TuvKdwNMS48C.

[75] John G. Proakis and Masoud Salehi. *Digital communications*. McGraw-Hill, 2008.

[76] Scott Robertson. “Sheaths in laboratory and space plasmas”. In: *Plasma Physics and Controlled Fusion* 55.9 (2013), p. 093001. URL: http://stacks.iop.org/0741-3335/55/i=9/a=093001.

[77] Joseph H Yuen. *Deep space telecommunications systems engineering*. Springer Science & Business Media, 2013.

[78] Barry G. Evans, ed. *Satellite Communication Systems*. Institution of Electrical Engineers, 1999.

[79] Floyd M. Gardner. *Phaselock Techniques*. Second. John Wiley and Sons, 1979.

[80] Marvin K. Simon, ed. *Bandwidth-Efficient Digital Modulation with Application to Deep-Space Communications*. DEEP SPACE COMMUNICATIONS AND NAVIGATION SERIES. NASA / Jet Propulsion Laboratory, 2001.

[81] Paul Muri and Janise McNair. "A Survey of Communication Sub-systems for Intersatellite Linked Systems and CubeSat Missions". In: *Journal of Communications* 7.4 (2012). URL: http://ojs.academypublisher.com/index.php/jcm/article/view/jcm0704290308.

[82] M. A. Bergamo. "Terminal system and capability for ARPA-NASA high-speed SONET/ATM experiments over NASA's Advanced Communications Technology Satellite". In: *Military Communications Conference, 1993. MILCOM '93. Conference record. Communications on the Move., IEEE*. Vol. 1. 1993, 235–241 vol.1. DOI: 10.1109/MILCOM.1993.408514.

[83] T. Dreischer et al. "System concept of an integrated RF-optical transceiver for deep space TT&C". In: *Aerospace Conference, 2004. Proceedings. 2004 IEEE* 3 (2004), 1531 Vol.3. ISSN: 1095-323X. DOI: 10.1109/AERO.2004.1367926.

[84] M. Guelman et al. "Acquisition and Pointing Control for Inter-Satellite Laser Communications". In: *IEEE Trans. on Aerospace and Electronic Systems* 40.4 (2004), pp. 1239 –1248.

[85] Walter Leeb et al. "Optical Terminals for Micro-satellite Swarms". In: *Technical University Wien, Austria* (2001).

[86] M. Sabatini and G.B. Palmerini. "Navigation issues in different baseline formation flying missions". In: *Aerospace conference, 2009 IEEE*. 2009, pp. 1–11. DOI: 10.1109/AERO.2009.4839335.

[87] Eberhard Gill, Simone D' Amico, and Oliver Montenbruck. "Autonomous Formation Flying for the PRISMA Mission". In: *Journal of Spacecraft and Rockets* 44 (2007), pp. 671–681.

[88] NASA. *Overview of the DART Mishap Investigation Results*. Tech. rep. online NASA, retrieved Jan 2010.

[89] *Experimental Spacecraft System (XSS)*. https://directory.eoportal.org/web/eoportal/satellite-missions/v-w-x-y-z/xss. Last Visited Nov 2016.

[90] J. A. C. Kentfield. "Formation Flight and Much More". In: *AIAA Journal* 45.8 (2007).

[91] Jesse Lietner. "Formation Flying System Design for a Planet-Finding Telescope-Occulter System". In: *Proc. of SPIE*. Vol. 6687. San Diego, CA, USA, 2007.

[92] Anne Long et al. *Relative Navigation of Formation-flying Satellites*. 2005.

[93] Balaji. "System design issues of formation flying spacecraft". In: *Aerospace Conference, 2003. Proceedings. 2003 IEEE*. Vol. 6. 2003, pp. 2587–2597.

[94] J. Leitner et al. *Formation Flight in Space Distributed Spacecraft Systems Develop New GPS Capabilities*. Tech. rep. 2. GPS World, 2002, pp. 22–31.

[95] Rich Burns et al. "TechSat 21: formation design, control, and simulation". In: *Aerospace conference proceedings, 2000 IEEE*. Vol. 7. IEEE. 2000, pp. 19–25.

[96] B. S. Sheard et al. "Intersatellite laser ranging instrument for the GRACE follow-on mission". In: *Journal of Geodesy* 86.12 (2012), pp. 1083–1095. ISSN: 1432-1394. DOI: 10.1007/s00190-012-0566-3. URL: http://dx.doi.org/10.1007/s00190-012-0566-3.

[97] J. Leitner. "A hardware-in-the-loop testbed for spacecraft formation flying applications". In: *Aerospace Conference, 2001, IEEE Proceedings.* Vol. 2. 2001, 2/615–2/620 vol.2. DOI: 10.1109/AERO.2001.931240.

[98] P.W.L. van Barneveld, O. Montenbruck, and P.N.A.M. Visser. "Epochwise prediction of GPS single differenced ionospheric delays of formation flying spacecraft". In: *Advances in Space Research* 44.9 (2009), pp. 987 –1001. ISSN: 0273-1177. DOI: DOI:10.1016/j.asr.2009.07.006. URL: http://www.sciencedirect.com/science/article/B6V3S-4WS2J0T-2/2/6c371224eea2806907dd361d250a9052.

[99] Jason W. Mitchell et al. *Development of a radio frequency space environment path emulator for evaluating spacecraft ranging hardware*. Tech. rep. NASA Goddard Space Flight Centre Technical Server, 2007.

[100] C. Long, C. Hunt, and M. Siemon. "Applications for a software programmable space platform". In: *Aerospace Conference, 2003. Proceedings. 2003 IEEE*. Vol. 5. 2003.

[101] C. Hunt et al. "Development of a crosslink channel simulator". In: *Aerospace Conference, 2004. Proceedings. 2004 IEEE*. Vol. 2. 2004, 1322–1328 Vol.2. DOI: 10.1109/AERO.2004.1367730.

[102] Ronald L Ticker and John D Azzolini. *2000 Survey of Distributed Spacecraft Technologies and Architectures for NASA's Earth Science Enterprise in the 2010-2025 Timeframe*. Tech. rep. Goddard Space Flight Center (GSFC), National Aeronautics and Space Administration (NASA), USA., 2000.

[103] C.F. Kwadrat, W.D. Horne, and B.L. Edwards. *Inter-Satellite Communications considerations and requirements for distributed spacecraft and formation flying systems*. Tech. rep. NASA/S-paceOps, 2002.

[104] Thomas E. Moore and et. al. *The Magnetic Constellation (MC), Global Dynamics of the Structured Magnetotail - Updated Synopsis*. Tech. rep. NASA Science and Technology definition team, 2004.

[105] ESA. *Cluster*. http://caa.estec.esa.int/caa/home.xml. Last Visited Jan 2010.

[106] ESA. *ACE*. http://www.esa.int/esaLP/ace.html. Last Visited Sep 2009.

[107] ESA. *SWARM*. http://www.esa.int/esaLP/LPswarm.html. Last Visited Sep 2009.

[108] Y.T. Yoon et al. "TerraSAR-X Precise Trajectory Estimation and Quality Assessment". In: *Geoscience and Remote Sensing, IEEE Transactions on* 47.6 (2009), pp. 1859–1868. ISSN: 0196-2892. DOI: 10.1109/TGRS.2008.2006983.

[109] NASA. *TPF*. http://www.terrestrial-planet-finder.com/. Last Visited Jan 2010.

[110] NASA/ESA. *Lisa*. http://sci.esa.int/science-e/www/object/index.cfm?fobjectid=31421. Last Visited Jan 2010.

[111] Gerhard Krieger. "MIMO-SAR: Opportunities and pitfalls". In: *IEEE Transactions on Geoscience and Remote Sensing* 52.5 (2014), pp. 2628–2645.

[112] NASA. *Solar terrestrial relations observatory (STEREO)*. http://stereo.gsfc.nasa.gov/. Last Visited Jan 2010.

[113] S. Gleason and M. Unwin. "Development and testing of a remote sensing instrument using GNSS reflectometry concepts". In: *Geoscience and Remote Sensing Symposium, 2003. IGARSS '03. Proceedings. 2003 IEEE International*. Vol. 7. 2003, 4332 –4334 vol.7.

[114] *DMC-3 (Disaster Monitoring Constellation-3)*. https://directory.eoportal.org/web/eoportal/satellite-missions/content/-/article/dmc3-2. Last Accessed May 2019.

[115] Maral Gerard, Sun Zhili, and Bousquet Michel. *Satellite communications systems: systems, techniques and technology*. John Wiley, 2009.

[116] K2UBC Martin Davidoff. *The Radio Amateur's Satellite Handbook*. 225 Main Street, Newington, CT 06111: The American Radio Relay League, 2003.

[117] Tanya Vladimirova et al. "Space-based wireless sensor networks: Design issues". In: *Aerospace Conference, 2010 IEEE*. 2010, pp. 1–14. DOI: 10.1109/AERO.2010.5447031.

[118] M. N. Sweeting. "UoSAT - An investigation into cost-effective spacecraft engineering". In: *Radio and Electronic Engineer* 52.8.9 (1982), pp. 363–378. ISSN: 0033-7722. DOI: 10.1049/ree.1982.0054.

[119] Robert Twiggs et al. "OPAL- A first generation microsatellite that provides picosat communications for the amateur radio community". In: *AMSAT-NA Space Symposium, 17 th, and AMSAT-NA Annual Meeting, San Diego, CA*. 1999, pp. 40–47.

[120] Christopher Kitts et al. "Emerald: a low-cost spacecraft mission for validating formation flying technologies". In: *Aerospace Conference, 1999. Proceedings. 1999 IEEE*. Vol. 2. IEEE. 1999, pp. 217–226.

[121] R. J. Twiggs. "A Cubesat: A new generation of picosatellite for education and industry low-cost space experimentation". In: *Proceedings of the 14th Annual AIAA/USU Conference on Small Satellites* (2000). URL: www.scopus.com.

[122] C.I. Underwood et al. "Using PALMSAT Pico-Satellite Technologies to Meet Mission Scenarios". In: *55th International Astronautical Congress*. 2004.

[123] D. J. Barnhart, T. Vladimirova, and M. N. Sweeting. "Design of self-powered wireless system-on-a-chip sensor nodes for hostile environments". In: *Circuits and Systems, 2008. ISCAS 2008. IEEE International Symposium on*. 2008, pp. 824–827. DOI: 10.1109/ISCAS.2008.4541545.

[124] Univ of Tokyo. *Xi-IV CubeSat*. http://www.space.t.u-tokyo.ac.jp/cubesat/index-e.html. Last Visited Sep 2016.

[125] Peter Fortescue, Graham Swinerd, and John Stark, eds. *Spacecraft Systems Engineering*. 4th. John Wiley & Sons, Ltd, Publications, 2011.

[126] *DARPA seeks high speed ISL technology*. http://www.networkworld.com/article/2934437/wireless/darpa-seeks-high-speed-inter-satellite-communication-technology.html. Visited Jan 2017.

[127] H. Zimmermann. "OSI Reference Model - The ISO Model of Architecture for Open Systems Interconnection". In: *IEEE Transactions on Communications* 28.4 (1980), pp. 425–432. ISSN: 0090-6778. DOI: 10.1109/TCOM.1980.1094702.

[128] *IEEE Standard for Information Technology, Telecommunications and information exchange systems, Local and metropolitan area networks, Specific Requirements: PART11: Wireless LAN Medium Access Control (MAC) and Physical Layer (PHY) Specifications*. IEEE Computer Society. 2007.

[129] Eustathia Ziouva and Theodore Antonakopoulos. "CSMA/CA performance under high traffic conditions: throughput and delay analysis". In: *Computer communications* 25.3 (2002), pp. 313–321.

[130] Hiromi Okada, Yoshifumi Nomura, and Yoshiro Nakanishi. “Multi-channel CSMA/CD method in broadband-bus local area networks”. In: *Proc. of IEEE GLOBECOM*. Vol. 84. 1984.

[131] Paul Muri. “DELAY TOLERANT NETWORKING FOR CUBESAT TOPOLOGIES AND PLATFORMS”. PhD thesis. The Graduate School, University of Florida, USA., 2013.

[132] Gyanappa A. Walikar and Rajashekar C. Biradar. “A survey on hybrid routing mechanisms in mobile ad hoc networks”. In: *Journal of Network and Computer Applications* 77 (2017), pp. 48 –63. ISSN: 1084-8045. DOI: http://dx.doi.org/10.1016/j.jnca.2016.10.014. URL: http://www.sciencedirect.com/science/article/pii/S1084804516302430.

[133] Amit Sarkar and T. Senthil Murugan. “Routing protocols for wireless sensor networks: What the literature says?” In: *Alexandria Engineering Journal* 55.4 (2016), pp. 3173 –3183. ISSN: 1110-0168. DOI: http://dx.doi.org/10.1016/j.aej.2016.08.003. URL: http://www.sciencedirect.com/science/article/pii/S1110016816302125.

[134] Kathleen Mary Stafford. “Characterization of blue whale calls from the Northeast Pacific and development of a matched filter to locate blue whales on the US Navy SOSUS (Sound Surveillance System) arrays”. MA thesis. Oregon State University, Graduate School, 1995.

[135] V. Potdar, A. Sharif, and E. Chang. “Wireless Sensor Networks: A Survey”. In: *Advanced Information Networking and Applications Workshops, 2009. WAINA ’09. International Conference on*. 2009, pp. 636–641. DOI: 10.1109/WAINA.2009.192.

[136] T. Vladimirova and M. N. Sweeting. “System-on-a-Chip Development for Small Satellite Onboard Data Handling”. In: *Journal of Aerospace Computing, Information and Communication, AIAA* (2004).

[137] Grant Bonin et al. “CanX–4 and CanX–5 Precision Formation Flight: Mission Accomplished”. In: *29th Annual AIAA / USU Conference on Small Satellites*. AIAA/USU. 2015.

[138] J. Costantine, Y. Tawk, and C. G. Christodoulou. “Deployable antenna concepts for CubeSats”. In: *2016 IEEE International Symposium on Antennas and Propagation (APSURSI)*. 2016, pp. 1541–1542. DOI: 10.1109/APS.2016.7696477.

[139] K. Sidibeh and T. Vladimirova. “The Effect of Angular Velocity on Inter-Satellite Links in LEO Satellite Networks”. In: *International Review of Aerospace Engineering (IREASE)* 1.2 (2008), pp. 181–186.

[140] Jian-Hao Hu, K. L. Yeung, and Tao Li. “Routing and re-routing in a LEO/MEO two-tier mobile satellite communications system with inter-satellite links”. In: *Communications, 2000. ICC 2000. 2000 IEEE International Conference on*. Vol. 1. 2000, 134–138 vol.1. DOI: 10.1109/ICC.2000.853079.

[141] L. Wood et al. “Taking Saratoga from space-based ground sensors to ground-based space sensors”. In: *2011 Aerospace Conference*. 2011, pp. 1–8. DOI: 10.1109/AERO.2011.5747332.

[142] John Gerard Walker. *Circular orbit patterns providing continuous whole earth coverage*. Tech. rep. ROYAL AIRCRAFT ESTABLISHMENT FARNBOROUGH (UNITED KINGDOM), 1970.

[143] John G Walker. *Continuous whole-earth coverage by circular-orbit satellite patterns*. Tech. rep. ROYAL AIRCRAFT ESTABLISHMENT FARNBOROUGH (UNITED KINGDOM), 1977.

[144] T. Henderson and d. Mortari. “Uni-flower: A novel proposal for university -Built Nanosatellites in Flower constellations”. In: *2006 AAS space Flight Mechanics Meeting Conference* AAS 06-204 (2006).

[145] Richard W. Middlestead, Robert E. LeLevier, and Mitchell D. Smith. “Satellite crosslink communications vulnerability in a nuclear environment”. In: *IEEE journal on selected areas in communications* 5.2 (1987), pp. 138–145.

[146] Qinglong Yang, Liying Tan, and Jing Ma. “Doppler characterization of laser inter-satellite links for optical LEO satellite constellations”. In: *Optics Communications* 282.17 (2009), pp. 3547 –3552. ISSN: 0030-4018. DOI: https://doi.org/10.1016/j.optcom.2009.05.058. URL: http://www.sciencedirect.com/science/article/pii/S0030401809004921.

[147] T. Vladimirova, X. Wu, and C. P. Bridges. “Development of a Satellite Sensor Network for Future Space Missions”. In: *2008 IEEE Aerospace Conference*. 2008, pp. 1–10. DOI: 10.1109/AERO.2008.4526248.

[148] R.S. Lawrence, C.G. Little, and H.J.A. Chivers. “A survey of ionospheric effects upon earth-space radio propagation”. In: *Proceedings of the IEEE* 52.1 (1964), pp. 4 –27. ISSN: 0018-9219.

[149] NiCT. *Ionospheric Working Group, Space Environment Laboratory, Applied Electromagnetic Research Institute, National Institute of Information and Communications Technology*. http://wdc.nict.go.jp/IONO/index_E.html. Last Visited Sep 2016.

[150] Kenneth Davies. *Ionospheric Radio*. London, UK.: The Institution of Engineering and Technology, 1990, Reprint 2008.

[151] Michael Finneran. *Thousand-fold Rise in Polar Flights Hikes Radiation Risk*. http://www.nasa.gov/centers/langley/science/polar-radiation.html. Last Visited 2016. 2016.

[152] Ljiljana R. Cander. “Ionospheric research and space weather services”. In: *Journal of Atmospheric and Solar-Terrestrial Physics* 70.15 (2008), pp. 1870 –1878. ISSN: 1364-6826. DOI: http://dx.doi.org/10.1016/j.jastp.2008.05.010. URL: http://www.sciencedirect.com/science/article/pii/S1364682608001326.

[153] Robert W. Schunk and Andrew F. Nagy. *Ionospheres; Physics, Plasma Physics and Chemistry*. Ed. by M.J. Roycroft J.T. Houghton and A.J. Dessler. 2nd. Cambridge Atmospheric and Space Science Series. Cambridge University Press, 2009.

[154] V. Korepanov et al. “IONOSAT – Ionospheric satellite cluster”. In: *Advances in Space Research* 42.9 (2008), pp. 1515 –1522. ISSN: 0273-1177. DOI: http://dx.doi.org/10.1016/j.asr.2008.02.022. URL: http://www.sciencedirect.com/science/article/pii/S0273117708001154.

[155] J.-P. Lebreton et al. “The ISL Langmuir probe experiment processing onboard DEMETER: Scientific objectives, description and first results”. In: *Planetary and Space Science* 54.5 (2006). First Results of the {DEMETER} Micro-Satellite, pp. 472 –486. ISSN: 0032-0633. DOI: http://dx.doi.org/10.1016/j.pss.2005.10.017. URL: http://www.sciencedirect.com/science/article/pii/S0032063305002084.

[156] David T. Young. “Space Plasma Particle Instrumentation and the New Paradigm: Faster, Cheaper, Better”. In: *Measurement Techniques in Space Plasmas:Particles*. American Geophysical Union, 2013, pp. 1–16. ISBN: 9781118664384. DOI: 10.1029/GM102p0001. URL: http://dx.doi.org/10.1029/GM102p0001.

[157] A. Belehaki, I. Stanislawska, and J. Lilensten. “An overview of Ionosphere—Thermosphere Models available for space weather purposes”. In: *Space Science Reviews* 147 (3 2009). 10.1007/s11214-009-9510-0, pp. 271–313. ISSN: 0038-6308. URL: http://dx.doi.org/10.1007/s11214-009-9510-0.

[158] A. Dalgarno et al. “The Atmosphere Explorer mission”. In: *Radio Science* 8.4 (1973), pp. 263–266. ISSN: 1944-799X. DOI: 10.1029/RS008i004p00263. URL: http://dx.doi.org/10.1029/RS008i004p00263.

[159] Herbert J. Kramer. *Observation of the Earth and Its Environment. Survey of Missions and Sensors*. Springer, 2002.

[160] Herbert O. Funsten and David J. McComas. “Limited Resource Plasma Analyzers: Miniaturization Concepts”. In: *Measurement Techniques in Space Plasmas:Particles*. American Geophysical Union, 2013, pp. 157–167. ISBN: 9781118664384. DOI: 10.1029/GM102p0157. URL: http://dx.doi.org/10.1029/GM102p0157.

[161] André Balogh. “Space Physics Instrumentation and Missions”. In: *Payload and Mission Definition in Space Sciences*. Ed. by V. Martínez Pillet, A. Aparicio, and F. Sánchez. Cambridge University Press, 2005.

[162] Tanya Vladimirova, Xiaofeng Wu, and Christopher P Bridges. “Development of a satellite sensor network for future space missions”. In: *Aerospace Conference, 2008 IEEE*. IEEE. 2008, pp. 1–10.

[163] CI Meng and PT Newell. *Investigations of Magnetosphere-Ionosphere Coupling Relevant to Operational Systems.* Tech. rep. JOHNS HOPKINS UNIV LAUREL MD APPLIED PHYSICS LAB, 1988.

[164] J. W. Ward. “Microsatellites for global electronic mail networks”. In: *Electronics Communication Engineering Journal* 3.6 (1991), pp. 267–272. ISSN: 0954-0695. DOI: 10.1049/ecej:19910044.

[165] *ProductBrief: HMR / HMC 2300 Magnetic Sensor Overview*. Last Visited Sep 2016. Solid State Electronics Center, Honeywell Inc.

[166] Larry H. Brace. “Langmuir Probe Measurements in the Ionosphere”. In: *Measurement Techniques in Space Plasmas:Particles*. American Geophysical Union, 2013, pp. 23–35. ISBN: 9781118664384. DOI: 10.1029/GM102p0023. URL: http://dx.doi.org/10.1029/GM102p0023.

[167] II Albarran and M Robert. “Cubesat Wakes in the Earth’s Ionosphere”. MA thesis. Embry-Riddle Aeronautical University - Daytona Beach, 2015. URL: https://commons.erau.edu/edt/57.

[168] Riki Munakata. *CubeSat Design Specifications v.11*. Tech. rep. California Polytechnic State University, 2008. URL: http://www.cubesat.org/images/developers/cds_rev11.pdf.

[169] Huang Xiangyu, Cui Hutao, and Cui Pingyuan. “An Autonomous optical navigation and guidance for soft landing on asteroids”. In: *Acta Astronautica* 54 (2004), pp. 763–771.

[170] Josef Sofka et al. “LASER Communications between Mobile Platforms”. In: *IEEE Trans. on Aerospace and Electronic Systems* 45.1 (2009), pp. 336 –346.

[171] T. Vladimirova et al. “First Draft of Preliminary Design Review Document for S-Cube”. VLSI Group in Surrey Space Center, University of Surrey, UK. 2009.

[172] *DataSheet: MAX2830, an integrated 2.4GHz CMOS transceiver and power amplifier*. Maxim Integrated Products, Inc. 2009.

[173] Constantine A Balanis. *Antenna theory: analysis and design*. John wiley & sons, 2016.

[174] Sophocles J. Orfanidis. *Electromagnetic Waves and Antennas*. http://eceweb1.rutgers.edu/~orfanidi/ewa/. 2016.

[175] David A. Vallado. *Fundamentals of Astrodynamics and Applications*. Kluwer Academic Publisher, 2004.

[176] Oliver Montenbruck and Eberhard Gill. *Satellite Orbits Models Methods and Applications*. 3rd. Springer, 2005.

[177] Franz T. Geyling and H. Robert Westerman. *Introduction to Orbital Mechanics*. Addison-Wesley, 1971.

[178] Jules Aarons. "Global morphology of ionospheric scintillations". In: *Proceedings of the IEEE* 70.4 (1982), pp. 360–378.

[179] Robert Thurman Lloyd Wood P. Worfolk. *Satellite Constellation Visualization software from the The Geometry Center*. 2016. URL: "http://savi.sf.net/","http://www.geom.uiuc.edu/~worfolk/SaVi/".

[180] Todd E Humphreys et al. "Simulating ionosphere-induced scintillation for testing GPS receiver phase tracking loops". In: *IEEE Journal of Selected Topics in Signal Processing* 3.4 (2009), pp. 707–715.

[181] David C. Miller and Joseph Gibbs. *Ionospheric Modelling and Propagation Analysis*. Tech. rep. RADC-TR- 78-163. ARGON Corporation, 1978.

[182] ISC Kosmotras. *Space Launch Systems DNEPR: User Guide*. ISC Kosmotras. 2001. URL: http://www.kosmotras.ru.

[183] ISC Kosmotras. visited:Dec 2015. 2015. URL: http://www.kosmotras.ru/img/resources/Leaflet_Dnepr_2012_part_2_ENG.jpg.

[184] Nathan Blaunstein and Eugeniu Plohotniuc. *Ionosphere and Applied Aspects of Radio Communication and RADAR*. CRC Press, 2008.

[185] John A Klobuchar. *Ionospheric effects on Earth-space propagation*. Tech. rep. AIR FORCE GEOPHYSICS LAB HANSCOM AFB MA, 1983.

[186] Lionel Loudet. *Sudden Ionospheric Distrubances Monitoring Station*. visited Mar 2016. URL: http://www.sidstation.loudet.org/ionosphere-en.xhtml.

[187] Yuji Sakamoto et al. "Development of low cost micro tethered satellite system". In: *23rd international symposium on space technology and science, Matsue, Japan*. Vol. 26. 1998.

[188] Giulio Avanzini and Manrico Fedi. "Refined dynamical analysis of multi-tethered satellite formations". In: *Acta Astronautica* 84 (2013), pp. 36 –48. ISSN: 0094-5765. DOI: https://doi.org/10.1016/j.actaastro.2012.10.031. URL: http://www.sciencedirect.com/science/article/pii/S0094576512004092.

[189] RS Nerem et al. "Gravity model development for TOPEX/POSEIDON: Joint Gravity Models 1 and 2". In: *Journal of Geophysical Research: Oceans* 99.C12 (1994), pp. 24421–24447.

[190] Bø D Tapley et al. "The joint gravity model 3". In: *Journal of Geophysical Research: Solid Earth* 101.B12 (1996), pp. 28029–28049.

[191] FG Lemoine et al. "The development of the NASA GSFC and NIMA joint geopotential model". In: *Gravity, geoid and marine geodesy*. Springer, 1997, pp. 461–469.

[192] Luigi Giuseppe Jacchia. "Revised static models of the thermosphere and exosphere with empirical temperature profiles". In: *SAO special report* 332 (1971).

[193] Luigi Giuseppe Jacchia. “Thermospheric temperature, density, and composition: New models”. In: *SAO special report* 375 (1977).

[194] Luigi G Jacchia and Jack W Slowey. *Analysis of Data for the Development of Density and Composition Models of the Upper Atmosphere.* Tech. rep. SMITHSONIAN ASTROPHYSICAL OBSERVATORY CAMBRIDGE MA, 1981.

[195] G. W. Hill. “Researches in Lunar theory”. In: *American Journal of Mathematics* (1878), pp. 5 –26.

[196] D. F. Lawden. “Fundamentals of space navigation”. In: *Journal of the british interplanetary society* 13.2 (1954), pp. 87–101.

[197] Yoshikazu Hashida and Philip L Palmer. “Epicyclic motion of satellites under rotating potential”. In: *Journal of Guidance, Control, and Dynamics* 25.3 (2002), pp. 571–581.

[198] Alvaro Gimeńez. “The life cycle of an ESA science mission and how to get involved”. In: *Payload and Mission Definition in Space Sciences*. Ed. by V. Martinez Pillet, A. Aparicio, and F. Sanchez. Cambridge University Press, 2005. Chap. 1.

[199] DNEPR. *Allocation of P-PODA on DNEPR*. Tech. rep. Cubesat.org, Calpoly USA, 2009. URL: http://cubesat.atl.calpoly.edu/media/Website\%20Images/D2\%20P-POD\%20A\%20Allocation.bmp.

[200] William E. Boyce and Richard C. DiPrima. *Elementary Differential Equations and Boundary Value Problems*. 9^{th}. John Wiley & sons, Inc., 2010.

[201] Boris V. Raushenbakh, Michael Yu. Ovchinnikov, and Susan Mckenna-Lawlor. *Essential Spaceflight Dynamics and Magnetospherics*. Microcosm Press and Kluwer Academic Press, 2003.

[202] Rolan E. Best. *Phase-Locked Loops, Design Simulation and Applications*. McGraw-Hill, 1999.

[203] Adel AM Saleh. “Frequency-independent and frequency-dependent nonlinear models of TWT amplifiers”. In: *IEEE Transactions on communications* 29.11 (1981), pp. 1715–1720.

[204] Rodger E. Ziemer and Roger L. Peterson. *Introduction to Digital Communications*. Macmillan Publishing Company, 1992.

[205] William C Jakes and Donald C Cox. *Microwave mobile communications*. Wiley-IEEE Press, 1994.

[206] Albert D. Wheelon. *Electromagnetic Scintillation, I. Geometrical Optics*. Second. Cambridge University Press, 2004.

[207] Albert D. Wheelon. *Electromagnetic Scintillation, II. Weak Scattering*. First. Cambridge University Press, 2003.

[208] Marc Engels. *Wireless OFDM Systems: how to make them work?* Kluwer, 2002.

[209] Heinrich Meyr, Marc Moeneclaey, and Stefan A. Fechtel. *Digital Communication Receivers: Synchronization, Channel Estimation, and Signal Processing*. John Wiley & Sons, Inc., 2001. ISBN: 9780471200574.

[210] B. Sklar. “Rayleigh fading channels in mobile digital communication system Part-I:Characterization”. In: *IEEE Communications Magazine* 35.7 (1997), pp. 90–100. ISSN: 0163-6804. DOI: 10.1109/35.601747.

[211] B. Sklar. “Rayleigh Fading Channels in Mobile Digital Communication Systems Part II: Mitigation”. In: *IEEE Communications Magazine* 35.9 (1997), pp. 148–155. ISSN: 0163-6804. DOI: 10.1109/MCOM.1997.621038.

[212] K. G. Budden. *The Propagation of radio waves: the theory of radio waves of low power in the ionosphere and magnetosphere*. Cambridge University Press, 1985.

[213] J. A. Ratcliffe. *The Magneto-ionic Theory and its Appplications to Ionosphere*. Cambridge Univeristy Press, 1959.

[214] Rodney Vaughan and Jorgen Bach Andersen. *Channels, Propagation and Antennas for Mobile Communication*. 1st. Institute of Engineering and Technology UK, 2003.

[215] Ray E. Sheriff and Y. Fun Hu. *Mobile satellite communication networks*. Wiley, 2001.

[216] K. G. Budden. *Lectures on Magnetoionic Theory*. Gordon and Breach, Science Publishers, 1964.

[217] Louis J. Ippolito. *Propagation Effects Handbook for Satellite Systems Design*. Tech. rep. Section 2 Prediction. Stanford Telecom ACS, 1999.

[218] Louis J. Ippolito. *Propagation Effects Handbook for Satellite Systems Design*. Tech. rep. Section 3 Applications. Stanford Telecom ACS, 1999.

[219] J. E. Allnut. *Satellite to ground radio wave propagation*. IEE, 1989.

[220] Gregory D Durgin, Theodore S Rappaport, and David A De Wolf. “New analytical models and probability density functions for fading in wireless communications”. In: *IEEE Transactions on Communications* 50.6 (2002), pp. 1005–1015.

[221] Matthias Patzold and Neji Youssef. “Modelling and Simulation of Direction-Selective and Frequency-Selective Mobile Radio Channels”. In: *AEU - International Journal of Electronics and Communications* 55.6 (2001), pp. 433 –442. ISSN: 1434-8411. DOI: 10.1078/1434-8411-54100064. URL: http://www.sciencedirect.com/science/article/pii/S1434841104700540.

[222] G. Dyer et al. “Mobile propagation measurements using CW and sliding correlator techniques”. In: *IEEE Antennas and Propagation Society International Symposium. 1998 Digest. Antennas: Gateways to the Global Network. Held in conjunction with: USNC/URSI National Radio Science Meeting (Cat. No.98CH36*. Vol. 4. 1998, pp. 1896–1899. DOI: 10.1109/APS.1998.701574.

[223] R. A. Ziegler and J. M. Cioffi. “Estimation of time-varying digital radio channels”. In: *IEEE Transactions on Vehicular Technology* 41.2 (1992), pp. 134–151. ISSN: 0018-9545. DOI: 10.1109/25.142772.

[224] F. Davarian. “Channel Simulation to Facilitate Mobile-Satellite Communications Research”. In: *IEEE Transactions on Communications* 35.1 (1987), pp. 47–56. ISSN: 0090-6778. DOI: 10.1109/TCOM.1987.1096663.

[225] E. Casas and C. Leung. “Performance of an OFDM/FM scheme for data transmission over fading mobile radio channels”. In: *Vehicular Technology Conference, 1986. 36th IEEE*. Vol. 36. 1986, pp. 103 –108.

[226] L. Mason. “Error Probability Evaluation for Systems Employing Differential Detection in a Rician Fast Fading Environment and Gaussian Noise”. In: *IEEE Transactions on Communications* 35.1 (1987), pp. 39–46. ISSN: 0090-6778. DOI: 10.1109/TCOM.1987.1096662.

[227] G.L. Stüber. *Principles of Mobile Communication*. Springer US, 2000. ISBN: 9780792379980. URL: https://books.google.com.pk/books?id=65_fF83bja0C.

[228] D. R. Hummels and F. W. Ratcliffe. “Calculation of error probability for MSK and OQPSK systems operating in a fading multipath environment”. In: *IEEE Transactions on Vehicular Technology* 30.3 (1981), pp. 112–120. ISSN: 0018-9545. DOI: 10.1109/T-VT.1981.23891.

[229] P. Bello. “Aeronautical Channel Characterization”. In: *IEEE Transactions on Communications* 21.5 (1973), pp. 548–563. ISSN: 0090-6778. DOI: 10.1109/TCOM.1973.1091707.

[230] Y. Miyagaki, N. Morinaga, and T. Namekawa. “Double Symbol Error Rates of M-ary DPSK in a Satellite-Aircraft Multipath Channel”. In: *IEEE Transactions on Communications* 31.12 (1983), pp. 1285–1289. ISSN: 0090-6778. DOI: 10.1109/TCOM.1983.1095775.

[231] P. Bello and B. Nelin. “The Influence of Fading Spectrum on the Binary Error Probabilites of Incoherent and Differentially Coherent Matched Filter Recievers”. In: *IRE Transactions on Communications Systems* 10.2 (1962), pp. 160–168. ISSN: 0096-2244. DOI: 10.1109/TCOM.1962.1088654.

[232] H. Salwen. “Differential Phase-Shift Keying Performance Under Time-Selective Multipath Fading”. In: *IEEE Transactions on Communications* 23.3 (1975), pp. 383–385. ISSN: 0090-6778. DOI: 10.1109/TCOM.1975.1092797.

[233] *Recommendation ITU-R P.531-10; Ionospheric Propagation data and prediction methods required for the design of satellite services and systems*. ITU-R. 2009. URL: http://www.itu.int/en/ITU-R/pages/default.aspx.

[234] Alison de Oliveira Moraes et al. “Extended ionospheric amplitude scintillation model for GPS receivers”. In: *Radio Science* 49.5 (2014). 2013RS005307, pp. 315–329. ISSN: 1944-799X. DOI: 10.1002/2013RS005307. URL: http://dx.doi.org/10.1002/2013RS005307.

[235] Jer-Chyi Liou et al. *The New NASA Orbital Debris engineering Model ORDEM2000*. NASA. 2002.

[236] Vincent L. Pisacane. “The Space Environment and its effects on Space Systems”. In: AIAA, 2008. Chap. 11, pp. 319–343.

[237] Donald L Schilling, ed. *Meteor Burst Communications: Theory and Practice*. Wiley-Interscience, 1993.

[238] Kenneth Davies. *Ionopheric Radio Propagation*. Vol. National Bureau of Standards Monograph 80. US Government Printing Office, 1965.

[239] David D. Meisel. “Meteor”. In: *AccessScience* (2014).

[240] Noah Brosch et al. “Unusual features in high statistics radar meteor studies at EISCAT”. In: *Monthly Notices of the Royal Astronomical Society* 401.2 (2010), pp. 1069–1079.

[241] J. Hant, V. Lin, and P. Anderson. “Verification of satellite-channel simulators with scintillation, terrestrial multipath, and shadowing effects”. In: vol. 2005. cited By 0. 2005. DOI: 10.1109/AERO.2005.1559468. URL: https://www.scopus.com/inward/record.uri?eid=2-s2.0-33751541726&doi=10.1109%2fAERO.2005.1559468&partnerID=40&md5=ba1d15674b86677afc35e6d4426c536b.

[242] Alison Oliveira Moraes et al. “Extended ionospheric amplitude scintillation model for GPS receivers”. In: *Radio Science* 49.5 (2014), pp. 315–329.

[243] Paul S. Cannon et al. "Signal distortion on VHF/UHF transionospheric paths: First results from the Wideband Ionospheric Distortion Experiment". In: *Radio Science* 41.5 (2006). RS5S40, n/a–n/a. ISSN: 1944-799X. DOI: 10.1029/2005RS003369. URL: http://dx.doi.org/10.1029/2005RS003369.

[244] KC Yeh and GW Swenson. "F-region irregularities studied by scintillation of signals from satellites". In: *Radio Sci. D* 68 (1964), p. 881.

[245] Nikolay Kostov. "Mobile Radio Channels Modeling in MATLAB". In: *Radioengineering* (2003).

[246] M.F. Pop and N.C. Beaulieu. "Design of wide-sense stationary sum-of-sinusoids fading channel simulators". In: *Communications, 2002. ICC 2002. IEEE International Conference on*. Vol. 2. 2002, 709 –716 vol.2. DOI: 10.1109/ICC.2002.996948.

[247] Michel C. Jeruchim, Philip Balaban, and K. Sam Shanmugan. *Simulation of Communication Systems*. Second. Kluwer Academic Publishers, 2002.

[248] R. W. Chang. "Synthesis of band-limited orthogonal signals for multichannel data transmission". In: *The Bell System Technical Journal* 45.10 (1966), pp. 1775–1796. ISSN: 0005-8580. DOI: 10.1002/j.1538-7305.1966.tb02435.x.

[249] R. Chang and R. Gibby. "A Theoretical Study of Performance of an Orthogonal Multiplexing Data Transmission Scheme". In: *IEEE Transactions on Communication Technology* 16.4 (1968), pp. 529–540. ISSN: 0018-9332. DOI: 10.1109/TCOM.1968.1089889.

[250] John M. Cioffi. *A Multicarrier Primer*. Tech. rep. 91-157. ANSI T1E1.4 Committee Contribution, 1991.

[251] Steven M. Kay. *Fundamentals of Statistical Signal Processing, Volume I: Estimation Theory*. Prentice Hall Signal Processing Series. Prentice Hall, 1993.

[252] Steven M. Kay. *Fundamentals of Statistical Signal Processing, Volume II: Detection Theory*. Prentice Hall Signal Processing Series. Upper Saddle River, New Jersey 07458: Prentice Hall, 1998.

[253] J.-J. van de Beek et al. "A time and frequency synchronization scheme for multiuser OFDM". In: *Selected Areas in Communications, IEEE Journal on* 17.11 (1999), pp. 1900 –1914. ISSN: 0733-8716. DOI: 10.1109/49.806820.

[254] A. Troya et al. "Efficient Inner Receiver Design for OFDM-Based WLAN Systems: Algorithm and Architecture". In: *Wireless Communications, IEEE Transactions on* 6.4 (2007), pp. 1374 –1385. ISSN: 1536-1276. DOI: 10.1109/TWC.2007.348334.

[255] A. Troya et al. "Low-Power VLSI Implementation of the Inner Receiver for OFDM-Based WLAN Systems". In: *Circuits and Systems I: Regular Papers, IEEE Transactions on* 55.2 (2008), pp. 672 –686. ISSN: 1549-8328. DOI: 10.1109/TCSI.2007.913732.

[256] Y. Mostofi and D.C. Cox. "Robust timing synchronization design in OFDM systems - Part II: high-mobility cases". In: *Wireless Communications, IEEE Transactions on* 6.12 (2007), pp. 4340 –4348. ISSN: 1536-1276. DOI: 10.1109/TWC.2007.05901.

[257] T.M. Schmidl and D.C. Cox. "Robust frequency and timing synchronization for OFDM". In: *Communications, IEEE Transactions on* 45.12 (1997), pp. 1613 –1621. ISSN: 0090-6778. DOI: 10.1109/26.650240.

[258] S.C. Thompson, J.G. Proakis, and J.R. Zeidler. “Noncoherent Reception of Constant Envelope OFDM in Flat Fading Channels”. In: *Personal, Indoor and Mobile Radio Communications, 2005. PIMRC 2005. IEEE 16th International Symposium on*. Vol. 1. 2005, pp. 517 –521. DOI: 10.1109/PIMRC.2005.1651490.

[259] S.C. Thompson et al. “Constant Envelope OFDM in Multipath Rayleigh Fading Channels”. In: *Military Communications Conference, 2006. MILCOM 2006. IEEE*. 2006, pp. 1 –7. DOI: 10.1109/MILCOM.2006.302187.

[260] A. Garcia Armada. “Understanding the effects of phase noise in orthogonal frequency division multiplexing (OFDM)”. In: *IEEE Transactions on Broadcasting* 47.2 (2001), pp. 153–159. ISSN: 0018-9316. DOI: 10.1109/11.948268.

[261] M. J. Fernandez-Getino Garcia, O. Edfors, and J. M. Paez-Borrallo. “Frequency offset correction for coherent OFDM in wireless systems”. In: *IEEE Transactions on Consumer Electronics* 47.1 (2001), pp. 187–193. ISSN: 0098-3063. DOI: 10.1109/30.920438.

[262] Char-Dir Chung and Shih-Ming Cho. “Constant-envelope orthogonal frequency division multiplexing modulation”. In: *Communications, 1999. APCC/OECC ’99. Fifth Asia-Pacific Conference on ... and Fourth Optoelectronics and Communications Conference*. Vol. 1. 1999, 629 –632 vol.1. DOI: 10.1109/APCC.1999.824966.

[263] P. Robertson and S. Kaiser. “Analysis of the loss of orthogonality through Doppler spread in OFDM systems”. In: *Global Telecommunications Conference, 1999. GLOBECOM ’99*. Vol. 1B. 1999, 701 –706 vol. 1b. DOI: 10.1109/GLOCOM.1999.830152.

[264] M. Schmidl and D.C. Cox. “Blind synchronisation for OFDM”. In: *Electronics Letters* 33.2 (1997), pp. 113 –114. ISSN: 0013-5194.

[265] M. Speth, F. Classen, and H. Meyr. “Frame synchronization of OFDM systems in frequency selective fading channels”. In: *Vehicular Technology Conference, 1997 IEEE 47th*. Vol. 3. 1997, 1807 –1811 vol.3. DOI: 10.1109/VETEC.1997.605870.

[266] F. Classen and H. Meyr. “Frequency synchronization algorithms for OFDM systems suitable for communication over frequency selective fading channels”. In: *Vehicular Technology Conference, 1994 IEEE 44th*. 1994, 1655 –1659 vol.3. DOI: 10.1109/VETEC.1994.345377.

[267] P. H. Moose. “A technique for orthogonal frequency division multiplexing frequency offset correction”. In: *IEEE Transactions on Communications* 42.10 (1994), pp. 2908–2914. ISSN: 0090-6778. DOI: 10.1109/26.328961.

[268] E.F. Casas and C. Leung. “OFDM for data communication over mobile radio FM channels. I. Analysis and experimental results”. In: *Communications, IEEE Transactions on* 39.5 (1991), pp. 783 –793. ISSN: 0090-6778. DOI: 10.1109/26.87141.

[269] E.F. Casas and C. Leung. “OFDM for data communication over mobile radio FM channels. II. Performance improvement”. In: *Communications, IEEE Transactions on* 40.4 (1992), pp. 680 –683. ISSN: 0090-6778. DOI: 10.1109/26.141422.

[270] Xilinx. *System Generator for DSP*. http://www.xilinx.com/tools/sysgen.htm. ver. 10.1. Last retrieved Jan 2010.

[271] *Manual: NuHorizon Spartan 3s1500 Development Board*. Nu Horizon Inc. 2009.

[272] Ettus Research. *USRP N210*. https://www.ettus.com/product/details/UN210-KIT. Last Visited 2015. 2013.

[273] Ettus Research. *USRP N210 Daughter Card SBX*. https://www.ettus.com/product/details/SBX. Last Visited 2015. 2013.

[274] Eric Blossom, Tom Rondeau, and Johnathan Corgan. *GnuRadio*. Last Visited 2019. 2016. URL: "http://gnuradio.org/".

[275] Barry Kauler. *Puppy Linux*. http://puppylinux.com/. Last Visited 2015. 2008.

[276] P. Banelli and S. Cacopardi. "Theoretical analysis and performance of OFDM signals in nonlinear AWGN channels". In: *IEEE Transactions on Communications* 48.3 (2000), pp. 430–441. ISSN: 0090-6778. DOI: 10.1109/26.837046.

[277] A. Leke and J.M. Cioffi. "Impact of imperfect channel knowledge on the performance of multicarrier systems". In: *Global Telecommunications Conference, 1998. GLOBECOM 98. The Bridge to Global Integration. IEEE*. Vol. 2. 1998, 951 –955 vol.2. DOI: 10.1109/GLOCOM.1998.776870.

[278] William W. Ward, David M. Snider, and Ronald F. Bauer. "REVIEW OF SEVEN YEARS OF ORBITAL SERVICE BY THE LES-8/9 EHF INTERSATELLITE LINKS." In: *Conference Record - International Conference on Communications*. Vol. 3. cited By 1. 1983, pp. 1171–1180. URL: https://www.scopus.com/inward/record.uri?eid=2-s2.0-0021002563&partnerID=40&md5=549e960a8dc4cf6764af052f485ca056.

[279] Donald H Martin. *Communication satellites*. 4th ed. AIAA, 2000.

[280] D. L. Brandel, W. A. Watson, and A. Weinberg. "NASA's advanced tracking and data relay satellite system for the years 2000 and beyond". In: *Proceedings of the IEEE* 78.7 (1990), pp. 1141–1151. ISSN: 0018-9219. DOI: 10.1109/5.56928.

[281] *Recommendations for Space Data System Standards, Proximity-1 Space Link Protocol – Data Link Layer*. http://ccsds.cosmos.ru/publications/http://public.ccsds.org/publications/BlueBooks.aspx. Consultative Committe for Space Data Systems Standards (Blue Book). CCSDS Secreteriat, NASA Washington, DC.

[282] *Recommendations for Space Data System Standards, Proximity-1 Space Link Protocol – Physical Layer*. http://ccsds.cosmos.ru/publications/http://public.ccsds.org/publications/BlueBooks.aspx. Consultative Committe for Space Data Systems Standards (Blue Book). CCSDS Secreteriat, NASA Washington, DC.

[283] Jim Taylor, Dennis K. Lee, and Shervin Shambayati. "Mars Reconnaissance Orbiter Telecommunications". In: *DESCANSO Design and Performance Summary Series*. Ed. by Joseph H. Yuen. DESCANSO Design and Performance Summary Series. California Institute of Technology,Pasadena, USA: NASA, JPL, 2006.

[284] ESA. *CANX4&5*. https://directory.eoportal.org/web/eoportal/satellite-missions/c-missions/canx-4-5#overview. Last Visited 2016.

[285] Yves Langevin. "Design Issues for space science missions". In: *Payload and Mission Definition in Space Sciences*. Ed. by V. Martiénez Pillet, A. Aparicio, and F. Sánchez. Cambridge, 2005. Chap. 2.

[286] Claude E. Shannon. "A mathematical theory of communication". In: *The Bell System Technical Journal* 27.3 (1948), pp. 379–423.

[287] Graham Hall. “Maxwell’s electromagnetic theory and special relativity”. In: *Philosophical Transactions of the Royal Society of London A: Mathematical, Physical and Engineering Sciences* 366.1871 (2008), pp. 1849–1860. ISSN: 1364-503X. DOI: 10.1098/rsta.2007.2192. eprint: http://rsta.royalsocietypublishing.org/content/366/1871/1849.full.pdf. URL: http://rsta.royalsocietypublishing.org/content/366/1871/1849.

[288] M.N.O. Sadiku. *Elements of Electromagnetics*. Oxf Ser Elec Series. Oxford University Press, 2010. ISBN: 9780195387759.

[289] H.M. Schey. *Div, Grad, Curl, and All that: An Informal Text on Vector Calculus*. W.W. Norton, 2005. ISBN: 9780393925166.

[290] L.D. Landau and E.M. Lifshitz. *Electrodynamics of Continuous Media*. 2nd ed. Vol. 8. Course of Theoretical Physics. Institute of Physical Problems, U.S.S.R. Academy of Sciences: Pergamon Press Ltd., 1984.

[291] L.D. Landau and E.M. Lifshitz. *Physical Kinetics*. 1st ed. Vol. 10. Course of Theoretical Physics. Institute of Physical Problems, U.S.S.R. Academy of Sciences: Pergamon Press Ltd., 1981.

[292] L.D. Landau and E.M. Lifshitz. *The Classical Theory of Fields*. 4th. Vol. 2. Course of Theoretical Physics. Translated from Russian by Morton Hamermesh. Institute of Physical Problems, U.S.S.R. Academy of Sciences: Butterworth-Heinenann, 1976.

[293] L.D. Landau and E.M. Lifshitz. *Mechanics*. 3rd. Vol. 1. Course of Theoretical Physics. Translated from Russian by J.B. Sykes and J.S. Bell. Institute of Physical Problems, U.S.S.R. Academy of Sciences: Butterworth-Heinenann, 1976.

[294] K. G. Budden. *Radio Waves in the Ionosphere*. Cambridge, 1961.

[295] P Shaft. “On the relationship between scintillation index and Rician fading”. In: *IEEE Transactions on Communications* 22.5 (1974), pp. 731–732.

[296] Minoru Nakagami. “The m-distribution-A general formula of intensity distribution of rapid fading”. In: *Statistical Method of Radio Propagation* (1960), pp. 3–34.

[297] B. Saltzberg. “Performance of an Efficient Parallel Data Transmission System”. In: *IEEE Transactions on Communication Technology* 15.6 (1967), pp. 805–811. ISSN: 0018-9332. DOI: 10.1109/TCOM.1967.1089674.

[298] J.A.C. Bingham. “Multicarrier modulation for data transmission: an idea whose time has come”. In: *Communications Magazine, IEEE* 28.5 (1990), pp. 5 –14. ISSN: 0163-6804. DOI: 10.1109/35.54342.

[299] R. David Luders. “Satellite Networks for Continuous Zonal Coverage”. In: *ARS Journal* 31.2 (1961). doi: 10.2514/8.5422, pp. 179–184.

[300] D. C. Beste. “Design of Satellite Constellations for Optimal Continuous Coverage”. In: *IEEE Transactions on Aerospace and Electronic Systems* AES-14.3 (1978), pp. 466–473. ISSN: 0018-9251. DOI: 10.1109/TAES.1978.308608.

[301] WS Adams and L Rider. “Circular polar constellations providing continuous single or multiple coverage above a specified latitude”. In: *Journal of the Astronautical Sciences* 35 (1987), pp. 155–192.

[302] Analytical Graphics. *Systems Tool Kit*. http://www.agi.com/. Last Visited 2015. 2015.

[303] Peter A. Sturrock. *Plasma Physics; An Introduction to the theory of Astrophysical, Geophysical & Laboratory Plasma*. Cambridge University Press, 1994.

[304] Graeme Lister. "Irving Langmuir and the light bulb". In: *Plasma Sources Science and Technology* 18.1 (2009), p. 014001. URL: http://stacks.iop.org/0963-0252/18/i=1/a=014001.

APPENDIX A

A.1 Selected Missions using Inter-Satellite Links

In the subsequent discussions, selected missions with a brief overview of their communications systems illustrates the wide variety of mission specific architectures in use.

A.1.1 Lincoln Experimental Satellites (LES 8&9) — *A Pair in GEO* - (1978)

The MIT* Lincoln laboratory‘s space communications program developed the LES-8&-9 identical satellites and its terminal under one roof. The two satellite were placed 90 deg apart in GEO. Several experiments were successfully demonstrated, including ground links with small terminals, and data relay via inter-satellite links [278] between the pair. The spacecraft using steerable parabolic dish antenna, fed with K-band (36/38 GHz) horn antenna feed, demonstrated precise pointing, initial acquisition of signal, and data transferred at rates of any one of the two modes 1 or 10 Mbps. The modulation scheme used is differential phase shift keying (DPSK). Although not stated, it is being assumed the underlying transmission scheme is spread spectrum to avoid unnecessary jamming (military application), which can be considered a remarkable achievement with the discrete component technology of that era. Salient features of the spacecraft, antenna, transmitter, receiver are summarised in Table 2.2.

A steerable antenna generates torque, which must be compensated by the spacecraft, a technically complex problem. Furthermore, with directional antennas, establishing a communications link requires scanning a predefined region for possible target and then establishing a link. In GEO the range between the two satellites is about 53475 km, aligning at such distances is a remarkable achievement, illustrating the attitude, and orbit control for precise pointing.

*Massachusetts Institute of Technology, Cambridge USA

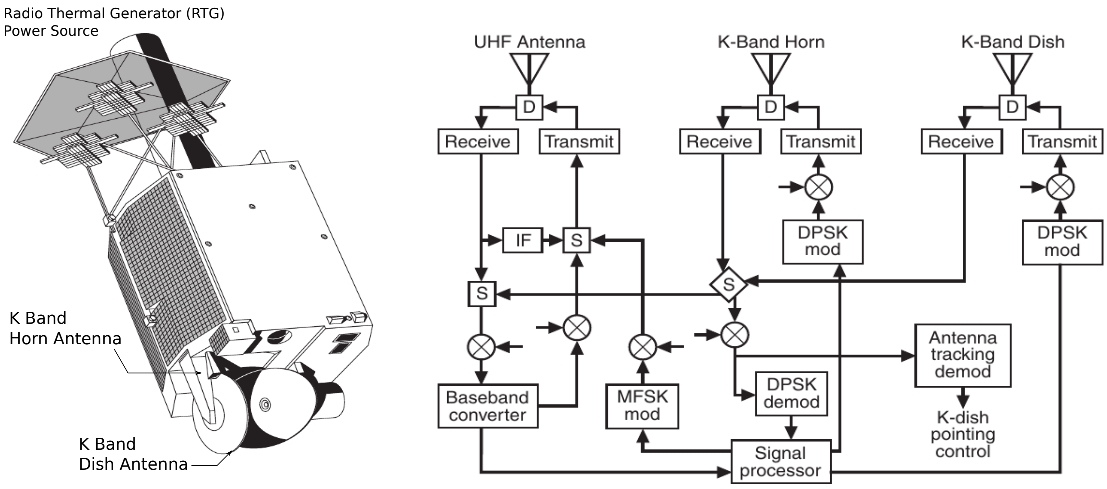

(a) LES-8/9 Satellite Strtructure (b) LES-8/9 Communications System

Fig. A.1 (a) LES-8&9 identical satellites in stowed position. Gyro based high gain antennas shown at the bottom. (b)The functional block diagram of communications system.(courtesy of [279, ch.1]).

A.1.2 Tracking and Data Relay Satellite (NASA) — A Fleet of 9 Satellites in GEO - (1983)

Tracking Data Relay Satellite (TDRS) programme, started in early 1970s, with the first deployment in 1983*, is the space segment of the NASA Space Network, providing tracking and data relay capability for fast moving spacecraft in lower Earth orbits, particularly the ones which are not visible to the ground station. Currently the fleet consists of 9 spacecraft, with the 3rd generation launched in 2014 TDRS-12 (TDRS-L). TDRS-L weighs about 3400 kg, with dimensions of 21.0 meters long by 13.1 meters wide, can generate power of 2200 watts. It houses two single access steerable dish antenna and an array with beam forming for multiple access, to provide inter-satellite link. A separate ground link antenna and an omni-directional antenna is used for spacecraft tracking, telemetry and telecommand (TT&C).

The TDRS can view the satellites above 1200 km altitude for 100% coverage, whereas, for spacecraft at altitudes less than 1200 km, Earth blocks the view for 15% of the orbit. The TDRS provides bent-pipe relay links, from user spacecraft to ground station, and vice versa. This service is based on successful experiments that involved ATS-6 † and the Nimbus-6 ‡ during the mid 70s. In order to use the TDRS service, a custom transponder is required by the user spacecraft [280].

*TDRS-A launched in April 1983, retired Fall 2009, disposed off in June 2010
†Advanced Technology Satellite (ATS) launched in GEO orbit carrying steerable 9.15 m dish antenna
‡One of the meteorological satellites of Nimbus programme launched in LEO at 1000 km altitude, inclined at 100°

A.1.3 Surrey Nanosatellite Applications Platform (SNAP-1) (SSTL) – *Single Satellite in LEO - 2000*

It was designed and built as a research mission by a joint academic-commercial team at the Surrey Space Centre (SSC) and Surrey Satellite Technology Limited . The SNAP-1 nanosatellite was designed to develop a modular, multi-mission nanosatellite bus (mass range of 1-10 kg), to demonstrate the use of miniature electrical and mechanical COTS (Commercial-Off-The-Shelf) product technologies in space and their use as autonomous robots for observing orbiting space vehicles. SNAP-1 is merely 6.3 kg, deployed in a circular orbit at about 680 km altitude, inclined at 98.13 deg. The SNAP program was also intended to demonstrate the feasibility of using clusters of low-cost satellites that can fly in formation and conduct multipoint remote sensing.

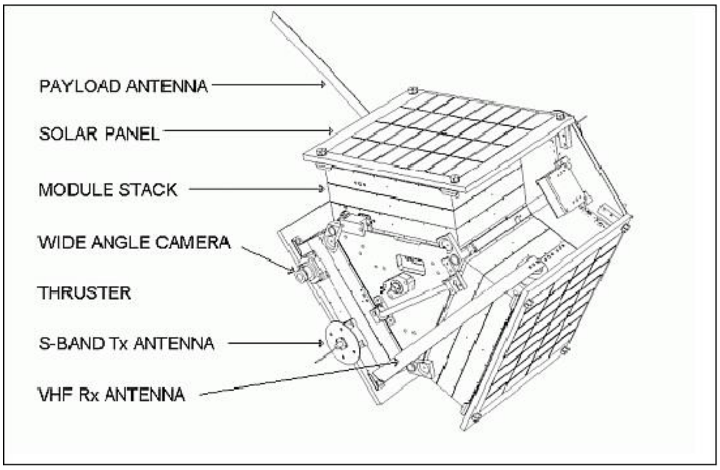

Fig. A.2 Isometric drawing of the SNAP-1 spacecraft (courtesy of SSTL).

The inter-satellite link with Tsinghua-1 (a microsatellite 50 kg) launched together, was to be tested. The communications systems uses S-band monopole antenna, and strip antenna for UHF and VHF links. The S-band data rate supports 38.4 kbps and 76.8 kbps (selectable) using BPSK and QPSK. The S-band transmitter is 0.5 kg the size of 120 mm x 160 mm x 20 mm operating at at 5.2 V DC drawing 670 mA. In addition VHF spread spectrum is also tested.

A.1.4 IRIDIUM — A Constellation of 66 Satellites in LEO (Motorola Inc. USA) - (1999)

Moving closer to Earth, in lower Earth orbits*, one of the successful use of continuous inter-satellite link is by IRIDIUM constellation. Comprising of 66 operational satellites, with 14 backup satellites, each weighing 690 kg, provides L-band links to Earth based users. Each spacecraft (Figure A.3) is linked with

*IRIDIUM constellation has 11 satellites phased out in one orbit at altitude of 670 km, inclined at 86.6°, each orbital plane spaced 30° apart from the other, thus a total of 66 active satellites (4 spares) cover the globe.

four adjacent satellites, two in-orbit while two cross-orbit links. Due to near circular orbits, the in-orbit inter-satellite distance remains constant (Figure A.4) , whereas cross plane distance varies, becoming closer near the poles, and moving farther away till they reach the equator. The ISL provides dedicated links operating at 22.55 to 23.55 GHz at 25 Mbps. Since the satellites are 3-axis stabilised, therefore, the horn antennas are fixed to the sides, no need for steering. The bidirectional links are continuous, unlike TDRS where links are available on demand.

The constellation design aspect stems from the requirement of constant ISL. The research is to provide complete ground coverage with the lowest number of satellites, optimising the communications systems power, antenna structures, and on-board propulsion for longer life time operations. That is why 700 km altitude in polar orbits is selected.

A.1.5 Advanced Relay and Technology Mission (ARTEMIS) (ESA) - (2001)

ARTEMIS is ESA's first GEO data relay communication satellite. It is designed to to demonstrate new communication technologies, principally for data relay and mobile services. "The technology demonstrations include an optical inter-satellite link, first European operational use of an electric ion

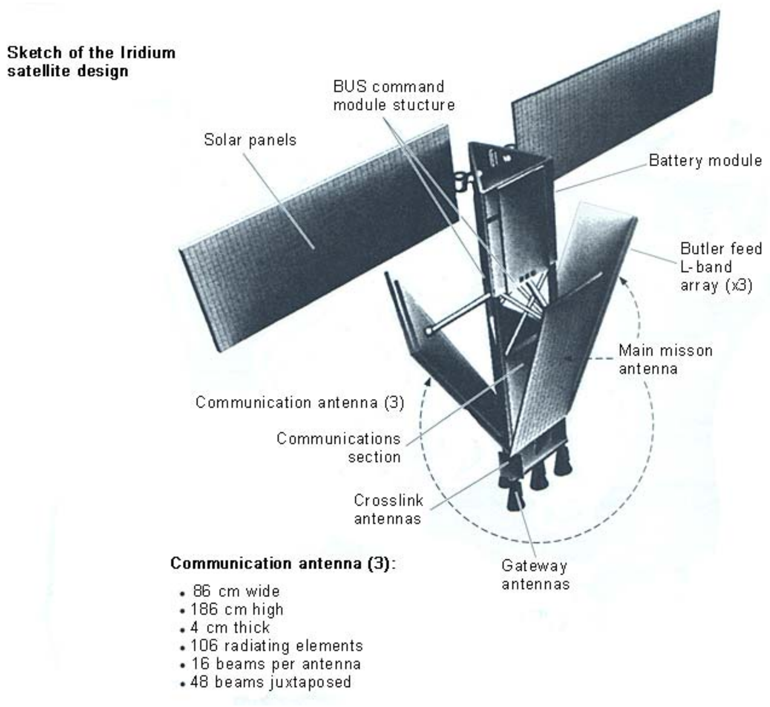

Fig. A.3 The IRIDIUM spacecraft structure indicating phased array antenna (courtesy of unknown).

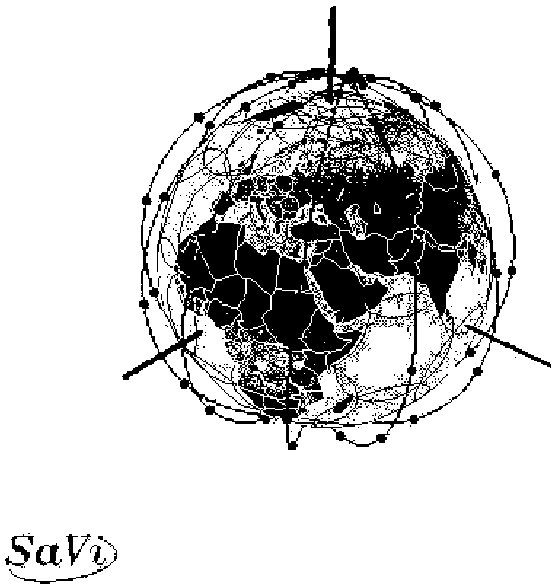

Fig. A.4 The IRIDIUM Constellation generated by Savi[179].

propulsion system, and a transponder for the support of EGNOS (European Geostationary Navigation Overlay Service) for signal enhancement of the GPS/GLONASS navigation satellite constellations."*

The spacecraft structure consists of a box-shaped three-axis bus of Italsat heritage (Alenia Spazio bus family, Alenia is also the prime contractor to ESA). The primary structure consists of the central cylinder

*From ESA Webportal: "https://directory.eoportal.org/web/eoportal/satellite-missions/a/artemis".

Table A.1 Artemis Spacecraft Characteristics.

Spacecraft Characteristics	
Mass at launch, power	3100 kg, 2.5 kW
Size: height, length, width	4.8 m, 25 m (solar array tip-to-tip), 8 m (antennas deployed)
Design life	10 years
Orbital position	21.5 deg East (GEO)
Communications: Data Relay Payload	
Feeder/downlink coverage	Western Europe
Inter-Satellite Link Experiment SKDR (S/Ka band Data Relay)	
Coverage	Approximately 65% of orbits up to 1000 km altitude
S-band (2 GHz)	Up to 1 Mbps in the forward direction (i.e. Artemis to low altitude spacecraft). Up to 3 Mbps in the return direction (i.e. low altitude spacecraft to ARTEMIS)
Ka-band (23/26 GHz)	10 Mbps in the forward direction 3 x 150 Mbps in the return direction
Optical link (800 nm)	2 Mbps in the forward direction 50 Mbps in the return direction

(aluminium honeycomb skinned with carbon fibre), the main platform, the propulsion platform, and four shear panels. The secondary structure is made up of the N/S radiators, the E/W panels, and the Earth-facing panel. The central propulsion module houses the propellant tanks, LAE (Liquid Apogee Engine), the East panel with the L-band antenna feed, the West panel with the IOL (Inter Orbit Link) antenna.

Spacecraft (S/C) electric power of 2.8 kW (at equinox after ten years to a 42.5 VDC bus) is provided by two solar wings (span of 25 m). BSR (Back Surface Reflecting) solar cells are mounted on each of the two solar wings. Two NiH2 batteries provide energy of 60 Ah for eclipse protection. A S/C design life of 10 years is provided. The S/C launch mass is 3100 kg (550 kg payload, 1538 kg propellant) The two antenna reflectors (2.85 m diameter) for Inter-Satellite link (ISL)* support are dominant features of the S/C structure.

Artemis established a successful optical link with SPOT-4, using its optical link via SILEX payload. It relayed images taken by EnviSat in 2003, using its Ka (23 GHz) inter-satellite link, demonstrating technology readiness levels.

A.1.6 Mars Reconnaissance Orbiter (NASA) - (2002)

ISL have been accomplished by the data link from rover to orbiting satellite (MRO) to NASA Deep space network ground stations on Earth. This is an example of great distances, and successful use of relay to overcome the limitations of direct ground links degraded by planetary atmosphere. The MRO and Odyssey are two NASA orbiters equipped with Proximity-1 [281, 282] relay communications capability, implemented in the Electra payload operating in UHF band. The X band and Ka band ground link is achieved via high gain steerable antenna, travelling wave tube (TWTA) amplifier. The X band transponder is called Small Deep Space Transponder (SDST).

A typical inter-spacecraft link is established when the orbiter passes over the rover for approximately 8 min, during which the link is initiated, data transferred and link closed. The orbiter relays the rover data to Earth using its high gain X band or Ka band transmitters. The major operating modes, functions and constraints of the Electra payload are stated in Table. It is evident that BPSK is used as the baseband modulation scheme, where flexible data rates have been set to overcome adverse impairments of channel. The operational frequency is in the 440 MHz band for forward links, and in 390 MHz band for the return link. The Electra transceiver is compatible with the CCSDS Proximity-1 Space Link Protocol [281, 282].

A helical low gain antenna is used, whose radiation pattern is nadir pointing on MRO orbiter, and a similar antenna on the rover. The important fact is that Electra is 12 kg, generates about 5 W RF power,

*ESA uses the term inter orbit link (IOL) for inter-satellite links (ISL).

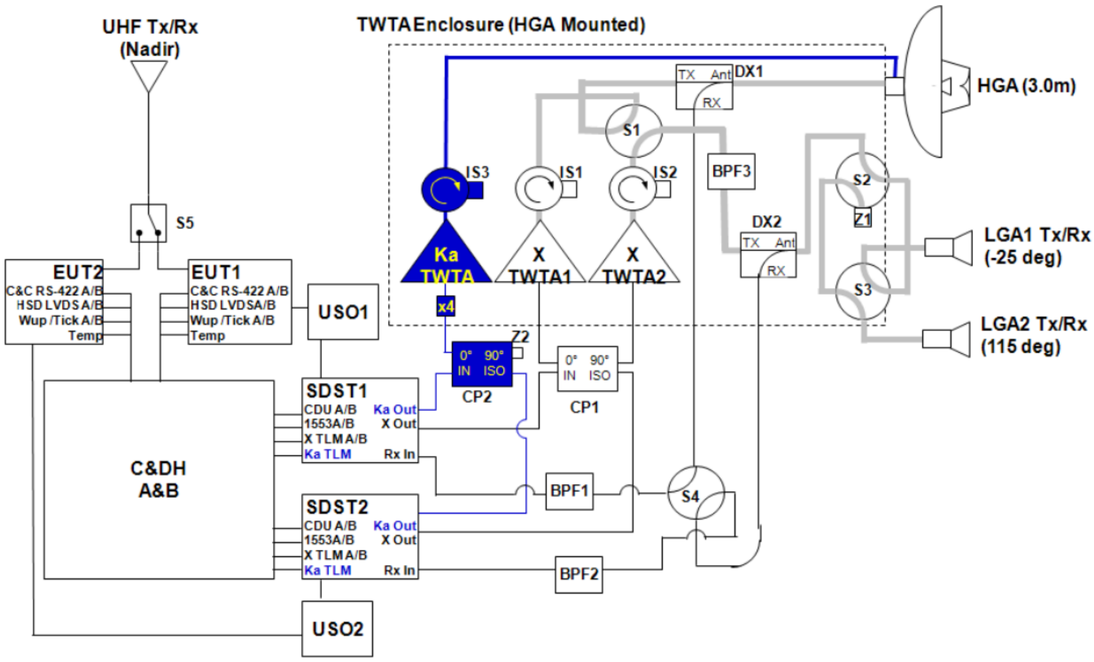

Fig. A.5 Mars orbiting relay satellite telecomm system

Table A.2 Electra modes, functions and performance [283, pg.38] also known as Small Deep Space Transponder (SDST) in Figure A.5.

Capability	Values
Protocol	Prox-1 (reliable and expedited link layer protocol)
Frequencies	440 MHz for front link and 390 Hz for return link
Modes of operation	Half-duplex Rx and Tx (no Prox-1 protocol in half duplex), Full-duplex transceiver.
Full-duplex carrier modes	Coherent , noncoherent
Transceiver RF output power	5.0 W full duplex 7.0 W half duplex
Circuit loss, EUT to antenna	- 0.42 dB
Receiver thresholds, at antenna	- 130.8 dBm (1 kbps) to - 99.6 dBm (1024 kbps) coded, - 126.0 dBm (1 kbps) to - 91.1 dBm (2048 kbps) uncoded
Carrier Modulation modes	Suppressed carrier, residual carrier (60 deg mod index)
Modulation Type	Residual binary phase-shift keying (BPSK) with Bi-phase-L (Manchester Line Coding). Suppressed-carrier BPSK.
Frequency reference	Ultra stable oscillator
Rx and Tx symbol rates	1,2,4,8,16,32,64,128,256,512,1024,2048 ksps. Also adaptive data rate mode.
Received signal power range	-140 to -70 dBm
Encoding	Uncoded, (k=7, r=1/2) convolutional, differntial symbol coding
Decoding	Uncoded, (k=7, r=1/2) convolutional (3-bit soft decode)
Scrambling & descrambling	V.38
Acquisition and tracking loop	Second-order PLL, with loop bandwidth 10 Hz to 10 kHz (for received signal from -140 dBm to -70 dBm)
Tracking range and rate	±20 kHz, ±200 Hz/s

The lessons learned from UHF transceiver are the problems arising from electromagnetic interference (EMI). The EMI were identified as harmonic overtones of sitching power supplies, data bus or clock mechanisms. One such tone from a science instrument was measured at -70 dBm centred near 400 MHz, a grave concern. The remedy taken was to reprogram the FPGA to include a digital filter, and shift the operational frequency by 3 MHz, so that onboard SAW filter could eliminate the interference completely.

A.1.7 Canadian Advanced Nanosat Experiment (CAN-X 4&5) – *A Pair in LEO* (2014)

The University of Toronto, Canada, nano satellite educational programme developed two identical cube shaped satellites to demonstrate autonomous in orbit formation flight. GPS based navigational data is exchanged when the satellites are with in 10 km range. The point to point link allows the satellites to exchange relative motion information as well as commands to maintain the relative motion with in desired limits. The mission successfully demonstrated its in orbit primary and extended mission objectives [137].

The CanX-4&5 mission objectives are as follows:

- Demonstrate the autonomous achievement and maintenance of along track (ATO) and projected circular orbit (PCO) at 1000, 100 and 50 meters. (Demonstrated perfectly for 11 orbits.)
- Demonstrate carrier-phase differential GPS techniques to perform relative position determination measurements with accuracies of 10 cm or less.
- Demonstrate sub-meter position control.
- Develop and validate fuel efficient formation flying algorithms.
- Demonstrate enabling technologies, such as CNAPS (Canadian Advanced Nanosatellite Propulsion System) and the S-band ISL (Inter satellite Link).

The low data rate ISL is sufficient for this purpose. It is not clear, whether, ISL provides range and range rate estimates. There is little information regarding the modulation scheme used, but BPSK is the most likely candidate.

It operates in S-band, supports 10 kbps at a range of 5 km. The patch antenna used is on one side of the spacecraft, and is only operational when the desired attitude is achieved. The ISL hardware consumes 600 mW power when transmitting and 400 mW when receiving. The transmitters delivers 21.8 dBm power to patch antenna which emits 15.3 dBm effective isotropic radiated power (EIRP). The link availability achieved during the formation was 100% and better than 90% at distances more than 5km.

This mission has set the benchmark for performance comparisons for nanosatellites.

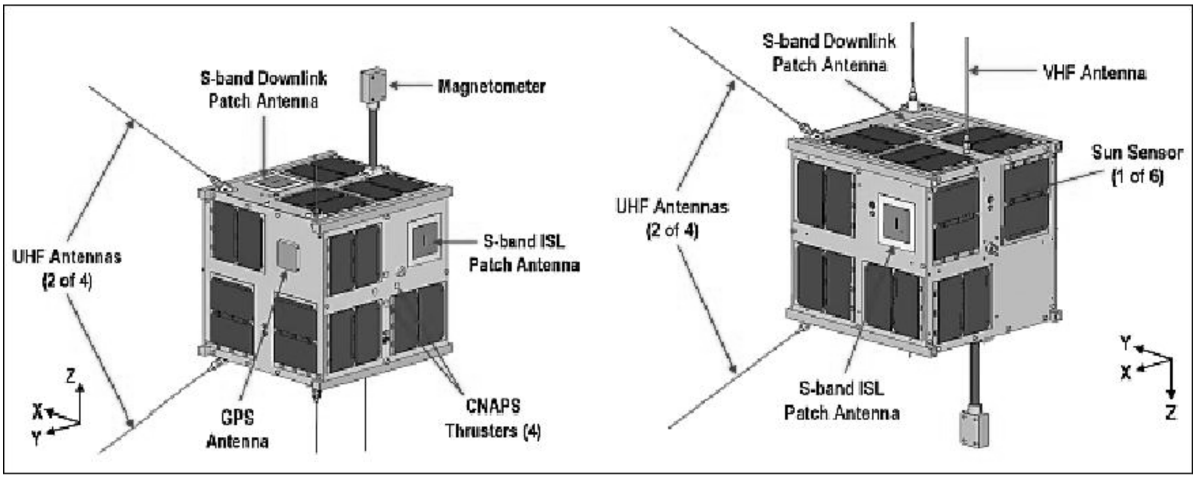

Fig. A.6 Identical spacecraft CANX-4&5 nano satellite sub-systems, and external mountings indicating the ISL patch antenna [284].

Table A.3 CANX 4&5 specifications [284]

Spacecraft Characteristics	
Mass at launch, power:	15 kg, 5.4 - 10 W (4.0 V bus voltage)
Size (height, length, width):	20 cm, 20 cm , 20 cm, Face mounted solar cells
Design life :	years
Orbit:	Sun Synchronous circular, 660 km altitude, 98.2 deg inclination
Attitude Control:	3 axis stabilised, 0.5 - 1.0 deg accuracy
Ground Link:	UHF, VHF
Communications: Data Relay Payload	
Feeder/downlink coverage	Western Europe
Inter satellite Link Characteristics	
Coverage	Approximately 65% of orbits up to 1000 km altitude
S-band (2 GHz):	5 km at 10 kbps, Patch antenna face mounted

A.2 A Survey of Space Science Missions

Science missions can be classified based on the field of interest for instance **space astronomy**, **solar-terrestrial physics** and **planetary exploration**. They can also be classified based on the complexity or capability build up through the technological developments.

A.2.1 Astronomy Missions

In the field of **Space Astronomy** the main driver is to cover the full range of electromagnetic spectrum, observed for a variety of objects. Each wavelength in the spectrum provides specific information, since it is related to the intrinsic temperature. High energy ranges are particularly interesting when active objects such as novae, supernovae etc are being observed. *Cold objects* such as molecular clouds and pro stars are best observed in the Infra Red region.

Advances in space astronomy relies on the improvement of focal plane instruments (quantum efficiency and resolution) and the increase in collecting areas. Missions can be divided in three categories as described by [285], and classified in figure A.7

1. The pioneer missions, which open up a new wavelength range, often with a whole sky survey at selected wavelengths,
2. The second generation missions which provide improved pointing and imaging capabilities,
3. The Observatory class missions which implement high-efficiency detectors to provide extensive capabilities for both imaging and spectroscopy,

As it is clear by 2010 all spectra would be observable and to a good quantum efficiency *.

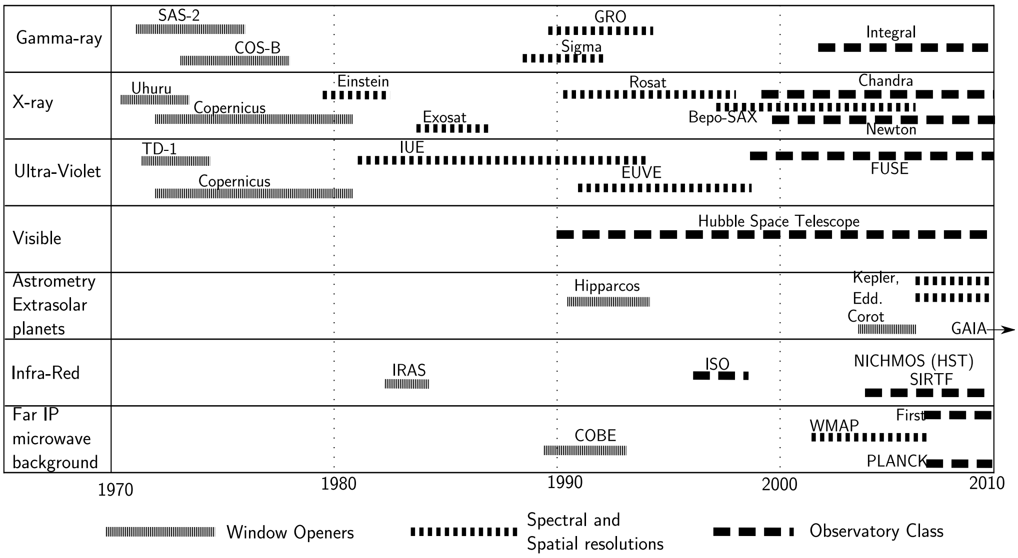

Fig. A.7 Space Astronomy Missions Current and planned [285]

A.2.2 Solar Terrestrial Physics

Solar Terrestrial physics developed by deploying satellites in Lower Earth Orbits to observe the Earth's magnetosphere and Solar activity. The International Solar Terrestrial Physics (ISTP) program has remarkable findings from the missions such as NASA Wind and Polar, and its current joint NASA/ESA Cluster mission.

*Measure of a device's electrical sensitivity to photons. The percentage of photons hitting the photoreactive surface that would produce an electron-hole pair

The present generation of solar terrestrial missions is dominated by SOHO for solar physics and Cluster for the study of Earth's magnetosphere.

Sun Earth L1 Lagrangian point has successfully demonstrated by SOHO mission is a strong candidate for future Solar observatory missions such as planned Solar Orbiter.

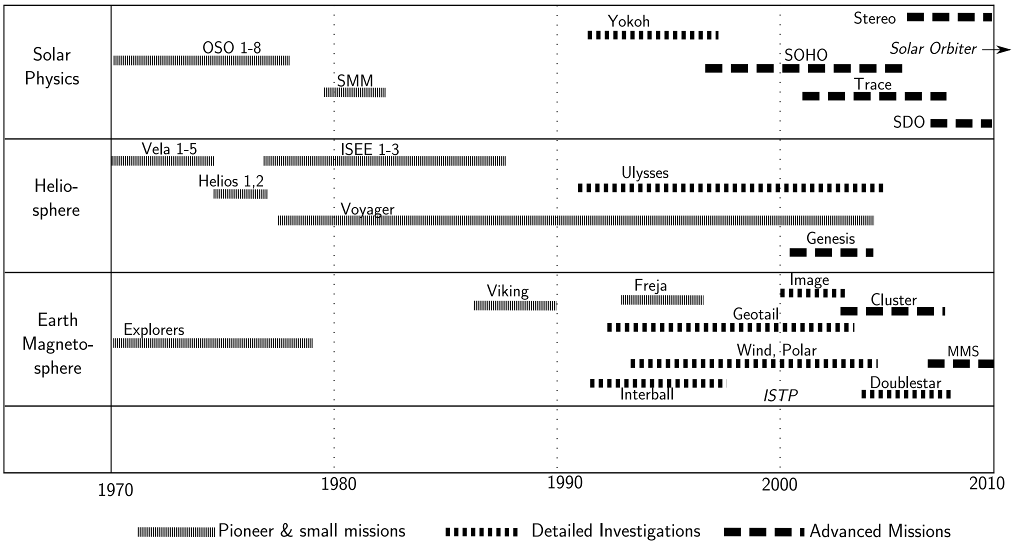

Fig. A.8 Solar Terrestrial Missions current and planned [285]

A.2.3 Solar System Exploration

Solar System exploration have not been far behind. Currently Mars has captured the fascination of scientists, and is actively being pursued for land rovers, and safe landing, as is observable from the figure A.9.

Studies carried out by ESA in their "Cosmic Vision for 2025" [65] for identifying the its next set of science mission, require multiple spacecraft constellations either for implementing interferometry techniques or for aggregating large collecting areas without incurring cost and complexity of a single large satellite. For instance the new generation of X-ray telescope beyond the Newton and Chandra.

A strong urge is towards non photonic space astronomy, with proposals for major observatories for gravity waves (Laser Interferometer Space Antenna (LISA)). LISA requires three satellites at millions of kilo-meter distances precisely controlled triangular configuration to measure gravitational waves.

Ambitious missions for extra solar planetary imaging Sun-Earth L2 point have already been selected for missions such as WMAP (NASA), Planck and Herschel (ESA) and Terrestrial planet finder (TPF) Darwin. The significance of choosing Earth-Sun L2 point which is 1.5 million km away from the Sun along the Sun Earth line, is to avoid the necessary contamination from Earths thermal Radiation.

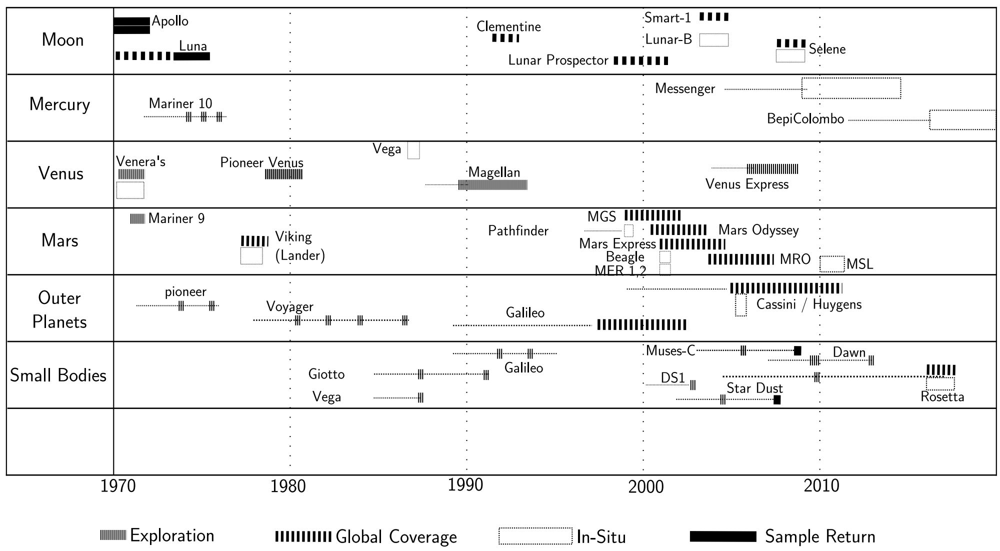

Fig. A.9 Solar System Exploration Missions current and planned [285]

APPENDIX B

B.1 Elements of Digital Baseband Processing in Communications Systems

> "The fundamental problem of communication is that of reproducing at one point either exactly or approximately a message selected at another point" - Claude Shannon[286], "A mathematical theory of communication".

In this section practical aspects of digital baseband processing telecommunications are described.

B.1.1 Foreword

The phenomenon of radiation is best understood when studied in the context of antennas and electromagnetic theory . A brief non technical history of events which lead to a uniform theory by Maxwell is presented in [287]. The fundamentals are well treated by Sadiku [288] and the mathematics of vector calculus is best illustrated by Schey [289]. A uniform treatment of EM theory with Matlab examples is covered by Orfanidis [174], but the lectures on Physics by Landau [290, 291, 292, 293] provide the fundamental mathematical expressions uniformly applied to a systematic treatise of wave propagation.. Wave involves differential equations, a treatment by Boyce [200] is easy to apply, for solutions both analytical and numerical examples abound. These sections are being written to avoid mathematics but the only language science knows is mathematics / algorithms. * Waves and vibrations hold the key to understanding the propagation of sound, light, ocean waves, earthquakes, the transmission of signals from brain and of course our interest the radio waves. However, in this section, electrical signals generated in the digital modem, and associated processes are briefly described with emphasis on graphical illustrations probably not available in text books. It is written for the reader with no engineering background, to grasp the basics helpful in selecting the modem for any project.

*We are indebted to the mathematical tools such as calculus, algebra and geometry which are being harnessed today with the advanced computational facilities, though the forms were developed hundreds of years ago. (A topic of history of mathematics describing the physics of astronomy, mechanics, electricity, magnetism, and quantum mechanics and like so).

The communications systems are studied using simulation techniques which have been discussed in depth for their pros and cons by Tranter [66]

B.1.2 Electrical Waveforms? *Signals Representing Bits*

The fundamental concept of telecommunications is that electrical current or voltages, when applied to one end of a copper wire can be measured or detected at the other end of the wire. That means electrical energy propagates from one point to the other.

The concept of telecommunications is illustrated in Figure B.1. Say we represent the bits by voltage levels +V for 1 and -V for 0. The voltage level is restricted to a time duration called symbol duration. This type of waveform is called a "pulse", which has a defined amplitude, time duration and a repetition rate. The concept is illustrated in Figure B.2.

Without going in to details of how the wave form is generated, or how the media effects the waveform, lets consider a simple waveform detector and decision maker, which decides which bits were sent by looking at the received waveform. In Figure B.2 left side represents the transmitter side, sending bits "1 0 1 1", which are represented by pulses of fixed time duration τ. As the pulse propagates through medium it gets distorted. A visible noise rides the amplitude, the level decreases called attenuation and the time duration expands, or the location of pulse shifts. A simple receiver would require a voltage level detector to distinguish in coming bits from the waveforms received. Each pulse is processed one at a time, and a corresponding bit is generated. A simple process for the voltage level detector would be to check the received signal level, compare it with a threshold voltage level γ, and then decide. When received level is above γ, the received signal represents 1, otherwise 0. There is an ambiguity at the exact level γ, therefore, the systems are designed so that the signals (waveforms levels also called amplitude) does not reach this level.

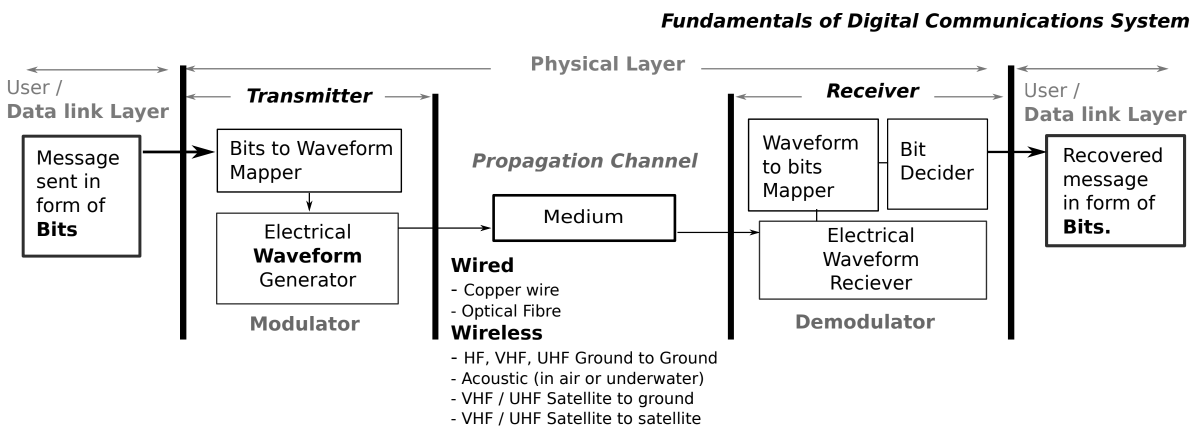

Fig. B.1 A simplified block diagram of digital communications system.

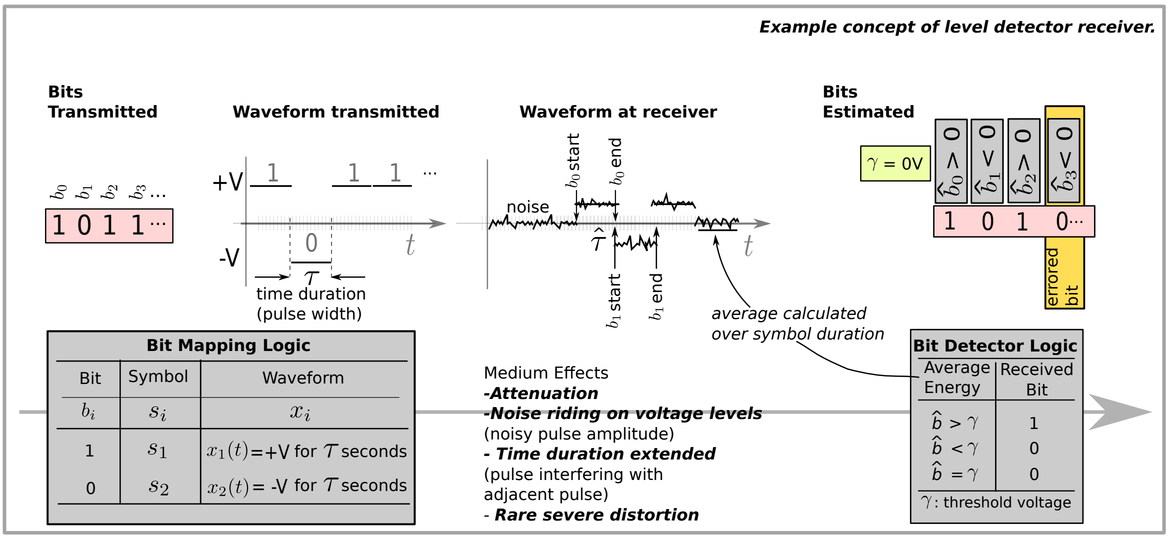

Fig. B.2 The functional level concept of bit to electrical waveform mapping at transmitter, and a complementary level detection process at the receiver end.

Notice, in the waveform at receiver, prior to waveform, there is constant noise, which does not carry information, then pulses arrive and the last pulse is distorted so much so that its level is near zero. These illustrations represent some of the manifestation by media on the propagating electrical signal. These form the study of channel characteristics. Say for instance, we decide to place the receiver close to the transmitter, then the received waveform would not show any distortion. However, as the distance increases, the receiver would observe noisy, attenuated signals, till the point the transmitted level and noise level is merged. This distance is the upper limit of how far the signal can travel. The above stated concept is illustrated in the form of "TIme snapshot" in Figure B.3, taken at arbitrary distances from transmitted.

Now lets discuss how the detector would take a decision. It can take a measurement at a single instance of time and based on the value, decide bit value. Or, it can take an average over the symbol duration τ. The latter method provides a better estimate than the former. The first type is simple to implement, but the second type is more robust to noise. For a simple proof of the above concept the reader is referred to estimation* theory by Kay [251, ch.3]. The problem of estimating the average (mean) DC level from several observed samples. It is noted that to take the average, the receiver needs to identify the start and end of symbol in time, thus the need for **symbol timing synchroniser**. Note, the bit b_3 whose amplitude has gone so down that the average went below the threshold, therefore it is incorrectly interpreted as 0, whereas a 1 was sent. This highlights the fact that average energy of the waveform should be high when compared to the noise energy to be correctly interpreted at the receiver highlighting the significance of signal to noise ratio (SNR) or bit energy to noise energy ratio (E_b/N_0).

*The estimation theory is not discussed here, to keep the discussion simple and without any mathematics.

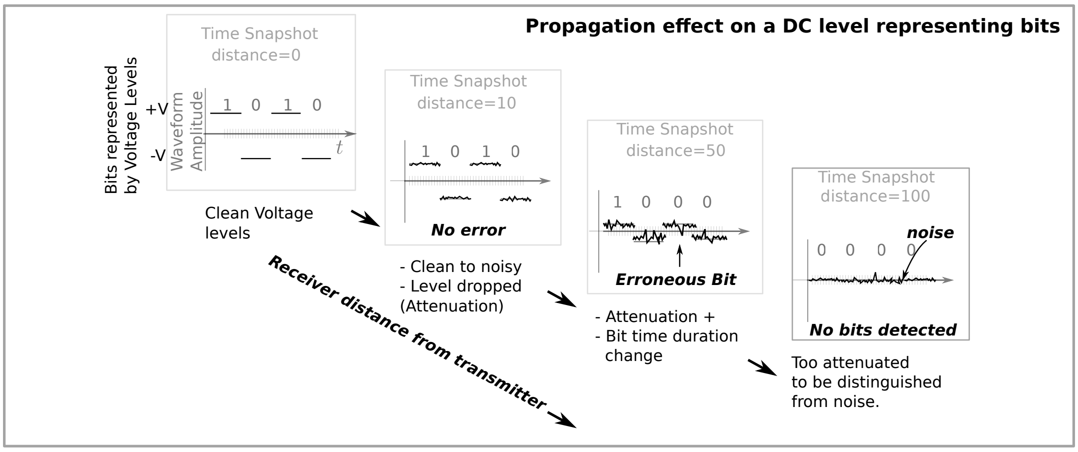

Fig. B.3 Illustration of medium effects on DC waveforms, as the receiver is placed at different distances from the transmitter. The waveform gets attenuated, noise starts to increase, and time duration changes (pulse width expands). The receiver is unable to decode the data bits after distance called the communications range.

The treatise above has highlighted simple but fundamental concepts in digital communications systems design, such as waveforms, manifests of channel, and requirements at the receiver. Now we turn our attention towards the generation of these waveforms, and their corresponding receiver architectures. Details are left to clarify the concept.

B.1.3 The concept of modulation

The concept called "modulation" is extensively used in communications and the following treatise would elaborate the basic concept. Before going into details, now we use another type of waveform to represent bits, a sinusoidal waveform which are mathematically represented by functions sine or cosine. Afterwards, the simple forms of modulations, amplitude, phase and frequency, are described. A simple modulator called I/Q modulator is described, which is commonly employed in digital communications. A simple receiver demodulator, and its other processing components are described, to identify, why some are used in space applications and other ignored?

Parameters of Sine Wave

The parameters which define a sinusoidal form of wave* are its amplitude A, time period T, and the phase ϕ. The inverse of time period is called frequency $f = 1/T$, i.e. the repetition rate. The wavelength $\lambda = c/f$, where c is the speed of wave in the medium. In vacuum it is fixed to a value 299792458 m/s in SI Units or $\approx 3 \times 10^8$, whereas it varies for other medium. These parameters are illustrated in Figure B.4.

*This is one of the solutions to the scalar wave equations which are derived from Maxwell's equations, see [174, p.13] or [288, ch.10], when the electric field is the form of a sinusoidal wave, also called harmonic wave with time dependence.

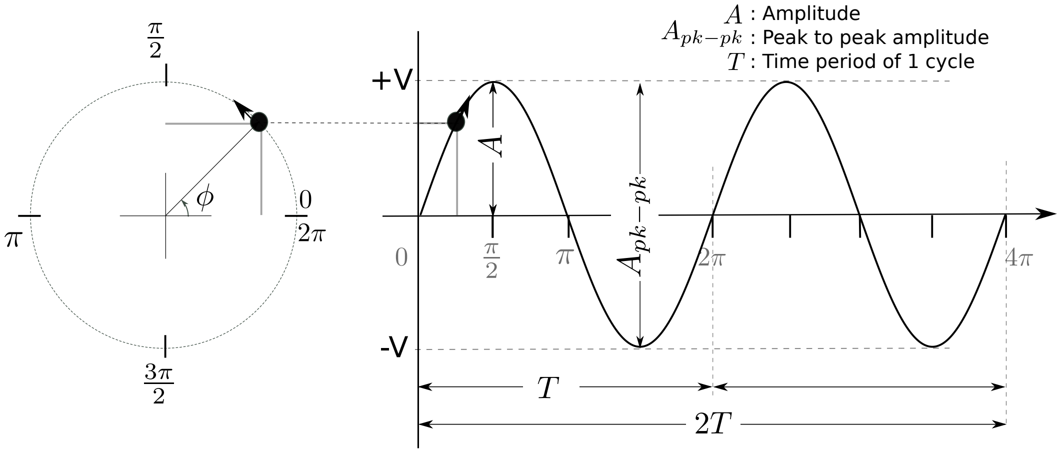

Fig. B.4 A sinusoidal wave propagating towards left side. It has a peak to peak voltage, a peak voltage and time duration T after which it repeats. Frequency in Hz is defined as $T = 1/f$, and wavelength in meters defined as $f \times \lambda = c$, where c is speed of wave in media, i.e. the speed with which dot moves away from origin.

The sine wave $c(t)$ is mathematically described as

$$c(t) = A\cos 2\pi f_c t + \phi \tag{B.1}$$

where A is the amplitude, f_c is the carrier frequency in Hz and ϕ is the phase angle which can be considered a random variable uniformly distributed in the interval $[-\pi, \pi]$.

A product of $c(t)$ with any other signal $s(t)$ is called the modulated signal, say $x(t)$ is

$$x(t) = s(t)c(t) = Ax(t)\cos 2\pi f_c t + \phi \tag{B.2}$$

which has a power spectral density of

$$S_{xx}(f) = \frac{A^2}{4}\left[S_{xx}(f - f_c) + S_{xx}(f + f_c)\right] \tag{B.3}$$

The eq. (B.3) also shows that the frequency shifts from the baseband to the carrier frequency in passband f_c. This is the fundamental concept of modulation. In reality the baseband signal occupies a bandwidth, which is shifted.

The significance of differentiating passband and baseband signal is from processing point of view. In digital signal processing, sampling of the signal takes the rate at least 2.1 times the highest frequency component in the signal. In general at least 3 to 4 times higher, so that information of the frequency components is preserved. So consider for instance the signal at 400 MHz, means sampling at 12 MHz, means 12 Msps, each represented by 32 or 64 bits, results in a large memory requirement. Therefore most functional signal processing is carried out in baseband. Modern computers come with high memory banks (4 to 16 GB RAM) allowing more sophisticated bandpass simulation studies.

The method to convert frequency is a simple mathematical multiplication, which in communications systems engineering is referred to modulation. It is one of the most important signal processing operation. It can effectively match the baseband signal with the channel characteristics, minimise the effects of channel noise and also provides capability of multiplexing many signals.

Modulation types: Amplitude, Phase and Frequency

Now to represent the data bits say “1 0 1 1” using oscillating time harmonic wave (sine wave), one of its parameters can be changed so that the change when detected at the receiver means the respective bit 0 or 1 was transmitted. The three parameters form the basis of amplitude, phase and frequency modulation. A suitable structure to generate these waveforms is also illustrated in Figure B.5.

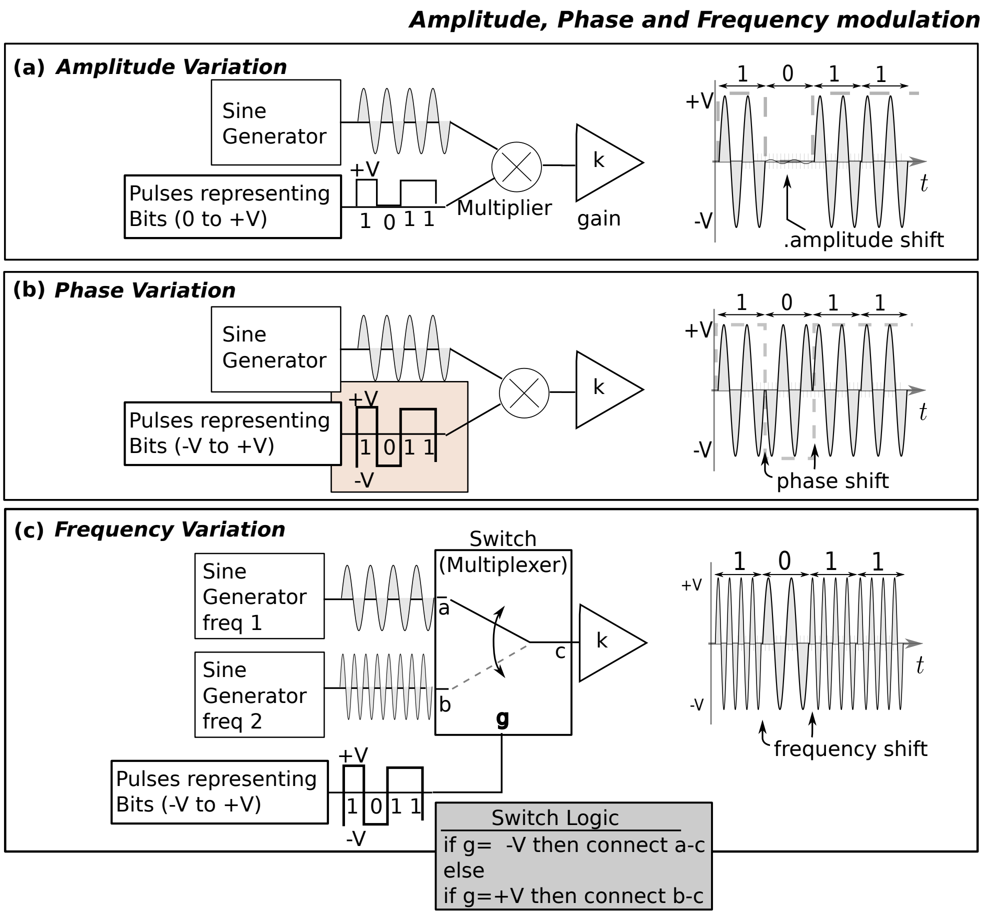

Fig. B.5 The three different types of waveforms carrying the same information bits. The first (a) uses amplitude variation to represent data, called pulse amplitude modulation (PAM) or amplitude shift keying (ASK). In (b) the phase is varied to represent bits, thus called phase shift keying (PSK). (c) shows how two different frequencies can be used to send binary bits, also called frequency shift keying (FSK). Note the pulse width or the symbol duration is kept same for the transmission.

a) When the amplitude A of sine wave is used to represent bits, then this method is called amplitude modulation (AM). At the receiver side, some form of amplitude (represented by the envelope of sine wave) detector is required. When discrete levels are used, then AM is called amplitude shift keying (ASK).

The parameter A is controlled by the amplitude of pulse, which represents the bits.

b) When the phase ϕ of wave representing bits is used then it is called phase modulation (PM). A phase detector and phase shift estimator is required to estimate the bits. When discrete values of phase shifts are employed, its called phase shift keying (PSK).

The pulse representing bits control the phase of the sine wave. A phase 0 is distinguishable from 180, which in sine wave means that wave is inverted (multiplication by -1). This feature has been used to generate two phase shifted waves representing 1 or 0. In this example only two phases can be generated, more phase variation is possible with the help of I/Q modulator described in section B.1.4.

c) If different frequencies $f = 1/T$ are assigned to each bit, then the method is called frequency modulation (FM). At the receiver some form of frequency shift detector is required to discern the bits. Obviously, when discrete frequencies represent bits, then the method is called frequency shift keying (FSK).

d) Any combination of the above three fundamental modulation schemes can be employed, generating interesting new waveforms, best suited for the application at hand.

Based on the modulation scheme, a corresponding demodulation method must be employed. The requisite functions in simplified form are shown in Figure B.6. We discuss one of the receiver architecture later to highlight the underlying functional blocks, concerns and issues.

B.1.4 IQ Modulator and Demodulator

Another way to generate waveforms which can vary the phase and amplitude arbitrarily is by the use of a structure shown in Figure B.7, called the I/Q modulator. There are two legs of the modulator, the I and Q paths. The data is separated in to two paths (serial to parallel conversion not shown in Figure B.7). The oscillator generates a cosine wave at a specific frequency $\omega = 2\pi f t$ in radians. The leg which is in phase with the oscillator wave is called I and the other leg is out of phase by 90°.

The pulses represented by I and Q manipulate the cosine and sine waves, and the resultant waveform represents bits, or combination of bits here to forth called symbols. Consider the timing diagram on the right side of Figure B.7. Top most plot shows bits representing pulse shapes, which are going to manipulate the cosine wave, called the I. The middle plot shows the pulses which are going to affect the sin wave, called the Q. The bottom plot is the resultant $x_i(t)$ ith symbol waveform. Note the duration of symbol is same for all.

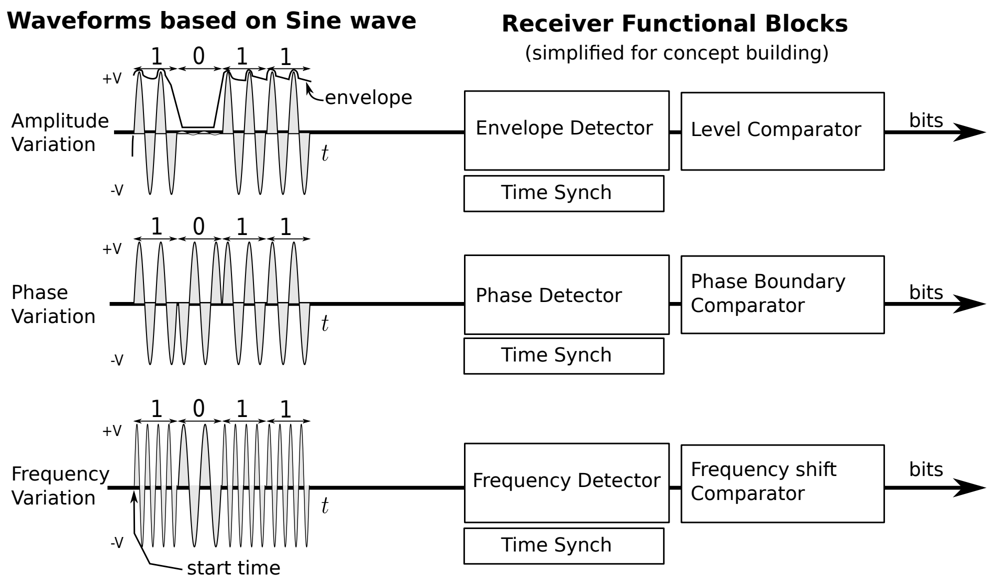

Fig. B.6 Simplified functions at the receiver side to detect the amplitude change, the phase change and the frequency shifts. The comparator compares the received value to a look up table, to decide bits corresponding to "shifts".

Lets consider the resultant wave $x_1(t)$ when I=1 and Q=0, then only cos wave is formed. When I=-1 and Q=0, $x_2(t)$ is -sine wave. The two symbols represent constant amplitude phase shift waveforms, commonly known as BPSK. So we can generate PSK type waveforms by changing the I and Q value.

For the 3rd symbol when I=2 and Q=0, $x_3(t)$ is a cos wave twice the amplitude. This highlights, that amplitude variations can be carried out as well. So where the need is to generate both amplitude and phase variations, this structure supports it with a simple manipulation of I and Q pulse levels.

A simplified form of the demodulator is shown in Figure B.8. The received signal is divided in to two paths, just like the modulator, and each leg is multiplied by the oscillator which is in quadrature phase. Then resultant is filtered using a low pass filter (LPF), so that the baseband voltage levels (pulses) could be retrieved. The retrieved I and Q are further processed for bit extraction, but before that, timings of the start and end of symbols must be done, any impairments caused by the medium, or hardware must be compensated, and then symbols to bit maps are consulted to extract the correct form of bits. The receiver structure is more complex than the transmitter, therefore we shall discuss one receiver in detail. Before that the concept of constellation diagrams is given.

Now we discuss the importance of symbol maps generated using constellation diagrams, and high light that at a time only one modulation scheme can be used at the receiver, since it needs it to extract bits from the symbols.

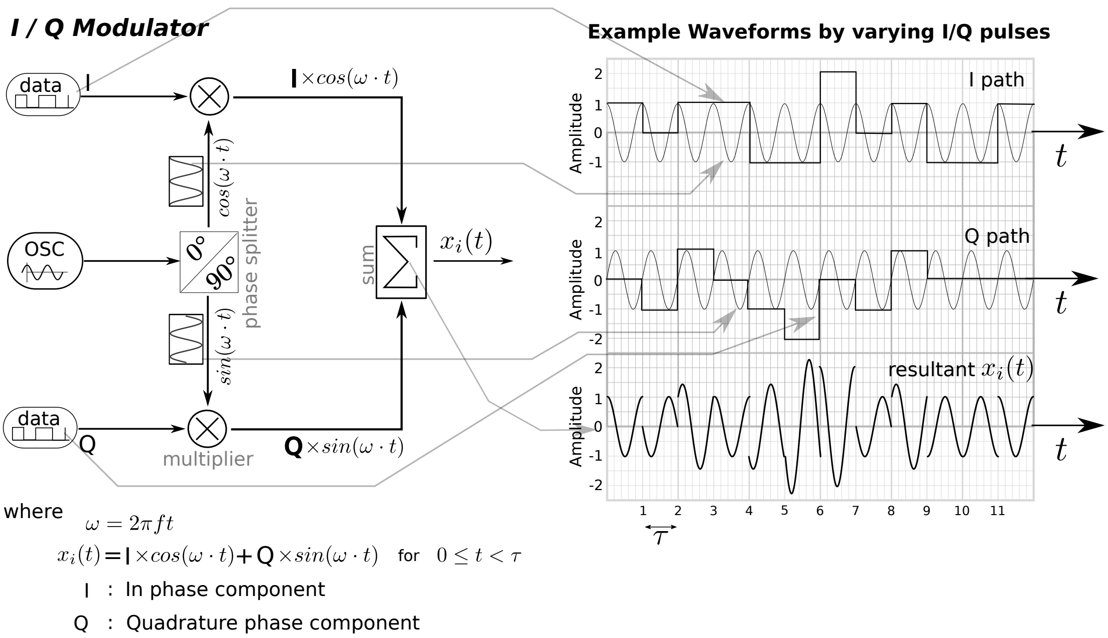

Fig. B.7 I/Q modulator structure.

B.1.5 Constellation Diagrams: Signal Space representation of digital symbols

Lets investigate further, how I and Q can be manipulated more systematically, with the aide of complex numbers and constellation diagrams, which is the basis of digital communications, and helpful in digital signal processing. Lets consider the complex number in rectangular form $a_i + jb_i$ whose real value represents I and imaginary value represents Q, and $j = \sqrt{-1}$, where i is a real number representing the ith symbol. In the context of the waveforms shown in Figure B.7, consider the values in the Table B.1, for the first seven pulses.

Now consider, we want to generate a waveform which represents not just bits, but the combination of bits. Taking two bits at a time, a symbol is formed. This type of signal can be represented by only amplitude variations, or only phase variations or a combination of both phase and amplitude variation. A constellation diagram having one axis representing real and the other imaginary values of the complex number, allows easy formulation of symbols. The constellation diagram is shown in Figure B.9, where the complex numbers shown in Table B.1 are marked on it to demonstrate the significance and ease of constellation diagrams.

In the constellation diagram Figure B.9, the amplitude is the circle marked 1, 2 and 3, where as the phase angle is marked positive counter clock wise from 0 axis. This is an arbitrary constellation which has waveforms having amplitude as well as phase modulation.

Now consider some generic constellations commonly employed in Figure B.10. The polar plot is used to represent M-PSK, constellations. Consider the two dots called Binary PSK (BPSK), two phases

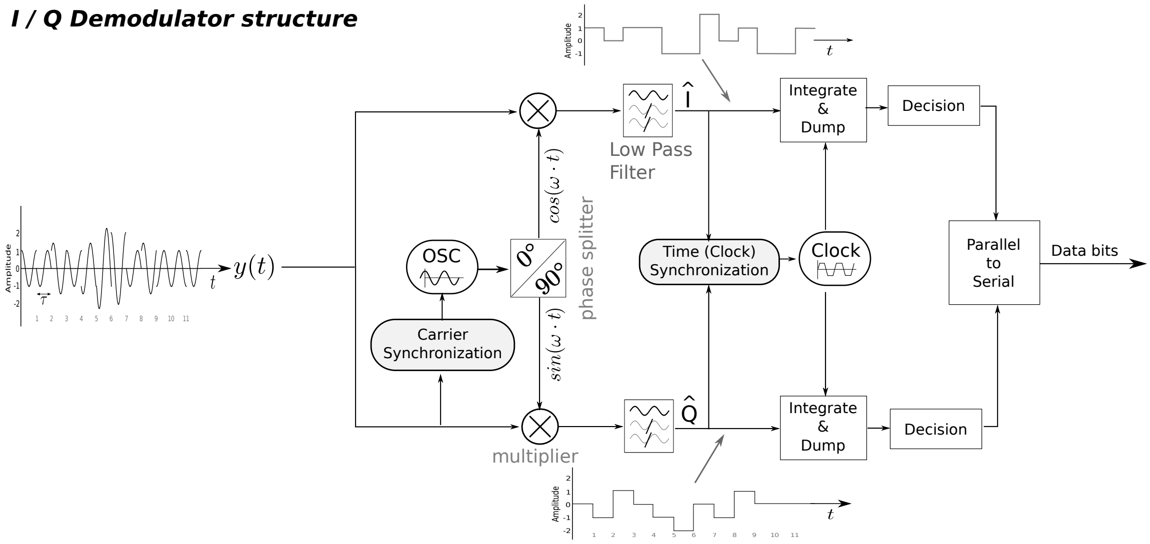

Fig. B.8 Simplified I/Q demodulator

representing 1 and 0. Consider the outer circle with square marks called Quadrature PSK (QPSK), it represents symbol of two bits grouped together i.e. 00, 10, 01, 11. And for the outer most circle star marked, 8-PSK, which can represent three bit groups i.e. 000, 001, 010, 011, 100, 101, 110, 111. Similarly, when the amplitude is also used to represent a variation, then quadrature amplitude modulation (QAM) constellation is formed, shown on the right side in Cartesian coordinate grid. The star marks represent constellation which is similar to QPSK, it can represent two bit symbols. The square marks represent 16-QAM, where four bits are used to represent one symbol i.e. 0000, 0001 ... 1111.

The combining of bits in to symbols supports higher bit transfer rate, measured in bits per second (bps). As can be inferred from the constellation diagrams, when BPSK sends 10 bps, QPSK can send 20 bps, and 8 PSK can send 30. However, as the constellation becomes packed, so does the complexity of decoding at the receiver and the manifestation of wireless channel significant, we shall talk more about it later.

It is easy to understand how the receiver takes decision with the help of constellation diagram. Lets consider the case of BPSK, QPSK and 8-PSK. We assume that the receiver is synchronised in time. The symbols have been marked, and the a_i and b_i value has been extracted. The magnitude and phase of the noise ridden symbols are shown with dull marks, which can be observed to be all over the place when noise levels are high as shown in BPSK but concentrated about the mean as shown in QPSK and 8-PSK. Occasional high noise effect is still observable. Note, that the decision boundary for BPSK is much relaxed than QPSK, which in turn is relaxed from 8-PSK. This shows, that for higher constellations, the signal to noise ratio requirement is also high, which is least for BPSK.

Symbol	(I) a_i	(Q) b_i	Ampl	Phase (deg)
x_1	1	0	1	0
x_2	0	-1	1	270
x_3	1	1	1.41	45
x_4	1	0	1	0
x_5	-1	-1	1.41	225
x_6	-1	-2	2.24	243.43
x_7	+2	0	2	0
x_8	0	-1	1	270
x_9	1	+1	1.41	45
x_{10}	-1	0	1	180
x_{11}	-1	0	1	180
x_{12}	1	0	1	0

Table B.1 Real part (I) and imaginary part (Q) for the waveforms Fig. B.7 in the form of a complex number $a_i + jb_i$. Corresponding constellation diagram in Fig. B.9.

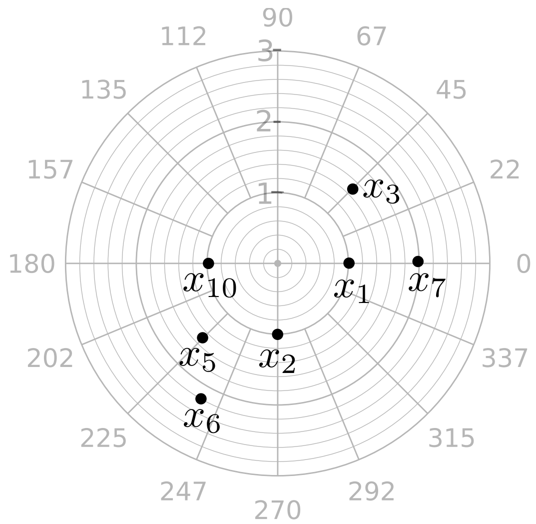

Fig. B.9 Constellation diagram with points representing the magnitude and phase as stated in Table B.1. Same points are not shown for clarity such as $x_3 = x_1$.

Signal constellation help in determining the impairments, which makes them a handy tool during design and testing of modulation demodulation schemes. A phase shift can easily be detected, when the whole constellation is shifted by that angle. A frequency shift means that the constellation is not static, and all symbols would rotated about a circle. When frequency shift is compensated, the rotation stops, and symbols align to a static position in the constellation.

B.1.6 Synchronization

In communications systems that are termed "coherent" the demodulator (receiver) requires a local carrier reference, whose phase should be a close approximation of that generated at transmitter. When the information being sent is in the form of digital symbols, a local symbol timing (clock) is also required, to control the sampling intervals.

There are several levels of synchronization. Besides carrier and symbol other problems include frame, word, code and packet synchronization. We discuss the carrier and symbol synchronization in this section. When an auxiliary signal is used to assist in achieving synchronization, the method is called data aided, other wise its called non-data aided. In data aided methods, a pilot symbol which is either an unmodulated carrier, or a sequence of alternating digital symbols is sent. In non-data aided methods, the structure of waveform is used for synchronization, for instance in the case of simple voltage levels, a crude but effective method is to keep a count between the level changes, corresponding to alternate bits.

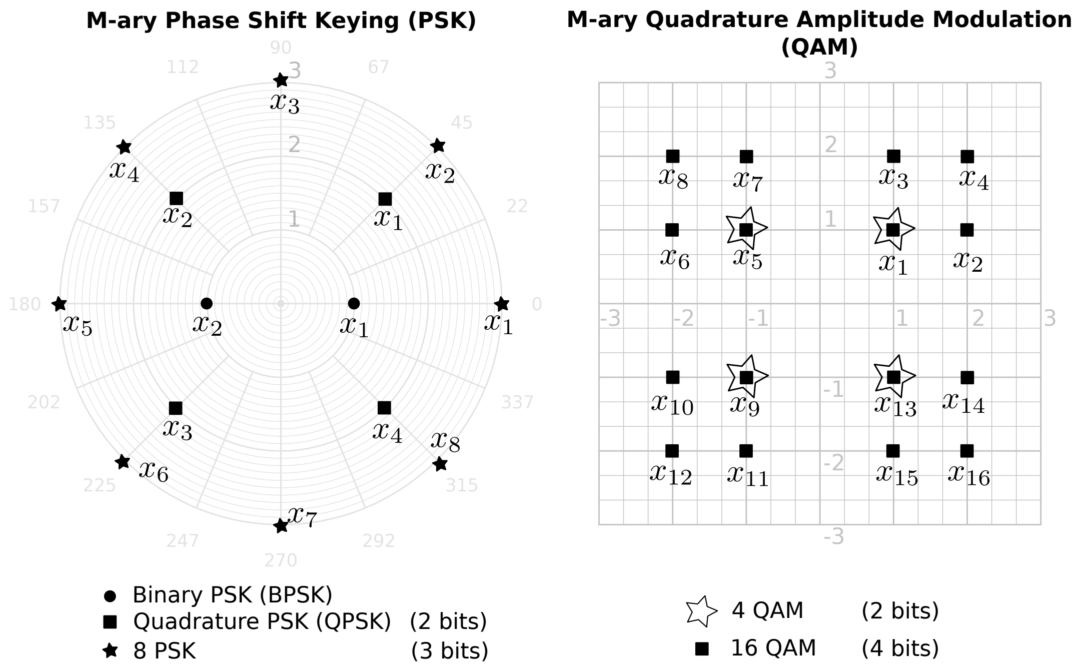

Fig. B.10 Common PSK and QAM constellations used in digital subscriber lines (ADSL) modems used in homes. BPSK requires two waveforms, QPSK requires four waveforms, and 8-PSK requires eight waveforms, 16 for 16-QAM. 2 bits combined to form a symbol can be represented by any one of the 4-QAM or QPSK waveforms.

Lets consider the **carrier synchronization** problem first. The problem is to replicate the local carrier as much as with the received carrier. Apart from the amplitude, the phase and frequency are the two parameters, which need to be synchronised. Lets consider the recovery process with the help of BPSK system. The received signal is of the form shown in Figure B.7, which can be stated in analytical form as follows;

$$y(t) = \pm A p(t) \cos(\omega_c t + \phi) \tag{B.4}$$

where $p(t)$ represents the pulse of duration τ. The local oscillator is to generate a carrier wave of the form

$$c_{lo}(t) = \hat{A} \cos \hat{\omega}_c t + \hat{\phi} \tag{B.5}$$

where $\hat{}$ means estimated values of the actual i.e. for the amplitude, phase and frequency of the local oscillator. The first step in demodulation is to extract the pulses representing data bits. The received signal with additional noise is multiplied with the local oscillator output, whose output has a lower frequency component and higher frequency component. The lower frequency components are at the baseband, which are extracted with the help of low pass filter (LPF). The signal after the filter, is of the following form.

$$d(t) = [(y(t) + n(t))c_{lo}(t)]_{lpf} = \pm \hat{A} p(t) \cos \varepsilon + n_d(t) \tag{B.6}$$

where $\varepsilon = \phi - \hat{\phi}$ and $n_d(t)$ is the demodulated noise. The simple analysis shows that the phase error reduces the signal by $\cos \varepsilon$ and the power by $\cos^2 \varepsilon$.

After the carrier is recovered, then the pulse needs to be integrated to estimate the average energy. This operation is called integrate and dump (I&D) in signal processing. Consider the rectangular pulse and the integration interval as shown in Figure B.11. The output of integrate and dump after one integration interval is reduced by a factor $(\tau - 2\zeta)/\tau$. For example a phase error in carrier recovery $\varepsilon = 18°$, which is 10% of 180° separation between two phasers, amounts to a power penalty of $\cos^2 18° \approx 0.5$ dB. Whereas for a timing error of 10% , $\zeta/\tau = 0.1$ results in a loss of $(1-0.2)^2 \approx 2.0$ dB. This also indicates that more severe penalty is observed for complex modulation schemes e.g. 16-PSK, 16-QAM. Unfortunately, the estimate of carrier and timing is also difficult to achieve with higher precision in these schemes.

Now we discuss some of the basic techniques to recover carrier in the case of BPSK. The carrier recovery can be implemented as shown in Figure B.14. This form is called open loop configuration. The frequency divider implementation is done using a loop back form called phase-locked loop (PLL). An alternative to the open loop is the closed loop configuration which is shown in Figure B.15.

Lets consider the **timing synchronization** problem, which recovers the symbol timing from the incoming signal. Lets consider the transmitted baseband signal as a pulse train is represented as

$$A(t) = \sigma_i A_i p(t - i\tau - D) \tag{B.7}$$

then its recovery follows the same method as its generation. A local clock generates the timing information in synchronization with the received signal. A clock is any signal $P(t)$, whose period is the same as symbol period τ, and whose zero crossings occur at $(i\tau - D)$, i.e.

$$P(t) = \sigma_i g(t - i\tau - D) \tag{B.8}$$

where g(t) is a pulse of duration less than the symbol duration τ. Thus like in carrier recovery, timing recovery is trying to reconstruct an unmodulated carrier waveform at the clock rate. A squaring loop method cannot work here, since $A^2(t)$ would be unity, where as zero crossings is desired.

A delay and multiply method would eliminate the above issue. The product of $A(t)$ with its delayed version $A(t - T_d)$ can provide necessary information to extract the clock. T_d is a fixed delay, whose value is chosen after experimentation and implementation. The product $M(t) = A(t)A(t - T_d)$ can be decomposed into a perioded and an aperiodic (random) component

$$M(t) = \tilde{P}(t) + R(t) \tag{B.9}$$

The periodic component $\tilde{P}(t)$ has harmonics at multiples of $1/\tau$ hence the tone at $f = 1/\tau$ can be filtered out to provide the basis of the clock. Further non linear processing is done to generate the clock. An alternative is to employ PLL and process its output to generate the clock. It is extensively used. A block diagram of the PLL based clock recovery method is shown in Figure B.16.

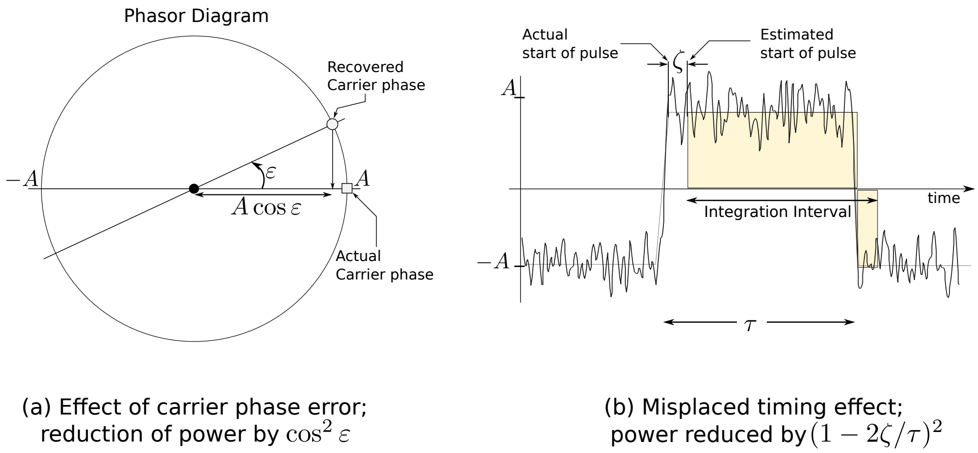

Fig. B.11 Effect of phase and timing error [247, p.497], on the power of received pulse.

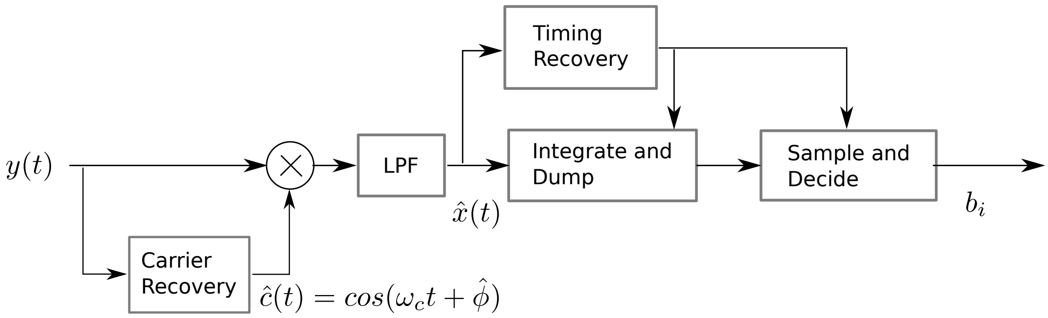

Fig. B.12 Simplified functional block diagram of synchronisation in BPSK.

It is obvious from the treatise above, that PLL plays an important role in synchronization. Also, the structure of receiver depends on the modulation / transmission scheme being employed. In all synchronisation techniques, an unmodulated wave is desirable. However, in some cases it can be overlooked. Therefore at the beginning of a transmission a pilot or synchronization symbol is sent for the receiver to synchronise and demodulate the data accordingly.

B.1.7 Phase-Locked Loop

Lets consider the functional block diagram of a PLL. The purpose is to keep the phase of the incoming signal clock and the local clock in phase, so that correct demodulation could be carried out. This architecture is called coherent means of detection, where the local oscillator of the same phase and frequency is used. There are three functional blocks of a PLL, a phase difference detector, a loop filter and a controllable oscillator.

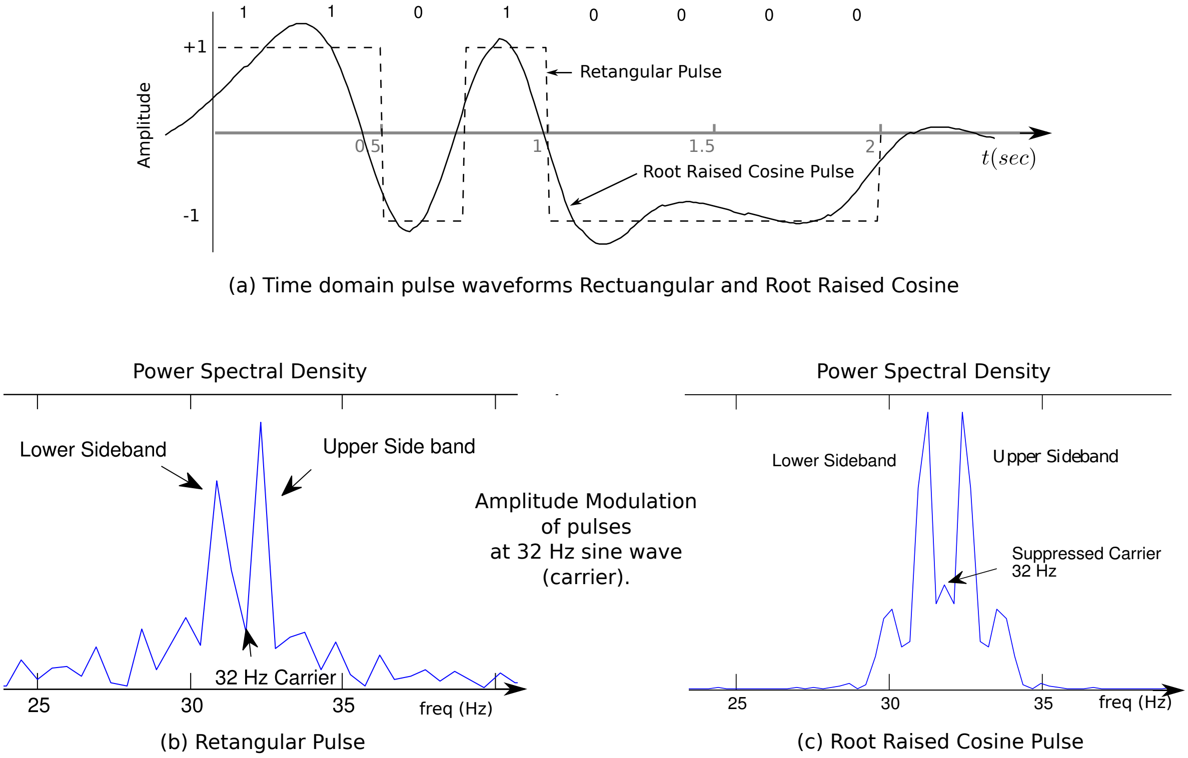

Fig. B.13 A crude comparison of rectangular pulse and root raised cosine shape on sideband suppression visible in passband amplitude modulation (double sideband).

A phase difference detector detects the difference between the locally generated clock and the incoming signal. Classically the output of the phase detector is the form of a voltage signal, which is the input to a voltage controlled oscillator (VCO)*. However, in our treatise, this differentiation is required at the implementation level. At functional level, the output of the phase detector is a number signifying the phase difference called phase error. The phase error can be positive or negative, changing abruptly as it is calculated instantaneously. A controller is required to cater to the abrupt variations in phase errors. This controller is in the form of a filter, whose purpose is to generate a signal for local oscillator, absorbing abrupt changes phase error.

It would not be fair to skip the transient behaviour. PLL operates in distinct modes of operations. The first is the acquisition mode, in which the incoming signal is not there, therefore, the local oscillator is made to run at a predefined frequency and phase. As soon as a reference signal is applied, the PLL tries to minimise the phase error, by adjusting the local oscillator output. In practice error can not be eliminated, but reduced to acceptable margins.

*Although in digital signal processing today a voltage controlled oscillator is not required, but a numerically controlled oscillator does the job, but most of the conventions have been retained from communications systems engineering texts, to ascertain their functionality.

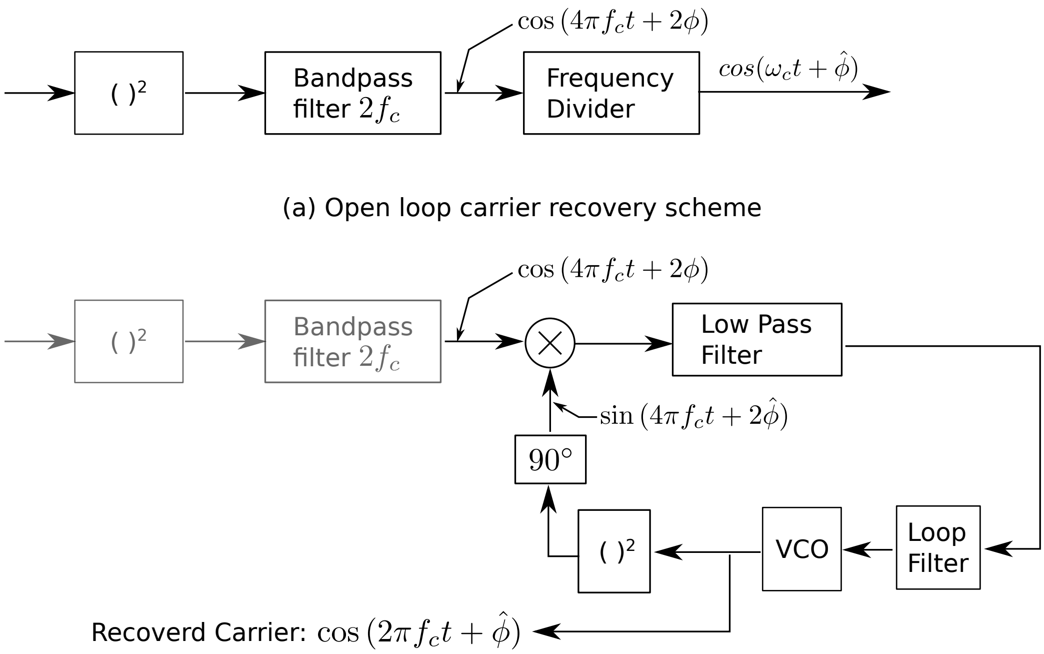

(a) Open loop carrier recovery scheme

(b An implementation using PLL to recover carrier for BPSK.

Fig. B.14 Functional block diagram of the carrier recovery in open loop configuration (a) and one of its implementation shown in (b).

After the lock is achieved, the PLL is shifted to a tracking mode. PLL is to track subtle changes in the phase error. An abrupt major change can make the PLL to lose its lock, making it to move again into acquisition mode.

There are particular parameters of interest to the designer, such as the time it takes to achieve a lock, the time it takes to lose the lock, the range of phase differences within which the lock is maintained, and the rate of change of phase difference to which the lock is maintained. It is also understood, that the noise level at the input plays a critical role in the performance of loop filter. So careful well designed loop filters play a critical role in the performance of the PLL, and directly on the overall receiver.

The complexities of PLL analysis, design, implementation as digital PLL and software PLL is well discussed by Gardner [79] and Best [202]. A note is required, the PLL requires a reference signal preferably an un-modulated wave with 50% duty cycle. So it cannot be used as it is in digital modulation schemes, where the carrier is suppressed, in other words, the recovery information is hidden.

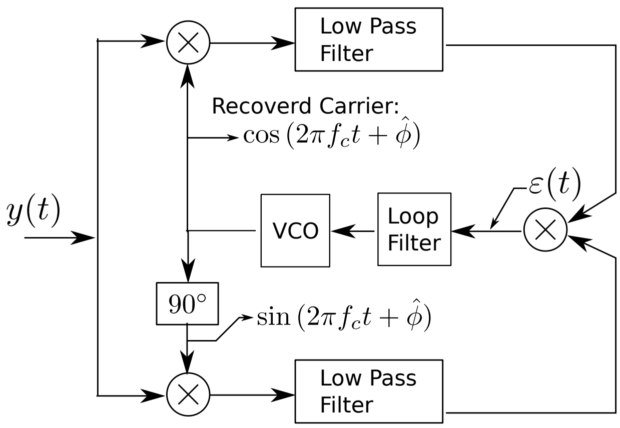

Fig. B.15 An alternative carrier recovery scheme for BPSK, called the Costas Loop.

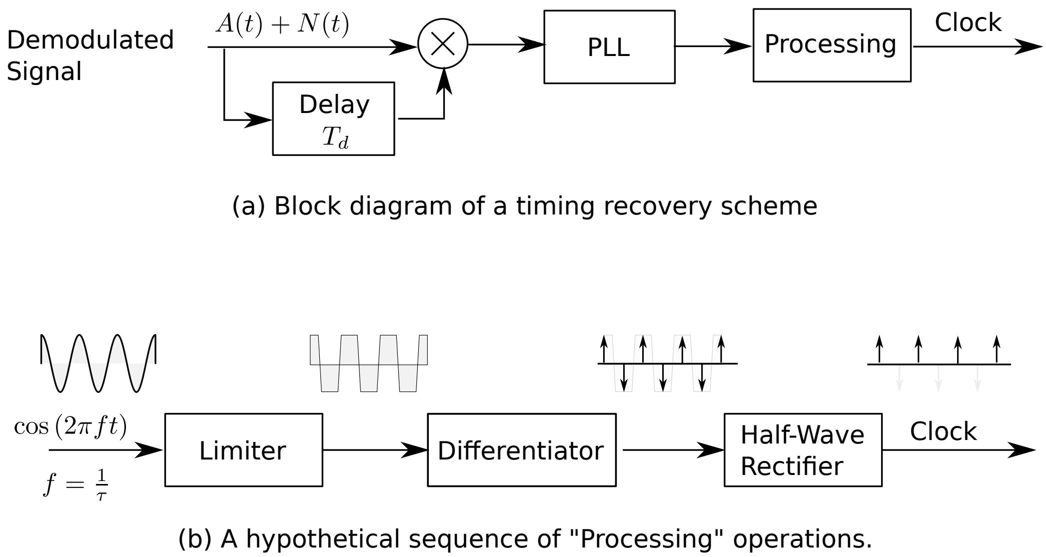

Fig. B.16 An alternative carrier recovery scheme for BPSK, called the Costas Loop.Clock recovery scheme for rectangular baseband signal. (a) PLL is used to generate a clock

B.2 Wireless Communications Channels : Fading Type Channels

A communication channel represents a physical medium (such as air, water, ionized gas) between the transmitter and the receiver. The channel model is a representation of the input-output relation of the channel in mathematical or algorithmic form. This model is derived either from measurements or is based on the theory of physical propagation phenomenon. Measurement based models lead to an empirical characterization of the channel in time or frequency domain and often involve statistical descriptions in the form of random variables or random processes. The parameters of the underlined distributions and power spectral densities are usually estimated from measured data. While measurement based models instill a high degree of confidence in their validity, however, the resulting empirical models often prove to be unwieldy and difficult to generalise unless extensive measurements are collected over the appropriate environment . For example, it is difficult to use measurements taken in one urban location unless a substantial amount of data is collected over a wide variety of urban locations and the necessary underlined theory is available to justify extrapolating the model to new locations.

Developing mathematical models for the propagation of signals over a transmission medium requires a good understanding of the underlying physical phenomenon. For example, to develop a model for an ionospheric radio channel, one must understand the physics of radio wave propagation (magneto ionic theory [212, 216, 294, 213] and references therein). One of the challenges in channel modelling is the translation of a detailed physical propagation model into a form that is suitable for simulation. Similarly, a fundamental understanding of optical sciences is needed to develop models for single mode and multi mode optical fibres.

Communication engineers rely on experts in the physical sciences to provide the fundamental models for different types of physical channels. For example, the mathematical model of a radio channel may take the form of Maxwell's Equation (as is the case in magneto ionic theories). While accurate, this model must be simplified and converted to a convenient form, prior to using it for simulation.

Physical communication channels such as wires, waveguides, free space and optical fibres often behave linearly . Some channels such as the mobile radio channels while linear, may behave in a random time-varying manner. The simulation models of these channels fall into one of the following two categories:

- Transfer function models for time-invariant channels.
- Tapped Delay line models for time-varying channels.

Transfer function models can be modelled into either time domain or frequency domain using finite impulse response (FIR) or infinite impulse response filters (IIR) . Empirical models in the form of measured or synthesised impulse or frequency responses are usually simulated using FIR techniques , whereas, analytical expressions for the transfer functions are easier to simulate using Infinite Impulse Response (IIR) techniques .

Simulation models for random time varying (fading channels) take the form of tapped delay lines with tap gains and delays that are random processes . Time varying channels require a number of special conditions while simulating the performance of a communication system. The methodology used depends on the objective of the simulation and whether the channel is varying slowly or rapidly with respect to the signals or subsystems that are being simulated. Another important factor is the relationship between the bandwidth of the applied signal and the bandwidth of the channel. The complexity of a useful channel model is a function of both the time and frequency characteristics of both the source and the channel.

In this article the focus is ionospheric channel model for mobile satellites having inter-satellite links. Before the details of the underlying physics is described, the basic theory of multi path fading is discussed from modelling point of view.

B.2.1 Fading Channel Types

Sklar [210, 211] defines the types based on stochastic properties of the channel. Bello [55] characterised the channel based on time and frequency transfer functions which are interlinked depicted in Figure B.18a, each of which provides an insight to the underlying behaviour in the respective domains. This insight has allowed us to better design the mobile communications systems, to support high data rates.

The "large scale fading" is a variation in the envelope of the received signal, generally determined by the path loss. When the variation in the envelope of the signal is of the order of wavelength, then it is called "small scale fading". It is the small scale fading that causes severe degradation in digital modulation schemes which manifests itself both in time and frequency domain (Figure B.18b). The end manifestation can be stated as either frequency selective, non frequency selective (flat), fast and slow fading. Flat fading is the type when the channel frequency response is flat over the used bandwidth (symbol bandwidth). It is the designers intention to design the baseband signals in such a manner, that the frequency selective fading appears to be flat for the duration of symbol transmission.

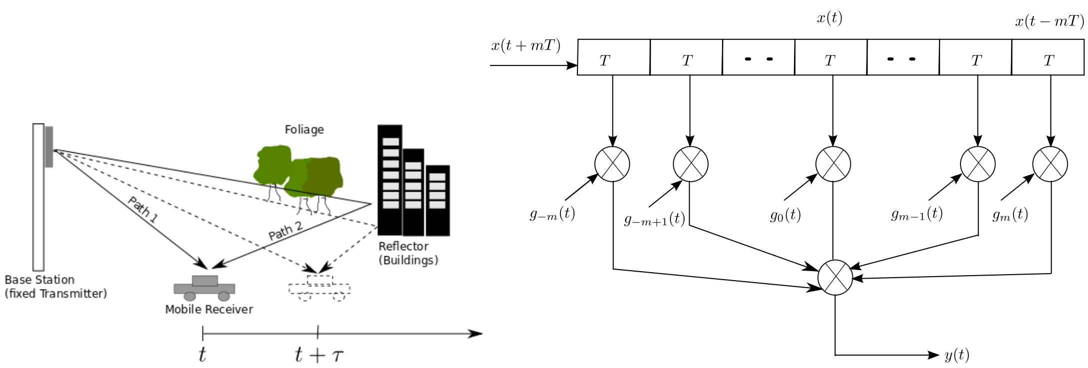

(a) Multipath on Terrestrial links.

(b) Tapped Delay Line model.

Fig. B.17 Multipath physical channel and its simulation model.

In the fading channel, when there is no direct line of sight component present, then the fading gain is governed by the Rayleigh probability distribution function, whereas, when there is a strong line of sight component present, the stochastic properties are governed by Rician distribution functions. The performance of the system is better in the presence of a line of sight component as compared to indirect multipath propagation environment.

To understand the performance, the probability of bit error ($P_b(\gamma)$) should be least for the given E_b/N_0 ratio. So a transmission scheme is to perform better if the bit error rate is better for the same E_b/N_0 ratio.

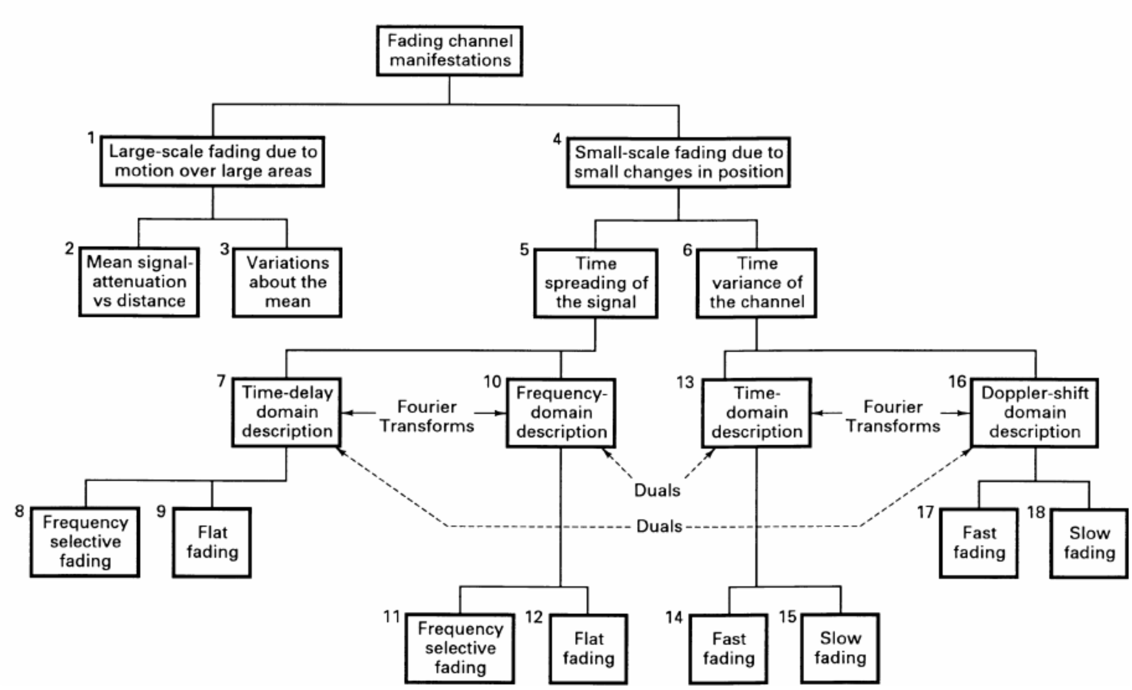

(a) Fading channel classification [74].

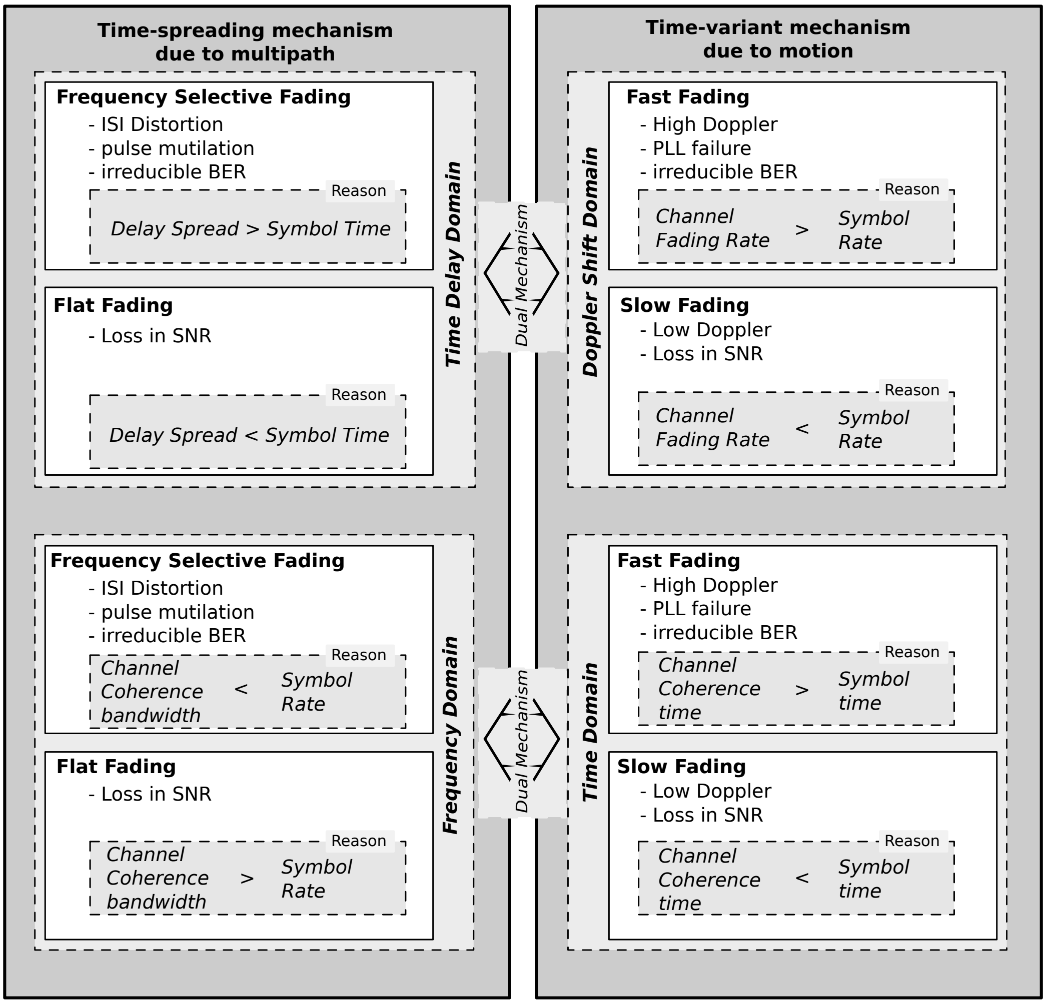

(b) Small scale fading channel manifests [211].

Fig. B.18 Fading channel classification and manifestation

To illustrate the marked difference three channels are used, additive white Gaussian noise (AWGN), Rayleigh and Rician fading models, in Figure B.20. The effects of the channel model are clearly visible, poorest performance in Rayleigh channel ("awful curve"), slightly better in Rician ("poor curve") and AWGN ("bad curve") is the best amongst themselves. Therefore, AWGN is considered the benchmark. The difference in performance also highlights the importance of the appropriate selection of channel models for performance evaluation of modem.

B.2.2 Distribution Functions

Although direct line-of-sight (LOS) radio propagation between the terminals, transmitter, and receiver occurs in the ionosphere – mostly for satellite–land and satellite–satellite communications; multi-diffraction, multi-reflection, and multi-scattering effects are usually observed owing to obstructions in the form of natural and artificial plasma structures. These plasma density irregularities cause additional losses compared to those observed when the ionospheric plasma is a uniform, homogeneous, regular-layered medium, and also cause multipath fading of the signal strength/intensity observed at the receiver.

The amplitude and phase variation is statistically given as probability distribution function (pdf). The following pdf are mentioned in literature.

Slow Fading The slow fading of radio signal also known as large-scale fading in mean signal level, tends to be log-normally distributed (expressed in decibels, dB) with a standard deviation depending on the degree of perturbation of the ionospheric region along the radio path.

The Gaussian or normal distribution of a random variable x representing the signal strength or voltage by introducing the following probability density function (PDF) of the received signal random level x:

$$PDF(x) = \frac{1}{\sqrt{2\pi\sigma^2}} \exp\left(-\frac{(x-\bar{x})^2}{2\sigma^2}\right) \tag{B.10}$$

where $\bar{x} \equiv < x >$, is the mean value of the random signal level and $\sigma^2 = < x^2 - \bar{x}^2 >$ is the variance or time-averaged power in dB.

Fast Fading Small scale fading is observed over distances of about half or one wavelength. Ionospheric channels are usually dynamic channels. In the case of dynamic multipath situation in which either the terminal antennas are in movement or the plasma structures move because of wind and ambient electrical and magnetic fields, the spatial variations of the resultant signal at each receiver will be seen as temporal variations. The fast fading due to ionospheric channel is stated by Rayleigh PDF and CDF.

The Rayleigh distribution describes the signal's spatial and temporal fast fading, and is defined as;

$$PDF(x) = \frac{x}{\sigma^2}\,\exp\left(-\frac{x^2}{2\sigma^2}\right), \qquad \forall\, x \geq 0 \tag{B.11}$$

The Rayleigh cumulative distribution function (CDF)

$$CDF(x) = prob(x \leq X) = \int_0^X PDF(x)\,dx = 1 - \exp\left(-\frac{X^2}{2\sigma^2}\right) \tag{B.12}$$

The Rician distribution is used when direct line of sight (LOS) path is clear in addition to multiple copies received due to forward scattering. The PDF is defined as

$$PDF(x) = \frac{x}{\sigma^2}\,\exp\left(-\frac{x^2 + A^2}{2\sigma^2}\right) \cdot I_0\left(\frac{Ax}{\sigma^2}\right) \quad \forall \quad A > 0,\, x \geq 0 \tag{B.13}$$

where A denotes the peak strength or voltage of the dominant component envelope and $I_0(\cdot)$ is the modified Bessel function of the first kind, zero-order. To estimate the contribution of each component dominant and multiple copies, for the resulting signal at the receiver, the Rician parameter K is introduced which is defined as

$$K = \frac{\text{LOS component power}}{\text{Multiple components power}} \tag{B.14}$$

The Rician factor can be rewritten as

$$K = \frac{A^2}{2\sigma^2} \tag{B.15}$$

Using the Rician factor the Rician PDF can be written as follows, from [184, pg.133];

$$PDF(x) = \frac{x}{\sigma^2}\,\exp\left(-\frac{x^2}{2\sigma^2}\right) \cdot \exp(-K) \cdot \left(\frac{x}{\sigma}\sqrt{2K}\right) \tag{B.16}$$

It should be noted that the Rician distribution is a general form, where when K is dominant then the distribution is Gaussian, where as when there is no dominant line of sight signal, then the distribution becomes Rayleigh, as illustrated in Figure B.19.

B.2.3 Relationship of K factor with Scintillation

The fading studied by two groups namely the ionosphere scientists and communications engineer, use two different terminologies.

Shaft [295] clarified the relationship of five different scintillation indices used in literature, with the probability distribution function the Rician probability density function, whose parameter K the Rician factor, which is also known as Nakagami-m pdf.

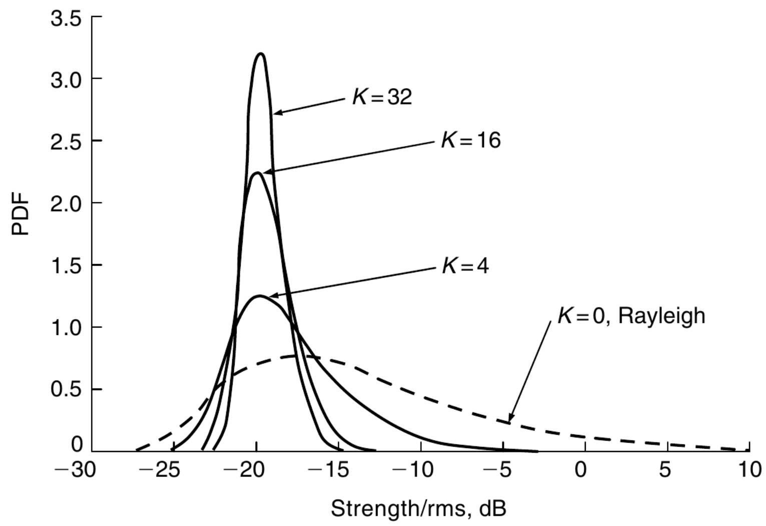

Fig. B.19 Rician distribution versus the normalised signal strength covering the Rayleigh PDF for $K = 0$ from [184, ch.4].

The conversion of scintillation index is accomplished in two steps

1. the scintillation index is related to the n-parameter of the Nakagami-m distribution, and then
2. the Nakagami-m distribution is related to the Rician distribution

The purpose here is to bring the results together in the context of communication theory.

The Nakagami-m distribution is defined by

$$p(R) = \frac{2m^m R^{2m-1}}{\Gamma(m)\Omega^m} \exp\left(\frac{m}{\Omega} R^2\right) \tag{B.17}$$

where

$$\begin{aligned} \Omega &= \bar{R^2} \\ m &= \frac{(\bar{R^2})^2}{(R^2 - \bar{R^2})^2} \geq \frac{1}{2} \end{aligned} \tag{B.18}$$

This distribution was derived by Nakagami [296] as an approximation to the Rician distribution. Computer evaluation has indicated that the agreement is excellent between the 1 and 99 percent points.

Chytil has shown that the scintillation index termed S_4 is mathematically related to the m-parameter through

$$m = \frac{1}{S_4^2} \tag{B.19}$$

Furthermore, the various scintillation indices are defined and approximately related (defined) as follows [59];

$$
\begin{aligned}
S_1 &:= \frac{\overline{|R-\bar{R}|}}{\bar{R}} \simeq 0.42\ S_4 && \text{(B.20)}\\
S_2 &:= \left[\frac{\overline{(R-\bar{R})^2}}{\bar{R}^2}\right]^{1/2} \simeq 0.52\ S_4 && \text{(B.21)}\\
S_3 &:= \frac{\overline{|(R-\bar{R})^2|}}{\overline{R^2}} \simeq 0.78\ S_4 && \text{(B.22)}\\
S_4 &:= \left[\frac{\overline{(R^2-\bar{R}^2)^2}}{\bar{R}^2}\right]^{1/2} && \text{(B.23)}\\
S_5 &\triangleq \frac{R_{max}-R_{min}}{R_{max}+R_{min}} \simeq 0.78\ S_4 && \text{(B.24)}
\end{aligned}
$$

where $R_{max},\ R_{min}$ are the third largest and smallest excursions.

The Nakagami-m distribution and the Rician distribution are related by

$$\gamma = \frac{(m^2-m)^{1/2}}{m-(m^2-m)^{1/2}} \tag{B.25}$$

Consequently the scintillation index S_4 and the ratio of the specular to random power are related through

$$\gamma = \frac{(1-S_4^2)^{1/2}}{1-(1-S_4^2)^{1/2}} \tag{B.26}$$

Therefore the theoretical models of scintillation and the measured values of scintillation are thus expressed in terms of meaningful to the communications engineer.

B.2.4 Mitigation Techniques in Fading Channels

When the channel introduces signal distortion as a result of fading, the system performance can exhibit an irreducible error rate at a level higher than the desired error rate[211] . In such cases, no amount of E_b/N_0 will help achieve the desired level of performance, and the only approach available for improving performance is to use some other form of mitigation to remove or reduce the signal distortion.

The mitigation method depends on whether the distortion is caused by frequency selective fading or fast fading. Once the signal distortion has been mitigated the performance curve can transition from the "awful" to merely "bad" curve. Next, it is possible to further ameliorate the effects of fading and strive to approach AWGN system performance by using some form of diversity to provide the receiver with a collection of uncorrelated replicas of the signal and by using a powerful error-correction code. Figure B.21 acts as a guide for ameliorating the effects of fading.

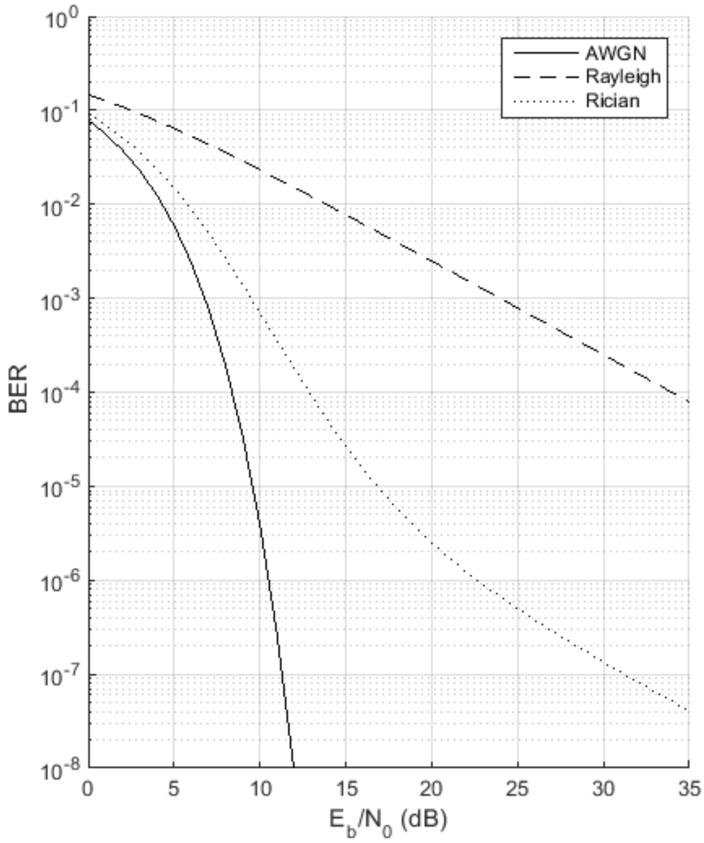

Fig. B.20 Bit error probability for AWGN ("bad"), Rayleigh ("worst") and Rician ("poor"), using theoretical expressions, simulated using BERTool in MATLAB [68].

The modulation type for a fading does not allow amplitude shift keying or quadrature amplitude modulation as they are inherently vulnerable to performance degradation in a fading environment. Thus for fading environment, the preferred choice for a signalling scheme is frequency or phase based modulation type. M-ary of 2 or 4 is practically useable, owing to the rapid and high phase distortions observed in fading channels caused by rapid motion[211].

In order to mitigate the fast fading distortion, non-coherent or differentially coherent modulation scheme that does not require phase tracking, and that reduces the detector integration time are used. Another method is to increase the symbol rate $1/T_{sym}$ such that it is greater than the fading rate $f_d \approx 1/T_0$, by adding signal redundancy, as is practiced in orthogonal frequency division multiplexing (OFDM) symbol generation.

In a conventional single carrier system, complex equalisation schemes are adopted to combat frequency selective fading. The ideal equaliser has a frequency response that is the exact inverse of that of the channel. This usually entails an infinite number of equaliser taps. What is worse, noises inflicted on the signal can be enhanced through the equaliser when a deep fade occurs. As a result even with the best equalisers a deep fade can still result in communication link failure in single-carrier systems [208]. The first proposal to use parallel data transmission to combat fading channels was published in around 1967 [297] and at Bell Laboratories [248], where OFDM theory had been established by 1968 [249]. In doing so, a small number of sub-channels used carriers that fell within deep faded frequency band, thus overcoming complete link outage.

However, the limited electronics and lack of digital processing systems, the technology was not widely accepted till the 90's, where processing technology improved and digital implementation was made possible in the form Multi-Carrier Modulation (MCM)[298].

Fast fading typically degrade OFDM by corrupting the orthogonality of the sub-carriers. A filtering technique [211] is used to provide time-domain shaping and partial-response coding, to reduce the spectral side lobes of the signal set and thus help preserve its orthogonality. The process introduces known inter-symbol-interference (ISI) and adjacent channel interference (ACI), which are then removed by a post processing equaliser and a cancelling filter. For high number of sub-carriers this filter is not required.

Error detection and correction can provide another type of gain, not by increasing the bit energy, but correcting the errored bits, thus improving the overall error rate, hence called coding gain. To utilise this benefit, the errors out of the de-modulator should be uncorrelated, which generally are, or an interleaver can be incorporated into the system design.

The mitigation approaches used when designing a system thus are considered in two steps;

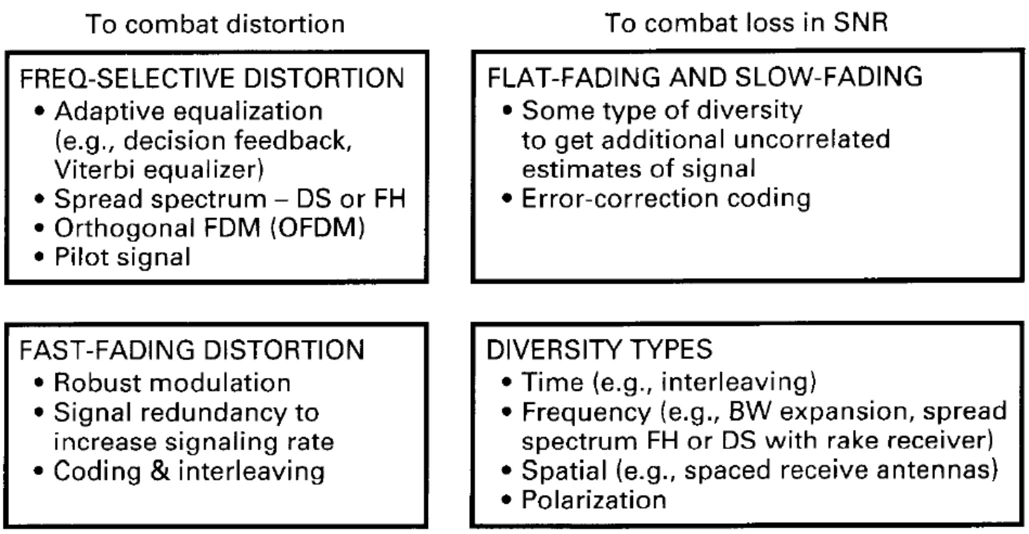

Fig. B.21 Small scale fading channel mitigation techniques adopted to improve system performance [211].

1. first, choose the type of mitigation to reduce or remove any distortion degradation;
2. next, choose a diversity type that can best approach AWGN system performance.

B.2.5 Modelling Multi path Fading Channels

Modelling an outdoor mobile channel is usually carried out as a two-step process which represents large-scale (macro) and small-scale (micro) effects of multi path and associated fading [66]. Large scale fading represents attenuation or path loss over a large area, and this phenomenon is affected by prominent terrain features like hills, buildings, etc., between the transmitter and the receiver . In terrestrial mobile communications, the receiver is often hidden or shadowed by such terrain features, and the statistics of large-scale fading provide a way of computing the estimated signal power or path loss as a function of distance. Small-scale fading deals with large dynamic variations in the received signal amplitude and phase as a result of very small changes in the spatial separation between the transmitter and the receiver

There are three mechanism that affect the quality of the received signal in a mobile channel: reflection, refraction and scattering. Reflection occurs when the radio wave impinges upon a large, smooth surface (water or large metallic surfaces), where large means as compared to the wavelength. Diffraction takes place when there is an obstruction in the radio path, causing secondary radio waves to form behind the obstruction. This phenomenon makes it possible to communicate when there is no line of sight (direct) path between transmitter and receiver and is known as shadowing. The third effect, scattering, results from rough surfaces whose dimensions are of the order of the wavelength, which causes the reflected energy to scatter in all directions.

While electromagnetic theory offers very complex models for these phenomena, it is possible to use simpler statistical models for the input-output relationship in a mobile channel. Specifically, the low pass equivalent response of a mobile channel can be modelled by a complex impulse response having the form

$$h(\tau,t) = \left\{ \left[\frac{k}{d^n} g_{sh}\left(p(t)\right) \right]^{1/2} \right\} \tilde{c}(\tau, p(t)), \quad d > 1km \tag{B.27}$$

where the term in braces models the large-scale fading and $\tilde{c}(\tau, p(t))$ accounts for the small scale fading as a function of position $p(t)$ at time t. The constant $K = -10\ log_{10}(k)$ is the median dB loss at a distance of 1 km. Typical the value of K is of the order of 87 dB at 900 MHz, d is the distance in meters between the transmitter and receiver, and the path loss exponent n has value of 2 for free space, and between 2 and 4 for most mobile channels, with higher values applying for obstructed paths . The factor $g_{sh}(p(t))$ accounts for shadowing due to buildings, tunnels, and other obstructions at a given location $p(t)$, and $G = 10log_{10}(g_{sh}(p(t))$ is usually modelled as a Gaussian variable with a mean of 0 dB and a standard deviation of 6 to 12 dB depending on the environment. This model is called log normal shadowing model . The path loss is expressed commonly as;

$$L(d)_{dB} = L(1km)_{dB} + 10nlog(d) + X_{\sigma} \tag{B.28}$$

where X_{σ} is a zero mean Gaussian variable with standard deviation of 6 to 12 dB.

In eq.(B.27), $c(\tau, p(t))$ represents the complex low pass equivalent impulse response of the channel at position $p(t)$, and the local multi path and fading that will result from small spatial displacements around the location $p(t)$. The path loss associated with large-scale fading, represented by the term in braces in eq. (B.27), as well as fading due to shadowing, changes very slowly as a function of time at normal vehicular speeds compared to the rate of change of $c(\tau, p(t))$. Hence the channel attenuation due to large-scale fading and shadowing may be treated as a constant within a small local area, and the large-scale effect on system performance is reflected in the average received signal. The dynamic behaviour of receiver subsystems such as tracking loops and equalisers, as well as the bit error rate of the system, will be affected significantly by the small-scale behavior modelled by $c(\tau, p(t))$.

B.3 Matlab Script to generate Multipath Profile

The path delays, and the attenuation based on inverse square frequency law, is used to determine a path profile. The problem geometry is depicted in Figure 5.10. The path profile for a single reflector is determined from the following code. In an iterative loop, it can easily find the values for all reflectors. The phase angle, needs to be given. We assumed equally distributed reflectors, and find the path lengths and attenuation for one half hemisphere. This makes up for the path profile.

```
%%
clear
close
%%
c = 300e6; % speed of light
f = [430e6;900e6;2400e6]; % operating frequency in Hz
z = c/f; % wavelengths
w = 2.*pi.*f; % operating freq in radians
n_samp = 20;
n_wavelengths = 10;
t = linspace(0,1/2*f,500); %
phi = 0.0; %
Amp = 1.0; % 1 Volt rms

% the radius of the circle representing the direct path range.
```

```
% d = [100 500 1000 100e3 200e3 300e3 400e3 ]
d = 1000;
% theta = randi(180,8,1).*pi/180.0;
% equally spaced angle for the placement of reflectors along
% the circumference. 8 discrete reflectors assumed
theta = linspace(0,180,8).*pi/180;
%% for the ith frequency lets evaluate the
ii = 1;

%Determine the path length from the
a = d.^2 + d.^2 - 2.*d.*d.*cos(theta);
d1 = sqrt(a);
p1 = d+d1;
t1 = p1./c;

p0 = d;
t0 = p0./c;

Lp = (4.*pi.*p0.*f(ii)./c).^2; % Path Loss
Amp0 = Amp./Lp
%x = (Amp./Lp).*sin(w(ii).*(t(ii,:)-t0)+ phi); %
%figure(1); plot(t(ii,:),x);
% Path loass
Lp1 = (4.*pi.*p1.*f(ii)./c).^2;
Amp1 = Amp./Lp1;

% Path delay
delay = t1 - t1(1)

% Normalized path gains with respect to direct path
atten = Amp1./Amp1(1);
atten_dB = mag2db(atten)
profile = [delay atten_dB]
stem(delay, atten_dB)
```

B.4 Experimental Verification of Reflections from 3U CubeSats

This experiment highlights the relationship of operational frequency (wavelength) and the reflected signal power from a surface area (radar cross section area) the size of a 3U CubeSat; to emulate the scenario when several tens or hundreds of sensors are deployed in close proximity of each other. A continuous wave (CW) signal transmitted in the direction of the object is measured for its reflected power at the receiver, for the relevant frequencies i.e. 400 MHz, 900 MHz, and 2400 MHz. Since inhouse equipment was available for 900 MHz and 10 GHz, therefore, the experiment is conducted for these two frequencies instead.

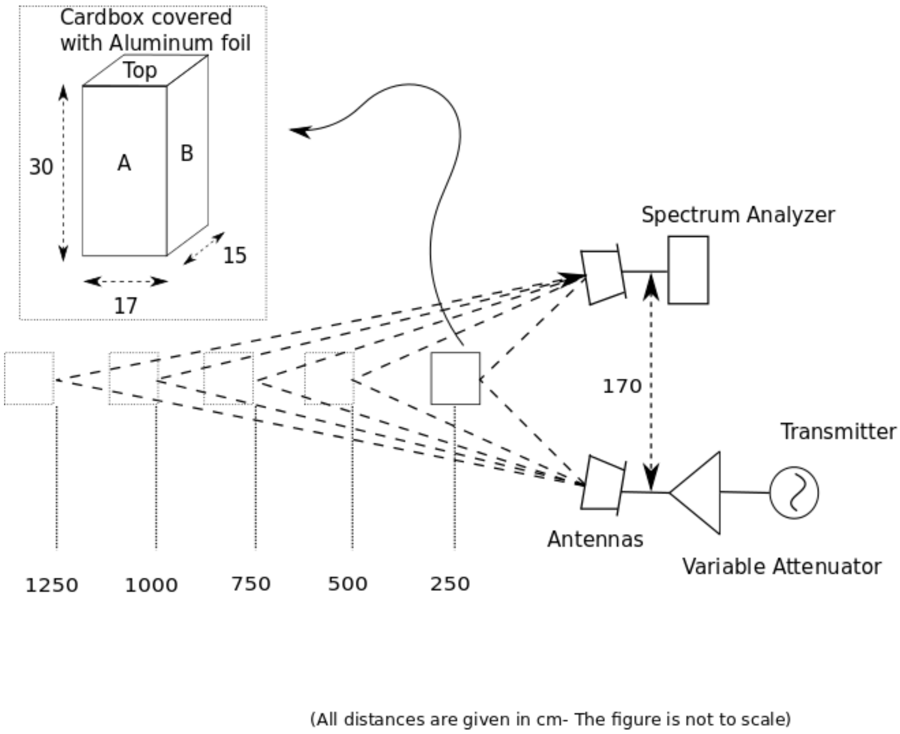

(a) Block diagram of experimental set up

(b) Field Set up

Fig. B.22 Experiment to quantify reflected power at frequencies 10 GHz and 900 MHz, from 3U CubeSat like structures.

A transmitter, the object and a spectrum analyser (acting as receiver) is set up as shown in Figure B.22a. A rectangular cardboard box covered with aluminium foil acts as the reflector, whose dimensions are shown in Figure B.22a. A continuous wave is generated using a signal generator for 900 MHz attached to a Yaggi-Udda type directional antenna. A spectrum analyzer attached to a similar Yaggi-Udda antenna acts as its receiver. The generated RF power can be controlled for this source.

For 10 GHz an inhouse training kit is used as a continuous wave source. It radiates using a horn antenna. A downconverter for the 10 GHz is used before the spectrum analyzer to act its receiver. In this setup, the transmitter power is unknown but can be controlled using builtin attenuator. We shall be able to measure at two different transmit powers. At the receiver, the difference will give us a good approximate of the reflected power.

The experiment is setup in open field away from other metallic objects in its vicinity. The field set up of the experiment is shown in Figure B.22b. Ideally a frequency sweep would have been best suited for this purpose, but unavailability of a wide bandwidth antenna prohibited a frequency sweep from 900 MHz to 10 GHz.

The transmitter and receiver are placed apart, in a manner that spillover power is not received. This is ensured by monitoring the signal level on the spectrum analyser, by keeping the transmitter antenna fixed (at right angle to the receiver antenna but directed towards the object), and rotating the receiver antenna. Starting from the direction of the transmitter then rotating clockwise, constantly monitore the receive signal. If any received signal is detected, the separation distance between transmitter and receiver is increased. It is also ensured that when the transmitter is off, there is no stray signal being picked up by the receiver. In this manner, any detected power, would be the one reflected from the object.

Table B.2 In-house equipment used in experiment.

Freq (GHz)	Antenna	Transmitter	Tx-Rx distance (cm)	Rx Attenuation (dB)	Tx Attenuation (dB)
10.351	Horn	Gunn Oscillator @7.6 V	170	10	10 – 20
0.900	Yagi-Udda	Vector Signal Generator	170	10	10 – 20

The available spectrum analyser could not read significant power above its noise floor for the 900 MHz when the object is illuminated with CW signal. Whereas directing the 900 MHz transmitter towards a metal air duct at the back , measurable reflected power was read on the spectrum analyser. This means that the object selected has a smaller surface area, and the reflected signals are so weak at 900 MHz transmission, that they are not detectable by the spectrum analyser. However, measurements could be made with a sensitive receiver.

Whereas, at 10 GHz the reflected power could be measured. The object was rotated, to determine the values of reflected powers from different sides. The received power for different sides of the object are given in Table B.3. This highlights the effects of rotating objects with uneven surfaces acting as reflectors.

Table B.3 Object Power Profile at distance of 250 cm

Sides	Side A	Corner A,B	Side B	Top
Rx Power (dBm)	-51	-65	-61	-56

For the 10 GHz transmitter, there was no setup to measure the transmitted power, however, by placing an attenuator in the waveguide, the reflected powers for two different attenuation were measured. The measured power levels after reflection from the object are recorded in Table B.4.

Table B.4 Results of experiment to determine the reflected power at 10 GHz.

Object Distance	Reflected Power (dBm)	
(cm)	10 dB att	20 dB att
250	-50.6	-59.9
500	-53.4	-62.8
750	-57	-66.6
1000	-60	-70
1250	-66	< -70

As a result of the experiment outlined above the following observations could be made:

- The radio receiver sensitivity level dictates what is the minimum power level it can sense. The spectrum analyser used for this experiment had a noise floor at around -70 dBm, which is far higher than of typical radios with noise floor at -100 dBm.
- The wavelength of the frequency should be comparable with the reflectors physical dimensions. That is why smaller wavelength of 10 GHz was easily reflected back. Whereas for 900 MHz, a larger size was required to detect the same strength signal. This also confirmed that the size of surface area should be comparable to wavelength 0.33 m for 900 MHz, whereas the object was 0.3 m high and 0.1 m wide.
- It can be safely deduced, that if frequencies less than 500 MHz are to be used, then CubeSat type structures cannot act as contributing reflecting surfaces, however, they may contributed minutely at frequencies above 1 GHz.

Appendix C

C.1 MATLAB script to solve the spring-mass problem

A MATLAB code which works in OCTAVE as well, is written to solve the coupled equations of motion for three masses attached at one end of a spring problem as discussed in section 4.2.2. The second order ODE are converted to first order ODE using the steps outlined in [200], and are entered in MATLAB following its online help / examples.

The script comprises of separate ODE solvers for each mass stated as `diff_springmass01(t,f)`, `diff_springmass02(t,f)`,`diff_springmass03(t,f)` which operate on passing the values of position `r1, r2, r3` and velocity `v1,v2,v3` of each of the three mass. The equivalent value of stiffness coefficient of two parallel springs is used denoted as `k1,k2,k3`.

The damping factor is represented with the variable `gamma1, gamma2, gamma3`, to incorporate the friction two sliding anodized metal surfaces i.e. CubeSat sliding inside P-POD.

Since the numerical problem assumes that the system is oscillatory, therefore, oscillating position and velocities are observed see Figure 4.7. However, in our case, as soon as the springs are decompressed, they lose contact, therefore no more force is applicable. The condition to find velocity of each CubeSat, is to determine the time, when springs have decompressed completely i.e. when the distance covered is equal to the value of l_c .

More complicated scenarios can be evolved or solved from this simple problem. For instance, incorporating the velocity of baseplate within the initial conditions of the system. Adding different values within predefined tolerance values, for the spring constant, the compressed lengths, and the length of CubeSat sliding or changing the values of mass.

C.1.1 The Script to Solve ODE

The script consists of two main functions. One is the ODE function in which first order ODEs are stated. The second is the main script, which calls the ODE function. The `function dfdt=diff_springmass03(t,f)` should be saved in a separate file called `diff_springmass03.m`, and the main script as a separate file called `main.m`. Both files should be in the same directory to execute. Run the main file either in debug mode or otherwise. The plots should be generated. The result of position and velocity of each CubeSat is in the Vector `Y`.

```
%%%%%%%%%%%%%%%%%%%%%%%%%%%%%%%%%%%%%%%%%%%%%%%%%%%%%%%%%%%%%%%%%%%%%%%%%
%% Save in separate file called diff_springmass03.m
%%%%%%%%%%%%%%%%%%%%%%%%%%%%%%%%%%%%%%%%%%%%%%%%%%%%%%%%%%%%%%%%%%%%%%%%%
%% ---- cut start ---- diff_springmass03.m
%
%
function dfdt = diff_springmass03(t,f)
% global variables
    global L gamma1 k1 m1 l1 gamma2 k2 m2 l2 gamma3 k3 m3 l3
    % initialization of dfdt vector to store and pass values
    dfdt = zeros((3*2),1);
    % positions of each mass first
    r1 = f(1);
    r2 = f(2);
    r3 = f(3);
    v1 = f(4);
    v2 = f(5);
    v3 = f(6);
    % now the governing equations for each mass in first
    % order diff form
    % for mass 3
    Fs3 = -k3*(r3-(r2+L)-l3);
    dv3 = Fs3/m3;
    dr3 = v3;
    % for mass 2
    Fs2 = -k2*(r2-(r1+L)-l2);
    dv2 = (1/m2)* (Fs2-Fs3);
    dr2 = v2;
    % for mass1
    Fs1 = -k1*(r1-0-l1);
    dv1 = (1/m1)*(Fs1-Fs2);
    dr1 = v1;
    dfdt = [
        dr1; ...
        dr2; ...
        dr3; ...

        dv1; ...
```

```
        dv2; ...
        dv3        ]; % must return the values of dfdt
%%%%%%%%%%%%%%%%%%%%%%%%%%%%%%%%%%%%%%%%%%%%%%%%%%%%%%%%%%%%%%%%%%%%%%%%%
%% ---- cut end ----


%%%%%%%%%%%%%%%%%%%%%%%%%%%%%%%%%%%%%%%%%%%%%%%%%%%%%%%%%%%%%%%%%%%%%%%%%
%% Save in a separate file called main.m
%%%%%%%%%%%%%%%%%%%%%%%%%%%%%%%%%%%%%%%%%%%%%%%%%%%%%%%%%%%%%%%%%%%%%%%%%%
%% ----- cut start ---- main.m
%%%%%%%%%%%%%%%%%%%%%%%%%%%%%%%%%%%%%%%%%%%%%
% -------- Main Script file to run ----------
%
%
clear ;
close ;
%
global L gamma1 k1 m1 l1 gamma2 k2 m2 l2 gamma3 k3 m3 l3
k = 2 * 19.231; %[lbs/inch] % 2 because in parallel
m = 1*2.205; %[kg->lbs] mass of one CubeSat
d = 0.052; %[inch] is the compressed length
l = 0.052; %[inch] displaced from equilibrium (compressed length ...
           % of spring)
gamma = 0.7; %unit less. For hard anodized surfaces
L = 10*0.3937; %[inch] 1U CubeSat is 10 cm long

k1 = k; k2=k; k3=k;  % same springs
l1 = l; l2=l; l3=l;  % the length of compression of all springs is the same
m1 = m; m2=m; m3=m; % the mass are the same
gamma1 = gamma; gamma2=gamma; gamma3=gamma; % the lengths of each mass is same

% Initial Conditions for the spring to be fully compresed the initial
% condition can be found from y1-0-l1 = -l1; y1 = 0; the origin is
% placed at the wall, from where the position is being determined.
r10 = 0; %
r20 = r10+L;
r30 = r20+L;

v10 = 0;
v20 = 0;
v30 = 0;

f0 = zeros(6,1);
```

```
f0 = [r10 r20 r30 v10 v20 v30];          % initial condition r0 and v0

% time constants
t = linspace(0,1,50);  % for 1 second


% options = odeset('RelTol',1e-6,'AbsTol',[1e-9 1e-9]);
[T,Y] = ode45(@diff_springmass03, t, f0);

% The resulting position and velocity of each CubeSat
% See the subplots for accessing the position and velocity
% vectors of each CubeSat from Y.

% plotting the results

figure(1);
subplot(3,2,1); plot(T,Y(:,1),'r:'); grid on;
xlabel ('time in sec'); ylabel('position in inch');
title ('CubeSat 1 position');
subplot(3,2,2); plot(T,Y(:,1+3),'r-'); grid on;
xlabel ('time in sec'); ylabel('velocity in inch/sec');
title ('CubeSat 1 Velocity');

subplot(3,2,3); plot(T,Y(:,2),'b:'); grid on;
xlabel ('time in sec'); ylabel('position in inch');
title ('CubeSat 2 position');
subplot(3,2,4); plot(T,Y(:,2+3),'b-'); grid on;
xlabel ('time in sec'); ylabel('velocity in inch/sec');
title ('CubeSat 2 velocity');

subplot(3,2,5); plot(T,Y(:,3),'m:'); grid on;
xlabel ('time in sec'); ylabel('position in inch');
title ('CubeSat 3 position');
subplot(3,2,6); plot(T,Y(:,3+3),'m-'); grid on;
xlabel ('time in sec'); ylabel('velocity in inch/sec');
title ('CubeSat 3 velocity');
%%%%%%%%%%%%%%%%%%%%%%%%%%%%%%%%%%%%%%%%%%%%%%%%%%%%%%%%%%%%%%%%%%%%%%%%%%%%%
% ---- cut end ---- main.m
%%%%%%%%%%%%%%%%%%%%%%%%%%%%%%%%%%%%%%%%%%%%%%%%%%%%%%%%%%%%%%%%%%%%%%%%%%%%%%
```

C.1.2 Script to Calculate new altitude and eccentricity

A script to calculate the difference in altitude and eccentricities due to the change in tangential velocity, as is observed in CubeSat ejection from P-POD. See section 4.2.3 for the impact of change in velocity vector on osculating elements eq. (4.16), eq. (4.17), eq. (4.18), eq. (4.19), eq. (4.20),eq. (4.21) and for details see [201].

See Table 4.3 for the reference values of semi-major axis a, the orbit parameter p and the eccentricity. The change in these values is computed using the change in tangential velocity determined earlier.

```
%% Script to calculate dela V tangential velocity effect on
%% corresponding orbital parameters
%% Chose values from
% deltaV is the difference in tangential Velocities of CubeSats wrt P
% V is the velocity vector
%    V is -2.0 m/s from the SHM
% Calculates the values of
% dp
% de
% To find the new values
% a  altitude
% e  eccentricity

 clear all
 close all
 % Including -2 m/s for the spring separation velocities.
 deltaV = [-0.0056 ; 0 ; +0.0056] %
 V = ([-2.0;-2.0;-2.0] .+ deltaV)/1000 % converted into km/s

 mu = 398600.4415; % km^3/s^2
 p = 7094.10; %km
 dp = 2*sqrt(p/mu).*V
 e = 0.0071;
 r = 7094.46 ; % km
 part1 = sqrt(p/mu).*V.*(1+(r/p))*cos(0);
 part2 = e*(r/(sqrt(mu*p))).*V;
 de = part1 + part2

 da = dp./(1-de.^2)

 preva = 7094.46; %km
 preve = 0.0071;
 format long
```

```
newa = preva + da  %km
newe = preve + de  %unitless
```

For the stated tangential velocity change, the change in respective osculating elements are stated as follows.

```
deltaV =
  -0.0056000
   0.0000000
   0.0056000

V =
  -0.0020056
  -0.0020000
  -0.0019944

dp =
  -5.3512e-04
  -5.3363e-04
  -5.3214e-04

de =
  -5.3704e-04
  -5.3554e-04
  -5.3404e-04

da =
  -5.3512e-04
  -5.3363e-04
  -5.3214e-04

newa =
   7094.45946487627
   7094.45946637044
   7094.45946786460

newe =
   0.00656296306506124
   0.00656446256986562
   0.00656596207466999
```

These values are used in Table 4.44.5

APPENDIX D

D.1 Satellite Constellation Design

Sheriff [215, ch.3 pg 104-114] gives a consolidated overview of the satellite constellation design for the purposes of improving Earth coverage, reducing number of satellites in orbit, and maintaining inter-satellite link connectivity, as the main constraints used in the theories. Savi can generate the constellation if the parameters are understood. In this section the parameters are defined, which allow one to visualise the constellation The following material is taken from the book chapter.

D.1.1 Design Considerations

The need for several satellites to operate in lower Earth orbits is to overcome longer propagation delays between Earth terminals and the GEO satellites. Whereas, a satellite in GEO is inherently at a higher altitude than the satellite in LEO, therefore, its antenna beam width is wider, thus covering larger areas on Earth, when compared with LEO based satellite of the same antenna type. Therefore, where a single satellite could cover around 1/3rd of the Earth's surface, several satellites are required for the same coverage.

The mission concepts arising in mid nineties constellation design rigorously from implementation point of view, of which the only constellation implemented in complete sense is IRIDIUM a set of 66 satellites, 10 satellites in an orbit, distributed over 6 orbital planes. Each orbit is polar.

D.1.2 Polar Orbit Constellation

For an optimal constellation of satellites, the most efficient plan is to have the satellites equally spaced within a given orbital plane and the planes equally spaced around the equator. The coverage obtained by successive satellites in a given orbital plane is described by a ground swath or street of coverage as shown in Figure D.1.

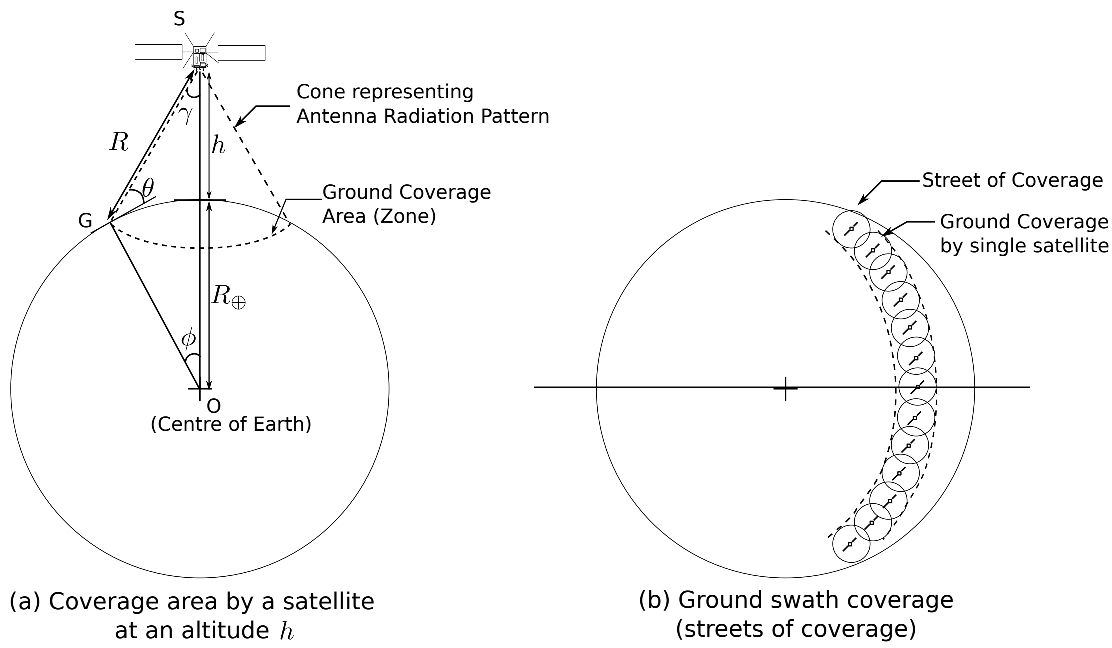

Fig. D.1 Satellite coverage parameter definitions. (a) Coverage zone at altitude (b) Swath or Street of Coverage by several coverage zones.

The problem of designing orbit constellations to provide continuous single-satellite coverage was first addressed by Luders. Luders [299] approach was later extended such that satellites were placed in orbital planes which have a common intersection for example in the polar region. The orbital plane separation and satellite spacing were then adjusted in order to minimise the total number of satellites requires. Beste [300] subsequently derived another method for polar constellation design for both single coverage and triple coverage by selecting orbital planes in such a way that a more uniform distribution of satellites over the Earth was obtained. Later on Adams and Riders [301] also derived another optimisation technique for designing such a constellation. The geometry used in optimising a polar orbit constellation is shown in Figure

D.1.3 Inclined Orbit Constellation

Constellations of satellites in inclined orbit has also been studied for optimum placement within the orbit as well as selection of inclination angle, to provide global coverage by a minimum number of satellites. Walker [143] showed that world-wide single satellite coverage can be accomplished by five satellites, while seven satellites are required for dual-coverage (two satellites over one spot). Walker constellation has been extended by Ballard [44] generally referred to by Rosette* Constellation and recently adopted by Ruggieri by the name of Flower Constellation [42, 45]. Ballard suggests using circular orbits, with

*The constellation traced footprints on ground are arranged like petals of a flower therefore the name *rosette*.

same inclination, which are uniformly distributed along the right ascension angle as they pass through a reference plane which is commonly set as the equatorial plane. The initial phase positions of satellites in each orbital plane is proportional to the right ascension of that plane. Generalised Rosette constellation having s satellites in each of the p orbital planes, a harmonic factor m takes the fractional values of $\{(0toN-1)/s\}$, is designated by (N,p,m).

In Ballard Constellation, the optimisation parameter is the coverage angle (angle between sub-satellite point to the user terminal). The purpose is to determine the critical phase and the optimum inclination which produces the smallest equi-distance for the largest triangle are obtained by a trial and error process. Ballard has tabulated the results for the best single visibility rosette for N between 5 and 15 as shown in Table D.1.

D.1.4 Emerging Formation Flying Missions

Formation Flying missions such as TandemX with TerraSAR [108], the requirement is not Earth coverage, rather reducing fuel consumption, while the two satellite maintain an acceptable relative distance, which has been addressed in the paper [87]. The orbits so defined are not deployed in a string of pearl configuration, rather there is a slight difference in eccentricity, which keeps the relative distance within acceptable margins of changes. These parameters can be used in the deployment of free flying sensor satellites in orbit as well.

Table D.1 Best single visibility rosette constellations for N = 5 to 15 calculated by Ballard [44], to allow minimum elevation angle of 10°

Constellation Dimensions			Optimum Inclination	Coverage Angle	Altitude	Time Period
N	P	m	$i(^\circ)$	$(^\circ)$	h	T
5	5	1	43.66	69.15	4.232	16.90
6	6	4	53.13	66.42	3.194	12.13
7	7	5	55.69	60.26	1.916	7.03
8	8	6	61.86	56.52	1.472	5.49
9	9	7	70.54	54.81	1.314	4.97
10	10	7	47.93	51.53	1.066	4.19
11	11	4	53.79	47.62	0.838	3.52
12	3	1/4, 7/4	50.73	47.90	0.853	3.56
13	13	5	58.44	43.76	0.7666	3.04
14	7	11/2	53.98	41.96	0.598	2.85
15	3	1/5, 4/5. 7/5, 13/5	53.51	42.13	0.604	2.87

D.2 SaVi — the satellite visualisation tool

SaVi [179](Satellite Constellation Visualisation) tool is a handy tool to easily visualise the above mentioned satellite constellations. It has built in scripts which can generate Walker as well as Ballard constellations. It has been extensively used in this dissertation during the study as well as visualising the design of a new type of orbit. As opposed to the industry standard Satellite Took Kit (STK) [302], which is licensed, Savi is open source, and has room for development. It can easily be modified to incorporate orbit dynamics code by Montenbruck and Gill [176]. The relative distances so found can be passed to network simulator such as NS-2 or NS-3, which are useful for network layer performance studies, but require a model for the physical layer to assess propagation delays, and disruption in the physical link, both of which actually affect the higher level protocol performance. Assuming a mobility model is common in such simulators, however, for satellites in orbit, the motion is certainly governed and predictable, if appropriate high precision models for gravitational fields, atmospheric pressures, radiation presuure and such are used, see [175] and Montenbruck and Gill [176] for details. Hashida and Palmer [197] developed an analytical form which incorporates several orders of the perturbation force models, overcoming the need for iterative numerical simulations.

APPENDIX E

E.1 Introduction to Plasma

The plasma state is referred to as ’fourth’ state of matter. As solid is heated it first goes through a transition in which bonds between adjacent molecules are loosened but not entirely broken, and the matter moves in liquid state, on further heating bonds adjacent particles close together are completely broken so that molecules can move more or less independently and the liquid becomes a gas. On further heating may also lead to the ionisation of the molecules or atoms of the gas, so that the gas then comprises neutral particles, ions and electrons. Although today it is known, that plasma state can exist under conditions, for solids, liquids, and gases.

Since the plasma state includes free particles, their movement produces electrical currents, and the constituents are influenced by electric and magnetic fields, the plasma can also produce electric and magnetic fields. A gas must be sufficiently highly ionized and even then there are limits on the density and temperature in order for the plasma to function as a system that is tightly knit by its electromagnetic interaction.

When the plasma is tenuous - i.e. has very low density - the way that particles interact with the macroscopic electromagnetic field becomes much more important than the way that they interact with the microscopic electromagnetic fields associated with individual particles. These orbits of charged particles are studied under ’orbit theory’. This theory helps in developing better fusion reactors, in which plasma is confined for sufficiently long periods of time that fusion reaction can take place, before the plasma gets unstable. Van Allen radiation belts were anticipated, because the charged particles from the sun gets trapped in Earth’s magnetic field. Same holds true for the electrons trapped in flux tubes joining nearby sunspots on the Sun’s outer region - i.e. corona.

Since the charged particles are tightly coupled to EM fields that permeate the ionized gas, the properties of EM waves in plasma differ significantly from those we observe in free space. Although charged particles can move freely along a magnetic field, their motion transverse to the field is very much inhibited. As a result plasma behaves as an anisotropic wave propagating medium. Furthermore the tendency of electrons to move rapidly in response to an electric field in such a way as to cancel that field has the tendency of preventing the propagation of waves of certain frequencies below a critical frequency called the ’plasma frequency’.

Magneto-ionic theory developed after World War I, explained the audible whistle like signal picked by HF receivers. It also explains the wave propagation in plasma.

Mechanisms studied for plasma have helped us explain the radio noise produced by the sun, called type II and type III radio bursts. The mechanism is that excitation of oscillations (’plasma oscillations’) produced by an electron beam travelling through the solar corona, accelerate electrons in the neighbourhood of a moving shock front. This phenomenon is studied as a beam producing oscillations in plasma.

A low density plasma can be confined, such confinement is never perfect. collisions between particles make it possible for particles to diffuse across magnetic field, leading to ’pitch-angle scattering’. Collisions also tend to dissipate the highly ordered motions involved in wave propagation , collisions of particles tend to lead to wave dissipation. Therefore properties of collisions in a fully ionized plasma is necessary study.

When the magneto-plasma system is subject to disturbances that are sufficiently slow and large-scale, it would be possible for electrons to prevent the build up of any electric field in the a frame that moves with the plasma. In such situations, the higher frequency modes of oscillation and wave propagation do not play a role in the behavior of system, and the behavior simplifies considerably and is called the ’magneto-hydrodynamic’ (MHD) approximation.

MHD has been able to identify waves propagating along the magnetic field analogous to waves propagating along a stretched string; these are now known as ’Alfven waves’.

In plasma containment systems such as Tokamaks [303], face the most important recurring problems of plasma physics, the stability.

The behaviour of a complex system can often be regarded as the sum of two different types of behaviours: coherent or collective behaviour, and noise. Since collisions between particles are effectively unpredictable, collisions contribute to the noise in a system. When instabilities occur, small random fluctuations are rapidly amplified, so that the system exhibits large-amplitude noise, called ’turbulence’. The behaviour of charged particles in a turbulent plasma differs markedly from the behaviour in a static plasma. Fermi(1949) proposed that cosmic rays are accelerated by the interaction of charged particles with randomly moving magnetised plasma clouds, the phenomenon known as ’Fermi acceleration’ retains a prominent role in astrophysics.

Stochastic acceleration can be regarded as the transfer of energy from waves to particles. The reverse process can also occur; single particles can emit radiation *, and a plasma can, acting collectively, generate

*(such as synchrotron radiation if they are moving in the presence of a magnetic field)

waves (for instance, a two-stream instability * develops electrostatic waves). Quantum mechanics yields simple mathematical relations (due to Einstein) between spontaneous emission, stimulated emission and absorption. The quantum-mechanical viewpoint when adopted, relations can be obtained between corresponding processes in a plasma.

E.1.1 Plasma Definition : Bulk Parameters

The term "plasma" introduced by Tonks and Langmuir [304] in 1929, "to designate that portion of an arc-type discharge in which the densities of ions and electrons are high but substantially equal." In discussing oscillations of this region, they noted that "when the electrons oscillate, the positive ions behave like a rigid jelly ...". Today the term plasma is used to refer to quasi-neutral assemblies of charged particles, and "plasma physica" is the study of the behaviour of these systems. Just as quantum mechanics shows how it is possible for matter to exhibit both particle-like and wave-like properties; so plasma physics shows how matter behaves as a collection of particles and a fluid.

Modified Gaussian system of units for electromagnetic quantities.

$$\nabla \times E = -\frac{1}{c}\frac{\partial B}{\partial t} \tag{E.1}$$

$$\nabla \cdot B = 0 \tag{E.2}$$

$$\nabla \cdot E = 4\pi\zeta \tag{E.3}$$

$$\nabla \times B = -\frac{1}{c}\frac{\partial E}{\partial t} + 4\pi\mathbf{j} \tag{E.4}$$

The conservation of charge relate current density with charge density.

$$-\frac{1}{c}\frac{\partial \zeta}{\partial t} + \nabla \cdot j = 0 \tag{E.5}$$

Lets consider that a simple plasma composed of fully ionized hydrogen. Lets denote electrons by e and ions (protons) i subscripts, then the charge, mass and number of density be denoted by e, m, n. Then the mass density, charge density and current density are given by

$$\rho = n_e m_e + n_i m_i, \tag{E.6}$$

$$\zeta = e_{elec} n_i + (-e_{elec}) n_e, \tag{E.7}$$

$$j = \tfrac{1}{c}(e_{elec} n_i v_i + (-e_{elec}) n_e v_e). \tag{E.8}$$

*Instabilities such as two stream instability and MHD instabilities can occur in an 'ideal' plasma, in which collisions play no role.

The v represent the averaged velocities of electrons and protons (positive ions).

E.2 Langmuir Probe Measurement in the Ionosphere

Langmuir Probe (LP) has extensively been used in the rockets and satellites to probe space plasma in the Earth's Ionosphere, for its simple construction. It has the ability to measure electron temperature T_e, electron and ion density N_e, N_i and the spacecraft potential V_s relative to the plasma.

E.2.1 Overview of the method

The LP technique involves measuring the volt-ampere characteristics of one or more bare metal collectors mounted on booms. A typical experimental setup is shown in figure which shows a radial probe and an axial probe on the spacecraft having an internal momentum v that allows it to operate in either spinning or de-spun modes. As in the Atmospheric Explorer (AE) and Dynamics Explorer (DE-2) missions. The radial probe is oriented perpendicular to the spin axis and is mounted on a deployable boom which is long enough to reach the undisturbed plasma beyond the spacecraft ion sheath. A length of 30 to 100 cm is adequate for most ionosphere applications (an outer plasma sphere mission would require a longer boom to accommodate the larger Debye shielding distances). The radial probe is perpendicular to the velocity vector when the spacecraft is de-spun thus permitting continuous measurement at the preferred angle of attack. In the spin mode the radial probe makes its most useful measurement as it passes through a 90^o angle of attack twice per spin. For reliability the axial probe is mounted on a boom short enough to avoid the need to stow it for launch and deploy it in orbit. If the spin axis is perpendicular to the orbit plane the axial probe remains at 90^o angle of attack whether or not the spacecraft is spinning. This approach essentially eliminates spin modulation and allows continuous measurement that the radial probe cannot provide when the spacecraft is spinning.

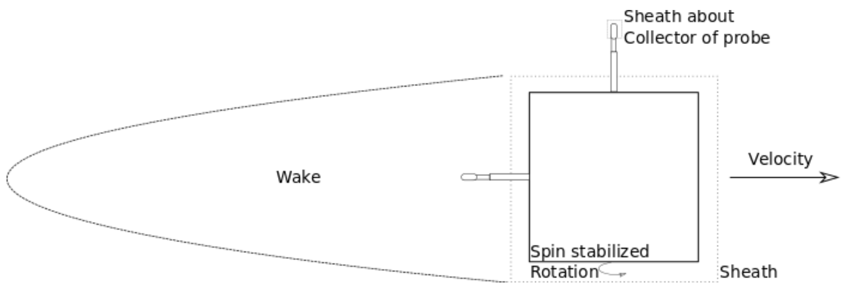

Fig. E.1 Langmuir probe arrangement on a spacecraft [166].

The axial probe is sometimes operated at a fixed potential to provide high resolution measurement of N_e or N_i but it can also be commanded to a sweeping mode which measures T_e and V_s in the event of damage, failure to deploy or contamination of the radial probe. The two probes can time share the same electro-meter if simultaneous operation and electronic redundancy are not required. Both probes have a guard electrode that is driven at the same potential as the collector to reduce electrical end effects.

Figure E.2 illustrates the measurement technique. Volt-ampere characteristics are obtained by repeatedly switching the collector voltage V_a with respect to the spacecraft potential V_s while measuring the net current I which is the sum of the ion current I_i and electron current I_e. The electronics contain an electro-meter, a sweep voltage generator and adaptive circuitry that adjust the gain and sweep amplitude to track the changing density and temperature. The electro-meter output is digitised and recorded for eventual telemetry to a ground station along with the necessary information on electro-meter gain and sweep voltage amplitude. The adaptive function [166] employs hardwired logic circuitry which examines the electro-meter output using each voltage sweep to determine the gain and sweep voltage settings required to achieve the so called "ideal curve" on the subsequent sweep. This adaptive compression accomplished two goals; (1) It focuses the limited telemetry bit rate on just the portion of the curve needed to derive N_e, N_i and T_e, and (2) It generates gain and amplitude settings that can be telecommunicated at low bit rate to serve as in-flight measurements of N_i and T_e.

The theoretical volt-ampere curve shown in the figure illustrates how the measurements are deduced from the curves. According to LP theory [166] the amplitude of the electron current I_e is proportional to N_e and ion current I_i is proportional to N_i. T_e determines the width of the electron retardation region. V_a is the sweep voltage that is applied to the probe with respect to the spacecraft potential V_s. In the ionosphere V_s assumes an equilibrium potential that is 3 or 4 kT_e negative with respect to the plasma potential V_p.

E.2.2 Theory of the Method

There is no general theory that applies to probe geometries, plasma conditions, spacecraft velocity and probe orientations [166]. Therefore, probes are usually designed for special limiting cases; such as orbital-motion-limited collection or sheath-area-limited collection [166]. To remain orbital limited the probe radius must be small compared with the thickness of the sheath that surrounds it while the radius of sheath-area-limited probe must be large compared to the sheath thickness. Dumbbell probes used on early rockets by Boggess and Spencer[158] are examples of sheath-area-limited probes. These probes were too large (radius approximately 10 cm) for satellite use, and they would have to have been even larger to remain sheath-area-limited at the lower densities of the upper F-region and the plasma sphere. Therefore satellite Langmuir probes have been made small enough to remain orbital motion limited. The probe can be either spherical or cylindrical. We have adopted the cylindrical geometry because the probe radius can be made small enough to remain orbital mission limited at very high ionosphere densities, while its length can be made great enough to collect a measurable current at very low densities. In the early missions the collector was a long thin stainless steel wire (23×0.056 cm) whose low mass made it easily boom mounted and whose strength made it rugged enough to withstand the rigors of the launch

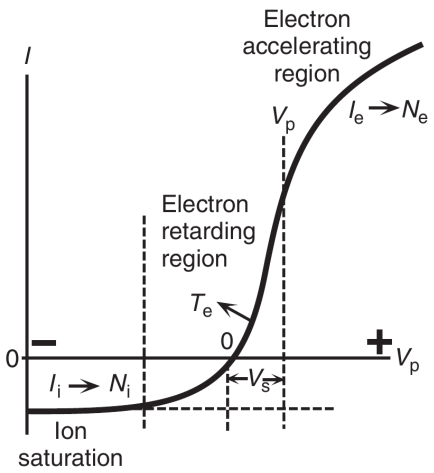

Fig. E.2 Langmuir probe electron current-voltage distribution curve. N_i,N_e and T_e are derived from different parts of the curve [166].

environment. The probes used in the later missions were shorter and larger in diameter (5×0.4 cm) to reduce the voltage induced in the collector as it cuts the geomagnetic field at high velocity.

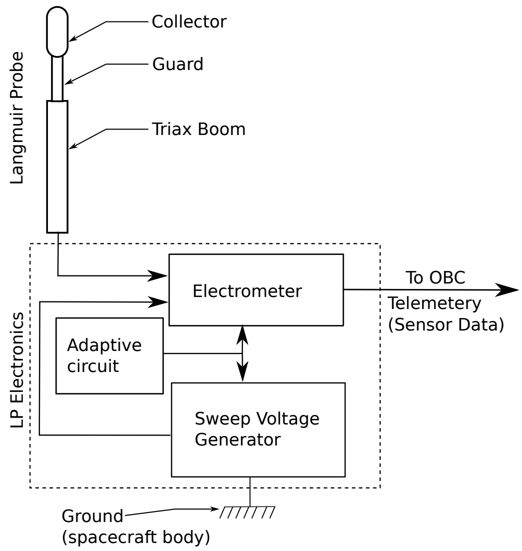

Fig. E.3 Langmuir probe electronic circuitry block diagram. The sweep voltage is applied with respect to the spacecraft voltage.[166]

The first step in the analysis of the volt-ampere curve is to employ the LP current equations to fit the ion saturation and electron retardation regions to obtain N_i, T_e and V_p. Now V_p is taken as the last point in the retardation region that provides a good fit to the exponential, or it may be taken as the inflexion point between the electron retardation and saturation region. All potentials referred to in the Langmuir probe equations are measured with respect to this point. Once V_p has been determined the electron saturation region has been fitted to obtain N_e. The appropriate equations for the orbital motion limited cylinder are discussed below.

The N_e measurement

The equation for the electron saturation current is given by [166]

$$I_e = N_e A e_{elec} 2\pi^{-1/2} \left(\frac{kT_e}{2\pi m_e}\right)^{1/2} \left(1 + \frac{e_{elec}V}{kT_e}\right)^{1/2} \tag{E.9}$$

where

A	$=$	probe surface area
e_{elec}	$=$	electron charge
k	$=$	Boltzmann constant
m_e	$=$	electron mass
V	$=$	probe potential relative to plasma potential V_p

By inspection the equation (E.9) has two terms, involving 1 and eV/kT_e respectively. The first term represent the random electron flux that strikes an uncharged cylindrical probe simply because it is physically there. The second term accounts for the additional current that is collected when the probe is driven positive with respect to V_p. I_e increases as the square root of eV/kT_e in this region.

An advantage of the cylindrical geometry can be appreciated by further inspection of equation (E.9). At higher voltage the electron saturation current ($eV/kT_e >> 1$) is essentially independent of T_e, since the kT_e term cancels. This feature makes it possible to measure N_e without the knowledge of T_e. Thus long cylindrical probes have the advantage of taking long continuous high precision measurements of N_e without interruption, because volt-ampere curves to determine T_e are not required. Since the spatial resolution is limited only be the electro-meter frequency response and the available telemetry rate, measurements made with a fixed V_a can resolve the small scale structure associated with ionospheric irregularities and plasma bubbles.

Because (E.9) represents a simple asymptotic form of the more general equation for orbital-motion-limited collection by an infinitely long probe, it overestimates N_e.

The N_i Measurements

For the N_i measurements the ion saturation current is described by equation (E.10), for the case where the probe axis is perpendicular to the ion velocity vector [166]

$$I_i = \frac{AN_i q_i v_i}{\pi} \left(1 + \frac{kT_i}{m_i v_i^2} + \frac{2e_{elec}V}{m_i v_i^2}\right)^{1/2} \tag{E.10}$$

where

q_i	=	ion charge
v_i	=	ion drift velocity in the spacecraft rest frame
T_i	=	ion temperature
m_i	=	ion mass
V	=	probe potential relative to the plasmaV_p

The ion current consists of three components involving the 1, kT_i and the V. The first term is an order of magnitude larger than the other at least in the E and F regions where m_i is large. It represents the ion current that is produced by ions being swept out by the side of the collector as it moves through the plasma at 8 or 9 km/s. These ions would be collected even if they had zero thermal velocity and if no attracting voltage were applied to the probe. The second term id the component of the current produced by the ion thermal motion at temperature T_i. The third term represents the additional ions that are attracted to the probe because of its accelerating potential V.

For ease of data processing N_i is usually derived by assuming that $m_i = 16$, $T_i = T_e$ and $v_i = v_s$ where v_s is the spacecraft velocity. These simplifying assumption are appropriate because of the dominance of the first term in the higher density regions of the ionosphere where the equation (E.10) is employed. It has been further suggested by Brace [166]. that the slope of the saturation region can be used to obtain the information of m_i in the upper F-region where the concentrations of H^+ and he^+ approach or exceed that of O^+.

The T_e Measurements

T_e is derived from the Langmuir equation for the electron retarding region given by

$$I_e = AN_e e_{elec} \left(\frac{kT_e}{2\pi m_e} \right)^{1/2} e^{eV/kT_e} \tag{E.11}$$

which applies to probes of any geometry. The T_e measurement relies on the fact that the exponential term involves only two variables; T_e and V. T_e is derived by fitting the volt-ampere curves using a linear approximation to the ion region and an exponential represntation of the electron retardation region. Note that the knowldge of the constants ahead of the exponential is not required to obtain T_e because only dV/dt and T_e affect the shape of the retading region and dV/dt is the known voltage sweep rate [166].

Measurement Accuracy

It has been described that if the sources of error are dealt with successfully then the accuracy of the LP measurements should be better than 10%, and perhaps better than 5% for T_e except for very low density ($N_e < 10^2 \text{cm}^{-3}$). The precision of the density measurments can be much greater depending on the number of bits employed in the telemetry words, the electrometer noise level and interference from other spacecraft systems. Relative accuracy of greater than 1% is typical [166].

It has been further suggested, that one can assess the accuracy achieved by (1) examining the internal consistency between LP theory and the shapes and amplitudes of the measured volt-ampere curves, (2) comparing the measurements by different probes on the same satellite and (3) comparing the probe measurements with those made by incoherent radars during over flights.

It has been found that good agreement between the measurement of N_e, N_i and T_e on similar LP on different satellites, rockets and even retarding potential analyser [166].

E.2.3 Implementation Issues

A number of factors have been highlighted which are critical to the successful measurement using Langmuir Probe;

- proper sensor placement,
- reduction of collector work function patchiness,
- reduction of collector surface contamination,
- limitation of Geo-magnetically indexed potentials in the collector,
- adequate resolution and recover of the volt-ampere curves, and
- attention to spacecraft design details.

It has been emphasised that in attention to some of these items can preclude the measurements completely especially for T_e [166]. We shall not discuss the actual manufacturing issues of the Langmuir Probe, but would consider the suggestion regarding the placement, spacecraft design and the electronics and in flight cleansing.

E.2.3.1 Boom and Sensor

The use of the boom is required to assure that the probe is placed in the undisturbed plasma i.e. beyond the spacecraft sheath and outside the spacecraft wake. To achieve this the boom length of 30cm to 100cm is adequate for ionosphere measurements. Two independent sensors are required particularly for spinning satellites to assure that at least one probe is in the undisturbed plasma at all times.

E.2.3.2 In-flight Cleansing

An in-flight cleansing of the probe is possible owing to the anticipated contamination during operations. A bake out temperature ($> 300°C$) is suggested which requires extensive electrical power.

Another method suggested to apply higher voltage (+150V) to one of the probes as the spacecraft traversed denser parts of ionosphere. There were no signs of contamination as the process was applied to the probes, and no significant disturbance observed in the volt-ampere curve obtained. Even applying the same method 18 months later also showed no significant disruption in volt-ampere curves, emphasising the validity of this method.

It is assumed that the probe gets contaminated due to exposure to the EUV and to chemically active atoms (O and O^+) which began to reduce the conductivity of the contaminating layer, however, one of the probes remained uncontaminated throughout the mission, whereas one showed disturbance, does not validate any confirm reason for contamination.

Therefore in-flight cleansing method is highly recommended.

E.2.3.3 Magnetically Induced Potentials

When a spacecraft travels with high velocity $\vec{v}$ through the Geo-magnetic field $\vec{B}$, a potential gradient of 300 mV/m is induced in the collector. For a collector of length l, the potential is $\vec{B} \times \vec{v} \cdot l$. The resulting potential gradient produces the same kind of energy smearing that is caused by surface contamination, that is error in T_e measurements especially in regions of very low temperature, resulting in incorrect identification of V_p [166].

The solution to energy smearing is to use short probes or keeping the probe aligned either with $\vec{B}$ or $\vec{v}$. Alignment with velocity is not desirable since it enhances the ion end effect [166], which makes the volt-ampere currents more difficult to interpret. However alignment with Geo-magnetic field is desirable, which eliminates the voltage induced in the probe.

If the spacecraft is not able to align itself with the Geo-magnetic field, then a short probe is recommended [166], where it was noted a maximum voltage induced smearing of 15mV which corresponds to 1kT_e at 150K. Thus use of short probe essentially removed the low temperature limit although it may have enhanced the errors in the N_e measurements.

E.2.3.4 Electronics

The electronics of the probe is required to apply the desired range of voltage to the probe, and to measure the resulting currents. If the full range of N_e (5 or 6 orders of magnitude) is to be measured then the electro meter should have a wide dynamic range. T_e typically varies by a factor of 30 from about 300 K in the E-region to greater than 10,000 K in the upper F-region at high latitudes. A single sweep amplitude is not adequate in such missions. If the sweep amplitude is kept high enough to reach full ion saturation at high T_e the retarding region will be crossed too quickly at low T_e to be followed by the electro meter or to be resolved at realistic telemetry sampling rates.

An adaptive circuitry is therefore suggested, which sets the electro meter gain and sweep amplitude so as to focus on the portion of the volt-ampere curve actually used to determine N_e,N_i and T_e.

The adaptive circuitry adjusts the electro meter gain using the ion current level observed at the beginning of each sweep. The gain is locked and a voltage sweep is initiated to generate a volt-ampere curve. Level detectors and time counters examine the retarding region to obtain an approximate value of kT_e for use in setting up the amplitude and start voltage to be used on the following sweep. The sweep amplitude ranges from about 300mV to 10V, corresponding to T_e variation from 300K to 10,000K.

The following pertinent questions affect the design of electronics to be used by the probe;

- What ranges of N_e and T_e are likely to be encounter in the selected orbit and at the level of solar activity expected during the mission?
- Does the mission science require the full range of N_e and T_e to be measured or is it possible to focus on narrower ranges of altitude latitude or local time?
- Is the spacecraft spin-stabilised or 3-axis stabilised?
- What sweep repetition rate is consistent with the spacecraft spin rate, the desired spatial resolution and the available telemetry rate?
- How many sensors are to be operated wand where they should be mounted to avoid or minimise spacecraft wake and sheath?
- Should each probe system be fully redundant to permit simulations measurements or can be probes time-share one electro meter and sweep generator?
- Is the available data rate adequate to permit the volt-ampere curves themselves to be recovered or will some form of electronic in flight processing be requires to obtain the desired spatial resolution along the orbit?
- Is in flight cleaning of the collectors likely to be required?
- Will the proposed spacecraft provide normal V_s or will design changes be required?

E.2.3.5 Spacecraft Design Factors

Since the LP sweep voltage is applied with respect to the spacecraft potential reference, the spacecraft design must be examined to identify if it includes any features that might affect V_s which should remain stable and low. Historically the most common spacecraft potential problems are caused by

- exposed metal connecting tabs on the solar arrays and
- insufficient external conducting area to return the LP current to the ionosphere without causing excessive changes in V_s.

It is essential that the net current to the spacecraft-probe system be zero, increases in I_e to the probes must be offset by identical reductions in I_e flowing to the spacecraft. The spacecraft design should support such changes in electron current without significant change to V_s.

To achieve a stable V_s requires an external conducting area that is several hundred times larger than the combined probe and guard areas. This conducting area must not be in the wake of the satellite because neither the ions nor the electrons have access to those surfaces. Although for typical space missions, the external area is typically more than 10,000 times than that of a LP, most of this area is non-conducting. Bare metal surfaces tend to have absorbtivity and emissivity coefficients that conflict with spacecraft thermal design requirement. This conflict can be resolved by painting some of the exposed surfaces with conductive thermal paint, or by adding conductive surfaces elsewhere.

It may be necessary to accept the smaller area ratio if an adequate area ratio is not achievable. In this situation, one must avoid using LPs in the the electron saturation regions where they collect the largest current. In this case T_e and N_i measurements are only possible. This approach has been employed on AE missions to reduce possible interference with the retarding potential analysers and the ion mass spectrometers.

It has been observed that cases of unusually high V_s have all been traced to the use of negative grounded solar arrays which interconnecting metal tabs were exposed to plasma. These tabs have voltages ranging from 0 to +40V with respect to spacecraft, so they act as small Langmuir probes that collectively attempt to draw a larger electron current than the rest of the spacecraft is able to return to the ionosphere. To maintain a net zero current, V_s shifts sufficiently negative to drop the array electron current to sustainable levels. Such high negative potential (0 - 40V) usually preclude the T_e and N_e measurements, since the available range of V_a is insufficient to drive the probe out of ions saturation. This problem is limited to the parts of the orbit where the spacecraft is sunlit.

Two solutions have been found successful. The first involves grounding the positive end of the solar array thus exposing only negative potentials to the plasma. While the array draws an enhanced ion current, this current is easily balanced by a slight decrease in V_s to draw the required additional electron current to spacecraft. This technique has been used on Explorer 22, 23, Tiros, AE, and DE spacecraft, and they experienced normal ranges of V_s [166]. The missions which had positive arrays, the problem had been solved by painting the solar cell tabs with silicon rubber to keep them from drawing electrons from the plasma. which proved to be a simple effective and low cost fix.

E.2.4 Probe Electronics

The voltage sweep generator is evaluated first. There are two options for its implementation. It requires an oscillator which controls the sweep frequency. Since variable sweep rates are desired, therefore a programmable sweep generator is evaluated. There are two options, an electrical hard-wired circuit, or a programmable micro-controller based oscillator. The micro-controller provides configurable sweep generation, much easier than the designed circuit.

The sweep functionality is programmed in a low power consuming micro-controller, which generates a digital waveform, which is converted to analog using digital to analog converter (DAC). This allows a precise control on the waveform to control the sweep rate. Apart from the passive components the processor and the DAC are major power consuming components. There is a wide range of micro-controllers and DAC available in the market. It is out of the scope of this thesis to conduct a detailed survey of the components, a quick search online can reveal the low power consuming MSP430 series from Texas Instruments, and PIC micro-controllers from Microchip.

An additional digital to analog converter (DAC) is used to generate the voltage sweep. A typical DAC consumes about 1.65 mW (based on AD5337 from Analog Devices), 8 bit 5.5V operations. An analog to digital (ADC) converter is also required, but 12 bit ADC is generally available on the micro-controller, which can be used instead of a separate component.

The only part missing is the analog electro-meter, which is essentially a charge sense amplifier. It is not a major current consuming component. However, its output must be converted to digital bits, which requires analog to digital converter (ADC). We opt to use the built-in ADC of micro-controller.

Another requirement is a dual polarity voltage source. If the main supply for spacecraft is unipolar (generates only +V volts), then we have to set up a dc-dc converter, which could provide -V from a +V supply. Commercially available converters (MURATA DC-DC converters) consume 0.7 W + 0.02 W, which is a a considerable power. In order to save this extra consumption of power, we propose the use of dual polarity electrical power supply system for the spacecraft.

A quick survey of the components required to build a voltage sweep generator, and a current sensor, with digital interface, would end up consuming at-least 3 Watts, requiring at least ± 7 V. It is recommended to decontaminate the probe, by applying high voltages so that accumulated charges on the surface disperse. It is a necessary step to keep the measurements as accurate as possible. For details of the implementation issues, see Appendix A higher power would be consumed when high potential cleansing process is implemented.

E.2.5 Estimates of generated Data

The probe is used in a symmetric sweep mode i.e. applied voltage is varied from a -V to a positive V value with in a time span. Typical value of V is between ± 7 Volts. The sweep duration can vary between time spans, assuming to be 500, 1000, 2000 ms*.

A typical measurement from the probe would be a sample of current at the applied voltage, as the voltage sweeps from a -V to +V voltage say ± 7 V. For the complete sweep, say 1000 discrete points between -V

*These assumptions are for preliminary analysis of the budgetary requirements of data, which might vary from the actual implementation.

and +v are measured. The voltage and current at each point is represented by 12 bits, which means, one sweep generates, $12 \times 2 \times 1000 = 24000$ bits. Lets consider that the next measurement is carried out after a second has elapsed. The time it takes a measurement to take is about 1 second average. Then every other second 24000 bits are being generated.

Furthermore, we would require a time stamp and the current magnetic field vector, say each being 12 bit and taken at the end of sweep. So the cumulative data comprises of sweep data, magnetic field vector, spin rate, time stamp, and orbit number which amounts to roughly (24x1000)+(12x3)+ 32 + 64 + 64 = 24196 bits. Add 5% overhead, 25405 bits of data per measurement are generates. This shows an estimate of data being generated per second.

With the measurement taken every minute over the orbit assuming an orbit period of say 100 min would yield a total of 2540500 bits. This means a data rate of 256 kbps is required to transfer the data on a link. The link should remain operational for at least one second for the data to pass on. However, there are further overheads involved in establishing the link, which is the responsibility of the data link layer.

Now consider that the link is available only for 1 second, then there is a chance of not being able to transfer the data as the link drops for some unknown reason. For the re-establishment of a successful link, there is going to be a handshaking procedure, in which a request is sent, an acknowledgement received, then the data is sent in the form of packets. These are intricacies of the data link layer protocol, which we are not considering for the moment. What we want to highlight is the fact that link needs a minimal time to complete transaction of the data which is called the **link window**, after which the link is not available for data transfers. Therefore a higher data rate than the data rate of instrument needs to be incorporated.

Now consider the deployment of say 10 sensor satellites, each generating the data as calculated in the previous paragraphs. Each sensor would send its data to its nearest satellite to be forwarded to the one which is to communicate with the micro-satellite acting as the relay satellite. Therefore, by the time the data is accumulated to the one satellite say after 10 hops, the data would be 10 times more at the end satellite. Taking the previous value of 25405 bits, would become 254050 bits. This shows a link 10 times faster than a single link is required, for the same available time, to pass the accumulated data.

E.2.6 Evaluating memory requirements to save data

For some unknown reason, the inter-satellite link is not available for say 30 orbits, then the data accumulated would have to be saved in to a memory. The memory capacity is limited. Any new data would require a space in the memory. There are two options, either discard the newer data, or discard the oldest data. In either case, a loss of data is inevitable. The memory is to be designed to keep at least the necessary data for say 10 orbits. In the case of FLASH type memory, one part of the memory has to be flushed, constantly, then double memory modules are used, including a memory handler. This discussion of selection of memory, and its intricate details are just highlighted indicative of one of the design factor in on-board data handler. Interested readers are suggested excellent books on spacecraft system design such as [125, 71]*.

The small discussion highlights that there are many design factors which actually determine the final link data rates. A compromise is always required to minimise the precision or accuracy of the converted measurements in digital form. The decision is with the science team, based on the available spacecraft resources.

In our mission, since multiple sensor satellites are being sent, therefore, moderate accuracy and precision is used. The final data rate is a compromise between the instrument measurement precision and accuracy, on-board memory capacities, and communications link rate. Therefore it is an iterative process, which cannot be finalised in one section or under a single scenario.

However, it does indicate, that high data rates in hundreds of kbps are required from the ISL. Therefore the modem should be able to support single burst like communications links, sending as much as data in one link as possible.

E.3 Magnetometer and Space Plasma Measurements

The accurate in situ measurement of the magnetic field is of fundamental importance to all Space Physics (Plasma) missions. Space plasma is always threaded by magnetic field lines, which provide the basic structural organization in different plasma regimes. The properties of plasma such as its temperature depends on the direction of magnetic field when the measurement is made. Generally the temperature measured perpendicular to magnetic field is different from when taken parallel, due to the random velocity distributions of ions. Energetic particles are guided by the magnetic fields, and it is often possible to describe the directional energetic flux intensity in the form of pitch angle distributions that are rotationally symmetric around the local magnetic field.

The magnetic field **B** being a vector requires measurements of its three components namely B_x, B_y, B_z, in a specified Cartesian coordinate system. Two main types of magneto-meters in use are the tri-axial flux-gate magnetometer (FGM) and the vector helium magnetometer. The detailed characteristics of both the magneto-meters is given in [161].

The performance of the magneto-meters is measured by their sensitivity (the smallest magnetic field that they can measure), that is related to their noise levels; measurement range and their frequency response. Magneto-meters used in all space missions have in general a noise level of <10 pT in the frequency range of 0.01-1 Hz. It is also possible to achieve accuracies better than 0.1 nT within a frequency range from DC to 10Hz.In and around the magnetosphere, the magnetic fields to be measured range from a

*An additional resource is the CubeSat community.

few nT to a few thousand nT * However, in interplanetary space, the magnetic field away from the Sun is less than 1 nT.

The dynamic range of the meter is the ratio of the maximum field to be measured to the resolution of the instrument, is usually dependent on the electronics and the analogue-to-digital converters (ADC).

Every magnetometer has a slight offset in its measurement, which means that the three magnetic sensors are not exactly zero in a zero field. These offsets are measured normally determined on ground and have typical values of 0.5-5nT. These offset are not constant, and in flight means of determining these offset is a must.

On a spinning spacecraft the offset can be easily determined, since the magnetic field measured perpendicular to the spin axis, must average out to be zero over one spin period. Provided the magnetic field is slowly varying, which is generally true at a certain altitude in most of the times in orbit. The offset along the spin axis is more difficult to assess, however, statistical methods have been devised to cater to this problem in inter-planetary missions [161]. Similarly offsets are difficult to determine on 3-axis stabilised spacecraft as well, again statistical properties of the plasma from long measurements is used to determine the offset.

E.3.1 Operations of a tri-axial flux-gate magnetometer

The tri-axial FGM consists of a set of three orthogonally placed sensors, each measuring the field along its axis, cumulatively making up the three components of magnetic field vector.

A single axis sensor consists of a magnetic core, which has a toroidal drive winding around it, and a coil transformer surrounding the sensor core and drive winding, around which another sense winding is placed. The two coils are orthogonal so their is no magnetic coupling in between them. Bipolar symmetric current pulses are used in the drive winding to drive the core material deep into saturation around the hysteresis loop at a frequency usually about $f_o = 15$kHz. In the absence of an external magnetic field, the symmetry of the hysteresis loop ensures there is no current in the winding. However, in the presence of an external magnetic field, along the axis of the sense winding, the hysteresis loop is slightly displaced, leading to a non symmetric magnetic signal which induces an alternating voltage in the sense winding, at a frequency $2f_o$. This signal of order of $< 1\mu V$, is proportional to the component of the magnetic filed along the axis of the sense winding. It is first amplified then detected using a synchronous detector. After some further amplification, the resultant voltage signal is fed back through a transconductance (voltage-to-current) amplifier and the sense winding, as a feedback current counteracting the effect of the external magnetic field. The voltage signal is fed to ADC which converts it into digital form for further processing.

*The Earth's magnetic field at the equator on the surface is about $30,000$nT.

Another alternative design of the meter uses the same sensors but replaces the analogue electronics with its digital counterpart. The signal processing is performed as a software function in the digital domain. Digital implementation has an advantage of being inherently tolerant to temperature variations. The sense signal is immediately fed to the ADC after amplification, and the process of filtering, synchronous detection and integration is carried out in the processor (digital controller). The feedback current is generated and converted via a digital-to-analogue converter. The calculated value if field -proportional to the magnetic field, and is ready for further processing.

We leave the functioning of the Vector Helium Magnetometer (VHM) which has flown on major missions such a Pioneer10,11, ISEE-3, Ulysses, Cassini Saturn Orbiter), which is relatively larger and complex. Its use is also restricted due to is power requirements and restricted availability *.

E.3.2 Implementation Issues

To enable measurements of considerable accuracy for weak magnetic fields, a few successive steps are used in space science mission design.

- To ensure that the spacecraft and its subsystems and its payloads have individually low magnetic moments, by attaching small magnets to counter their fields such as valves used for attitude manoeuvres.
- To minimise the current loops generated due to power subsystem, particularly in the wiring of solar panels.
- To place sensors on the boom to be deployed as far away from the vicinity of spacecraft as is possible (constrained by mechanical strength and cost) about 1m to > 10m.
- For a better accuracy the residual magnetic field of the spacecraft needs to be measured , compensated, and the residual field then be calibrated at the location of magnetometer.

E.3.3 AC Magnetic field measurements

The AC magnetic fields are measured using magnetic antennas, which are essentially of two types typically used on board missions (a) the magnetic loop antenna [161], and (b) the search coil magnetometer . In both cases the time dependent magnetic field vector $\mathbf{B}(t)$ is detected through the application of Faraday's law, by measuring the voltage induced in a sensing loop or coil, as a function of frequency by the variation of the magnetic flux $\Phi = NA(\mathbf{B} \cdot \mathbf{n}$. Where N is the number of turns in the sensing coil, A is the area of sensing loop , while $\mathbf{n}$ being the unit normal to the area. The time rate of change of the component of the magnetic field vector parallel to unit vector is thus obtained from the voltage induced in the coil. This means that if all three components of the derivative of $\mathbf{B}$ are to be measured, then in principle, three simultaneous measurements along three orthogonal directions are needed.

*JPL science team developed and designed the instrument, and have the only access to use it.

APPENDIX F

CUBESAT COMMERCIAL BUS SYSTEM

The commercially available bus systems after a quick search online, are listed in the Figure F.1 & F.2. The main on board computer, electrical power system, and the ground link are the essential systems. A separate beacon signal generator is placed from experience, to maintain redundancy if for some reason there is a failure of main communications systems which generally is a case. Beacon signal generator is directly powered from the solar panels, so that even an issue with the electrical power system could be bypassed.

Attitude determination and control system is required to maintain a spin stabilised satellite, so that Langmuir Probe and magneto meter could carry out their measurements as discussed in section E.2.3.5. An angular rate of 5 to 10 revolution per minute would suffice.

Parameters		Units	Beacon
Manufacturer			MicroChip
Model			rfPIC12F675F
Output Power		dBm	<= 10
I/O Pins			6
ADC Channels			4
ADC Resolution		bits	10
RF frequency range		MHz	380-450
Electrical Power Requirement	Voltage	V	2 to 5.5
	Current	A	0.014 (while transmitting +6 dBm at 434 MHz)
	Power	W	
Mass		g	
Dimensions	length x width x height	mm	7.34 x 8.18 x 1.98
Data Interface			ICSP
Data Rates		kbps	40
Memory	EEPROM Data Memory	Bytes	1024
	Flash Memory		1024 x 14 words
	SRAM	Bytes	512
Pointing Requirement			
Price			$2.30
Weblink			http://www.microchip.com/

Parameters		Units	ADCS	
Manufacturer			Clyde Space	CubesatShop
Model			CS-ADCS-INT-01	Cube ADCS
Electrical Power Requirement	Voltage	V		3.3/5
	Current	A		
	Power	W		1(nominal – depends on configuration)
Mass		g		<=351 g
Dimensions	length x width x height	mm		PC 104
Data Interface				UART, I2C, CAN
Data Rates				
Memory	SDRAM			
	Flash			
Configurations				(Magnetic, Y-Momentum, 3-Axis)
Pointing Requirement				
Attitude				
Price			$ 18,850 (hardware only)	>= € 14,200
Weblink			http://www.clyde-space.com/	http://www.cubesatshop.com/

Fig. F.1 A sample of available COTS for IMM Bus. Beacon signal generator using rfPIC a Micro-controller with integrated RF transceiver. A solution for attitude determination and control system for CubeSat.

Parameters		Units	Ground Link		
Manufacturer			CubesatShop		Clyde Space
Model			ISIS TXS	HISPICO	STX
RF Power		dBm	<=28	<=27	21-30 (dB)
RF Interface			SMA/MCX	SMA	
RF frequency range		MHz	2100-2500	2200-2300	2400-2483
	Voltage	V		3.3 (nominal) to 5	
Electrical Power Requirement	Current	A		1.5 @ 27 dBm	
	Power	W	<3.5		<6 (for max RF output Power)
Mass		g	62	75	
Dimensions	length x width x height	mm	PC 104	95 x 46 x 15	PC 104
Data Interface			I2C	SPI	I2C(control,telemetry)/SPI(payload data)
Data Rates		kbps	<= 100	<=1060	<=2000
Memory	SDRAM				
	Flash				
Pointing Requirement			nadir	nadir	nadir
Price			€ 8,500	€ 6,500	$8,900.00
Weblink			http://www.cubesatshop.com		http://www.clyde-space.com/cubesat_shop

Parameters		Units	Electrical Power System	Battery Pack
Manufacturer			GOM Space	
Model			Nano Power P31u	Nano Power BPX
	Voltage	V	3.3 / 5	6-33.6
Electrical Power Output	Current	A	5 / 4	
	Power	W	<= 30	
Capacity		mAh	2600	<=10400
Mass		g		>500
Dimensions	length x width x height	mm	PC 104	PC 104
Conversion efficiency		%	93	
Output Channels			6	
Input Channels			3	
Data Interface			I2C	I2C
Pointing Requirement				
Attitude				
Price				
Weblink			http://gomspace.com/	http://gomspace.com/

Parameters		Units	OBC OBDH	
Manufacturer			GOM Space	
Model			NanoMind A3200	NanoMind A712D
	Voltage	V	3.3	3.3
Electrical Power Requirement	Current	A	0.04 (peripherals add to this)	0.07 (peripherals add to this)
	Power	W		
Mass		g	14	55
Dimensions	length x width x height		PC104	PC 104
MCU			AVR32	ARM7
ADC Channel			8	8
Data Interface			I2C, UART, CAN-Bus, SPI	CAN, I2C, USART
Data Rates				
	SDRAM	MB	32	2
Memory	Flash	MB	128	4
	microSD Card Support			Upto 2 GB
Pointing Requirement				
Attitude				
Price				
Weblink			http://gomspace.com	http://gomspace.com/

Fig. F.2 Example components after market survey of COTS for IMM BUS, including the ground link, electrical power system with batteries and on board data handling.